DEVELOPMENT OF GREEN'S FUNCTIONS AND ITS APPLICATION FOR CYLINDRICALLY STRATIFIED MEDIA

SUN JIN

(M.S., WUHAN UNIVERSITY, CHINA)

A THESIS SUBMITTED

FOR THE DEGREE OF DOCTOR OF PHILOSOPHY

DEPARTMENT OF ELECTRICAL AND COMPUTER ENGINEERING

NATIONAL UNIVERSITY OF SINGAPORE

2004

Acknowledgement

I would like to express my sincere gratitude to my supervisors, Associate Professor Li Le-Wei and Professor Leong Mook-Seng, for their valuable guidance and strong support during my PhD research work program. Particularly, I would express appreciation to my principal supervisor Associate Professor Li Le-Wei and acting supervisor Dr. Wang Chao-Fu for their great assistance in the research work and to co-supervisor Professor Leong Mook-Seng for his useful opinions and suggestions on many parts of this thesis, without which this thesis would not be possible.

My thanks are also extended to Mr. Ng Tiong Huat, Mr. Li Zhong Cheng and many friends in Microwave Division for their help, advice and instructive discussions.

Last but not least, I take this opportunity to express my deep thanks to my parents and my wife Zhou YunYun, for their support and understanding.

Contents

List of Tables

List of Figures

List of Symbols

$\overline{\boldsymbol{G}}_E$	Electric field dyadic Green's function in spatial domain
$\widetilde{\overline{\boldsymbol{G}}}_E$	Electric field dyadic Green's function in spectral domain
$\overline{\boldsymbol{G}}_A$	Magnetic vector potential dyadic Green's function in spatial domain
$\widetilde{\overline{\boldsymbol{G}}}_A$	Magnetic vector potential dyadic Green's function in spectral domain
$\overline{\boldsymbol{G}}_\phi$	Electric scalar potential dyadic Green's function in spatial domain
$\widetilde{\overline{\boldsymbol{G}}}_\phi$	Electric scalar potential dyadic Green's function in spectral domain
$\boldsymbol{E}$	Electric field
$\boldsymbol{H}$	Magnetic field
$\boldsymbol{J}$	Electric current
$\boldsymbol{E}_s$	Transverse component of electric field
$\boldsymbol{H}_s$	Transverse component of magnetic field
E_z	z component of electric field
H_z	z component of magnetic field
E_ϕ	ϕ component of electric field
H_ϕ	ϕ component of magnetic field
$\overline{\boldsymbol{T}}_{ij}$	Local transmission matrix when waves travel from layer i to layer j
$\overline{\boldsymbol{R}}_{ij}$	Local reflection matrix when waves travel from layer i to layer j

$\widetilde{\overline{\boldsymbol{T}}}_{ij}$	Generalized transmission matrix when waves travel from layer i to layer j
$\widetilde{\overline{\boldsymbol{R}}}_{ij}$	Generalized reflection matrix when waves travel from layer i to layer j
$\widetilde{\overline{\boldsymbol{M}}}_{i}$	Multi-reflection matrix when waves travel in layer i
$\overline{\boldsymbol{I}}$	Identity matrix of 2×2 dimension
J_n	Bessel function of the first kind
N_n	Bessel function of the second kind
$H_n^{(1)}$	Hankel function of the first kind
ϵ_i	Relative permittivity for the ith layer
μ_i	Relative permeability for the ith layer
ϵ_0	Relative permittivity for the free space
μ_0	Relative permeability for the free space
k_z	Wavenmber in z direction
$k_{i\rho}$	Wavenmber in ρ direction for the ith layer
k_i	Propagation constant for the ith layer
$\boldsymbol{e}^i$	Tangential electric fields at the cylindrical surface $\rho = \rho_i$
$\boldsymbol{h}^i$	Tangential magnetic fields at the cylindrical surface $\rho = \rho_i$
$\overline{\boldsymbol{T}}$	Transfer matrix for tangential fields at two successive cylindrical surfaces
$\boldsymbol{A}$	Magnetic vector potential
ϕ	Electric scalar potential
$\tilde{G}_{\rho\rho}^{E_n}$	ρ component of electric field Green's function due to a $\widehat{\boldsymbol{\rho}}$-oriented dipole
$\tilde{G}_{\rho\phi}^{E_n}$	ρ component of electric field Green's function due to a $\widehat{\boldsymbol{\phi}}$-oriented dipole
$\tilde{G}_{\rho z}^{E_n}$	ρ component of electric field Green's function due to a $\widehat{\boldsymbol{z}}$-oriented dipole
$\tilde{G}_{\phi\rho}^{E_n}$	ϕ component of electric field Green's function due to a $\widehat{\boldsymbol{\rho}}$-oriented dipole
$\tilde{G}_{\phi\phi}^{E_n}$	ϕ component of electric field Green's function due to a $\widehat{\boldsymbol{\phi}}$-oriented dipole
$\tilde{G}_{\phi z}^{E_n}$	ϕ component of electric field Green's function due to a $\widehat{\boldsymbol{z}}$-oriented dipole

$\tilde{G}^{E_n}_{z\rho}$	z component of electric field Green's function due to a $\widehat{\boldsymbol{\rho}}$-oriented dipole
$\tilde{G}^{E_n}_{z\phi}$	z component of electric field Green's function due to a $\widehat{\boldsymbol{\phi}}$-oriented dipole
$\tilde{G}^{E_n}_{zz}$	z component of electric field Green's function due to a $\widehat{\boldsymbol{z}}$-oriented dipole
$\tilde{G}^{H_n}_{\rho\rho}$	ρ component of magnetic field Green's function due to a $\widehat{\boldsymbol{\rho}}$-oriented dipole
$\tilde{G}^{H_n}_{\rho\phi}$	ρ component of magnetic field Green's function due to a $\widehat{\boldsymbol{\phi}}$-oriented dipole
$\tilde{G}^{H_n}_{\rho z}$	ρ component of magnetic field Green's function due to a $\widehat{\boldsymbol{z}}$-oriented dipole
$\tilde{G}^{H_n}_{\phi\rho}$	ϕ component of magnetic field Green's function due to a $\widehat{\boldsymbol{\rho}}$-oriented dipole
$\tilde{G}^{H_n}_{\phi\phi}$	ϕ component of magnetic field Green's function due to a $\widehat{\boldsymbol{\phi}}$-oriented dipole
$\tilde{G}^{H_n}_{\phi z}$	ϕ component of magnetic field Green's function due to a $\widehat{\boldsymbol{z}}$-oriented dipole
$\tilde{G}^{H_n}_{z\rho}$	z component of magnetic field Green's function due to a $\widehat{\boldsymbol{\rho}}$-oriented dipole
$\tilde{G}^{H_n}_{z\phi}$	z component of magnetic field Green's function due to a $\widehat{\boldsymbol{\phi}}$-oriented dipole
$\tilde{G}^{H_n}_{zz}$	z component of magnetic field Green's function due to a $\widehat{\boldsymbol{z}}$-oriented dipole
$\tilde{G}^{A}_{\rho\rho}$	ρ component of vector potential Green's function due to a $\widehat{\boldsymbol{\rho}}$-oriented dipole
$\tilde{G}^{A}_{\rho\phi}$	ρ component of vector potential Green's function due to a $\widehat{\boldsymbol{\phi}}$-oriented dipole
$\tilde{G}^{A}_{\rho z}$	ρ component of vector potential Green's function due to a $\widehat{\boldsymbol{z}}$-oriented dipole
$\tilde{G}^{A}_{\phi\rho}$	ϕ component of vector potential Green's function due to a $\widehat{\boldsymbol{\rho}}$-oriented dipole
$\tilde{G}^{A}_{\phi\phi}$	ϕ component of vector potential Green's function due to a $\widehat{\boldsymbol{\phi}}$-oriented dipole
$\tilde{G}^{A}_{\phi z}$	ϕ component of vector potential Green's function due to a $\widehat{\boldsymbol{z}}$-oriented dipole
$\tilde{G}^{A}_{z\rho}$	z component of vector potential Green's function due to a $\widehat{\boldsymbol{\rho}}$-oriented dipole
$\tilde{G}^{A}_{z\phi}$	z component of vector potential Green's function due to a $\widehat{\boldsymbol{\phi}}$-oriented dipole
$\tilde{G}^{A}_{zz}$	z component of vector potential Green's function due to a $\widehat{\boldsymbol{z}}$-oriented dipole
$\tilde{G}^{\phi}_{\rho\rho}$	ρ component of scalar potential Green's function due to a $\widehat{\boldsymbol{\rho}}$-oriented dipole
$\tilde{G}^{\phi}_{\phi\phi}$	ϕ component of scalar potential Green's function due to a $\widehat{\boldsymbol{\phi}}$-oriented dipole
$\tilde{G}^{\phi}_{zz}$	z component of scalar potential Green's function due to a $\widehat{\boldsymbol{z}}$-oriented dipole

Abstract

Due to the advantages of microstrip antennas, such as their low weight, low cost, and flexibility, microstrip antennas mounted on layered structures have become very popular in various applications, ranging from satellite, vehicular communications and remote sensing to radiators in biomedical applications. Among these advantages, conformability is a very important feature for applications of microstrip antennas. After over two decades of research, the development of planar microstrip antennas has now reached maturity. However, the progress of research on conformal or nonplanar microstrip antennas lags far behind that for planar microstrip antennas. The conformal microstrip antennas are printed on nonplanar surfaces, such as cylindrical, spherical, and conical bodies. This thesis studies: (1) the propagation of electromagnetic waves in cylindrically stratified media and the electric field closed-form (fast computational form) Green's functions; (2) fast computation of mixed potential Green's functions and the corresponding mixed potential integral equation (MPIE) for cylindrically stratified media; (3) the application of MPIE in full wave analysis of microstrip structures, such as microstrip line, microstrip patch antenna and helical microstrip antenna mounted on cylindrically stratified media and (4) the creeping waves propagating along the dielectric coated perfect conducting cylinder. The principal activity is to find the fast computational form of dyadic Green's functions for cylindrically stratified media, which can act as the basis for further research.

In the study of closed-form Green's functions for cylindrically stratified media, a

method based on 2×2 matrix in field analysis is applied, where only the z components of field are used to represent the modes guided through layers. In order to get the closed-form electric field Green's functions, the discrete complex image method (DCIM) is applied with the help of the generalized pencil of function (GPOF) method. All the nine components of the dyadic Green's functions are explicitly derived and their closed-form expressions are obtained. The final results were all examined by a comparison to those obtained by a direct inverse Fourier transform, which shows that these results are reasonable and reliable. The study suggests that the spatial domain Green's functions can be represented by several complex images much akin to the planarly stratified media case.

In the study of mixed potential Green's functions and MPIE for cylindrically stratified media, scalar potential Green's functions and magnetic vector potential Green's functions are introduced by considering the relation between the potential Green's functions and the electric field Green's functions. To obtain the fast computational form of mixed potential Green's functions, recursive relations which correspond to two different derivation methods are first investigated thoroughly. Then a series acceleration technique, i.e., Kummer's transformation, is applied. Finally, with the help of DCIM, fast computational forms of mixed potential Green's functions are obtained.

In the study of the applications of MPIE for cylindrically stratified media, three different kinds of microstrip structures, i.e., microstrip line, microstrip rectangular patch antenna and helical microstrip antenna, are investigated. The MPIE is solved in the spatial domain with rooftop basis functions. For the fist two geometries, current distributions are calculated when the incident field is a plane wave. Then the resonant behaviours are obtained based on the current distributions. The results of a reduced case are compared with those of a commercial software and close agreement is found. For the helical microstrip antenna, far field radiation patterns are calculated based on the

current distributions when the antenna is center fed.

Finally, creeping waves guided along a perfectly conducting cylinder with a lossy magnetic coating are studied and characterized. The creeping waves are a kind of surface waves guided along the dielectric coated PEC cylinder, which relate to the poles of the Green's functions. The effect of the surface waves is implicitly contained in the spatial domain Green's functions; however, a varied form of Green's functions, i.e, a double integral spectral representation over a continuum of azimuthal and axial wave number, is employed to explicitly investigate the surface wave propagating along the cylindrically layered media

keywords: Dyadic Green's Functions, Discrete Complex Image Method, Electromagnetic Waves, Cylindrically Stratified Media

Chapter 1

Introduction

1.1 Layered Media

The properties of electromagnetic waves propagating in layered media have for a very long time been a major issue in widespread areas such as radio frequency design, microwave theory and techniques, and optical communications. Among various applications, microstrip antennas have attracted more and more attention because of their low profile, light weight and conformalbility. Microstrip antenna consists of a patch of metalization on a grounded substrate. These multilayered dielectric structures can be roughly divided into two classes according to their geometries: planarly multilayered media and nonplanar multilayered media such as cylindrically, spherically, and conically multilayered bodies.

The study on microstrip antennas mounted on a grounded substrate (Figs. 1.1-1.2) started at the beginning of 1970s [1, 2]. With the rapid development of material science and photolithographic techniques, extensive research and development of microstrip antennas and arrays, aimed at exploiting their numerous advantages such as low profile, light weight, conformal configuration and compatibility with integrate circuits, have been carried out. Much of this work has been well reviewed in [3–7]. Compared with the matured research work on planar microstrip antennas, the progress of research on

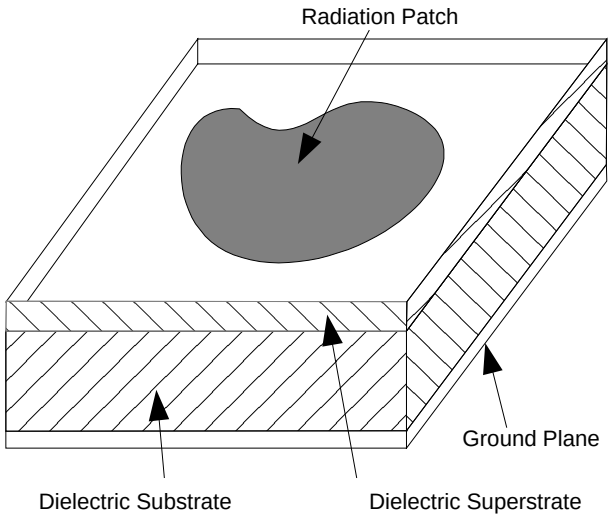

Figure 1.1: A microstrip patch mounted on planarly grounded substrate with a superstrate.

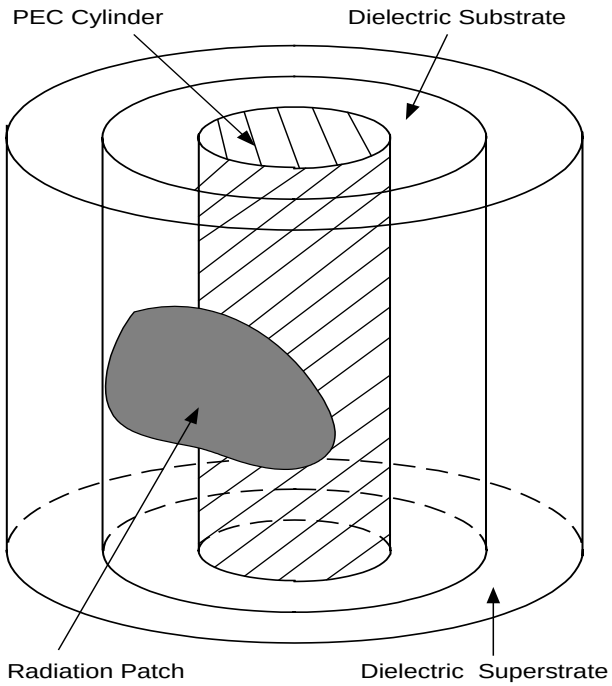

Figure 1.2: A microstrip patch mounted on a dielectric-coated circular cylinder with a superstrate.

conformal or nonplanar microstrip antennas lags far behind. The following subsections, 1.1.1 and 1.1.2, discuss these two classes of layered media and give reviews of the published research work on them separately. Next, the studies on the Green's functions for layered media are reviewed.

1.1.1 Plannarly Stratified Media

Generally speaking, all microstrip antennas can be thought of as conformal. The planar microstrip antennas are one special group of the conformal antennas. So it is worthwhile to summarize the main methods to analyze the planar microstrip antennas.

- Simple transmission line model [2,8,9] was firstly employed to analyze a rectangular microstrip antenna by Munson in 1974 [2]. In this method, the interior region of the patch antenna is modeled as a section of transmission line.

- The generalized transmission line model (GTLM) has been used to study rectangular patch [10], circular patch [11], annular and circular sector [12], and concentric array of circular rings [13]. The major difference between the transmission line model and GTLM is that a patch in GTLM is modeled in the form of transmission lines in orthogonal directions and thus include the variation of fields in the transverse direction.

- The cavity model proposed by Lo *et al* [14] has been applied to various shapes of patches [15–17]. The interior region of the patch is modeled ad a cavity which is bounded by electric wall on the top and bottom, and magnetic wall along the periphery. This model is based on the fact that microstrip antennas are narrow-band resonant antennas.

- Other variations of the cavity model include generalized cavity model [18] and multiport network model [4].

Although the implementation of aforementioned analytic methods are relatively simple compared with the full-wave techniques, they have some limitations. For example, they have limited capabilities to handle problems such as surface waves effects, mutual coupling, large array, and different substrate configurations. To overcome the limitations, full-wave techniques are proposed. The finite-difference time-domain (FDTD) approach [19] and the finite element method [20] are two powerful methods for conformal antanna analysis. The other two popular full-wave techniques are spectral domain full-wave analysis [21, 22] and spatial domain full-wave analysis or the mixed potential integral equation (MPIE) technique [23–25]. The methods are named according to the ways in which the integral equations are solved for the stratified media problems:

- The integral equations are solved in spectral domain. Green's functions are written in the spectral domain and there is no need of the inverse Fourier transform spectral domain Green's functions.

- The integral equations are solved in spatial domain. Before solving the integral equations, the inverse Fourier transform is applied to the spectral domain Green's functions, which result in the spatial domain Green's functions. When the integral equations take the mixed potential form, i.e., the scalar potential and vector potential, the technique is referred to as MPIE technique.

The MPIE technique is more computationally efficient than spectral domain analysis. The numerical efficiency of the MPIE is obtained due to the use of fast computational form or closed-form spatial domain Green's functions [26,27]. The MPIE has been used to analyze various types of planar microstrip antennas configurations [28–33]. The detailed discussions of closed-form Green's functions are presented in section 1.2.

1.1.2 Cylindrically Stratified Media

The methods for analyzing planar microstrip antennas can be applied to nonplanar microstrip antennas in principle. One of the most commonly used nonplanar stratified structures is the cylindrically stratified structure. Cylindrically stratified structures can be used as practical models in a wide variety of applications. The typical examples include microstrip and patch antennas and their arrays mounted on dielectric, or dielectric-coated conducting cylinders, as well as the microwave and millimeter-wave integrated circuit printed on cylindrical surface. Patch antennas or integrated circuits can be modeled as various shapes of conductors with zero thickness printed on the interface of different layers, conformal to cylindrical surface of certain radius. Similar to the methods employed for the analysis of planar microstrip antennas, the main techniques used for cylindrical microstrip antennas are the spectral domain full-wave approach, cavity model analysis and GTLM theory. The fact that the spatial domain full-wave analysis has not been fully developed for the analysis of nonplanar microstrip structures reminds us of some difficulties in this area, but also something worthwhile to be done. This will be discussed in section 1.2. The spectral domain full-wave approach used by [34–37] is described briefly here:

- An integral equation which governs the unknown patch surface current density is constructed by imposing the total electric field tangential to the patch surface to zero. The Green's functions involved in this equation is in the spectral domain.

- Expand the unknown surface current density on the patch in terms of linear combinations of basis or expansion functions in the spatial domain. A convenient choice of the basis function is the cavity model function. Find the Fourier transform of the spatial domain basis function and substitute the spectral domain basis function into the integral equation.

- Select the basis functions as test functions (Galerkin's moment method [38]) and transform the integral equation into a matrix equation. Solve this matrix equation for the unknown current density.

The choice of basis function is especially important for the spectral domain full-wave approach applied to the cylindrical microstrip antenna problem, since the numerical convergence depends strongly on the basis function chosen for the expansion of the patch surface current density. Secondly, the Fourier transform of the basis function should be easily obtained. Closed-form Fourier transform of the basis function will make the calculation of the element of the impedance matrix easy. The work on the microstrip structures on cylindrically layered media is well reviewed in [39].

Another issue related to the microstrip antennas mounted on the dielectric coated PEC cylinder is the surface waves supported by the dielectric coated PEC cylinder. The study of wave propagation along the surface of the coated cylinder is also a canonical problem for the analysis of conformal antenna arrays mounted on cylindrically layered media. Some researchers studied the creeping wave propagation constant and model impedance for a dielectric and lossy dielectric coated cylinder [40–42]. It is found that, similar to the planar configuration, no cutoff frequencies exist for the creeping waves associated with the coated cylinder. In fact, the coated cylinder can support an infinite number of surface wave modes. However, depending upon the thickness of coating, only a few Elliott type creeping wave modes with low attenuation can exist [41]. As a further extension, Nashadham and Felsen examined the dispersion of waves guided along cylindrical substrate-superstrate layered media [43]. He related the complex azimuthal propagation constant with the poles of the Green's functions and located the poles by solving the dispersion equation using Davidenko's method [44]. The dispersion curve showed that wave propagation for thin superstrate layer were anisotropic in (ϕ, z) space. In the visible spectrum, the surface wave poles were classified as leaky, creeping, or

trapped, depending on the magnitude of the ratio of azimuthal to radial wave number relative unity. In the invisible spectrum, the surface waves were evanescent along the ϕ and ρ directions. The work on the cylindrical microstrip structure and cylindrically multilayered media is summarized as follows:

- The problem of surface wave propagation along the dielectric coated cylinder is an important issue in designing the microstrip antennas. The surface wave behaviour for one-layer dielectric coated PEC cylinder [40–42] and two-layer dielectric coated PEC cylinder [43] have been studied.

- The resonant behaviour and radiation characteristic of a cylindrical rectangular patch antenna [45,46,35,37], triangular patch antenna [47,48], and wrapped around patch antenna [49, 35, 50] mounted on dielectric coated PEC cylinder have been studied.

- Conformal microstrip transmission line such as cylindrical microstrip lines [51,52], coupled cylindrical microstrip lines [53], cylindrical microstrip discontinuity [54], slot-coupled double-sided cylindrical microstrip lines [55], and cylindrical coplanar waveguides [56]have also been studied.

- Conformal microstrip arrays mounted on curved surfaces have received attention [2,57,58,36]. Most of the arrays are mounted on cylindrical bodies which can model the typical structure of a missile or aircraft.

1.2 Green's Functions for Layered Media

The spectral domain full-wave analysis and MPIE technique can be grouped into one category: integral equation technique. This technique makes an assumption that the substrate and ground plane are infinite in lateral dimension. The formulation of the solution is based on rigorously solving the boundary value problem. This is done by

using the exact Green's functions for the layered media. The Green's functions include the effects of dielectric loss, conductor loss, fringing effect, surface wave modes, and space wave radiation, if there is any. The Green's functions take different forms in the spectral domain full-wave analysis and MPIE technique. Normally, the electric field Green's functions are used in the former one and potential Green's functions are used in the latter one. The electric field integral equation (EFIE) for a perfect conductor is

$$\boldsymbol{E} = -\iint \overline{\boldsymbol{G}}_E(\boldsymbol{r}, \boldsymbol{r}') \cdot \boldsymbol{J}_s(\boldsymbol{r}') dS', \tag{1.1}$$

where $\boldsymbol{E}$ is the electric field due to the excitation current, $\overline{\boldsymbol{G}}_E(\boldsymbol{r}, \boldsymbol{r}')$ is dyadic electric field Green's functions, and $\boldsymbol{J}_s$ is the current density. The MPIE for a perfect conductor is

$$\boldsymbol{E} = j\omega \iint \overline{\boldsymbol{G}}_A(\boldsymbol{r}, \boldsymbol{r}') \cdot \boldsymbol{J}_s(\boldsymbol{r}') dS' + \nabla \iint G_\phi(\boldsymbol{r}, \boldsymbol{r}') q_s(\boldsymbol{r}') dS', \tag{1.2}$$

where $\overline{\boldsymbol{G}}_A(\boldsymbol{r}, \boldsymbol{r}')$ is the vector potential dyadic Green's functions, $G_\phi(\boldsymbol{r}, \boldsymbol{r}')$ is the scalar potential Green's functions, and q_s is the charge density. The $e^{-j\omega t}$ time dependence is suppressed throughout this thesis.

1.2.1 Green's Functions for Planarly Layered Media

The electric field Green's functions for planarly layered media can be easily obtained in spectral domain by using transmission line model, where the original problem is reduced to that of solving an equivalent transmission line network along the z coordinates [59–61]; and also can be found using the eigenfunction expansion technique [62–64]. When using the eigenfunction expansion technique, the method of scattering superstition is used: the Green's function is expressed into two parts, the unbounded Green's function and the scattering Green's function. The unbounded Green's function represents the contribution of the direct waves form radiation sources in an unbounded medium, and the scattering Green's function describes an additional contribution of the multiple reflection

and transmission waves from the cylindrical interfaces of the stratified media. The scattering Green's function is expressed in terms of cylindrical vector wave functions and scattered coefficients to be solved. The boundary conditions at each layer interface are then imposed to develop a matrix equation satisfied by the unknown coefficients. The resultant coefficients matrix equations are then solved in a recurring manner for the scattering coefficients. The general expression for the scattering Green's function, and hence the Green's functions for multilayered media are defined in a rather compact form. In the equivalent transmission line model, a uniform transmission line section corresponds to each layer of the media. Generally, two dual transmission line networks must be considered, one for the TE waves, and one for TM waves. The electric and magnetic fields anywhere in the layered media are firstly expressed in terms of the transmission line Green's functions, and then in terms of vector potential and scalar potential Green's functions. Finally, the potential Green's functions can be postulated in different forms [65]. Due to the non-uniqueness of the potentials, three formulations of the mixed potential Green's functions for PEC objects of arbitrary shape in a layered medium were derived, where the vector potential dyadic kernel is modified so that only one scalar potential kernel is needed. These formulations are amenable to increasing the capability of the well-established triangular patch MoM procedure, initially developed by Rao *et al.* [66] for arbitrary shaped geometries in free space. An advantage of the MPIE formulation is that vector and scalar potential are employed, and they are expressed, respectively, in terms of the current and charge densities. MPIE is in fact the same as EFIE. The only difference is the transfer of a "∇" operator. This result in less singular kernels and more rapidly convergent spectral integrals in the evaluation of Green's functions components.

It is well known that in planarly layered media, the scalar potential, which is related to the vector potential via Lorenze gauge, cannot be described with a single scalar kernel. This is due to fact that the scalar potentials of a single point charge associated with a

horizontal and vertical dipole in mutilayered media are, in general, not identical. In other words, the scalar potential depends not only on the value, but also the flow direction of the charge. A static point charge, on the other hand, produces a unique potential. In Michalski's method [65], the authors keep the scalar potential Green's function in its simple scalar form while introduce some new entries into the vector potential Green's functions. By appropriately choosing the forms of potential Green's functions, the scalar potential Green's function can be continuous at the interface of multilayered media. Some researchers [67] developed a different MPIE from that of Michalski *et al.*. They expressed the scalar potential in dyadic form, while keeping the dyadic kernel of the vector potential in its simple form originally developed by Sommerfeld [68]. An extra line integral term, which is well behaved and nonsingular, will appear when the PEC object penetrates an interface.

The scalar and vector potential Green's functions obtained so far are represented by Sommerfeld Integration (SI) or the inverse Fourier transform of their spectral domain counterparts, like

$$\overline{\boldsymbol{G}}(\rho) = \frac{1}{4\pi}\int_{-\infty}^{\infty} \widetilde{\overline{\boldsymbol{G}}}(k_\rho) H_0^{(1)}(k_\rho\rho) k_\rho dk_\rho, \tag{1.3}$$

where $\overline{\boldsymbol{G}}(\rho)$ and $\widetilde{\overline{\boldsymbol{G}}}(k_\rho)$ are the Green's functions in the spatial and spectral domains, repectively, and $H_0^{(1)}(\bullet)$ is the zeroth-order Hankel function of the first kind. The integration route is called the Sommerfeld integration path (SIP). The Sommerfeld integration is very time-consuming because of the slowly decaying behaviour of the integrand. To overcome the difficulty, discrete complex image method (DCIM) was used [26]. In this technique, the spectral domain Green's functions are approximated by the sum of series of exponentials using the generalized pencil of function (GPOF) method [69, 70], then the integration in Eq. (1.3) can be evaluated analytically using the Sommerfeld identity [62]. This fast computational form of Green's functions are also referred to as closed-form Green's functions. The work on the closed-form Green's

functions for planarly layered media can be found in [27, 71–75].

1.2.2 Green's Functions for Cylindrically Layered Media

The Green's functions for cylindrically layered media are necessary for the full-wave analysis of microstrip antennas and circuits mounted on cylindrically multilayered structure. Unlike those in planarly and spherically layered media, TE and TM waves are coupled together at the interface of the cylindrically layered media. This requires simultaneous solution of the fields corresponding to TM and TE cases, the only exceptions being the rotationally symmetric ($n = 0$) and z-invariant ($k_z = 0$) cases for which separate analysis of TE and TM modes are possible. The coupled-mode analysis requires for cylindrical structures results in reflection and transmission matrices rather than reflection and transmission coefficients.

The electromagnetic wave propagation from cylindrical structures was studied first intensively by Wait [76]. Later on, the electric field Green's functions for cylindrically layered media in spectral domain have appeared in [62, 77–80]. Some of them used 4×4 matrix [77–79], others used 2×2 matrix in field analysis [62, 80]. In this thesis, 2×2 and 4×4 matrices method are both used to derive the Green's functions. In Chapters 4 and 5, electric field Green's functions using the above two different methods are given respectively, and numerical results demonstrate their equality.

The electric field Green's functions obtained using above two methods are in the form:

$$\overline{\boldsymbol{G}}(z, z'; \phi, \phi') = \sum_{n=-\infty}^{\infty} e^{jn(\phi-\phi')} \int_{-\infty}^{\infty} \widetilde{\overline{\boldsymbol{G}}}(k_z, n) e^{jk_z(z-z')} dk_z, \tag{1.4}$$

where k_z is the wave number in z direction and n represents the wave number in ϕ direction. $\widetilde{\overline{\boldsymbol{G}}}(k_z, n)$ is the spectral domain Green's functions, which can also be referred to as *cylindrical eigenmodes* later on. To perform the inverse Fourier transform, one must sum all the cylindrical eigenmodes from minus infinity to positive infinity. Besides, Sommerfeld integration in k_z complex plane is needed. Compared with Eq. (1.3), the

inverse Fourier transform seems not as straightforward as in the planarly stratified media case.

One type of closed-form Green's functions for cylindrically stratified media was first reported in [81], where a two-step DCIM technique [82] was used for obtaining the spatial domain Green's functions in closed-form due to $\widehat{\boldsymbol{z}}-$and $\widehat{\boldsymbol{\phi}}-$ oriented electrical and magnetic sources in cylindrically layered media. Firstly, due to the singularities encountered along the original path of integration [83], a new path is obtained by the deformation of the original SIP. The deformed path is divided into three contours. In the third contours, the Green's functions are sampled uniformly and approximated in terms of complex exponentials by the GPOF method. These functions are then represented by the zeroth-order Hankel functions using large argument approximation before being transformed into the spatial domain via the Sommerfeld identity. Secondly, the prior spectral domain Green's functions approximated are subtracted from the original Green's functions to yield the Green's functions vanishing beyond the second portion. These Green's functions are then sampled uniformly along the first two contours and approximated in terms of complex exponentials by the GPOF method. The approximate Green's functions in the spatial domain are then obtained from simple contour integrals of exponential functions. Finally, addition of the contributions of each region gives the spatial domain Green's functions in closed-form. Careful study shows that the source point and field point are located far away in $\widehat{\boldsymbol{\rho}}$ direction in above closed-form Green's functions. If the source point and field point lie in the same cylindrical surface, the Green's functions represent the surface fields. The series formed by the cylindrical eigenmodes is slowly convergent or even divergent. This problem was studied in [84, 85] using Watson transform [86], where the infinite summation over order n was transformed to an integration along the steep decent path on a complex plane.

The derivation of mixed potential Green's functions for cylindrically layered media,

however, turns out to be a nontrivial thing compared with that for the planarly layered media case. The difficulty lies in the fact that TM and TE waves are coupled together in the cylindrically layered media. No explicit transmission line equations can be formulated for separated TM and TE waves, as that in the planarly stratified media case. Instead, the Green's functions for the electrical field is much more complicated by introducing the reflection and transmission matrices, rather than the reflection and transmission coefficients for planarly stratified media case. Though it is difficult to derive, the MPIE formulation does exist according to Maxwell's theory, which states that the field can be determined solely by its vector potential and scalar potential, although the choices of vector potential and scalar potential are not unique. Hall [87] presented one way to construct the mixed potential Green's functions for one-layer dielectric coated PEC cylinder. He started from the electric field Green's functions first, and subtracted the gradient part of electric field Green's functions, assuming the gradient part was corresponding to the scalar potential by introducing a dyadic scalar potential Green's function; and the remaining part was the vector potential, which is less singular because the gradient part had been subtracted. In this manner, the gradient operator on the scalar potential Green's function can be transferred to the source current, which can furthermore reduce the singularity of the integral equation.

Numerical evaluation of the spatial domain mixed potential Green's functions must be carefully conducted. It contains an infinite summation over n and an infinite integral over k_z. A cut off of infinite summation of the series and a convergence criteria must be made. Secondly, calculation of the special functions, i.e., Bessel function and Hankel function will be difficult due to the highly unstable behaviours for large order and large argument. Finally, numerical overflow and underflow will occur if Bessel function and Hankel function are evaluated independently. Nakatani provided a method to calculate large order cylindrical eignmodes [79]. He rearranged the spectral domain Green's functions and expressed them in terms of certain ratios of special functions. These

ratios of special functions can be accurately evaluated using recursive relations of the special functions. However, these type of ratios are not adequate enough for the Green's functions for the case of more than one-layer dielectric coated cylinder.

1.3 Motivation and Objectives

With the rapid applications of conformal microstrip antennas, fast and accurate analysis of such structures is necessary. Of the various theoretical techniques, the full-wave analysis is the most accurate, yet less efficient in the computing sense, since most full-wave analysis of conformal microstrip antennas are confined to applying the method of moment (MoM) in spectral domain. This technique is only applicable to the case in which the Fourier transforms of the basis function are easily obtained. Moreover, it cannot be readily applied to the arbitrary shape conformal antennas, since the basis function is not easy to choose. The convergence problem of the spectral domain full-wave analysis is also crucial, since it is sensitive to the basis functions. Therefore, the spatial domain full-wave analysis has received more and more attention for the last decades. The closed-form Green's functions are important to the spatial domain full-wave analysis. Much research work has been done for the planarly stratified media, but much remains undeveloped for the cylindrically stratified media.

In this thesis, the spectral domain Green's functions for cylindrically stratified media both in electric form and mixed potential form are derived. The spatial domain mixed potential Green's functions, and the complete set of spatial domain electric field Green's functions for multilayer coated PEC cylinder are developed for the first time. Compared with the problems of one-layer coated PEC cylinder, the problems involving multilayer coated PEC cylinder are astonishingly complicated. Using these spatial domain Green's functions, mixed potential integral equation can be used to analyze cylindrically conformal microstrip antennas and circuits. The work could provide an new

approach for solving more complex problems, such as irregular shaped patch and large scale problems.

1.4 Development of the Thesis

This thesis is divided into nine chapters.

Chapter 1 gives a brief introduction on the problem of layered media. A review of the work on planarly and cylindrically microatrip antennas and circuits is presented and different approaches used are summarized. Green's functions method, which is essential to the full-wave technique, is highlighted. The work on closed-form Green's functions for planarly and cylindrically layered media is also reviewed.

Chapter 2 summarizes the methods employed in this thesis. The dyadic Green's function technique, DCIM and series acceleration techniques are used in the following chapters to obtain the fast computational form of spatial domain Green's functions.

Chapter 3 presents the formulation of the Green's functions in their eigenfunction expansion forms for cylindrically stratified media where both the source and field points are arbitrarily located. The 2×2 matrix method is used. A correction of the formulation is made for the typo in [62]. The correctness is proved by numerical results in Chapter 5, in which the Green's functions are derived using 4×4 matrix method.

The complete set of fast computational form of electric field Green's functions is presented in Chapter 4. The Green's functions considered here have the source and field points located on different cylindrical surface. This condition makes the cylindrical eigenmodes a fast convergent series. Two-step approximation process by using the GPOF method is used perform the inverse Fourier transform.

The evaluations of large order cylindrical eigenmodes are discussed in Chapter 5. The recursive relations of ratios of special functions and their certain combinations are

investigated first, followed by the rearrangement of Green's functions in 2×2 and 4×4 forms. Numerical results between the *Mathematica* and our method confirm the validity of the *Fortran* program we have developed.

Chapter 6 presents the the formulation of mixed potential Green's functions in spectral domain and in spatial domain. Numerical evaluation of spatial domain mixed potential Green's functions is highlighted.

Applications of the mixed potential Green's functions are presented in Chapter 7. The resonant behaviour of a microstrip line and a rectangular patch antenna mounted on dielectric coated PEC cylinder are studied using MPIE. The effect of the superstrate on the resonance frequency is investigated. As another application, the radiation patterns of a helical antenna mounted on dielectric coated PEC cylinder is calculated. Rigorous current distributions are obtained by solving the MPIE.

Surface wave propagation along dielectric coated PEC cylinder is discussed in Chapter 8, since it is also an important issue in designing microstrip antennas. A magnetic lossy material is considered there and some new phenomena are found.

In Chapter 9, concluding remarks on the present work are made, and future work are proposed.

1.5 Original Contributions

Closed-form Green's functions in the spatial domain for multilayered media have for a long time been hot research topics in electromagnetics and microwave fields. They are useful in the full-wave analysis of microstrip antennas or circuits. The investigation of spatial domain closed-form Green's functions and MPIE for planarly layered structure has reached its maturity for the last ten years [7], but much is to be investigated for the spatial domain closed-form Green's functions for cylindrically layered media. More

precisely, for cylindrically layered media, the closed-form should be referred to as fast computational form. It is because the so-called closed-form Green's functions are not completely analytical and it still requires numerical evaluation to obtain the final solution.

A complete set of closed-form electric field Green's functions are developed in this thesis. This is a further development of the work in [81], where only $\hat{\boldsymbol{z}}-$ and $\hat{\boldsymbol{\phi}}-$ oriented electrical or magnetic sources are considered. Two different methods are presented for deriving the Green's functions and some errors in literature [62] are identified and the corrections are made. In order to obtain the mixed potential Green's functions in the spatial domain, large order cylindrical eigenmodes are to be evaluated. The spectral domain Green's functions are rearranged for two cases, which are the 2×2 and 4×4 matrix method. Some new recursive relations are presented for the first time to enable the Green's functions to be calculated in recursive algorithm.

The mixed potential Green's functions are derived for general cylindrically mutilayered media in this study. In literature [87], one form of mixed potential Green's functions for one-layer coated PEC cylinder was given in a very simple way, with many details either left out or in a haphazard manner. In this thesis, the formulation of mixed potential Green's functions for cylindrically mutilayered media are derived systematically and completely. The evaluation of the mixed potential Green's functions in spatial domain is also studied in detail. Series acceleration technique and DCIM are used to perform the inverse Fourier transform of the spectral domain Green's functions. Using the spatial domain Green's functions obtained, MPIE is, for the first time, applied to analyze a helical antenna, a patch antenna and a microstrip line as examples, with substrate and superstrate in all cases. Finally, the surface wave supported by the multilayered cylinder, which is also an important issue in designing the microstrip antennas on multilayered cylinder, is considered. Some new phenomena are revealed for the coated material which has magnetic loss.

1.6 Publications

During the present research, a portion of the results obtained has been published in or accepted by international refereed journals and some conference papers presented as well.

1.6.1 Journal Papers

1. Jin Sun, Chao-Fu Wang, Le-Wei Li, and Mook-Seng Leong, "A complete set of spatial domain dyadic Green's function components for cylindrically stratified media in fast computational form", *Journal of Electromagnetic Waves and Applications*, vol. 16, no. 11, pp. 1491-1509, November, 2002.

2. Jin Sun, Chao-Fu Wang, Le-Wei Li, and Mook-Seng Leong, "Mixed Potential Spatial Domain Green's Functions in Fast Computational Form for Cylindrically Stratified Media", *Journal of Electromagnetic Waves and Applications*, vol. 18, no. 2, February 2004. The full content is accepted by, and appears in, Progress In Electromagnetics Research, vol. 45, pp. 181-199, 2004, EMW Publishing: Boston, Massachusetts.

3. Jin Sun, Chao-Fu Wang, Le-Wei Li, and Mook-Seng Leong, "Creeping Waves along a Perfectly Conducting Cylinder with a Lossy Magnetic Coating", *IEEE Antennas and Wireless Propagation Letters*, vol. 2, pp. 298-301, December 2003.

4. Jin Sun, Chao-Fu Wang, Le-Wei Li, and Mook-Seng Leong, "Characterizing Helical Microstrip Antenna Mounted on a Dielectric-Coated Circular Cylinder Using MoM and Closed Form Green's Function", *IEEE Antennas and Wireless Propagation Letters*, vol. 3, February, 2004.

5. Jin Sun, Chao-Fu Wang, Le-Wei Li, and Mook-Seng Leong, "Further improvement for fast computation of mixed potential Green's function for cylindrically stratified media", *IEEE Trans. Antennas Propagat.*, vol. 54, no. 10, October, 2004.

1.6.2 Conference Papers

1. Jin Sun, Chao-Fu Wang, Le-Wei Li, Mook-Seng Leong, "Closed form Green's functions for ρ-oriented electrical source in cylindrically stratified media', in*Proc. 2002 IEEE AP-S International Symposium And USNC/URSI National Radio Science Meeting*, San Antonio, Texas, USA, June 16-21, 2002, pp. 804-807

2. Jin Sun, Chao-Fu Wang, Le-Wei Li, and Mook Seng Leong, "Curve fitting in fast computation of mixed potential Green's functions for cylindrically stratified media", in *Proc. 2003 Progress In lectromagnetics Research (PIERS'03)*, Pan Pacific, Singapore, Jan. 7-10, 2003, p. 19.

3. Jin Sun, Chao-Fu Wang, Le-Wei Li, and Mook-Seng Leong, "Application of Kummer's transformation in fast computation of mixed potential Green's function for cylindrically stratified structure", in *Proc. 2003 IEEE AP-S International Symposium And USNC/URSI National Radio Science Meeting*, Columbus, Ohio, USA, June 23-27, 2003, vol. 4, pp. 954-957.

4. Jin Sun, Chao-Fu Wang, Le-Wei Li, and Mook-Seng Leong, "Radiation patterns of helical microstrip antenna mounted on multilayered dielectric coated PEC cylinder", accepted by *Proc. 2004 IEEE AP-S International Symposium And USNC/URSI National Radio Science Meeting*, Monteret, Califorlia USA, June 20-26, 2004.

5. Jin Sun, Er-Ping Li, Le-Wei Li, and Mook-Seng Leong, "Application of mixed potential integral equation for cylindrically stratified structure", accepted by *Proc. 2004 IEEE AP-S International Symposium And USNC/URSI National Radio Science Meeting*, Monteret, Califorlia USA, June 20-26, 2004.

6. Jin Sun, Er-Ping Li, Le-Wei Li, and Mook-Seng Leong, "Recursive Relations in Accurate Computation of Green's Function for Cylindrical Stratified Media",

accepted by *Proc. 2004 IEEE AP-S International Symposium And USNC/URSI National Radio Science Meeting*, Monteret, Califorlia USA, June 20-26, 2004.

Chapter 2

Methodologies

2.1 Dyadic Green's Functions Technique

Among various approaches available to electromagnetic problems involving layered media, the dyadic Green's functions [63] play a fairly important role, especially in those boundary value problems. The dyadic Green's functions technique was developed from scalar Green's functions technique by introducing dyadic algebra. A Green's function represents the fields due to a point source. Fields for arbitrary sources in linear media can be obtained by integrating the Green's functions with respect to the source distribution. On the other hand, dyadics provide a compact form to express different properties such as boundary or interface conditions, medium equations, solutions of Green's functions, and transformations between field problems. The resultant method that combines the Green's functions and dyadic algebra is referred to as dyadic Green's functions technique. Dyadic Green's functions sometimes are also referred to as Green's functions later on in this thesis, as they always appear in dyadic form by default. The Green's functions technique is a powerful tool and provides physical insight into the relationships between the behavior of electromagnetic waves and material parameters, having already been widely applied in the boundary value problems of complex media [62, 86, 88].

2.1.1 Dyadics

Dyadic function (or *dyadic* for short) is a product of two vectors. This product is neither dot (scalar) product nor cross (vector) product, and instead is a bi-vector. In a general orthogonal coordinates system whose coordinate variables are denoted by (e_1, e_2, e_3) and the corresponding unit vectors are denoted by ($\widehat{\boldsymbol{e}}_1$, $\widehat{\boldsymbol{e}}_2$, $\widehat{\boldsymbol{e}}_3$), the arbitrary two vectors can be expressed by

$$\boldsymbol{V} = \sum_{i=1}^{3} V_i \widehat{\boldsymbol{e}}_i, \tag{2.1a}$$

$$\boldsymbol{V}' = \sum_{j=1}^{3} V_j' \widehat{\boldsymbol{e}}_j. \tag{2.1b}$$

The definition of the *dyadic product* is

$$\begin{aligned} \overline{\boldsymbol{F}} &= \boldsymbol{V}\boldsymbol{V}' \\ &= \Big(\sum_i V_i \widehat{\boldsymbol{e}}_i\Big)\Big(\sum_j V_j' \widehat{\boldsymbol{e}}_j\Big) \\ &= \sum_i \sum_j V_i V_j' \widehat{\boldsymbol{e}}_i \widehat{\boldsymbol{e}}_j, \end{aligned} \tag{2.2}$$

where the juxtaposed unit vectors, $\widehat{\boldsymbol{e}}_i\widehat{\boldsymbol{e}}_j$, are designated as *dyads*. Summarized from Eqn. (2.2), a dyadic can always be expressed by

$$\overline{\boldsymbol{F}} = \sum_i \sum_j F_{ij} \widehat{\boldsymbol{e}}_i \widehat{\boldsymbol{e}}_j. \tag{2.3}$$

The properties of the dyadic $\overline{\boldsymbol{F}}$ and some of its mathematical operations used in this thesis are given briefly below. Detailed description of dyadic and its operations can be found in [63, 88–90].

2.1.2 Properties of Dyadics

- The dyads $\widehat{\boldsymbol{e}}_i\widehat{\boldsymbol{e}}_j$ are not commutative, i.e.,

$$\widehat{\boldsymbol{e}}_i\widehat{\boldsymbol{e}}_j \neq \widehat{\boldsymbol{e}}_j\widehat{\boldsymbol{e}}_i, \tag{2.4}$$

  when $i \neq j$.

- The transpose of a dyadic $\overline{\boldsymbol{F}}$ is defined by

$$\begin{aligned}\overline{\boldsymbol{F}}^T &= \Big(\sum_i \sum_j F_{ij}\widehat{\boldsymbol{e}}_i\widehat{\boldsymbol{e}}_j\Big)^T \\ &= \sum_i \sum_j F_{ji}\widehat{\boldsymbol{e}}_i\widehat{\boldsymbol{e}}_j. \end{aligned} \tag{2.5}$$

  When $F_{ij} = F_{ji}$, $\overline{\boldsymbol{F}}$ is a symmetric dyadic.

2.1.3 Basic Operations

- Anterior products:

$$\begin{aligned}\boldsymbol{u}\cdot\overline{\boldsymbol{F}} &= \boldsymbol{u}\cdot\boldsymbol{V}\boldsymbol{V}' \\ &= (\boldsymbol{u}\cdot\boldsymbol{V})\boldsymbol{V}'; \end{aligned} \tag{2.6}$$

$$\begin{aligned}\boldsymbol{u}\times\overline{\boldsymbol{F}} &= \boldsymbol{u}\times\boldsymbol{V}\boldsymbol{V}' \\ &= (\boldsymbol{u}\times\boldsymbol{V})\boldsymbol{V}'. \end{aligned} \tag{2.7}$$

- Posterior products:

$$\begin{aligned}\overline{\boldsymbol{F}}\cdot\boldsymbol{u} &= \boldsymbol{V}\boldsymbol{V}'\cdot\boldsymbol{u} \\ &= \boldsymbol{V}(\boldsymbol{V}'\cdot\boldsymbol{u}); \end{aligned} \tag{2.8}$$

$$\begin{aligned}\overline{\boldsymbol{F}}\times\boldsymbol{u} &= \boldsymbol{V}\boldsymbol{V}'\times\boldsymbol{u} \\ &= \boldsymbol{V}(\boldsymbol{V}'\times\boldsymbol{u}). \end{aligned} \tag{2.9}$$

2.1.4 Electromagnetic Fields in Terms of Dyadic Green's Functions

The electric and magnetic fields can be related to the source directly through

$$\boldsymbol{E}(\boldsymbol{r}) = \iiint \overline{\boldsymbol{G}}_e(\boldsymbol{r},\boldsymbol{r}')\cdot\boldsymbol{J}(\boldsymbol{r}')dV', \tag{2.10a}$$

$$\boldsymbol{H}(\boldsymbol{r}) = \iiint \overline{\boldsymbol{G}}_m(\boldsymbol{r},\boldsymbol{r}')\cdot\boldsymbol{J}(\boldsymbol{r}')dV', \tag{2.10b}$$

where $\overline{\boldsymbol{G}}_e(\boldsymbol{r},\boldsymbol{r}')$ is the dyadic Green's function of electric type and $\overline{\boldsymbol{G}}_m(\boldsymbol{r},\boldsymbol{r}')$ is the dyadic Green's function of magnetic type. They are both associated with the arbitrary electric

source $\boldsymbol{J}(\boldsymbol{r}')$. The vectors $\boldsymbol{r}$ and $\boldsymbol{r}'$ represent the field point and the source point, respectively. Once the dyadic Green's functions are known, the electric and magnetic fields can be readily calculated.

The dyadic Green's functions can be solved and represented either in spatial domain or in spectral domain. With the help of the vector wave functions in different coordinates systems, the dyadic Green's function for various structures can be expressed in spectral domain in terms of eigenfunction expansion.

2.2 DCIM and GPOF Methods

The GPOF method [70] finds poles by solving a generalized eigenvalue problem. In order to optimize the performance of the GPOF method, subspace decomposition is used. The new method developed is more efficient than the conventional Prony and pencil of function methods, which yield the solution in two steps, namely, the solution of an ill-conditioned matrix equation and finding the roots of a polynomial. Compared to the least square or total least square Prony method, the GPOF method was shown to be more robust to noise [69].

In the GPOF method, the EM transient signal is described by the following expression:

$$y_k = \sum_{i=1,M} b_i e^{(s_i \delta t k)}, \tag{2.11}$$

where $k = 0,\ 1\ ,...\ N-1$, b_i are the complex residues, s_i are the complex poles, and δt is the sampling interval.

Two matrices, $\overline{\boldsymbol{Y}}_1$ and $\overline{\boldsymbol{Y}}_2$ are defined in terms of a set of information vectors as

$$\overline{\boldsymbol{Y}}_1 = [\boldsymbol{y}_0, \boldsymbol{y}_1, \cdots, \boldsymbol{y}_{L-1}], \tag{2.12}$$

$$\overline{\boldsymbol{Y}}_2 = [\boldsymbol{y}_1, \boldsymbol{y}_2, \cdots, \boldsymbol{y}_L], \tag{2.13}$$

where

$$\boldsymbol{y}_i = [y_i, y_{i+1}, \cdots, y_{i+N-L-1}]^T. \tag{2.14}$$

By using singular value decomposition (SVD), $\overline{\boldsymbol{Y}}_1$ can be further broken down into

$$\overline{\boldsymbol{Y}}_1 = \overline{\boldsymbol{U}}\,\overline{\boldsymbol{D}}\,\overline{\boldsymbol{V}}^H, \tag{2.15}$$

where superscript H denotes the conjugate transpose of a matrix, and $\overline{\boldsymbol{U}}$ and $\overline{\boldsymbol{V}}$ are the matrices of left and right singular vector respectively. Here, $\overline{\boldsymbol{D}}$ is a diagonal matrix and subsequently only M of the most significant singular values are selected, so that depending on the number of singular values chosen, the $\overline{\boldsymbol{U}}$ and $\overline{\boldsymbol{V}}$ matrices are also truncated correspondingly as $\overline{\boldsymbol{U}} = [\boldsymbol{U}_1, \cdots, \boldsymbol{U}_M]$ and $\overline{\boldsymbol{V}} = [\boldsymbol{V}_1, \cdots, \boldsymbol{V}_M]$, respectively.

By computing the eigenvalues of $\overline{\boldsymbol{Z}}$,

$$\overline{\boldsymbol{Z}} = \overline{\boldsymbol{D}}^{-1}\overline{\boldsymbol{U}}^H\overline{\boldsymbol{Y}}_2\overline{\boldsymbol{V}}, \tag{2.16}$$

poles $z_i = e^{(s_i\delta t)}$, $i = 1, \cdots, M$ in the Z-plane can be obtained.

At the same time, $\overline{\boldsymbol{Y}}_1$ and $\overline{\boldsymbol{Y}}_2$ may be express as

$$\overline{\boldsymbol{Y}}_1 = \overline{\boldsymbol{Z}}_1\overline{\boldsymbol{B}}\overline{\boldsymbol{Z}}_2, \tag{2.17}$$

and

$$\overline{\boldsymbol{Y}}_2 = \overline{\boldsymbol{Z}}_1\overline{\boldsymbol{B}}\overline{\boldsymbol{Z}}_0\overline{\boldsymbol{Z}}_2, \tag{2.18}$$

where, $\overline{\boldsymbol{Z}}_1$ and $\overline{\boldsymbol{Z}}_2$ are both matrices composed of the poles z_i in the z-plane:

$$\overline{\boldsymbol{Z}}_1 = \begin{bmatrix} 1 & 1 & 1 & 1 \\ z_1 & z_2 & \cdots & z_M \\ . & . & \cdots & . \\ z_1^{N-L-1} & z_2^{N-L-1} & \cdots & z_M^{N-L-1} \end{bmatrix}, \tag{2.19}$$

$$\overline{\boldsymbol{Z}}_2 = \begin{bmatrix} 1 & z_1 & \cdots & z_1^{L-1} \\ 1 & z_2 & \cdots & z_2^{L-1} \\ . & . & \cdots & . \\ 1 & z_M & \cdots & z_M^{L-1} \end{bmatrix}, \tag{2.20}$$

$$\overline{\boldsymbol{Z}}_0 = diag[z_1, z_2, z_3, \cdots, z_M], \tag{2.21}$$

where the optimal choice of L is around $N/2$. In addition, $\overline{\boldsymbol{B}} = diag[b_1, b_2, \cdots, b_M]$ is a diagonal matrix of the complex residues. Hence with $\overline{\boldsymbol{Z}}_1$ and $\overline{\boldsymbol{Z}}_2$ known, the $\overline{\boldsymbol{B}}$ matrix, i.e., the complex residues can be obtained.

The DCIM is implemented with the help of GPOF method. The general procedure is:

- Divide the Sommerfeld integration path into three contours, which are named near, middle and far contours. In the far contour, the spectral domain Green's functions are approximated in terms of complex exponentials by the GPOF method. Transform the approximating Green's functions into the spatial domain via the Sommerfeld identity.

- The prior spectral domain Green's functions approximated are subtracted from the original Green's functions to yield the Green's functions vanishing beyond the middle contour. These Green's functions are again approximated in terms of complex exponentials by the GPOF method. Integrate these approximating Green's functions on the near and middle contours.

- Finally, addition of the contributions of each contours gives the spatial domain Green's functions in closed-form.

2.3 Methods Applied in Cylindrically Layered Media Problems

The Green's functions for cylindrically layered media are derived using two methods, but they are equivalent in physical meaning. The first method starts from the the vector wave functions M, N and L. The free space Green's functions are then expressed in terms of these vector wave functions. Then a local reflection and transmission matrices of an outgoing and standing wave for a single cylindrical interface is defined. General reflection and transmission matrices for a cylindrically multilayered media are developed by making use of the local reflection and transmission matrices. The Green's functions due to an arbitrary source in a cylindrically multilayered media are then derived by expanding the field due to the source in terms of cylindrical wave functions and expressed in terms of the generalized reflection and transmission matrices. This method can be referred to as 2×2 matrix method, since transmission and reflection matrices are in 2×2 matrix form. In the second method, the cylindrically multilayered medium is modeled as a transmission line. This transmission line is different from that of the planarly multilayered media, where TE and TM wave are decoupled. A field transfer equation is developed where a 4×4 transfer matrix relates the fields on two successive cylindrical surfaces. Green's functions are then obtained by imposing boundary conditions on the transfer equation. The following two subsections give more details on these two methods.

2.3.1 Cylindrical Vector Wave Functions

In the cylindrical coordinates system (ρ, ϕ,z), the scalar potential function is

$$\psi_{mk_\rho}(k_z) = J_m(k_\rho \rho) e^{jm\phi} e^{ik_z z}, \tag{2.22}$$

where $J_m(k_\rho \rho)$ denotes the m-th order Bessel function of the first kind, $k = \sqrt{k_\rho^2 + k_z^2}$, and k_ρ and k_z are the wavenumbers in transverse and propagating directions, respectively.

The cylindrical vector wave functions can be generated from the scalar potential function similarly. The solenoidal vector wave functions are given by

$$\begin{aligned}
\boldsymbol{M}_{mk_\rho}(k_z) &= \nabla \times \left[\psi_{mk_\rho}(k_z)\widehat{\boldsymbol{z}}\right] \\
&= \left[jm\frac{J_m(k_\rho\rho)}{\rho}\widehat{\boldsymbol{\rho}} - \frac{\partial J_m(k_\rho\rho)}{\partial\rho}\widehat{\boldsymbol{\phi}}\right]e^{j(m\phi+k_z z)}, \qquad (2.23a) \\
\boldsymbol{N}_{mk_\rho}(k_z) &= \frac{1}{k}\nabla\times\nabla\times\left[\psi_{mk_\rho}(k_z)\widehat{\boldsymbol{z}}\right] \\
&= \frac{1}{k}\left[jk_z\frac{\partial J_m(k_\rho\rho)}{\partial\rho}\widehat{\boldsymbol{\rho}} - mk_z\frac{J_m(k_\rho\rho)}{\rho}\widehat{\boldsymbol{\phi}}\right. \\
&\quad \left.+k_\rho^2 J_m(k_\rho\rho)\widehat{\boldsymbol{z}}\right]e^{j(m\phi+k_z z)}, \qquad (2.23b)
\end{aligned}$$

and the irrotational vector wave function is

$$\begin{aligned}
\boldsymbol{L}_{mk_\rho}(k_z) &= \nabla\psi_{mk_\rho}(k_z) \\
&= \left[\frac{\partial J_m(k_\rho\rho)}{\partial\rho}\widehat{\boldsymbol{\rho}} + jm\frac{J_m(k_\rho\rho)}{\rho}\widehat{\boldsymbol{\phi}}\right. \\
&\quad \left.+jk_z J_m(k_\rho\rho)\widehat{\boldsymbol{z}}\right]e^{j(m\phi+k_z z)}. \qquad (2.23c)
\end{aligned}$$

From these vector wave functions, the derivation of the Green's functions can be summarized into the following steps [62]:

- The fields $[E_z, H_z]^T$ are expressed in terms of scalar potential function ψ. The transmission and reflection of $[E_z, H_z]^T$ in cylindrically layered media are studied first. General transmission and reflection matrices are introduced to characterize the wave propagation.

- Express free space Green's functions in terms of the vector wave functions in (2.23). Eliminate vector wave function $\boldsymbol{L}$ by using the singularity extraction and principal value integral techniques.

- Express the Green's functions, which contain only vector wave functions $\boldsymbol{M}$ and $\boldsymbol{N}$, in terms of scalar potential function ψ, a quantity that is proportional to $[E_z, H_z]^T$ is factored out.

- The quantity proportional to $[E_z, H_z]^T$ will transmit and reflect like $[E_z, H_z]^T$, which has been studied in the first step. Hence the Green's functions for cylindrically layered media are obtained through the generalization of the free space Green's functions.

2.3.2 Transfer Matrix $\overline{\boldsymbol{T}}$

The $\overline{\boldsymbol{T}}$ transfer matrix method used in this thesis for the derivation of the Green's functions is very similar to the method used in [91]. Fig. 2.1 is the TE and TM wave coupled transmission line model. The tangential field E_z, E_ϕ, H_z and H_ϕ are considered at each cylindrical interface. A 4×4 matrix $\overline{\boldsymbol{T}}_{i+1,i}$ relates these tangential field on two successive interface, i.e., the ith and $i+1$th interface, by

$$\begin{bmatrix} E_z^{i+1} \\ E_\phi^{i+1} \\ H_z^{i+1} \\ H_\phi^{i+1} \end{bmatrix} = \overline{\boldsymbol{T}}_{i+1,i} \cdot \begin{bmatrix} E_z^{i} \\ E_\phi^{i} \\ H_z^{i} \\ H_\phi^{i} \end{bmatrix} \tag{2.24}$$

or

$$\begin{bmatrix} E_z^{i} \\ E_\phi^{i} \\ H_z^{i} \\ H_\phi^{i} \end{bmatrix} = \overline{\boldsymbol{T}}_{i+1,i}^{-1} \cdot \begin{bmatrix} E_z^{i+1} \\ E_\phi^{i+1} \\ H_z^{i+1} \\ H_\phi^{i+1} \end{bmatrix}. \tag{2.25}$$

If there is a current source, J_z and J_ϕ on the ith cylindrical surface, we know that the fields on the two side of this cylindrical surface are discontinuous and they are restricted by the boundary conditions. Generally, the derivation of the Green's functions can be summarized into the following steps:

- Express the field on the inner side of the ith cylindrical surface in terms of the fields on the innermost cylindrical surface using Eq. (2.24), in which two unknown coefficient C_{TE}^{in} and C_{TM}^{in} are involved.

- Similarly, express the field on the outer side of the ith cylindrical surface in terms of the fields on the outermost cylindrical surface using Eq. (2.25), in which two unknown coefficient C_{TE}^{out} and C_{TM}^{out} are involved.
- Impose the boundary conditions on the field of both side of the ith cylindrical surface and obtain a matrix equation which can be solved for the 4 unknown coefficients.
- Once the unknown coefficients are obtained, the fields anywhere in the layered media can be obtained, hence the Green's functions are known.

2.4 Series Acceleration Techniques

The statement that the rate of convergence of a series is determined by the asymptotic form of the series is the basis for Kummer's method [92–94]. Suppose a series $f(n)$ has an asymptotic form $f_\infty(n)$. An equivalent expression to the summation of $f(n)$ can be found if the asymptotic series is subtracted from and added back to the original series as seen below,

$$\sum_{n=-\infty}^{\infty} f(n) = \sum_{n=-\infty}^{\infty} [f(n) - f_\infty(n)] + \sum_{n=-\infty}^{\infty} f_\infty(n). \tag{2.26}$$

Usually, $f_\infty(n)$ is chosen in such a way that the last series has a known closed-form expression. For complicated series, however, obtaining a closed-form expression for the asymptotic series can be a tedious task. If the closed-form expression for the asymptotic series is possible, the right hand side of Eq. (2.26) converges much more rapidly than the direct sum of $f(n)$.

Another effective transform for alternating series is the Shanks' transform [95]. The algorithm for the Shanks' transform of a sequence of partial sums is

$$S = e_1(S_{n+1}) + \frac{1}{e_1(S_{n+1}) - e_1(S_n)},$$

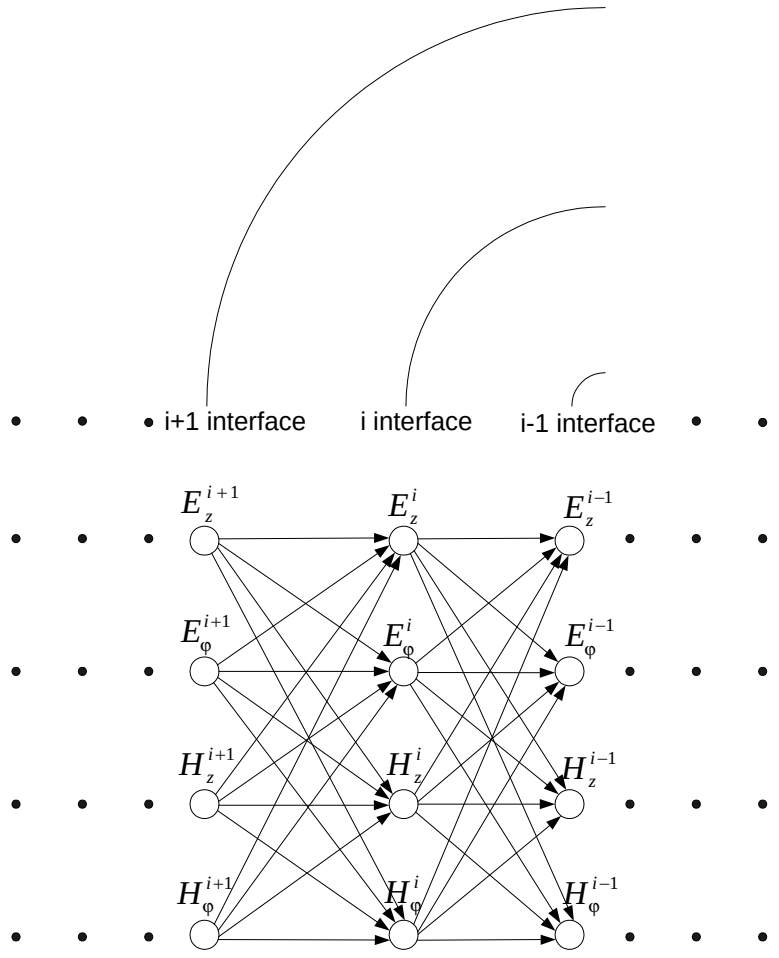

Figure 2.1: Signal-flow graph representation of the field relations between two successive cylindrical interface.

where

$$e_0(S_n) = S_n, \qquad e_1(S_n) = \frac{1}{e_0(S_{n+1}) - e_0(S_n)}.$$

Higher order Shanks' transform can be carried out using Wynn's ϵ-algorithm [96]:

$$e_{s+1}(S_n) = e_{s-1}(S_{n+1}) + \frac{1}{e_s(S_{n+1}) - e_s(S_n)}, \qquad s = 1, 2, ...$$

where

$$e_0(S_n) = S_n, \qquad e_1(S_n) = \frac{1}{e_0(S_{n+1}) - e_0(S_n)}.$$

Only the even order terms $e_{2r}(S_n)$ are Shanks' transform of order r approximating S.

2.5 Summary

The dyadic Green's functions technique and the methods applied in this thesis for cylindrically layered media are introduced and discussed briefly in this chapter. In the following chapters, specific problems are studied by applying one or more of these methods. The dyadic Green's functions are derived using aforementioned two methods, i.e., the 2×2 and 4×4 matrix methods. DCIM and series acceleration techniques are used to obtained the fast computational form of spatial domain Green's functions.

Chapter 3

Waves in Cylindrically Stratified Media

Over the past several decades, the dyadic Green's functions technique has been employed widely to investigate the interaction of the electromagnetic waves with the layered media in boundary-value problems [63]. When the dyadic Green's functions for a medium are known, its electromagnetic fields can be formulated in terms of an integral containing the Green's functions and an arbitrary current. In contrast to the planar and spherical layered media, TE and TM waves are coupled together at an interface in cylindrically layered media. Hence, reflection and transmission matrices (2×2 matrices) rather than reflection and transmission coefficients are used in the coupled-mode analysis of cylindrical structures [59, 62]. In this Chapter, a method based on 2×2 matrices is used to derive the electric field Green's functions for cylindrically stratified media. Much of the content can be found in [62]. However, the derivation is given here in detail in order to: 1) correct some typos in the formulation in [62] and 2) provide a full theoretical basis for the reader to have a smoother understanding of the following chapters.

3.1 Transmission and Reflection of Waves in Cylindrically One-Layered Media

3.1.1 Vector Wave Equation in Cylindrical Coordinates

In a cylindrical geometry of circular symmetry, a wave can be broken into cylindrical harmonics with different $e^{jn\phi}$ dependence. In principle, only two of the six electromagnetic field components are needed to characterize the wave. To characterize the TM and TE waves, the E_z and H_z components are used, respectively. The vector wave equations in a homogeneous, isotropic, source-free medium are

$$\nabla \times \nabla \times \boldsymbol{E} - k^2 \boldsymbol{E} = 0, \tag{3.1}$$

$$\nabla \times \nabla \times \boldsymbol{H} - k^2 \boldsymbol{H} = 0. \tag{3.2}$$

In cylindrical coordinates , the z components are extracted to yield

$$(\nabla^2 + k^2) E_z = 0, \tag{3.3}$$

$$(\nabla^2 + k^2) H_z = 0. \tag{3.4}$$

The general solutions to the above equations are

$$\begin{bmatrix} E_z \\ H_z \end{bmatrix} = [A_n J_n(k_\rho \rho) + B_n H_n^{(1)}(k_\rho \rho)] e^{jk_z + jn\phi}, \tag{3.5}$$

where $k_\rho^2 + k_z^2 = k^2$.

Given the z component of the field, the transverse components of the field in cylindrical coordinates can be determined from the following equations:

$$\boldsymbol{E}_s = \frac{1}{k_\rho^2}[jk_z \nabla_s E_z - j\omega\mu \hat{z} \times \nabla_s H_z], \tag{3.6}$$

$$\boldsymbol{H}_s = \frac{1}{k_\rho^2}[jk_z \nabla_s H_z + j\omega\mu \hat{z} \times \nabla_s E_z], \tag{3.7}$$

where $\nabla_s = \hat{\rho}\frac{\partial}{\partial \rho} + \hat{\phi}\frac{1}{\rho}\frac{\partial}{\partial \phi} = \hat{\rho}\frac{\partial}{\partial \rho} + \hat{\phi}\frac{jn}{\rho}$. The above equations are only valid in a

homogeneous region. By using E_z and H_z, all six components of the electromagnetic field can be derived in cylindrical coordinates.

3.1.2 Transmission and Reflection of Outgoing Waves

The reflection and transmission of waves at a cylindrical interface can be categorized into two cases: outgoing wave incident on a cylindrical boundary and standing wave on a cylindrical boundary. Consider the case where there is an outgoing($+\rho$ direction)

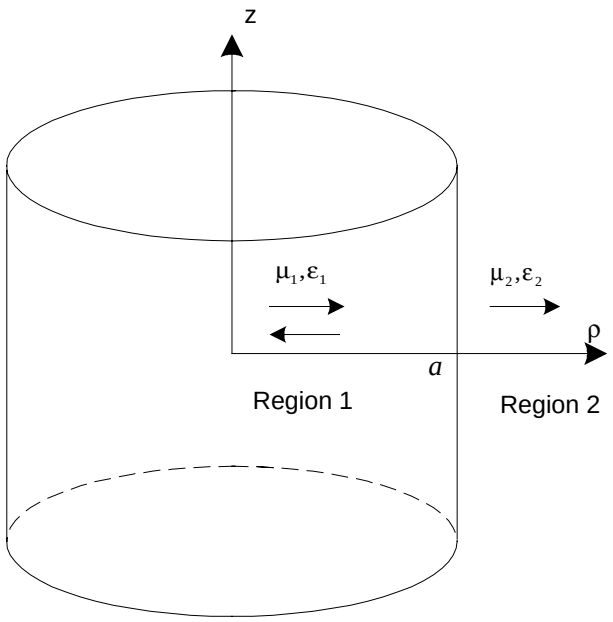

Figure 3.1: Reflection and transmission of an outgoing wave.

cylindrical wave in region 1 as shown in Fig. 3.1. In general, the wave in region 1 will have an outgoing wave for the n-th harmonic with $e^{jn\phi}$, as well as an incoming wave. The outgoing wave for the n-th harmonic is

$$\begin{bmatrix} E_{1z} \\ H_{1z} \end{bmatrix} = H_n^{(1)}(k_{1\rho}\rho) \begin{bmatrix} e_{1z} \\ h_{1z} \end{bmatrix} = H_n^{(1)}(k_{1\rho}\rho) \cdot \boldsymbol{a}_1 \tag{3.8}$$

Because of the closed nature of a cylindrical geometry, the incoming wave, represented by a Hankel function of the first kind, is always perfectly reflected at the origin, resulting in a standing wave. The total field in region 1 is then expressed as

$$\begin{bmatrix} E_{1z} \\ H_{1z} \end{bmatrix} = H_n^{(1)}(k_{1\rho}\rho) \cdot \boldsymbol{a}_1 + J_n(k_{1\rho}\rho)\overline{\boldsymbol{R}}_{12} \cdot \boldsymbol{a}_1. \tag{3.9}$$

Here, the field has been assumed to have e^{jk_z} dependence in all region. In addition, the wave is expressed for the n-th harmonic with $e^{in\phi}$ dependence. The field in region 2 is an outgoing wave and expressed as

$$\begin{bmatrix} E_{2z} \\ H_{2z} \end{bmatrix} = H_n^{(1)}(k_{2\rho}\rho)\overline{\boldsymbol{T}}_{12} \cdot \boldsymbol{a}_1, \tag{3.10}$$

where $k_{2\rho} = \sqrt{k_2^2 - k_z^2}$.

The ϕ components of the field in each of the homogeneous region 1 and region 2 is then derived from Eqs. (3.9) and (3.10) to yield

$$\begin{bmatrix} E_{1\phi} \\ H_{1\phi} \end{bmatrix} = \overline{\boldsymbol{H}}_n^{(1)}(k_{1\rho}\rho) \cdot \boldsymbol{a}_1 + \overline{\boldsymbol{J}}_n(k_{1\rho}\rho)\overline{\boldsymbol{R}}_{12} \cdot \boldsymbol{a}_1, \tag{3.11a}$$

$$\begin{bmatrix} E_{2\phi} \\ H_{2\phi} \end{bmatrix} = \overline{\boldsymbol{H}}_n^{(1)}(k_{2\rho}\rho)\overline{\boldsymbol{T}}_{12} \cdot \boldsymbol{a}_1, \tag{3.11b}$$

where $\overline{\boldsymbol{H}}_n^{(1)}(k_{1\rho}\rho)$ and $\overline{\boldsymbol{J}}_n(k_{1\rho}\rho)$ take the following form

$$\overline{\boldsymbol{B}}(k_{i\rho}\rho) = \frac{1}{k_{i\rho}^2\rho} \cdot \begin{bmatrix} j\omega\epsilon_i k_{i\rho}\rho B_n'(k_{i\rho}\rho) & -nk_z B_n(k_{i\rho}\rho) \\ -nk_z B_n(k_{i\rho}\rho) & j\omega\mu_i k_{i\rho}\rho B_n'(k_{i\rho}\rho) \end{bmatrix}. \tag{3.12}$$

Here, B_n represent $H_n^{(1)}$ or J_n. Boundary conditions are imposed at $\rho = a$, which require the continuity of the tangential components of the electromagnetic field. Solving the subsequent system of equations, expressions for $\overline{\boldsymbol{R}}_{12}$ and $\overline{\boldsymbol{T}}_{12}$ are derived to be

$$\overline{\boldsymbol{R}}_{12} = \overline{\boldsymbol{D}}^{-1} \cdot [H_n^{(1)}(k_{1\rho}a) \cdot \overline{\boldsymbol{H}}_n^{(1)}(k_{2\rho}a) - H_n^{(1)}(k_{2\rho}a) \cdot \overline{\boldsymbol{H}}_n^{(1)}(k_{1\rho}a)], \tag{3.13a}$$

$$\overline{\boldsymbol{T}}_{12} = \overline{\boldsymbol{D}}^{-1} \cdot [H_n^{(1)}(k_{1\rho}a) \cdot \overline{\boldsymbol{J}}_n(k_{1\rho}a) - J_n(k_{1\rho}a) \cdot \overline{\boldsymbol{H}}_n^{(1)}(k_{1\rho}a)], \tag{3.13b}$$

where

$$\overline{\boldsymbol{D}} = [\overline{\boldsymbol{J}}_n(k_{1\rho}a) \cdot \overline{H}_n^{(1)}(k_{2\rho}a) - \overline{\boldsymbol{H}}_n^{(1)}(k_{2\rho}a) \cdot J_n(k_{1\rho}a)]. \tag{3.14}$$

$\overline{\boldsymbol{R}}_{12}$ and $\overline{\boldsymbol{T}}_{12}$ are both functions of n. Furthermore, by applying the Wronskian for Hankel functions as

$$H_n^{(1)}(x)J_n'(x) - J_n(x)H'^{(1)}_n(x) = -\frac{2j}{\pi x}, \tag{3.15}$$

$\overline{\boldsymbol{T}}_{12}$ can be further simplified to

$$\overline{\boldsymbol{T}}_{12} = \frac{2\omega}{\pi k_{i\rho}^2 a} \cdot \overline{\boldsymbol{D}}^{-1} \cdot \begin{bmatrix} \epsilon_1 & 0 \\ 0 & -\mu_1 \end{bmatrix}. \tag{3.16}$$

3.1.3 Transmission and Reflection of Standing Waves

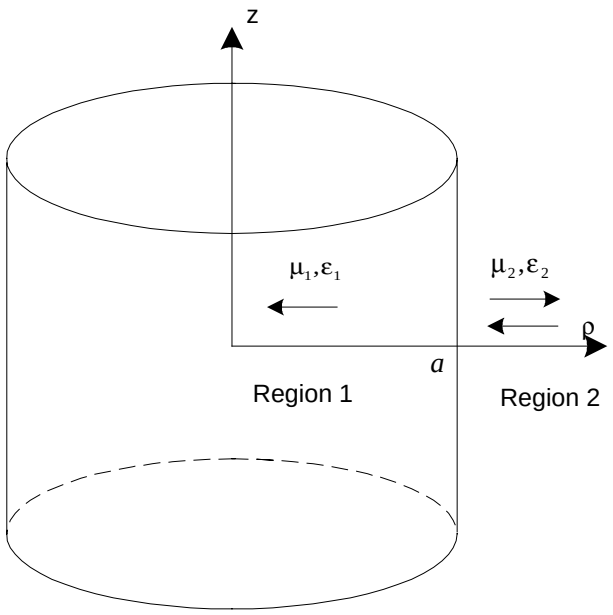

Figure 3.2: Reflection and transmission of a standing wave.

Consider the case where there is a standing wave as in Fig. 3.2. The field in region 1

and 2 is then given by

$$\begin{bmatrix} E_{2z} \\ H_{2z} \end{bmatrix} = H_n^{(1)}(k_{2\rho}\rho)\overline{\boldsymbol{R}}_{12} \cdot \boldsymbol{a}_2 + J_n(k_{2\rho}\rho) \cdot \boldsymbol{a}_2, \tag{3.17}$$

$$\begin{bmatrix} E_{1z} \\ H_{1z} \end{bmatrix} = J_n(k_{1\rho}\rho)\overline{\boldsymbol{T}}_{12} \cdot \boldsymbol{a}_2, \tag{3.18}$$

respectively.

Similar to the previous case, the ϕ components of the fields are derived from Eq. (3.17) and Eq. (3.18) via the use of Eq. (3.6) and Eq. (3.7),

$$\begin{bmatrix} E_{2\phi} \\ H_{2\phi} \end{bmatrix} = \overline{\boldsymbol{H}}_n^{(1)}(k_{2\rho}\rho) \cdot \overline{\boldsymbol{R}}_{21} \cdot \boldsymbol{a}_2 + \overline{\boldsymbol{J}}_n(k_{2\rho}\rho) \cdot \boldsymbol{a}_2, \tag{3.19a}$$

$$\begin{bmatrix} E_{1\phi} \\ H_{1\phi} \end{bmatrix} = \overline{\boldsymbol{J}}_n(k_{1\rho}\rho)\overline{\boldsymbol{T}}_{21} \cdot \boldsymbol{a}_2. \tag{3.19b}$$

Then, the boundary conditions at $\rho = a$ can be imposed to solve for $\overline{\boldsymbol{R}}_{21}$ and $\overline{\boldsymbol{T}}_{21}$, yielding

$$\overline{\boldsymbol{R}}_{21} = \overline{\boldsymbol{D}}^{-1} \cdot [J_n(k_{1\rho}a) \cdot \overline{J}_n(k_{2\rho}a) - J_n(k_{2\rho}a) \cdot \overline{J}_n(k_{2\rho}a)], \tag{3.20a}$$

$$\overline{\boldsymbol{T}}_{21} = \frac{2\omega}{\pi k_{2\rho}^2 a} \cdot \overline{\boldsymbol{D}}^{-1} \cdot \begin{bmatrix} \epsilon_2 & 0 \\ 0 & -\mu_2 \end{bmatrix}. \tag{3.20b}$$

The $\overline{\boldsymbol{D}}$ is defined in Eq. (3.14). The reflection and transmission matrices of an interface for outgoing and standing waves are thus obtained.

3.2 Transmission and Reflection of Waves in Cylindrically Multilayered Media

3.2.1 Transmission and Reflection of Outgoing Waves

Reflection and transmission matrices for cylindrically multilayered media can be derived from the reflection and transmission matrices for a single interface, which were obtained in above. Consider the outgoing wave case. A three-layer medium is shown in Fig. 3.3.

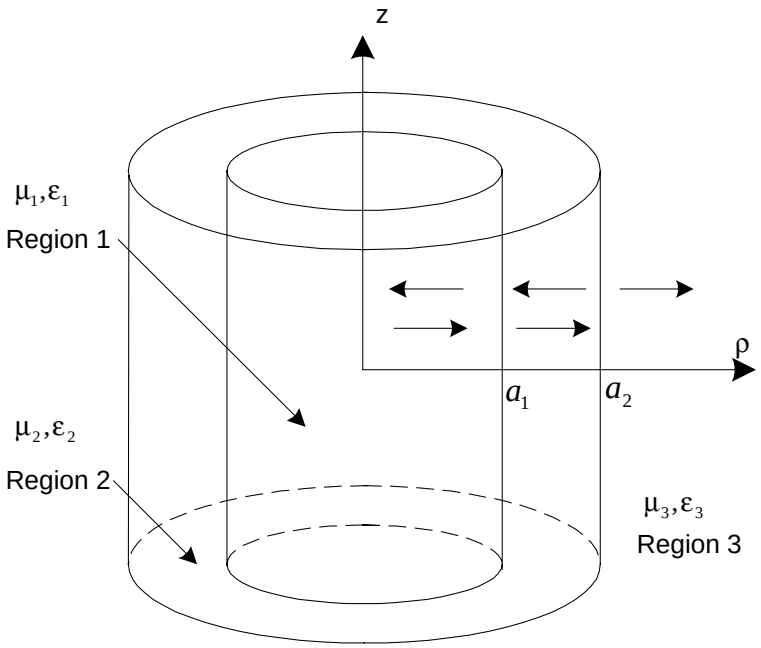

Figure 3.3: Reflection and transmission through a three-layered cylindrical medium: the outgoing wave case.

The fields in region 1 and region 2 are composed of standing and outgoing waves, while there is only an outgoing wave in region 3. The fields in the three regios can be express

as

$$\begin{bmatrix} E_{1z} \\ H_{1z} \end{bmatrix} = [H_n^{(1)}(k_{1\rho}\rho)\overline{\boldsymbol{I}} + J_n(k_{1\rho}\rho)\widetilde{\overline{\boldsymbol{R}}}_{12}] \cdot \boldsymbol{a}_1, \tag{3.21}$$

$$\begin{bmatrix} E_{2z} \\ H_{2z} \end{bmatrix} = [H_n^{(1)}(k_{2\rho}\rho)\overline{\boldsymbol{I}} + J_n(k_{2\rho}\rho)\overline{\boldsymbol{R}}_{23}] \cdot \boldsymbol{a}_2, \tag{3.22}$$

and

$$\begin{bmatrix} E_{3z} \\ H_{3z} \end{bmatrix} = H_n^{(1)}(k_{3\rho}\rho) \cdot \boldsymbol{a}_3. \tag{3.23}$$

respectively. Here, $\boldsymbol{a}_2$ and $\boldsymbol{a}_3$ are defined similar to $\boldsymbol{a}_1$ in Eq. (3.8). $\widetilde{\overline{\boldsymbol{R}}}_{12}$ is a generalized reflection matrix that relates standing wave to outgoing wave and $\overline{\boldsymbol{R}}_{23}$ is the local reflection matrix between region 2 and region 3.

An outgoing wave in region 2 is a consequence of the transmission of an outgoing wave in region 1 plus the reflection of a standing wave in region 2, leading to the following equations,

$$\boldsymbol{a}_2 = \overline{\boldsymbol{T}}_{12} \cdot \boldsymbol{a}_1 + \overline{\boldsymbol{R}}_{21} \cdot \overline{\boldsymbol{R}}_{23} \cdot \boldsymbol{a}_2. \tag{3.24}$$

Furthermore, the standing wave in region 1 is a result of the reflection of an outgoing wave in region 1 plus the transmission of a standing wave in region 2, yielding

$$\widetilde{\overline{\boldsymbol{R}}}_{12} \cdot \boldsymbol{a}_1 = \overline{\boldsymbol{R}}_{12} \cdot \boldsymbol{a}_1 + \overline{\boldsymbol{T}}_{12} \cdot \overline{\boldsymbol{R}}_{23} \cdot \boldsymbol{a}_2. \tag{3.25}$$

Solving Eq. (3.25) gives

$$\boldsymbol{a}_2 = (\overline{\boldsymbol{I}} - \overline{\boldsymbol{R}}_{21} \cdot \overline{\boldsymbol{R}}_{23})^{-1} \cdot \overline{\boldsymbol{T}}_{12} \cdot \boldsymbol{a}_1, \tag{3.26}$$

and

$$\widetilde{\overline{\boldsymbol{R}}}_{12} = \overline{\boldsymbol{R}}_{12} + \overline{\boldsymbol{T}}_{21} \cdot \overline{\boldsymbol{R}}_{23} \cdot (\overline{\boldsymbol{I}} - \overline{\boldsymbol{R}}_{21} \cdot \overline{\boldsymbol{R}}_{23})^{-1} \cdot \overline{\boldsymbol{T}}_{12}. \tag{3.27}$$

Eq. (3.27) expresses the generalized reflection matrix $\widetilde{\overline{\boldsymbol{R}}}_{12}$ in terms of the local reflection and transmission matrix between region 1 and region 2. This is in fact the result of the

physics of the multiple reflection in region 2. Consequently, Eq. (3.27) is expressed by a general recursive relation as

$$\widetilde{\overline{\boldsymbol{R}}}_{i,i+1} = \overline{\boldsymbol{R}}_{i,i+1} + \overline{\boldsymbol{T}}_{i+1,i} \cdot \widetilde{\overline{\boldsymbol{R}}}_{i+1,i+2} \cdot (\overline{\boldsymbol{I}} - \overline{\boldsymbol{R}}_{i+1,i} \cdot \widetilde{\overline{\boldsymbol{R}}}_{i+1,i+2})^{-1} \cdot \overline{\boldsymbol{T}}_{i,i+1}. \quad (3.28)$$

Eq. (3.28) can be used to find the generalized reflection matrices for an N-layer medium. In general, the field in region i can be written as

$$\begin{bmatrix} E_{iz} \\ H_{iz} \end{bmatrix} = [H_n^{(1)}(k_{i\rho}\rho)\overline{\boldsymbol{I}} + J_n(k_{i\rho}\rho)\widetilde{\overline{\boldsymbol{R}}}_{i,i+1}] \cdot \boldsymbol{a}_i, \quad (3.29)$$

where $\widetilde{\overline{\boldsymbol{R}}}_{N,N+1} = 0$, if $i = N$, since no reflection exists beyond region N. Therefore, Eq. (3.28) can be used recursively to find $\widetilde{\overline{\boldsymbol{R}}}_{N,N+1}$ for all regions. Similarly, from (3.26) it can be deduced in general,

$$\boldsymbol{a}_{i+1} = (\overline{\boldsymbol{I}} - \overline{\boldsymbol{R}}_{i+1,i} \cdot \widetilde{\overline{\boldsymbol{R}}}_{i+1,i+2})^{-1} \cdot \overline{\boldsymbol{T}}_{i,i+1} \cdot \boldsymbol{a}_i = \overline{\boldsymbol{S}}_{i,i+1} \cdot \boldsymbol{a}_i, \quad (3.30)$$

where

$$\overline{\boldsymbol{S}}_{i,i+1} = (\overline{\boldsymbol{I}} - \overline{\boldsymbol{R}}_{i+1,i} \cdot \widetilde{\overline{\boldsymbol{R}}}_{i+1,i+2})^{-1} \cdot \overline{\boldsymbol{T}}_{i,i+1}. \quad (3.31)$$

Since $\boldsymbol{a}_1$ is known, Eq. (3.30) can be used recursively to find $\boldsymbol{a}_i$ for all i, in general,

$$\boldsymbol{a}_N = \overline{\boldsymbol{T}}_{N-1,N} \cdot \overline{\boldsymbol{S}}_{N-2,N-1} \cdot \cdots \cdot \overline{\boldsymbol{S}}_{12} \cdot \boldsymbol{a}_1 = \widetilde{\overline{\boldsymbol{T}}}_{1N} \cdot \boldsymbol{a}_1 \quad (3.32)$$

where

$$\widetilde{\overline{\boldsymbol{T}}}_{1N} = \overline{\boldsymbol{T}}_{N-1,N} \cdot \overline{\boldsymbol{S}}_{N-2,N-1} \cdot \cdots \cdot \overline{\boldsymbol{S}}_{12}. \quad (3.33)$$

3.2.2 Transmission and Reflection of Standing Waves

Consider the standing wave case. If a standing wave is in region 3 as shown in Fig. 3.4, it will set up both standing and outgoing wave in region 2 and 3, but only a standing wave in region 1, as the field has to be regular at the origin. The field in each region may

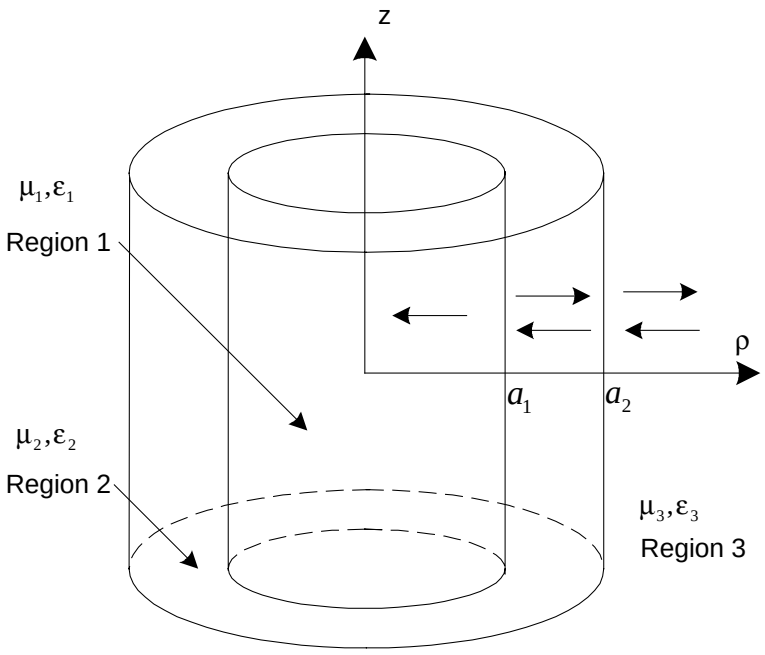

Figure 3.4: Reflection and transmission through a three-layered cylindrical meda: the standing wave case.

be expressed as follows:

$$\begin{bmatrix} E_{3z} \\ H_{3z} \end{bmatrix} = [H_n^{(1)}(k_{3\rho}\rho)\widetilde{\overline{\boldsymbol{R}}}_{32} + J_n(k_{3\rho}\rho)\overline{\boldsymbol{I}}] \cdot \boldsymbol{a}_3, \tag{3.34}$$

$$\begin{bmatrix} E_{2z} \\ H_{2z} \end{bmatrix} = [H_n^{(1)}(k_{2\rho}\rho)\overline{\boldsymbol{R}}_{21} + J_n(k_{2\rho}\rho)\overline{\boldsymbol{I}}] \cdot \boldsymbol{a}_2, \tag{3.35}$$

$$\begin{bmatrix} E_{1z} \\ H_{1z} \end{bmatrix} = J_n(k_{1\rho}\rho) \cdot \boldsymbol{a}_1. \tag{3.36}$$

$\widetilde{\overline{\boldsymbol{R}}}_{32}$ in Eq. (3.34) is the generalized matrix that relates an outgoing wave to a standing wave. In a similar procedure outline in previous section, the expression for the standing wave in region 2 and the generalized reflection matrix $\widetilde{\overline{\boldsymbol{R}}}_{32}$ is derived to be

$$\boldsymbol{a}_2 = (\overline{\boldsymbol{I}} - \overline{\boldsymbol{R}}_{23} \cdot \overline{\boldsymbol{R}}_{21})^{-1} \cdot \overline{\boldsymbol{T}}_{32} \cdot \boldsymbol{a}_3, \tag{3.37}$$

and

$$\widetilde{\overline{\boldsymbol{R}}}_{32} = \overline{\boldsymbol{R}}_{32} + \overline{\boldsymbol{T}}_{23} \cdot \widetilde{\overline{\boldsymbol{R}}}_{21} \cdot (\overline{\boldsymbol{I}} - \overline{\boldsymbol{R}}_{23} \cdot \widetilde{\overline{\boldsymbol{R}}}_{21})^{-1} \cdot \overline{\boldsymbol{T}}_{32}. \tag{3.38}$$

Consequently, a generalized recursive relation can be obtained for an N-layer medium,

$$\widetilde{\overline{\boldsymbol{R}}}_{i,i-1} = \overline{\boldsymbol{R}}_{i,i-1} + \overline{\boldsymbol{T}}_{i-1,i} \cdot \widetilde{\overline{\boldsymbol{R}}}_{i-1,i-2} \cdot (\overline{\boldsymbol{I}} - \overline{\boldsymbol{R}}_{i-1,i} \cdot \widetilde{\overline{\boldsymbol{R}}}_{i-1,i-2})^{-1} \cdot \overline{\boldsymbol{T}}_{i,i-1}. \tag{3.39}$$

The field in region i can be written as

$$\begin{bmatrix} E_{iz} \\ H_{iz} \end{bmatrix} = [H_n^{(1)}(k_{i\rho}\rho)\widetilde{\overline{\boldsymbol{R}}}_{i,i+1} + J_n(k_{i\rho}\rho)\overline{\boldsymbol{I}}] \cdot \boldsymbol{a}_i. \tag{3.40}$$

Since $\widetilde{\overline{\boldsymbol{R}}}_{10} = 0$ in the above recursive relation, one can use (3.39) recursively to find $\widetilde{\overline{\boldsymbol{R}}}_{i,i-1}$ for all i, starting from the innermost layer. In addition, by generalizing Eq. (3.37), a recursive relation can be obtained as follows,

$$\boldsymbol{a}_{i-1} = (\overline{\boldsymbol{I}} - \overline{\boldsymbol{R}}_{i-1,i} \cdot \widetilde{\overline{\boldsymbol{R}}}_{i-1,i-2})^{-1} \cdot \overline{\boldsymbol{T}}_{i,i-1} \cdot \boldsymbol{a}_i = \overline{\boldsymbol{S}}_{i,i-1} \cdot \boldsymbol{a}_i, \tag{3.41}$$

where

$$\overline{\boldsymbol{S}}_{i,i-1} = (\overline{\boldsymbol{I}} - \overline{\boldsymbol{R}}_{i-1,i} \cdot \widetilde{\overline{\boldsymbol{R}}}_{i-1,i-2})^{-1} \cdot \overline{\boldsymbol{T}}_{i,i-1}. \tag{3.42}$$

In general,

$$\boldsymbol{a}_1 = \overline{\boldsymbol{T}}_{21} \cdot \overline{\boldsymbol{S}}_{32} \cdot \cdots \cdot \overline{\boldsymbol{S}}_{N,N-1} \cdot \boldsymbol{a}_N = \widetilde{\overline{\boldsymbol{T}}}_{N1} \cdot \boldsymbol{a}_N, \tag{3.43}$$

where

$$\widetilde{\overline{\boldsymbol{T}}}_{N1} = \overline{\boldsymbol{T}}_{21} \cdot \overline{\boldsymbol{S}}_{32} \cdot \cdots \cdot \overline{\boldsymbol{S}}_{N,N-1} \tag{3.44}$$

is a generalized transmission matrix for cylindrically layered media.

3.3 Field in Cylindrically Layered Media

In order to obtain the field due to a point source in cylindrically layered media, the field due to a point source is expanded in terms of cylindrical wave functions. By using

identity (Appendix C-1), it can be shown that

$$\frac{e^{jk|r-r'|}}{|r-r'|} = \sum_{n=-\infty}^{\infty} \frac{je^{jn(\phi-\phi')}}{2} \int_{-\infty}^{\infty} dk_z e^{jk_z(z-z')} J_n(k_\rho \rho_<) H_n^{(1)}(k_\rho \rho_>). \tag{3.45}$$

where $\rho_<$ is the smaller of ρ and ρ', and $\rho_>$ is the larger of ρ and ρ'. For a point electric dipole pointing in the $\hat{\alpha}$ direction denoted by a current

$$\boldsymbol{J}(\boldsymbol{r}) = \hat{\alpha}\delta(\boldsymbol{r}-\boldsymbol{r}'), \tag{3.46}$$

since the electric field due to an electric current source $\boldsymbol{J}$ is

$$\boldsymbol{E}(\boldsymbol{r}) = j\omega\mu \iiint_{V'} \overline{\boldsymbol{G}}(\boldsymbol{r},\boldsymbol{r}') \cdot \boldsymbol{J}(\boldsymbol{r}') dV', \tag{3.47}$$

then the z component of the electric field can be obtained from (3.47), yielding

$$E_z = \frac{j}{\omega\epsilon}[\hat{z}\cdot\alpha k^2 + \frac{\partial}{\partial z'}\nabla'\cdot\hat{\alpha}]\frac{e^{jk|r-r'|}}{4\pi|\boldsymbol{r}-\boldsymbol{r}'|}. \tag{3.48}$$

Since $\boldsymbol{H} = (\nabla\times\boldsymbol{E})/(j\omega\mu)$, the z component of $\boldsymbol{H}$ is

$$H_z = -\hat{z}\cdot\nabla'\times\hat{\alpha}\frac{e^{jk|r-r'|}}{4\pi|\boldsymbol{r}-\boldsymbol{r}'|}. \tag{3.49}$$

Using Eq. (3.45), the field generated by source (3.46) is

$$\begin{bmatrix} E_z \\ H_z \end{bmatrix} = \frac{j}{4\pi\omega\epsilon}\boldsymbol{D}' \sum_{n=-\infty}^{\infty} \frac{je^{in(\phi-\phi')}}{2} \int_{-\infty}^{\infty} dk_z e^{jk_z(z-z')} J_n(k_\rho\rho_<) H_n^{(1)}(k_\rho\rho_>), \tag{3.50}$$

where

$$\boldsymbol{D}' = \begin{bmatrix} \nabla'\times\nabla'\times\hat{z}' \\ j\omega\epsilon_j\nabla\times\hat{z}' \end{bmatrix}\cdot\hat{\alpha}. \tag{3.51}$$

Consider Fig. 3.5, where a point source is placed in region j so that reflection of wave takes place at $\rho = a_j$, and $\rho = a_{j-1}$. The field in region j is then given by

$$\begin{aligned}\begin{bmatrix} E_{jz} \\ H_{jz} \end{bmatrix} = \frac{j}{4\pi\omega\epsilon_j} \sum_{n=-\infty}^{\infty} e^{jn(\phi-\phi')} \int_{-\infty}^{\infty} dk_z e^{jk_z(z-z')} \{ & J_n(k_\rho\rho_<) H_n^{(1)}(k_\rho\rho_>)\overline{\boldsymbol{I}} \\ & + H_n^{(1)}(k_{j\rho}\rho)\bar{\boldsymbol{a}}_{jn}(\rho') + J_n(k_{j\rho}\rho)\bar{\boldsymbol{b}}_{jn}(\rho')\} \cdot \overleftarrow{\boldsymbol{D}'}_j, \end{aligned} \tag{3.52}$$

where

$$\overleftarrow{\boldsymbol{D}'}_j = \begin{bmatrix} (\hat{z}k_j^2 - jk_z\nabla') \\ -j\omega\epsilon_j\nabla\times\hat{z}' \end{bmatrix}\cdot\hat{\alpha} \tag{3.53}$$

is an operator that acts on functions to its left. As a consequence of the $(e^{-jn\phi'-jk_zz'})$ dependence, $\nabla' = \hat{\rho}'\frac{\partial}{\partial\rho'} - \hat{\rho}'\frac{jn}{\rho'} - \hat{z}jk_z$, the additional standing and outgoing waves generated in region j is a result of reflection of the primary field. By imposing the

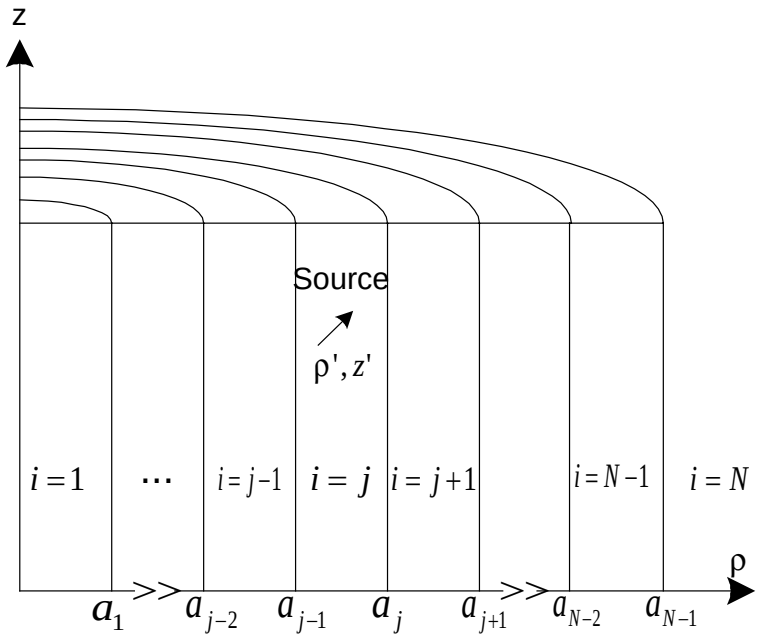

Figure 3.5: A source in cylindrically multilayered media.

constraint conditions at $\rho = a_{j-1}$ and $\rho = a_j$, the expression for $\bar{\boldsymbol{a}}_{jn}$ and $\bar{\boldsymbol{b}}_{jn}$ can be found. Upon simplification, part integrand in Eq. (3.52) is given by

$$\begin{aligned}
&\left[J_n(k_{j\rho}\rho_<)H_n^{(1)}(k_{j\rho}\rho_>)\overline{\boldsymbol{I}} + H_n^{(1)}(k_{j\rho})\overline{\boldsymbol{a}}_{jn} + J_n(k_{j\rho}\rho)\overline{\boldsymbol{b}}_{jn}\right]\cdot\overleftarrow{\boldsymbol{D}'}_j \\
&\quad = \begin{cases} \left[H_n^{(1)}(k_{i_\rho}\rho)\overline{\boldsymbol{I}} + J_n(k_{i_\rho}\rho)\widetilde{\overline{\boldsymbol{R}}}_{i,i+1}\right]\cdot\widetilde{\overline{\boldsymbol{M}}}_j \\ \qquad\cdot\left[J_n(k_{i_\rho}\rho')\overline{\boldsymbol{I}} + H_n^{(1)}(k_{i_\rho}\rho')\widetilde{\overline{\boldsymbol{R}}}_{i,i-1}\right]\overleftarrow{\boldsymbol{D}'}_j, & \rho > \rho' \\ \left[J_n(k_{i_\rho}\rho)\overline{\boldsymbol{I}} + H_n^{(1)}(k_{i_\rho}\rho)\widetilde{\overline{\boldsymbol{R}}}_{i,i-1}\right]\cdot\widetilde{\overline{\boldsymbol{M}}}_j \\ \qquad\cdot\left[H_n^{(1)}(k_{i_\rho}\rho')\overline{\boldsymbol{I}} + J_n(k_{i_\rho}\rho')\widetilde{\overline{\boldsymbol{R}}}_{i,i+1}\right]\overleftarrow{\boldsymbol{D}'}_j, & \rho < \rho' \end{cases}
\end{aligned} \tag{3.54}$$

where

$$\widetilde{\overline{\boldsymbol{M}}}_j = \begin{cases} (\overline{\boldsymbol{I}} - \widetilde{\overline{\boldsymbol{R}}}_{i,i-1} \cdot \widetilde{\overline{\boldsymbol{R}}}_{i,i+1})^{-1}, & \rho > \rho' \\ (\overline{\boldsymbol{I}} - \widetilde{\overline{\boldsymbol{R}}}_{i,i+1} \cdot \widetilde{\overline{\boldsymbol{R}}}_{i,i-1})^{-1}, & \rho < \rho' \end{cases} \tag{3.55}$$

is a factor accounting for multiple reflection within the source region j.

For $i > j$, the field in region i is given by

$$\begin{bmatrix} E_{jz} \\ H_{jz} \end{bmatrix} = \frac{j}{4\pi\omega\epsilon_j} \sum_{n=-\infty}^{\infty} e^{jn(\phi-\phi')} \int_{-\infty}^{\infty} dk_z e^{jk_z(z-z')} [H_n^{(1)}(k_\rho \rho_>)\overline{\boldsymbol{I}} + J_n(k_{i\rho}\rho)\widetilde{\overline{\boldsymbol{R}}}_{i,i+1}] \cdot \boldsymbol{a}_{in}, \tag{3.56}$$

where $\boldsymbol{a}_{in}$ is the amplitude of the outgoing wave in region i and it can be obtained via the recursive Eq. (3.32). Similarly, $\widetilde{\overline{\boldsymbol{R}}}_{i,i+1}$ can be found from (3.28).

For $i < j$, the field in region i is of the form

$$\begin{bmatrix} E_{iz} \\ H_{iz} \end{bmatrix} = \frac{j}{4\pi\omega\epsilon_j} \sum_{n=-\infty}^{\infty} e^{jn(\phi-\phi')} \int_{-\infty}^{\infty} dk_z e^{jk_z(z-z')} [J_n(k_{i\rho}\rho_>)\overline{\boldsymbol{I}} + H_n^{(1)}(k_{i\rho}\rho)\widetilde{\overline{\boldsymbol{R}}}_{i,i-1}] \cdot \boldsymbol{a}_{in}. \tag{3.57}$$

In this case, $\boldsymbol{a}_{in}$ is the amplitude of standing wave in region i. Expressions for $\boldsymbol{a}_{in}$ and $\widetilde{\overline{\boldsymbol{R}}}_{i,i-1}$ are given by the recursive relation (3.41) and (3.39), respectively.

Hence, the z components of the field are summarized as follows for three cases:

$$\begin{bmatrix} E_{jz} \\ H_{jz} \end{bmatrix} = \frac{j}{4\pi\omega\epsilon_j} \sum_{n=-\infty}^{\infty} e^{jn(\phi-\phi')} \int_{-\infty}^{\infty} dk_z e^{jk_z(z-z')} \overline{\boldsymbol{F}}_n(\rho,\rho') \cdot \overleftarrow{\boldsymbol{D}}'_j, \tag{3.58}$$

where

$$\overline{\boldsymbol{F}}_n(\rho,\rho') = \begin{cases} \left[H_n^{(1)}(k_{i_\rho}\rho)\overline{\boldsymbol{I}} + J_n(k_{i_\rho}\rho)\widetilde{\overline{\boldsymbol{R}}}_{i,i+1}\right] \cdot \widetilde{\overline{\boldsymbol{M}}}_j \\ \quad \cdot \left[J_n(k_{i_\rho}\rho')\overline{\boldsymbol{I}} + H_n^{(1)}(k_{i_\rho}\rho')\widetilde{\overline{\boldsymbol{R}}}_{i,i-1}\right], & \rho > \rho' \\ \left[J_n(k_{i_\rho}\rho)\overline{\boldsymbol{I}} + H_n^{(1)}(k_{i_\rho}\rho)\widetilde{\overline{\boldsymbol{R}}}_{i,i-1}\right] \cdot \widetilde{\overline{\boldsymbol{M}}}_j \\ \quad \cdot \left[H_n^{(1)}(k_{i_\rho}\rho')\overline{\boldsymbol{I}} + J_n(k_{i_\rho}\rho')\widetilde{\overline{\boldsymbol{R}}}_{i,i+1}\right], & \rho < \rho' \end{cases} \tag{3.59}$$

and

$$\widetilde{\overline{\boldsymbol{M}}}_j = \begin{cases} (\overline{\boldsymbol{I}} - \widetilde{\overline{\boldsymbol{R}}}_{j,j-1} \cdot \widetilde{\overline{\boldsymbol{R}}}_{j,j+1})^{-1}, & \rho > \rho' \\ (\overline{\boldsymbol{I}} - \widetilde{\overline{\boldsymbol{R}}}_{j,j+1} \cdot \widetilde{\overline{\boldsymbol{R}}}_{j,j-1})^{-1}, & \rho < \rho' \end{cases} \tag{3.60}$$

when both ρ and ρ' are in the same region j, i.e., $i = j$.

When $i > j$, $\rho \in$ region i and $\rho' \in$ region j, $\rho > \rho'$,

$$\begin{aligned} \overline{\boldsymbol{F}}_n(\rho, \rho') = \left[H_n^{(1)}(k_{i_\rho}\rho)\overline{\boldsymbol{I}} + J_n(k_{i_\rho}\rho)\widetilde{\overline{\boldsymbol{R}}}_{i,i+1}\right] \cdot \widetilde{\overline{\boldsymbol{M}}}_i \cdot \widetilde{\overline{\boldsymbol{T}}}_{ji} \cdot \widetilde{\overline{\boldsymbol{M}}}_j \\ \cdot \left[J_n(k_{i_\rho}\rho')\overline{\boldsymbol{I}} + H_n^{(1)}(k_{i_\rho}\rho')\widetilde{\overline{\boldsymbol{R}}}_{i,i-1}\right], \end{aligned} \tag{3.61}$$

where

$$\widetilde{\overline{\boldsymbol{M}}}_i = (\overline{\boldsymbol{I}} - \overline{\boldsymbol{R}}_{i,i-1} \cdot \widetilde{\overline{\boldsymbol{R}}}_{i,i+1})^{-1}, \tag{3.62}$$

$$\widetilde{\overline{\boldsymbol{M}}}_j = (\overline{\boldsymbol{I}} - \widetilde{\overline{\boldsymbol{R}}}_{j,j-1} \cdot \widetilde{\overline{\boldsymbol{R}}}_{j,j+1})^{-1}, \tag{3.63}$$

and $\widetilde{\overline{\boldsymbol{T}}}_{ji}$ is

$$\widetilde{\overline{\boldsymbol{T}}}_{ji} = \overline{\boldsymbol{T}}_{i-1,i} \cdot \overline{\boldsymbol{S}}_{i-2,i-1} \cdots \overline{\boldsymbol{S}}_{j,j+1}, \tag{3.64}$$

where

$$\overline{\boldsymbol{S}}_{i,i+1} = (\bar{\boldsymbol{I}} - \overline{\boldsymbol{R}}_{i+1,i} \cdot \widetilde{\overline{\boldsymbol{R}}}_{i+1,i+2})^{-1} \cdot \overline{\boldsymbol{T}}_{i,i+1}. \tag{3.65}$$

When $i < j$, $\rho \in$ region i and $\rho' \in$ region j, $\rho < \rho'$,

$$\begin{aligned} \overline{\boldsymbol{F}}_n(\rho, \rho') = \left[J_n(k_{i_\rho}\rho)\overline{\boldsymbol{I}} + H_n^{(1)}(k_{i_\rho}\rho)\widetilde{\overline{\boldsymbol{R}}}_{i,i-1}\right] \cdot \widetilde{\overline{\boldsymbol{M}}}_i \cdot \widetilde{\overline{\boldsymbol{T}}}_{ji} \cdot \widetilde{\overline{\boldsymbol{M}}}_j \\ \cdot \left[H_n^{(1)}(k_{i_\rho}\rho')\overline{\boldsymbol{I}} + J_n(k_{i_\rho}\rho')\widetilde{\overline{\boldsymbol{R}}}_{i,i+1}\right]. \end{aligned} \tag{3.66}$$

where

$$\widetilde{\overline{\boldsymbol{M}}}_i = (\overline{\boldsymbol{I}} - \overline{\boldsymbol{R}}_{i,i+1} \cdot \widetilde{\overline{\boldsymbol{R}}}_{i,i-1})^{-1}, \tag{3.67}$$

$$\widetilde{\overline{\boldsymbol{M}}}_j = (\overline{\boldsymbol{I}} - \widetilde{\overline{\boldsymbol{R}}}_{j,j+1} \cdot \widetilde{\overline{\boldsymbol{R}}}_{j,j-1})^{-1}, \tag{3.68}$$

and $\widetilde{\overline{\boldsymbol{T}}}_{ji}$ is

$$\widetilde{\overline{\boldsymbol{T}}}_{ji} = \overline{\boldsymbol{T}}_{i+1,i} \cdot \overline{\boldsymbol{S}}_{i+2,i+1} \cdots \overline{\boldsymbol{S}}_{j,j-1}, \tag{3.69}$$

where

$$\overline{\boldsymbol{S}}_{i,i-1} = (\overline{\boldsymbol{I}} - \overline{\boldsymbol{R}}_{i-1,i} \cdot \widetilde{\overline{\boldsymbol{R}}}_{i-1,i-2})^{-1} \cdot \overline{\boldsymbol{T}}_{i,i-1}. \tag{3.70}$$

The z components of the field due to a point source have been obtained now. The transverse components of the field can be derived through Eqs. (3.6) and (3.7). Then the Green's functions can be obtained. The explicit expressions will be given in Chapter 4.

It is important that the expression of multi-reflection matrix $\widetilde{\overline{\boldsymbol{M}}}$ is given for different cases, i.e., $i = j$, $i > j$ and $i < j$. However in [62], there is no difference shown in the expressions of $\widetilde{\overline{\boldsymbol{M}}}$ for these cases. Also, the forms of $\widetilde{\overline{\boldsymbol{M}}}_i$ and $\widetilde{\overline{\boldsymbol{M}}}_j$ are different: in $\widetilde{\overline{\boldsymbol{M}}}_i$, the local and generalized reflection matrices are included; while in $\widetilde{\overline{\boldsymbol{M}}}_j$, only generalized reflection matrices are involved. With careful investigations, the expression of $\widetilde{\overline{\boldsymbol{M}}}$ should be in the present form. The correctness will be proved in Chapter 4 and Chapter 5 by numerical results.

3.4 Summary

The z components of the field due to a point source for cylindrically multilayered media are derived using 2×2 matrix method. The local reflection and transmission matrices of an outgoing wave and a standing wave by considering a single interface case are first provided. The generalized reflection and transmission matrices for cylindrically multilayered media are then developed by making use of the local reflection and transmission matrices. Finally, the z components of the field due to a point source in a layered media are derived by expanding the field due to a point source in terms of cylindrical wave functions and expressed in terms of the generalized reflection and transmission matrices. The typos in [62] are identified and the correct expressions are given instead. The correctness will be proved in Chapter 4 and Chapter 5 by numerical

results.

Chapter 4

Electric Field Green's Function in Cylindrically Layered Media

---

The electric field Green's functions can be derived from Chapter 3, where the z components and hence the transverse components of the electromagnetic field due to a point source are obtained. In this chapter, the Green's functions are derived and given in explicit form, where there are no operator $\boldsymbol{D}$, as represented by Eqs. (3.51) and (3.53), in the Green's functions expressions. Then the closed-form electric field Green's functions are studied when the source point and observation point are not located on the same cylindrical surface.

4.1 Closed-Form Green's Functions

Multilayered cylindrical structures are often used as physical models in many practical applications. Such examples include typical conducting and dielectric cylindrical waveguides, cylindrically-rectangular and wrap-around microstrip and patch antennas and their arrays, the inlet of airplanes, missile bodies, and some optical fibers with step-varying refractive indexes. Numerical modeling of such structures can be efficiently

and rigorously performed by employing the MoM although other techniques such as finite element method and finite-difference methods (in both time-domain and frequency-domain) are also available. It is well-known that the MoM procedure for such a problem can be applied either in the spatial domain or in the spectral domain. Although the spectral domain analysis is more suitable and quite efficient for planar structures where the Fourier transform and inverse transform are applied to simplify the problem, the spatial domain analysis is still considered to be more general in that it can be easily applied to objects of arbitrary shape and particularly when the Fourier transform cannot be directly applied to formulate and simplify the Green's functions.

When the spatial domain Green's functions are used in the numerical MoM procedure, it is, however, very time-consuming sometimes because the Sommerfeld-type integrals are usually involved and numerical evaluation of these integrals is not actually very easy. Therefore, the closed-form solution to the Green's functions becomes necessary. The procedure for this kind solution was reported [27, 73, 82, 97] for the planarly layered media [63, 64]. For cylindrically multilayered media, the dyadic Green's functions have been formulated using 4×4 matrix method [78, 79], and 2×2 matrix method [62]. The corresponding closed-form Green's functions in spatial domain were recently reported in [81], where the fast computational solutions to the spatial domain Green's function components due to $\widehat{\boldsymbol{z}}$- and $\widehat{\boldsymbol{\phi}}$-oriented electric and magnetic sources embedded in arbitrary cylindrically multilayered media are obtained by using the GPOF method [70]. The key concept there was that the large argument behavior of the zeroth-order Hankel functions enables complex exponentials of k_ρ to be represented in terms of Hankel functions in the first step of GPOF method. These Green's functions are then approximated in terms of complex exponentials along a deformed path, which avoids the branch point singularity and pole singularities. In the second step of GPOF method, only two simple contour integrals of exponential functions need to be performed to get the so-called closed-form Green's functions.

However, electric or magnetic sources along the radial direction are often encountered in practice, such as a radial probe frequently used as a feeding element of the aforementioned microstrip antennas or patches. This motivates the present work in this chapter; and it actually presents spatial domain Green's functions components due to $\widehat{\boldsymbol{\rho}}$-oriented electric source in fast computational form and also $\widehat{\boldsymbol{\rho}}$-components of Green's functions due to $\widehat{\boldsymbol{z}}$- and $\widehat{\boldsymbol{\phi}}$-oriented electric source embedded in cylindrically multilayered media for a complete set of Green's functions. The explicit Green's functions are given in Section 4.2 followed by a summary of two-step GPOF method in Section 4.3. In Section 4.4, some numerical examples of the fast computational form Green's functions are presented for a specific cylindrically multilayered medium and the corresponding approximate Green's functions are obtained and compared with the exact Green's functions obtained by the direct numerical evaluation of the corresponding integrals.

4.2 General Formulation of Electric Green's Functions

Consider cylindrically stratified media as shown in Fig. 3.5. In the case of source point in layer j and field point in layer i, the electric field Green's functions can be written as [62]:

$$\begin{aligned}\overline{\boldsymbol{G}}_E(\boldsymbol{r},\boldsymbol{r}') &= \frac{j}{8\pi}\sum_{n=-\infty}^{\infty}\int_{-\infty}^{\infty}dk_z\frac{1}{(k_j k_{i_\rho})^2}\overline{\boldsymbol{D}}_{i\mu} \\ &\quad\cdot\overline{\boldsymbol{F}}_n(\rho,\rho')f_n(z,\phi;z',\phi')\cdot\overline{\overline{\boldsymbol{D}}}_{j\epsilon}^{\Leftarrow} - \frac{\widehat{\boldsymbol{\rho}}\widehat{\boldsymbol{\rho}}}{k_j^2}\delta(\boldsymbol{r}-\boldsymbol{r}') \qquad (4.1)\end{aligned}$$

where

$$\overline{\boldsymbol{D}}_{i\mu} = \left[\ \nabla\times\nabla\times\widehat{\boldsymbol{z}}, j\omega\mu_i\nabla\times\widehat{\boldsymbol{z}}\ \right], \qquad (4.2a)$$

$$\overline{\overline{\boldsymbol{D}}}_{j\epsilon}^{\Leftarrow} = \left[\ \nabla'\times\nabla'\times\widehat{\boldsymbol{z}}', -i\omega\epsilon_j\nabla\times\widehat{\boldsymbol{z}}'\ \right]^t\cdot\widehat{\boldsymbol{\alpha}}, \qquad (4.2b)$$

$$f_n(z,\phi;z',\phi') = e^{jn(\phi-\phi')+jk_z(z-z')}, \qquad (4.2c)$$

$$\overline{\boldsymbol{F}}_n(\rho,\rho') = \begin{bmatrix} f_{11} & f_{12} \\ f_{21} & f_{22}\end{bmatrix} \qquad (4.2d)$$

$$= \begin{cases} \left[H_n^{(1)}(k_{i_\rho}\rho)\overline{\boldsymbol{I}} + J_n(k_{i_\rho}\rho)\widetilde{\overline{\boldsymbol{R}}}_{i,i+1}\right]\widetilde{\overline{\boldsymbol{A}}}, & \rho > \rho'; \\ \\ \left[J_n(k_{i_\rho}\rho)\overline{\boldsymbol{I}} + H_n^{(1)}(k_{i_\rho}\rho)\widetilde{\overline{\boldsymbol{R}}}_{i,i-1}\right]\widetilde{\overline{\boldsymbol{A}}}, & \rho < \rho'. \end{cases} \tag{4.2e}$$

In Eq. (4.2), $\widehat{\boldsymbol{\alpha}}$ denotes the direction of the source and $\widetilde{\overline{\boldsymbol{A}}}$ is a 2×2 amplitude matrix for the standing and outgoing waves, given by

$$\widetilde{\overline{\boldsymbol{A}}} = \widetilde{\overline{\boldsymbol{M}}}_i \cdot \widetilde{\overline{\boldsymbol{T}}}_{ji} \cdot \widetilde{\overline{\boldsymbol{M}}}_j \cdot \overline{\boldsymbol{B}}, \tag{4.3}$$

where $\widetilde{\overline{\boldsymbol{M}}}_i$ and $\widetilde{\overline{\boldsymbol{M}}}_j$ denote the generalized multi-reflection matrices in region i and region j, respectively. They are defined in Eqs. (3.60), (3.62-3.63) and (3.67-3.68). $\widetilde{\overline{\boldsymbol{T}}}_{ji}$ stands, as defined in Eqs. (3.64) and (3.69), for the generalized transmission matrix from region j to region i, and the matrix $\overline{\boldsymbol{B}}$ is defined as [62]

$$\overline{\boldsymbol{B}} = \begin{cases} \left[J_n(k_{j_\rho}\rho')\overline{\boldsymbol{I}} + H_n^{(1)}(k_{j_\rho}\rho')\widetilde{\overline{\boldsymbol{R}}}_{j,j-1}\right], & \rho > \rho'; \\ \\ \left[H_n^{(1)}(k_{j_\rho}\rho')\overline{\boldsymbol{I}} + J_n(k_{j_\rho}\rho')\widetilde{\overline{\boldsymbol{R}}}_{j,j+1}\right], & \rho < \rho'. \end{cases} \tag{4.4}$$

Based on above expressions and considering Eq. (1.4), we have obtained the complete set of spectral domain Green's functions expressions and these expressions are given subsequently.

4.2.1 The $\widehat{\rho}$-Oriented Electrical Dipole

$$\tilde{G}_{z\rho}^{E_n} = -\frac{1}{8\pi\epsilon_j\omega}\Big(- ik_z\frac{\partial f_{11}}{\partial\rho'} - \frac{n\omega\epsilon_j}{\rho'}f_{12}\Big), \tag{4.5a}$$

$$\begin{aligned}\tilde{G}_{\phi\rho}^{E_n} = &-\frac{1}{8\pi\epsilon_j\omega k_{i\rho}^2}\Big[\frac{k_z n}{\rho}(ik_z\frac{\partial f_{11}}{\partial\rho'} + \frac{n\omega\epsilon_j}{\rho'}f_{12}) \\ &+i\omega\mu_i(ik_z\frac{\partial^2 f_{21}}{\partial\rho\partial\rho'} + \frac{n\omega\epsilon_j}{\rho'}\frac{\partial f_{22}}{\partial\rho})\Big],\end{aligned} \tag{4.5b}$$

$$\begin{aligned}\tilde{G}_{\rho\rho}^{E_n} = &-\frac{1}{8\pi\epsilon_j\omega k_{i\rho}^2}\Big[ik_z(- ik_z\frac{\partial^2 f_{11}}{\partial\rho\partial\rho'} - \frac{n\omega\epsilon_j}{\rho'}\frac{\partial f_{12}}{\partial\rho}) \\ &+\frac{\omega n\mu_i}{\rho}(ik_z\frac{\partial f_{21}}{\partial\rho'} + \frac{n\omega\epsilon_j}{\rho'}f_{22})\Big],\end{aligned} \tag{4.5c}$$

$$\tilde{G}^{H_n}_{z\rho} = \frac{1}{8\pi\epsilon_j\omega}\Big[ik_z\frac{\partial f_{21}}{\partial\rho'} + \frac{n\omega\epsilon_j}{\rho'}f_{22}], \tag{4.5d}$$

$$\begin{aligned}\tilde{G}^{H_n}_{\phi\rho} = &-\frac{1}{8\pi\epsilon_j\omega k^2_{i\rho}}\Big[-i\omega\epsilon_j(ik_z\frac{\partial^2 f_{11}}{\partial\rho\partial\rho'} + \frac{n\omega\epsilon_j}{\rho'}\frac{\partial f_{12}}{\partial\rho})\\ &+\frac{k_z n}{\rho}(ik_z\frac{\partial f_{21}}{\partial\rho'} + \frac{n\omega\epsilon_j}{\rho'}f_{22})\Big],\end{aligned} \tag{4.5e}$$

$$\begin{aligned}\tilde{G}^{H_n}_{\rho\rho} = &-\frac{1}{8\pi\epsilon_j\omega k^2_{i\rho}}\Big[-\frac{n\omega\epsilon_j}{\rho}(ik_z\frac{\partial f_{11}}{\partial\rho'} + \frac{n\omega\epsilon_j}{\rho'}f_{12})\\ &-ik_z(ik_z\frac{\partial^2 f_{21}}{\partial\rho\partial\rho'} + \frac{n\omega\epsilon_j}{\rho'}\frac{\partial f_{22}}{\partial\rho})\Big].\end{aligned} \tag{4.5f}$$

4.2.2 The $\hat{\rho}$-Oriented Magnetic Dipole

$$\tilde{G}^{H_n}_{z\rho} = \frac{1}{8\pi\mu_j\omega}\Big(ik_z\frac{\partial f_{22}}{\partial\rho'} - \frac{n\omega\mu_j}{\rho'}f_{21}\Big), \tag{4.6a}$$

$$\begin{aligned}\tilde{G}^{H_n}_{\phi\rho} = &\frac{1}{8\pi\mu_j\omega k^2_{i\rho}}\Big[\frac{k_z n}{\rho}(-ik_z\frac{\partial f_{22}}{\partial\rho'} + \frac{n\omega\mu_j}{\rho'}f_{21})\\ &-i\omega\epsilon_i(-ik_z\frac{\partial^2 f_{12}}{\partial\rho\partial\rho'} + \frac{n\omega\mu_j}{\rho'}\frac{\partial f_{11}}{\partial\rho})\Big],\end{aligned} \tag{4.6b}$$

$$\begin{aligned}\tilde{G}^{H_n}_{\rho\rho} = &-\frac{1}{8\pi\mu_j\omega k^2_{i\rho}}\Big[-ik_z(ik_z\frac{\partial^2 f_{22}}{\partial\rho\partial\rho'} - \frac{n\omega\mu_j}{\rho'}\frac{\partial f_{21}}{\partial\rho})\\ &+\frac{\omega n\epsilon_i}{\rho}(-ik_z\frac{\partial f_{12}}{\partial\rho'} + \frac{n\omega\mu_j}{\rho'}f_{11})\Big],\end{aligned} \tag{4.6c}$$

$$\tilde{G}^{E_n}_{z\rho} = \frac{1}{8\pi\mu_j\omega}(ik_z\frac{\partial f_{12}}{\partial\rho'} - \frac{n\omega\mu_j}{\rho'}f_{11}), \tag{4.6d}$$

$$\begin{aligned}\tilde{G}^{E_n}_{\phi\rho} = &\frac{1}{8\pi\mu_i\omega k^2_{i\rho}}\Big[i\omega\mu_i(-ik_z\frac{\partial^2 f_{22}}{\partial\rho\partial\rho'} + \frac{n\omega\mu_j}{\rho'}\frac{\partial f_{21}}{\partial\rho})\\ &+\frac{k_z n}{\rho}(-ik_z\frac{\partial f_{12}}{\partial\rho'} + \frac{n\omega\mu_j}{\rho'}f_{11})\Big],\end{aligned} \tag{4.6e}$$

$$\begin{aligned}\tilde{G}^{E_n}_{\rho\rho} = &-\frac{1}{8\pi\mu_j\omega k^2_{i\rho}}\Big[-\frac{n\omega\mu_i}{\rho}(-ik_z\frac{\partial f_{22}}{\partial\rho'} + \frac{n\omega\mu_j}{\rho'}f_{21})\\ &+ik_z(-ik_z\frac{\partial^2 f_{12}}{\partial\rho\partial\rho'} + \frac{n\omega\mu_j}{\rho'}\frac{\partial f_{11}}{\partial\rho})\Big].\end{aligned} \tag{4.6f}$$

4.2.3 The $\hat{z}$-Oriented Electrical Dipole

$$\tilde{G}^{E_n}_{zz} = -\frac{1}{8\pi\epsilon_j\omega}k^2_{j\rho}f_{11}, \tag{4.7a}$$

$$\tilde{G}^{E_n}_{\phi z} = -\frac{1}{8\pi\epsilon_j\omega k_{i\rho}^2}k_{j\rho}^2\Big(-\frac{k_z n}{\rho}f_{11} - i\omega\mu_i\frac{\partial f_{21}}{\partial\rho}\Big), \tag{4.7b}$$

$$\tilde{G}^{E_n}_{\rho z} = \frac{1}{8\pi\epsilon_j\omega k_{i\rho}^2}k_{j\rho}^2\Big(-ik_z\frac{\partial f_{11}}{\partial\rho} + \frac{n\omega\mu_i}{\rho}f_{21}\Big), \tag{4.7c}$$

$$\tilde{G}^{H_n}_{zz} = -\frac{1}{8\pi\epsilon_j\omega}k_{j\rho}^2 f_{21}, \tag{4.7d}$$

$$\tilde{G}^{H_n}_{\phi z} = \frac{1}{8\pi\epsilon_j\omega k_{i\rho}^2}k_{j\rho}^2\Big(-i\omega\epsilon_i\frac{\partial f_{11}}{\partial\rho} + \frac{k_z n}{\rho}f_{21}\Big), \tag{4.7e}$$

$$\tilde{G}^{H_n}_{\rho z} = \frac{1}{8\pi\epsilon_j\omega k_{i\rho}^2}k_{j\rho}^2\Big(-\frac{n\omega\epsilon_i}{\rho}f_{11} - ik_z\frac{\partial f_{21}}{\partial\rho}\Big). \tag{4.7f}$$

4.2.4 The $\hat{z}$-Oriented Magnetic Dipole

$$\tilde{G}^{H_n}_{zz} = -\frac{1}{8\pi\mu_j\omega}k_{j\rho}^2 f_{22}, \tag{4.8a}$$

$$\tilde{G}^{H_n}_{\phi z} = -\frac{1}{8\pi\mu_j\omega k_{i\rho}^2}k_{j\rho}^2\Big(-\frac{k_z n}{\rho}f_{22} + i\omega\epsilon_i\frac{\partial f_{12}}{\partial\rho}\Big), \tag{4.8b}$$

$$\tilde{G}^{H_n}_{\rho z} = -\frac{1}{8\pi\mu_j\omega k_{i\rho}^2}k_{j\rho}^2\Big(ik_z\frac{\partial f_{22}}{\partial\rho} + \frac{n\omega\epsilon_i}{\rho}f_{12}\Big), \tag{4.8c}$$

$$\tilde{G}^{E_n}_{zz} = -\frac{1}{8\pi\mu_j\omega}k_{j\rho}^2 f_{12}, \tag{4.8d}$$

$$\tilde{G}^{E_n}_{\phi z} = \frac{1}{8\pi\mu_j\omega k_{i\rho}^2}k_{j\rho}^2\Big(i\omega\mu_i\frac{\partial f_{22}}{\partial\rho} + \frac{k_z n}{\rho}f_{12}\Big), \tag{4.8e}$$

$$\tilde{G}^{E_n}_{\rho z} = -\frac{1}{8\pi\mu_j\omega k_{i\rho}^2}k_{j\rho}^2\Big(-\frac{n\omega\mu_i}{\rho}f_{22} + ik_z\frac{\partial f_{12}}{\partial\rho}\Big). \tag{4.8f}$$

4.2.5 The $\hat{\phi}$-Oriented Electrical Dipole

$$\tilde{G}^{E_n}_{z\phi} = -\frac{1}{8\pi\epsilon_j\omega}\Big(i\omega\epsilon_j\frac{\partial f_{12}}{\partial\rho'} - \frac{k_z n}{\rho'}f_{11}\Big), \tag{4.9a}$$

$$\begin{aligned}\tilde{G}^{E_n}_{\phi\phi} = -\frac{1}{8\pi\epsilon_j\omega k_{i\rho}^2}\Big[&\frac{k_z n}{\rho'}\Big(\frac{k_z n}{\rho}f_{11} + i\omega\mu_i\frac{\partial f_{21}}{\partial\rho}\Big)\\ &-i\omega\epsilon_j\Big(\frac{k_z n}{\rho}\frac{\partial f_{12}}{\partial\rho'} + i\omega\mu_i\frac{\partial^2 f_{22}}{\partial\rho\partial\rho'}\Big)\Big],\end{aligned} \tag{4.9b}$$

$$\begin{aligned}\tilde{G}^{E_n}_{\rho\phi} = -\frac{1}{8\pi\epsilon_j\omega k_{i\rho}^2}\Big[&ik_z\Big(i\omega\epsilon_j\frac{\partial^2 f_{12}}{\partial\rho\partial\rho'} - \frac{k_z n}{\rho'}\frac{\partial f_{11}}{\partial\rho}\Big)\\ &-\frac{n\omega\mu_i}{\rho}\Big(i\omega\epsilon_j\frac{\partial f_{22}}{\partial\rho'} - \frac{k_z n}{\rho'}f_{21}\Big)\Big],\end{aligned} \tag{4.9c}$$

$$\tilde{G}^{H_n}_{z\phi} = -\frac{1}{8\pi\epsilon_j\omega}\Big(i\omega\epsilon_j\frac{\partial f_{22}}{\partial\rho'} - \frac{k_z n}{\rho'}f_{21}\Big), \tag{4.9d}$$

$$\begin{aligned}\tilde{G}^{H_n}_{\phi\phi} = &-\frac{1}{8\pi\epsilon_j\omega k_{i\rho}^2}\Big[\frac{k_z n}{\rho'}(-i\omega\epsilon_i\frac{\partial f_{11}}{\partial\rho} + \frac{k_z n}{\rho}f_{21})\\ &-i\omega\epsilon_j(-i\omega\epsilon_i\frac{\partial^2 f_{12}}{\partial\rho\partial\rho'} + \frac{k_z n}{\rho}\frac{\partial f_{22}}{\partial\rho'})\Big],\end{aligned} \tag{4.9e}$$

$$\begin{aligned}\tilde{G}^{H_n}_{\rho\phi} = &-\frac{1}{8\pi\epsilon_j\omega k_{i\rho}^2}\Big[\frac{n\omega\epsilon_i}{\rho}(i\omega\epsilon_j\frac{\partial f_{12}}{\partial\rho'} - \frac{k_z n f_{11}}{\rho'})\\ &-ik_z(-i\omega\epsilon_j\frac{\partial^2 f_{22}}{\partial\rho\partial\rho'} + \frac{k_z n}{\rho'}\frac{\partial f_{21}}{\partial\rho})\Big].\end{aligned} \tag{4.9f}$$

4.2.6 The $\hat{\phi}$-Oriented Magnetic Dipole

$$\tilde{G}^{H_n}_{z\phi} = \frac{1}{8\pi\mu_j\omega}\Big(i\omega\mu_j\frac{\partial f_{21}}{\partial\rho'} + \frac{k_z n}{\rho'}f_{22}\Big), \tag{4.10a}$$

$$\begin{aligned}\tilde{G}^{H_n}_{\phi\phi} = &-\frac{1}{8\pi\mu_j\omega k_{i\rho}^2}\Big[\frac{k_z n}{\rho'}(\frac{k_z n}{\rho}f_{22} - i\omega\epsilon_i\frac{\partial f_{12}}{\partial\rho})\\ &+i\omega\mu_j(\frac{k_z n}{\rho}\frac{\partial f_{21}}{\partial\rho'} - i\omega\epsilon_i\frac{\partial^2 f_{11}}{\partial\rho\partial\rho'})\Big],\end{aligned} \tag{4.10b}$$

$$\begin{aligned}\tilde{G}^{H_n}_{\rho\phi} = &\frac{1}{8\pi\mu_j\omega k_{i\rho}^2}\Big[ik_z(i\omega\mu_j\frac{\partial^2 f_{21}}{\partial\rho\partial\rho'} + \frac{k_z n}{\rho'}\frac{\partial f_{22}}{\partial\rho})\\ &+\frac{n\omega\epsilon_i}{\rho}(i\omega\mu_j\frac{\partial f_{11}}{\partial\rho'} + \frac{k_z n}{\rho'}f_{12})\Big],\end{aligned} \tag{4.10c}$$

$$\tilde{G}^{E_n}_{z\phi} = \frac{1}{8\pi\mu_j\omega}\Big(i\omega\mu_j\frac{\partial f_{11}}{\partial\rho'} + \frac{k_z n}{\rho'}f_{12}\Big), \tag{4.10d}$$

$$\begin{aligned}\tilde{G}^{E_n}_{\phi\phi} = &-\frac{1}{8\pi\mu_j\omega k_{i\rho}^2}\Big[\frac{k_z n}{\rho'}(i\omega\mu_i\frac{\partial f_{22}}{\partial\rho} + \frac{k_z n}{\rho}f_{12})\\ &+i\omega\mu_j(i\omega\mu_i\frac{\partial^2 f_{21}}{\partial\rho\partial\rho'} + \frac{k_z n}{\rho}\frac{\partial f_{11}}{\partial\rho'})\Big],\end{aligned} \tag{4.10e}$$

$$\begin{aligned}\tilde{G}^{E_n}_{\rho\phi} = &-\frac{1}{8\pi\mu_j\omega k_{i\rho}^2}\Big[\frac{n\omega\mu_i}{\rho}(i\omega\mu_j\frac{\partial f_{21}}{\partial\rho'} + \frac{k_z n f_{22}}{\rho'})\\ &+ik_z(-i\omega\mu_j\frac{\partial^2 f_{11}}{\partial\rho\partial\rho'} - \frac{k_z n}{\rho'}\frac{\partial f_{12}}{\partial\rho})\Big].\end{aligned} \tag{4.10f}$$

4.3 Two-Step DCIM Procedure

Fig. 4.1 is the deformed SIP on the complex k_z plane. k_s is the propagation constant for the source layer. Parameters T_1, T_2 and T_3 as well as k_s define the shape of the SIP. The

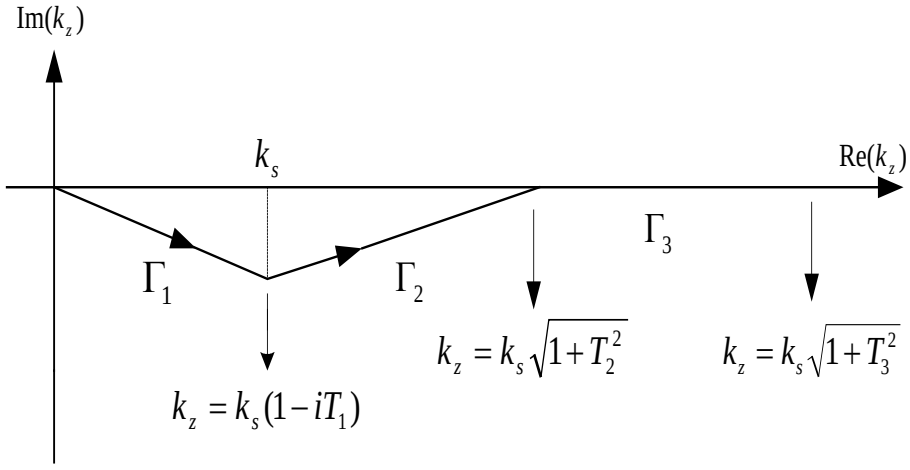

Figure 4.1: Deformed Sommerfeld Integral Path (SIP) on the complex k_z plane.

two-step DCIM procedure [81,82], which is performed on this path, is outlined briefly as follows:

a) The spectral domain Green's functions are sampled uniformly along the path Γ_3 to avoid the singularites [83]:

$$\begin{aligned} k_{\rho_s} &= jk_s(t_3 + T_2), \\ k_z &= k_s\sqrt{1 + (t_3 + T_2)^2} \end{aligned} \tag{4.11}$$

for $0 \leq t_3 < T_3 - T_2$, where k_{ρ_s} are the wavenumbers of the sampling region that is chosen as the source layer.

b) The sampled Green's functions are multiplied by $\sqrt{k_{\rho_s}}$ and approximated in terms of N_3 complex exponentials of k_{ρ_s} by the GPOF method,

$$\sqrt{k_{\rho_s}}\tilde{G}_{k_{\rho_s}} \cong \sum_{l=1}^{N_3} b_{l_t} e^{s_{l_t} t_3} = \sum_{l=1}^{N_3} b_{l_k} e^{k_{\rho_s} s_{l_k}}. \tag{4.12}$$

c) The resulting exponential functions are represented by the zeroth-order Hankel function using the large argument approximation,

$$\tilde{G}_{k_{\rho_s}} \cong \sum_{l=1}^{N_3} b_{l_k} \frac{e^{k_{\rho_s} s_{l_k}}}{\sqrt{k_{\rho_s}}} \cong \sum_{l=1}^{N_3} b_{l_h} H_0^{(1)}(k_{\rho_s} s_{l_h}). \tag{4.13}$$

d) By using the Sommerfeld identity (Appendix C), the spatial domain Green's functions G_{k_ρ} are obtained as

$$G_{k_{\rho s}} \cong \frac{2}{i} \sum_{l=1}^{N_3} b_{l_h} \frac{e^{-jk_{\rho s}|r_l|}}{|r_l|}, \tag{4.14}$$

where $r_l = \sqrt{(z-z')^2 + s_{l_h}^2}$.

e) The spectral domain Green's functions approximated on the path Γ_3 are subtracted from the original Green's functions to yield the Green's functions vanishing on the path Γ_3. Then the resulting Green's functions are sampled uniformly along the two deformed paths Γ_1 and Γ_2.

f) The sampled Green's functions are approximated in terms of N_1 and N_2 complex exponentials of k_z by the GPOF method on the deformed paths Γ_1 and Γ_2, respectively, as

$$k_z = k_s(1 - jT_1)\frac{t_1}{T1}, \qquad 0 \le t_1 < T_1; \tag{4.15}$$

$$k_z = k_s[1 - jT_1 + (\sqrt{1+T_2^2} - 1 + jT_1)\frac{t_2}{T_2 - T1}], \qquad 0 \le t_2 < T_2 - T_1; \tag{4.16}$$

$$\tilde{G}_{k_z} \cong \sum_{m=1}^{N_1} b_{m_t} e^{k_z s_{m_k}} + \sum_{n=1}^{N_2} b_{n_k} e^{k_z s_{n_k}}. \tag{4.17}$$

g) Transformation of the approximated Green's functions into the spatial domain turns out to be simple contour integrals of exponentials as

$$G_{k_z} = \int_{\Gamma_1+\Gamma_2} dk_z \tilde{G}_{k_z} e^{ik_z(z-z')}. \tag{4.18}$$

4.4 Numerical Results and Discussion

As the numerical procedure and results form primary parts of the current work, typical and representative results are presented in this chapter. As an example, we subsequently consider a 2-layer coated PEC cylinder structure, as shown in Fig. 4.2. Some new results of the $\widehat{\boldsymbol{\rho}}$-associated components of electric field Green's functions are first provided.

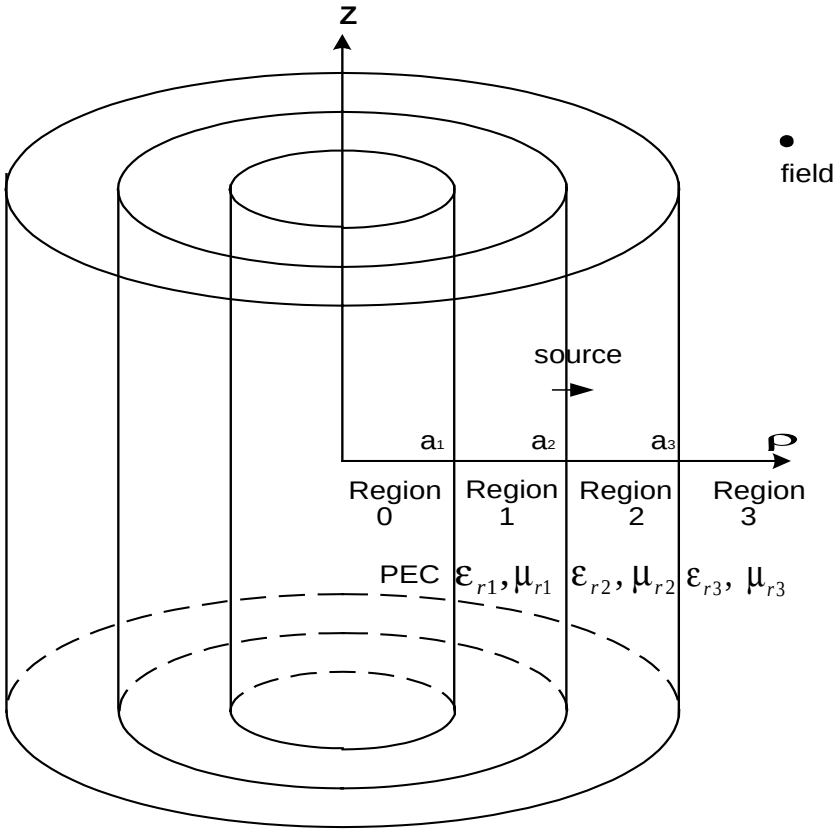

Figure 4.2: A two-layer coated PEC cylinder.

And more results of the other components of the dyadic Green's functions than those presented in [81] are provided and shown in 3-dimensional plots. Comparison between the approximate results obtained herein using the GPOF method and those exact values obtained by direct numerical evaluations of the inverse Fourier integral is also made to verify the correctness of the present work, the accuracy of the proposed approach, and applicability of the fast computational form.

In the numerical analysis, the complex images in each segment are chosen as 10 for the segment $0 \leq t_1 < T_1$, 4 for the segment $0 \leq t_2 < T_2 - T_1$, and 2 for the segment $0 \leq t_3 < T_3 - T_2$, respectively. Because the integral in segment $0 \leq t_1 < T_1$ dominates the inverse Fourier integral, so more images for this segment are chosen to maintain a good accuracy, but less images for other segments are chosen so as to increase the computational speed.

The geometry of the multilayered cylinder is shown in Fig. 4.2. Region 0 is considered to be a PEC cylinder. The dielectric parameters for other regions are: in Region 1, $\epsilon_{r_1} = 2.5$ and $\mu_{r_1} = 1$; in Region 2, $\epsilon_{r_2} = 3.8$ and $\mu_{r_2} = 1$; and in Region 3, $\epsilon_{r_3} = 1$ and $\mu_{r_3} = 1$. The dimensions of the structure are assumed to be $a_1 = 51$ mm, $a_2 = 52$ mm, and $a_3 = 53$ mm, while observation and source points are assumed to be located at $\rho = 70$ mm and $\rho' = 52$ mm, respectively for $\phi - \phi' = \pi/4$ and at $f = 6.8$ GHz. Different from the source orientation in the existing results where the source is $\widehat{\boldsymbol{\phi}}$- and $\widehat{\boldsymbol{z}}$-oriented, the source is assumed in the following computation to be a $\widehat{\boldsymbol{\rho}}$-oriented electric dipole located at ρ' while the observation point is located at ρ. The deformed path parameter T_1, T_2, T_3 are carefully chosen herein as $T_1 = 0.12$, $T_2 = 3.0$, and $T_3 = 6.0$ after the accuracy and convergence checks. For the specified cylindrically layered media, Fig. 4.3 to Fig. 4.5 depict three component amplitudes of electric field Green's function components, i.e., the $\widehat{\boldsymbol{\rho}}$-, $\widehat{\boldsymbol{\phi}}$-, and $\widehat{\boldsymbol{z}}$-components of electric field components due to a $\widehat{\boldsymbol{\rho}}$-oriented electric source while Fig. 4.6 to Fig. 4.8 show magnetic fields due to a $\widehat{\boldsymbol{\rho}}$-oriented electric source. To

demonstrate the correctness of the results, the numerically exact results are also obtained from the direct numerical integrations of the Sommerfeld-type integrals and depicted in Fig. 4.3 to Fig. 4.8. It is seen from the comparison that the agreement between the two sets of results is excellent, thus confirming the good accuracy and applicability of the applied approach and the developed source codes. Figs.(4.9-4.14) show the corresponding Green's functions components displayed in Figs.(4.3-4.8) but in larger $(z - z')$. In order to seen the wave phenomenon in this range, $k_0(z - z')$ rather than $\log_{10}|k_0(z - z')|$ is used for the horizontal axial scale.

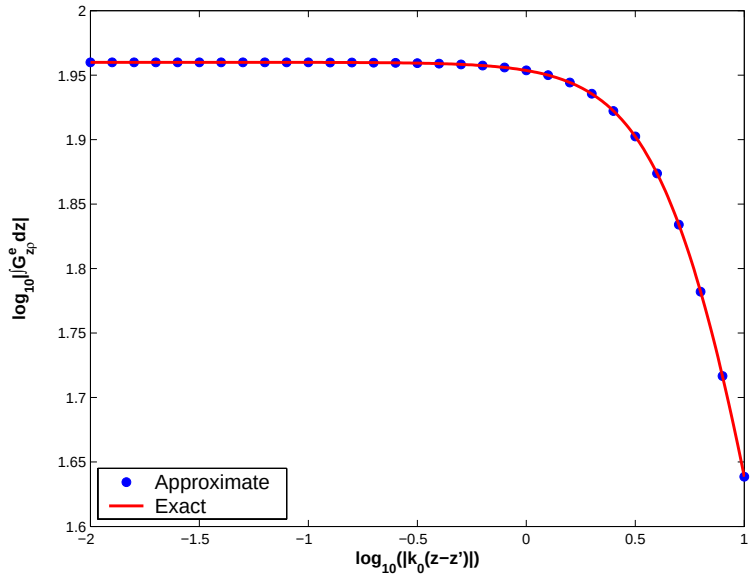

Figure 4.3: Magnitude of the Green's function component $\int G^e_{z\rho} dz$. The dielectric and geometrical parameters in Fig. 4.2 are: $\epsilon_{r_1} = 2.5$, $\mu_{r_1} = 1$; $\epsilon_{r_2} = 3.8$, $\mu_{r_2} = 1$; $\epsilon_{r_3} = 1$, $\mu_{r_3} = 1$; $a_1 = 51$ mm, $a_2 = 52$ mm, and $a_3 = 53$ mm.

As in [81], the other components of the electric field Green's functions for cylindrically multilayered media have been obtained for a specific angle. In this work, we extend the work by including more angles from 0 to 360 degrees and plotted them in three-dimension(due to ϕ-oriented and z-oriented electric source) in Fig. 4.15 to Fig. 4.18.

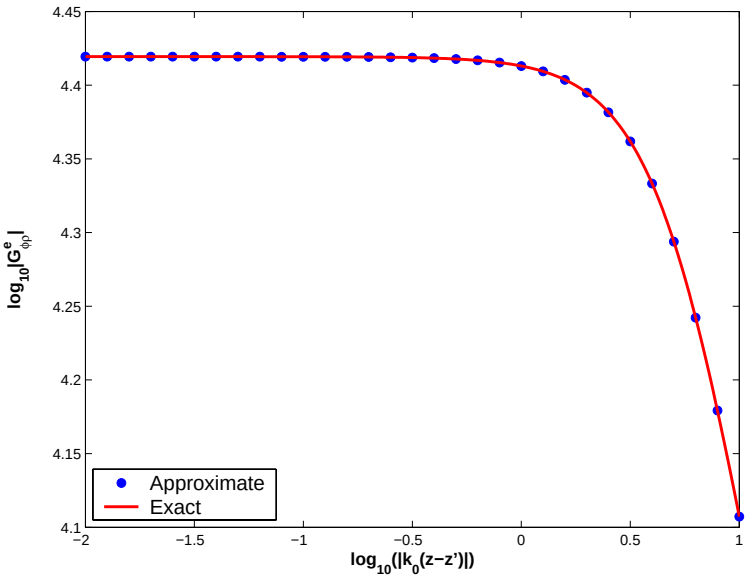

Figure 4.4: Magnitude of the Green's function component $G^e_{\phi\rho}$. The dielectric and geometrical parameters in Fig. 4.2 are: $\epsilon_{r_1} = 2.5$, $\mu_{r_1} = 1$; $\epsilon_{r_2} = 3.8$, $\mu_{r_2} = 1$; $\epsilon_{r_3} = 1$, $\mu_{r_3} = 1$; $a_1 = 51$ mm, $a_2 = 52$ mm, and $a_3 = 53$ mm.

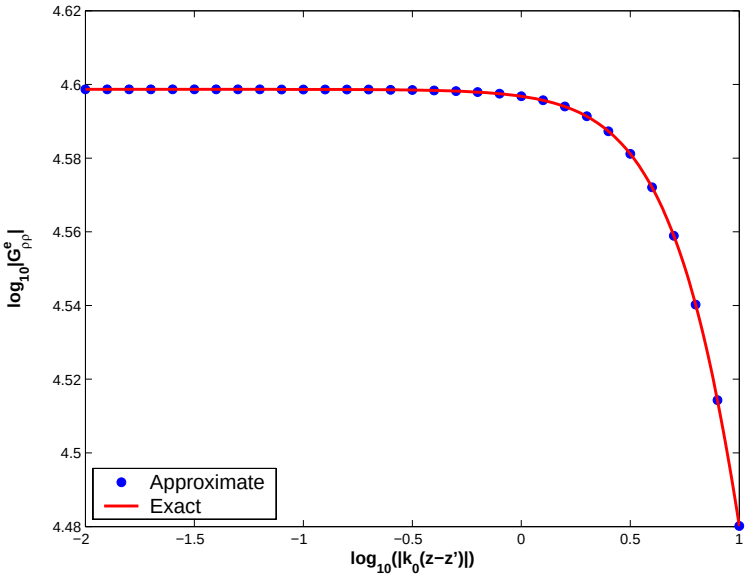

Figure 4.5: Magnitude of the Green's function component $G^e_{\rho\rho}$. The dielectric and geometrical parameters in Fig. 4.2 are: $\epsilon_{r_1} = 2.5$, $\mu_{r_1} = 1$; $\epsilon_{r_2} = 3.8$, $\mu_{r_2} = 1$; $\epsilon_{r_3} = 1$, $\mu_{r_3} = 1$; $a_1 = 51$ mm, $a_2 = 52$ mm, and $a_3 = 53$ mm.

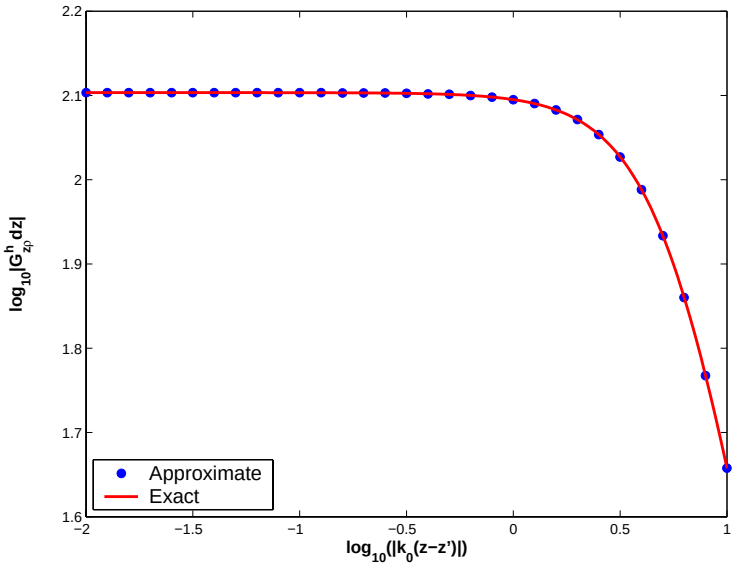

Figure 4.6: Magnitude of the Green's function component $G^h_{z\rho}$. The dielectric and geometrical parameters in Fig. 4.2 are: $\epsilon_{r_1} = 2.5$, $\mu_{r_1} = 1$; $\epsilon_{r_2} = 3.8$, $\mu_{r_2} = 1$; $\epsilon_{r_3} = 1$, $\mu_{r_3} = 1$; $a_1 = 51$ mm, $a_2 = 52$ mm, and $a_3 = 53$ mm.

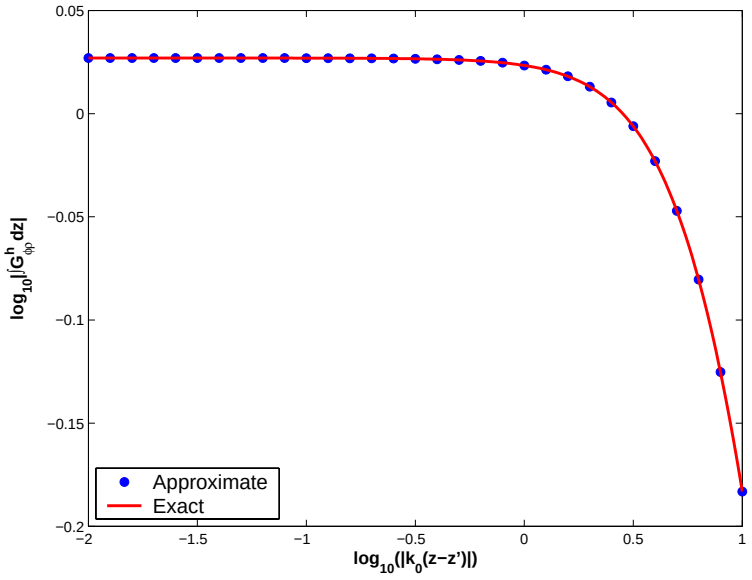

Figure 4.7: Magnitude of the Green's function component $\int G^h_{\phi\rho} dz$. The dielectric and geometrical parameters in Fig. 4.2 are: $\epsilon_{r_1} = 2.5$, $\mu_{r_1} = 1$; $\epsilon_{r_2} = 3.8$, $\mu_{r_2} = 1$; $\epsilon_{r_3} = 1$, $\mu_{r_3} = 1$; $a_1 = 51$ mm, $a_2 = 52$ mm, and $a_3 = 53$ mm.

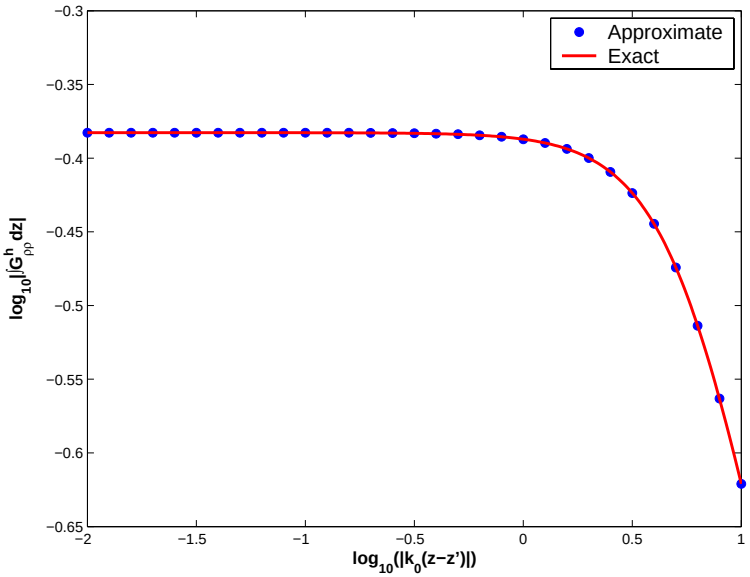

Figure 4.8: Magnitude of the Green's function component $\int G^h_{\rho\rho} dz$. The dielectric and geometrical parameters in Fig. 4.2 are: $\epsilon_{r_1} = 2.5$, $\mu_{r_1} = 1$; $\epsilon_{r_2} = 3.8$, $\mu_{r_2} = 1$; $\epsilon_{r_3} = 1$, $\mu_{r_3} = 1$; $a_1 = 51$ mm, $a_2 = 52$ mm, and $a_3 = 53$ mm.

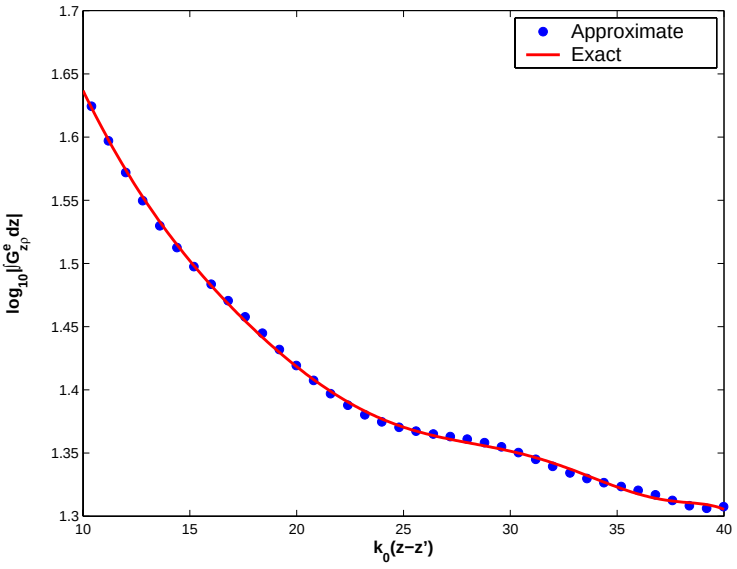

Figure 4.9: Magnitude of the Green's function component $\int G^e_{z\rho} dz$. The dielectric and geometrical parameters in Fig. 4.2 are: $\epsilon_{r_1} = 2.5$, $\mu_{r_1} = 1$; $\epsilon_{r_2} = 3.8$, $\mu_{r_2} = 1$; $\epsilon_{r_3} = 1$, $\mu_{r_3} = 1$; $a_1 = 51$ mm, $a_2 = 52$ mm, and $a_3 = 53$ mm.

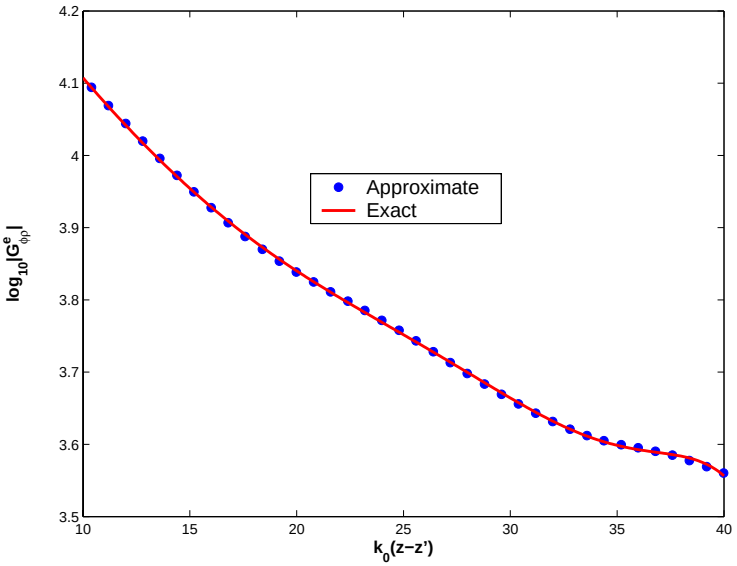

Figure 4.10: Magnitude of the Green's function component $G^e_{\phi\rho}$. The dielectric and geometrical parameters in Fig. 4.2 are: $\epsilon_{r_1} = 2.5$, $\mu_{r_1} = 1$; $\epsilon_{r_2} = 3.8$, $\mu_{r_2} = 1$; $\epsilon_{r_3} = 1$, $\mu_{r_3} = 1$; $a_1 = 51$ mm, $a_2 = 52$ mm, and $a_3 = 53$ mm.

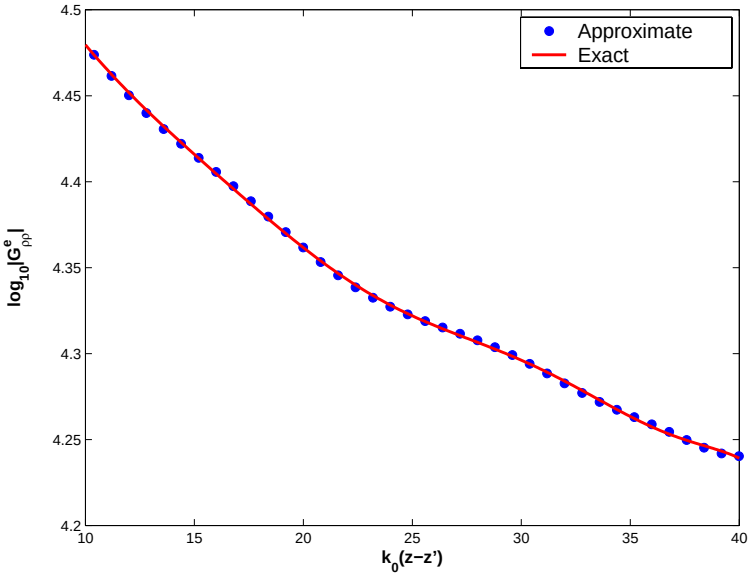

Figure 4.11: Magnitude of the Green's function component $G^e_{\rho\rho}$. The dielectric and geometrical parameters in Fig. 4.2 are: $\epsilon_{r_1} = 2.5$, $\mu_{r_1} = 1$; $\epsilon_{r_2} = 3.8$, $\mu_{r_2} = 1$; $\epsilon_{r_3} = 1$, $\mu_{r_3} = 1$; $a_1 = 51$ mm, $a_2 = 52$ mm, and $a_3 = 53$ mm.

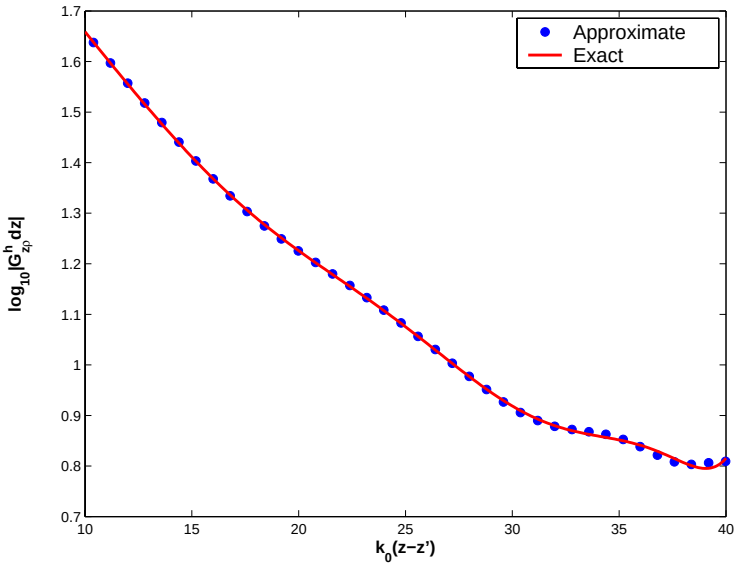

Figure 4.12: Magnitude of the Green's function component $G^h_{z\rho}$. The dielectric and geometrical parameters in Fig. 4.2 are: $\epsilon_{r_1} = 2.5$, $\mu_{r_1} = 1$; $\epsilon_{r_2} = 3.8$, $\mu_{r_2} = 1$; $\epsilon_{r_3} = 1$, $\mu_{r_3} = 1$; $a_1 = 51$ mm, $a_2 = 52$ mm, and $a_3 = 53$ mm.

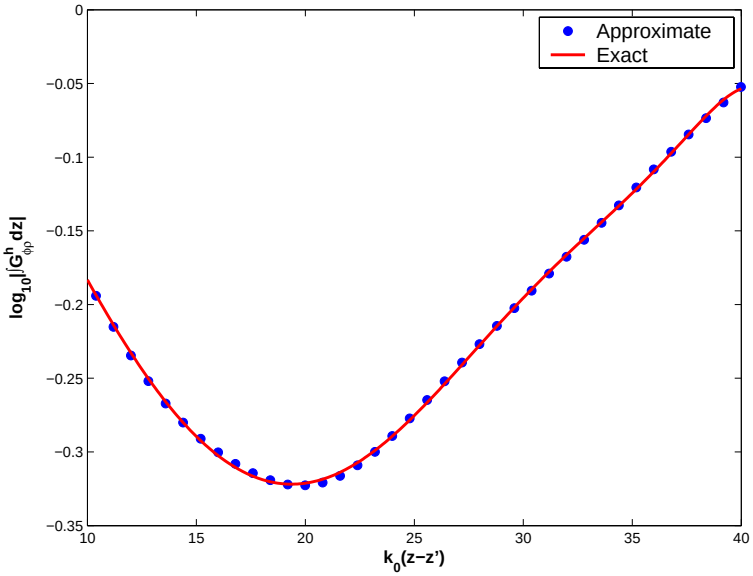

Figure 4.13: Magnitude of the Green's function component $\int G^h_{\phi\rho} dz$. The dielectric and geometrical parameters in Fig. 4.2 are: $\epsilon_{r_1} = 2.5$, $\mu_{r_1} = 1$; $\epsilon_{r_2} = 3.8$, $\mu_{r_2} = 1$; $\epsilon_{r_3} = 1$, $\mu_{r_3} = 1$; $a_1 = 51$ mm, $a_2 = 52$ mm, and $a_3 = 53$ mm.

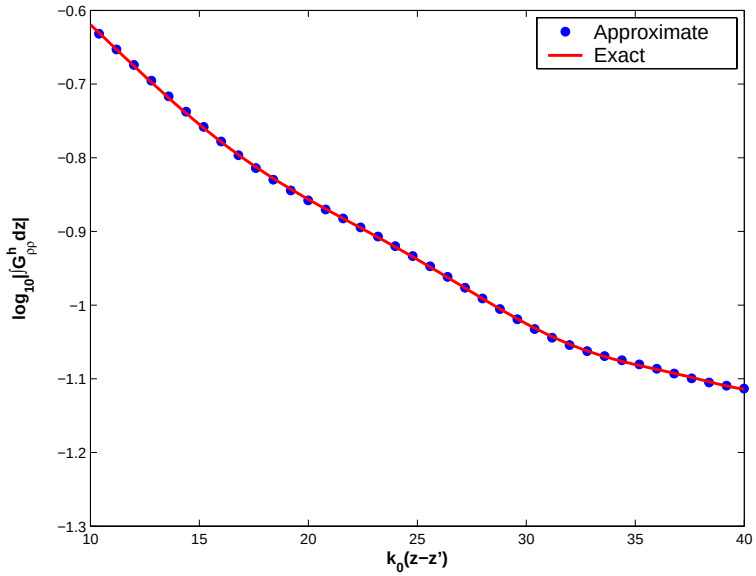

Figure 4.14: Magnitude of the Green's function component $\int G^h_{\rho\rho} dz$. The dielectric and geometrical parameters in Fig. 4.2 are: $\epsilon_{r_1} = 2.5$, $\mu_{r_1} = 1$; $\epsilon_{r_2} = 3.8$, $\mu_{r_2} = 1$; $\epsilon_{r_3} = 1$, $\mu_{r_3} = 1$; $a_1 = 51$ mm, $a_2 = 52$ mm, and $a_3 = 53$ mm.

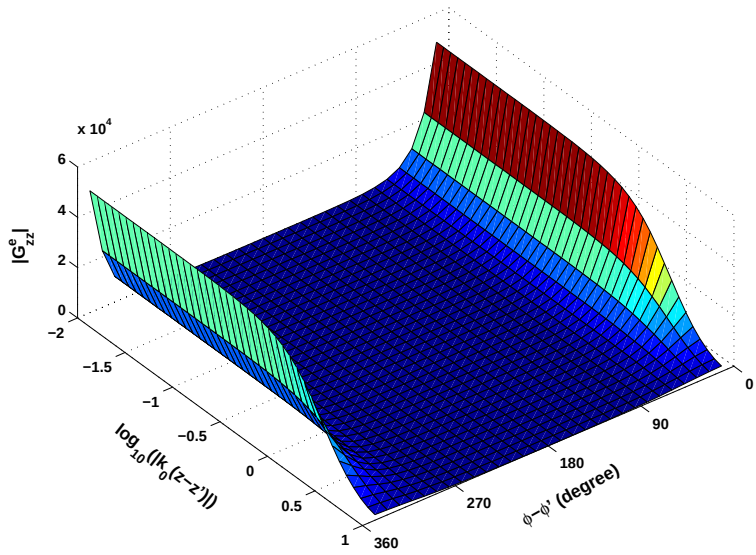

Figure 4.15: Magnitude of the Green's function component G^e_{zz}. The dielectric and geometrical parameters in Fig. 4.2 are: $\epsilon_{r_1} = 2.5$, $\mu_{r_1} = 1$; $\epsilon_{r_2} = 3.8$, $\mu_{r_2} = 1$; $\epsilon_{r_3} = 1$, $\mu_{r_3} = 1$; $a_1 = 51$ mm, $a_2 = 52$ mm, and $a_3 = 53$ mm.

Compared with the existing data, the current results agree very well, but cover more azimuth angles.

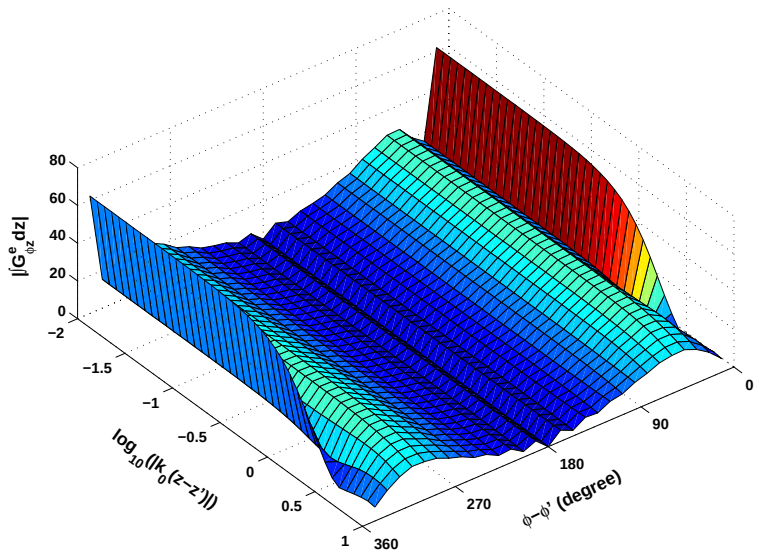

Figure 4.16: Magnitude of the Green's function component $\int G^e_{\phi z} dz$. The dielectric and geometrical parameters in Fig. 4.2 are: $\epsilon_{r_1} = 2.5$, $\mu_{r_1} = 1$; $\epsilon_{r_2} = 3.8$, $\mu_{r_2} = 1$; $\epsilon_{r_3} = 1$, $\mu_{r_3} = 1$; $a_1 = 51$ mm, $a_2 = 52$ mm, and $a_3 = 53$ mm.

4.5 Summary

This chapter has presented for the first time the complete dyadic Green's functions components in fast computational form for defining electromagnetic field components due to an arbitrary oriented electric or magnetic source located in a conducting cylinder coated with multilayered dielectric materials. The exact results of these dyadic Green's functions components are also obtained and compared with the newly obtained approximate results. The comparison shows that the approximate results are very close to the exact data and the accuracy of the GPOF approach is very good. In addition, the same procedure as in [81] has been repeated, but more results are obtained for different

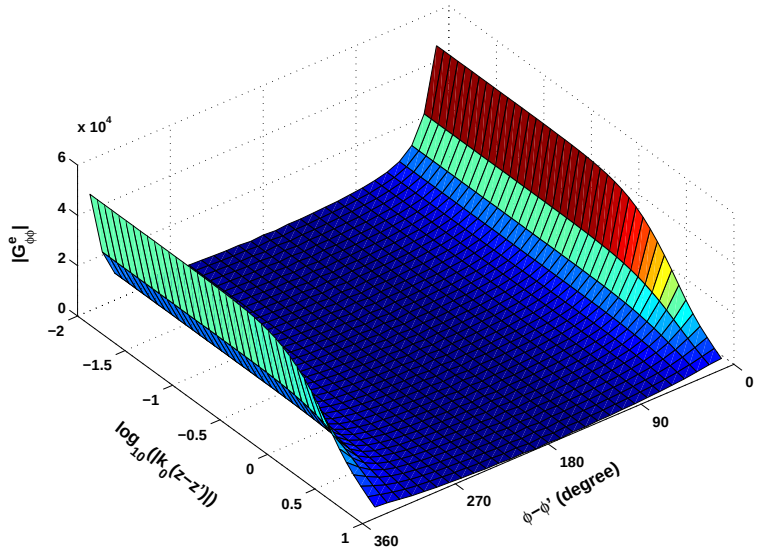

Figure 4.17: Magnitude of the Green's function component $G^e_{\phi\phi}$. The dielectric and geometrical parameters in Fig. 4.2 are: $\epsilon_{r_1} = 2.5$, $\mu_{r_1} = 1$; $\epsilon_{r_2} = 3.8$, $\mu_{r_2} = 1$; $\epsilon_{r_3} = 1$, $\mu_{r_3} = 1$; $a_1 = 51$ mm, $a_2 = 52$ mm, and $a_3 = 53$ mm.

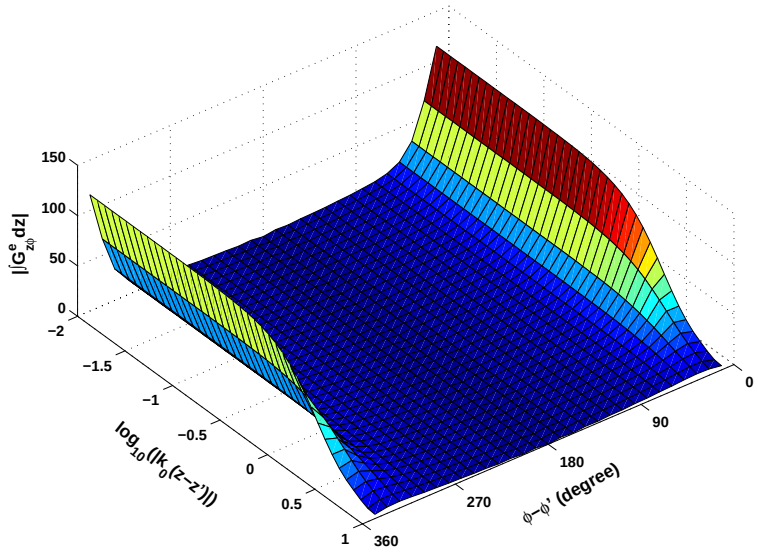

Figure 4.18: Magnitude of the Green's function component $\int G^e_{z\phi} dz$. The dielectric and geometrical parameters in Fig. 4.2 are: $\epsilon_{r_1} = 2.5$, $\mu_{r_1} = 1$; $\epsilon_{r_2} = 3.8$, $\mu_{r_2} = 1$; $\epsilon_{r_3} = 1$, $\mu_{r_3} = 1$; $a_1 = 51$ mm, $a_2 = 52$ mm, and $a_3 = 53$ mm.

azimuth angles ranging from 0 to 360 degrees. The Green's functions studied in this chapter are for the case where the source point and the observation point are not located on the same cylindrical surface, i.e., $\rho \neq \rho'$, where no convergence problem occurs in Eq. (4.1) for the summation of cylindrical eigenmodes. However, it is found that the convergence problem will appear for the summation of cylindrical eigenmodes in Eq. (4.1) when $\rho = \rho'$. How to calculate the spatial domain Green's functions when $\rho = \rho'$ will be discussed in Chapter 6. A study on the recursive relations in Chapter 5 will be presented first as the basis of discussions in Chapter 6.

Chapter 5

Accurate Calculation of Integer Order Cylindrical Eigenmodes

The spatial domain Green's functions are the inverse Fourier transform of the spectral domain Green's functions. The inverse Fourier transform includes a summation of the cylindrical eigenmodes over integer index n, which is also the order of the special function, and a integral of the resultant summation over complex number k_z, which is the wavenumber in z direction. When the source point and the observation point are not located on the same cylindrical surface, the evaluation of the spatial domain Green's functions becomes difficult because convergence problems occur in the summation process. Evaluation of larger cylindrical eigenmodes is necessary, and it is an extremely challenging task because of numerical overflow and highly oscillating behaviour of the special functions involved in the cylindrical eigenmodes. In [79] which dealt with one-layer coated PEC cylinder, the problem was solved by using recursive relations. For multilayer coated PEC cylinder, the expressions of Green's functions become extremely complex and hence the recursive relations provided in [79] are not adequate enough for the calculation purpose. In this chapter, more general recursive relations are summarized

for cylindrically multilayered media. In order to make use of these recursive relations, the spectral domain Green's functions derived using 2×2 matrix method, which are presented in Chapter 4, are re-arranged into an new form. To verify the validity, the Green's functions based on the 4×4 matrix method are newly presented in the recursive form. The Green's functions in 4×4 matrix form also provide us another choice of programming.

5.1 Recursive Formulations of Ratios of Special Functions

In this section, in total seventeen recursive formulations are presented with detailed derivations subsequently. They are categorized into three groups: the basic ratios, simple ratios and ratios of certain combinations of special functions according to their similarities.

5.1.1 Basic Ratios of Special Functions

First, we introduce three basic recursive relations of the ratios of special functions. These special functions are Bessel functions of the first and second kind, Hankel function of the first kind.

$$P_m(a) = \frac{J_{m+1}(a)}{J_m(a)}, \tag{5.1}$$

$$Q_m(a) = \frac{N_{m+1}(a)}{N_m(a)}, \tag{5.2}$$

$$R_m(a) = \frac{H^{(1)}_{m+1}(a)}{H^{(1)}_m(a)}, \tag{5.3}$$

$P_m(a)$, $Q_m(a)$, $R_m(a)$ are the three basic quantities that can be evaluated using recursive relations. More discussion on these three quantities will appear in Section 5.4. The quantities in the following two subsections are obtained in recursive forms if the above three basic quantities are in used.

5.1.2 Simple Ratios of Special Functions

In the basic ratios of special functions, only one argument a is involved. The following simple ratios of special functions include two arguments a and b.

$$\begin{aligned} G_m^J(a,b) &= \frac{J_m(b)}{J_m(a)}, \\ G_{m+1}^J(a,b) &= \frac{P_m(b)}{P_m(a)} \cdot G_m^J(a,b), \end{aligned} \tag{5.4}$$

$$\begin{aligned} G_m^H(a,b) &= \frac{H_m^{(1)}(b)}{H_m^{(1)}(a)}, \\ G_{m+1}^H(a,b) &= \frac{R_m(b)}{R_m(a)} \cdot G_m^H(a,b), \end{aligned} \tag{5.5}$$

$$\begin{aligned} G_m^{JH}(a,b) &= J_m(a) \cdot H_m^{(1)}(b), \\ G_{m+1}^{JH}(a,b) &= P_m(b) \cdot R_m(a) \cdot G_m^{JH}(a,b), \end{aligned} \tag{5.6}$$

$$\begin{aligned} G_m^{JN}(a,b) &= \frac{N_m(a) \cdot J_m(b)}{N_m(b) \cdot J_m(a)}, \\ G_{m+1}^{JN}(a,b) &= \frac{Q_m(a) \cdot P_m(b)}{Q_m(b) \cdot P_m(a)} \cdot G_m^{JN}(a,b). \end{aligned} \tag{5.7}$$

Eqs. (5.4-5.7) are in explicit recursive forms.

$$\begin{aligned} G_m'^J(a,b) &= \frac{J_{m+1}(b)}{J_m(a)} \\ &= \frac{J_{m+1}(b)}{J_{m+1}(a)} \cdot \frac{J_{m+1}(a)}{J_m(a)} \\ &= G_{m+1}^J(a,b) \cdot P_m(a), \end{aligned} \tag{5.8}$$

$$\begin{aligned} G_m'^H(a,b) &= \frac{H_{m+1}^{(1)}(b)}{H_m^{(1)}(a)} \\ &= \frac{H_{m+1}^{(1)}(b)}{H_{m+1}^{(1)}(a)} \cdot \frac{H_{m+1}^{(1)}(a)}{H_m^{(1)}(a)} \\ &= G_{m+1}^H(a,b) \cdot R_m(a), \end{aligned} \tag{5.9}$$

$$\begin{aligned} G_m^{\prime\prime J}(a,b) &= \frac{J_m'(b)}{J_m(a)} \\ &= \frac{-J_{m+1}(b)+\frac{m}{b}\cdot J_m(b)}{J_m(a)} \\ &= -G_m^{\prime J}(a,b)+\frac{m}{b}\cdot G_m^J(a,b), \end{aligned} \tag{5.10}$$

$$\begin{aligned} G_m^{\prime\prime H}(a,b) &= \frac{H_m^{'(1)}(b)}{H_m^{(1)}(a)} \\ &= \frac{-H_{m+1}^{(1)}(b)+\frac{m}{b}\cdot H_m^{(1)}(b)}{H_m^{(1)}(a)} \\ &= -G_m^{\prime H}(a,b)+\frac{m}{b}\cdot G_m^H(a,b). \end{aligned} \tag{5.11}$$

Eqs. (5.8-5.11) are in recursive forms if recursive relations (5.1-5.7) are taken into account.

5.1.3 Ratios of Certain Combinations of Special Functions

Consider some ratios of certain combinations of special functions as follows,

$$\begin{aligned} \frac{r(a,b)}{p(a,b)} &= \frac{N_m(a)\cdot J_m(b)-J_m(a)\cdot N_m(b)}{N_m(a)\cdot J_m(b)-J_m(a)\cdot N_m(b)} \\ &= \frac{m}{b}-\frac{N_m(a)\cdot J_{m+1}(b)-J_m(a)\cdot N_{m+1}(b)}{N_m(a)\cdot J_m(b)-J_m(a)\cdot N_m(b)} \\ &= \frac{m}{b}-\frac{\frac{J_{m+1}(b)}{J_m(b)}-\frac{J_m(a)\cdot N_{m+1}(b)}{N_m(a)\cdot J_m(b)}}{1-\frac{N_m(b)\cdot J_m(a)}{N_m(a)\cdot J_m(b)}} \\ &= \frac{m}{b}-\frac{J_{m+1}(b)}{J_m(b)}-\frac{2}{\pi b}\cdot\frac{J_m(a)}{J_m(b)}\cdot\frac{1}{N_m(a)\cdot J_m(b)-N_m(b)\cdot J_m(a)} \\ &= \frac{m}{b}-P_m(b)-\frac{P_m(b)-Q_m(b)}{G_m^{JN}(a,b)-1}, \end{aligned} \tag{5.12}$$

$$\begin{aligned} \frac{q(a,b)}{p(a,b)} &= \frac{N_m'(a)\cdot J_m(b)-J_m'(a)\cdot N_m(b)}{N_m(a)\cdot J_m(b)-J_m(a)\cdot N_m(b)} \\ &= \frac{m}{a}-\frac{N_{m+1}(a)\cdot J_m(b)-J_{m+1}(a)\cdot N_m(b)}{N_m(a)\cdot J_m(b)-J_m(a)\cdot N_m(b)} \\ &= \frac{m}{a}-\frac{N_{m+1}(a)}{N_m(a)}-\frac{\frac{N_m(b)}{J_m(b)}\cdot\frac{N_{m+1}(a)\cdot J_m(a)-J_{m+1}(a)\cdot m(a)}{N_m(a)\cdot N_m(a)}}{1-\frac{J_m(a)\cdot N_m(b)}{N_m(a)\cdot J_m(b)}} \\ &= \frac{m}{a}-\frac{N_{m+1}(a)}{N_m(a)}+\frac{2}{\pi a}\cdot\frac{N_m(b)}{N_m(a)}\frac{1}{N_m(a)\cdot J_m(b)-N_m(b)\cdot J_m(a)} \end{aligned}$$

$$= \frac{m}{a} - Q_m(a) + \frac{P_m(a) - Q_m(a)}{G_m^{JN}(a,b) - 1}, \tag{5.13}$$

$$\begin{aligned}
\frac{s(a,b)}{p(a,b)} &= \frac{N'_m(a)\cdot J'_m(b) - J'_m(a)\cdot N'_m(b)}{N_m(a)\cdot J_m(b) - J_m(a)\cdot N_m(b)} \\
&= \frac{m^2}{ab} - \frac{m}{a}\frac{N_m(a)\cdot J_{m+1}(b) - J_m(a)\cdot N_{m+1}(b)}{N_m(a)\cdot J_m(b) - J_m(a)\cdot N_m(b)} \\
&\quad -\frac{m}{b}\cdot\frac{N_{m+1}(a)\cdot J_m(b) - J_{m+1}(a)\cdot N_m(b)}{N_m(a)\cdot J_m(b) - J_m(a)\cdot N_m(b)} \\
&\quad +\frac{N_{m+1}(a)\cdot J_{m+1}(b) - J_{m+1}(a)\cdot N_{m+1}(b)}{N_m(a)\cdot J_m(b) - J_m(a)\cdot N_m(b)} \\
&= \frac{m^2}{ab} - \frac{m}{a}\cdot\left[P_m(b) + \frac{P_m(b) - Q_m(b)}{G_m^{JN}(a,b) - 1}\right] - \frac{m}{b}\cdot\left[Q_m(a) - \frac{P_m(a) - Q_m(a)}{G_m^{JN}(a,b) - 1}\right] \\
&\quad +\frac{Q_m(a)\cdot P_m(b)\cdot G_m^{JN}(a,b) - Q_m(b)\cdot P_m(a)}{G_m^{JN}(a,b) - 1},
\end{aligned} \tag{5.14}$$

$$\begin{aligned}
\frac{r(a,b)}{q(a,b)} &= \frac{N_m(a)\cdot J'_m(b) - J_m(a)\cdot N'_m(b)}{N'_m(a)\cdot J_m(b) - J'_m(a)\cdot N_m(b)} \\
&= \frac{\frac{m}{b}\left[N_m(a)\cdot J_m(b) - J_m(a)\cdot N_m(b)\right] - \left[N_m(a)\cdot J_{m+1}(b) - J_m(a)\cdot N_{m+1}(b)\right]}{\frac{m}{a}\left[N_m(a)\cdot J_m(b) - J_m(a)\cdot N_m(b)\right] - \left[N_{m+1}(a)\cdot J_m(b) - J_{m+1}(a)\cdot N_m(b)\right]} \\
&= \frac{\frac{m}{b} - \left[P_m(b) + \frac{P_m(b) - Q_m(b)}{G_m^{JN}(a,b) - 1}\right]}{\frac{m}{a} - \left[Q_m(a) - \frac{P_m(a) - Q_m(a)}{G_m^{JN}(a,b) - 1}\right]},
\end{aligned} \tag{5.15}$$

$$\begin{aligned}
\frac{s(a,b)}{q(a,b)} &= \frac{N'_m(a)\cdot J'_m(b) - J'_m(a)\cdot N'_m(b)}{N'_m(a)\cdot J_m(b) - J'_m(a)\cdot N_m(b)} \\
&= \frac{m}{b} - \frac{N'_m(a)\cdot J_{m+1}(b) - J'_m(a)\cdot N_{m+1}(b)}{N'_m(a)\cdot J_m(b) - J'_m(a)\cdot N_m(b)} \\
&= \frac{m}{b} - \frac{m}{a}\frac{N_m(a)\cdot J_{m+1}(b) - J_m(a)\cdot N_{m+1}(b)}{N'_m(a)\cdot J_m(b) - J'_m(a)\cdot N_m(b)} \\
&\quad -\frac{N_{m+1}(a)\cdot J_{m+1}(b) - J_{m+1}(a)\cdot N_{m+1}(b)}{N'_m(a)\cdot J_m(b) - J'_m(a)\cdot N_m(b)} \\
&= \frac{m}{b} - \frac{m}{a}\cdot\frac{P_m(b) + \frac{P_m(b) - Q_m(b)}{G_m^{JN}(a,b) - 1}}{\frac{m}{a} - \left[Q_m(a) - \frac{P_m(a) - Q_m(a)}{G_m^{JN}(a,b) - 1}\right]} - \frac{\frac{Q_m(a)\cdot P_m(b)\cdot G_m^{JN}(a,b) - Q_m(b)\cdot P_m(a)}{G_m^{JN}(a,b) - 1}}{\frac{m}{a} - \left[Q_m(a) - \frac{P_m(a) - Q_m(a)}{G_m^{JN}(a,b) - 1}\right]},
\end{aligned} \tag{5.16}$$

$$\begin{aligned}
\frac{s(a,b)}{r(a,b)} &= \frac{N'_m(a)\cdot J'_m(b) - J'_m(a)\cdot N'_m(b)}{N_m(a)\cdot J'_m(b) - J_m(a)\cdot N'_m(b)} \\
&= \frac{m}{b} - \frac{N_{m+1}(a)\cdot J'_m(b) - J_{m+1}(a)\cdot N'_m(b)}{N_m(a)\cdot J'_m(b) - J_m(a)\cdot N'_m(b)}
\end{aligned}$$

$$
\begin{aligned}
&= \frac{m}{a} - \frac{\frac{m}{b}\cdot\frac{N_{m+1}(a)\cdot J_m(b)-J_{m+1}(a)\cdot N_m(b)}{N_m(a)\cdot J_m(b)-J_m(a)\cdot N_m(b)} - \frac{N_{m+1}(a)\cdot J_{m+1}(b)-J_{m+1}(a)\cdot N_{m+1}(b)}{N_m(a)\cdot J_m(b)-J_m(a)\cdot N_m(b)}}{\frac{m}{b} - \frac{N_m(a)\cdot J_{m+1}(b)-J_m(a)\cdot N_{m+1}(b)}{N_m(a)\cdot J_m(b)-J_m(a)\cdot N_m(b)}} \\
&= \frac{m}{a} - \frac{\frac{m}{b}\cdot\left[Q_m(a) - \frac{P_m(a)-Q_m(a)}{G_m^{JN}(a,b)-1} - \frac{Q_m(a)\cdot P_m(a)\cdot G_m^{JN}(a,b)-Q_m(b)\cdot P_m(a)}{G_m^{JN}(a,b)-1}\right]}{\frac{m}{b} - \left[P_m(b) + \frac{P_m(b)-Q_m(b)}{G_m^{JN}(a,b)-1}\right]}.
\end{aligned}
\tag{5.17}
$$

Eqs. (5.12)-(5.17) are in recursive forms when we consider the recursive relations (5.1-5.4) and (5.7). These formulations will be used in the next two sections to reformulate the expressions of electric field Green's functions. The implementation and numerical stability of these recursive relations are to be discussed in Section 5.4.

5.2 Reformulation of the Green's Functions: 2×2 Matrix Method

The Green's functions are first re-arranged based on the 2×2 matrix method [62], then re-arrangement is also made for the Green's functions derived using 4×4 matrix method [78, 79]. The equivalence between these two forms of Green's functions will be shown by numerical results in Section 5.4.

5.2.1 Original Transmission and Reflection Matrices

For convenient discussion, the quantities used in Chapter 3 are rewritten here, referred to as original quantities. The j and i represent the indexes of source layer and field layer, respectively.

Multi-reflection matrix $\widetilde{\overline{\boldsymbol{M}}}$:

$$\text{for } i > j: \tag{5.18}$$

$$\widetilde{\overline{\boldsymbol{M}}}_i = (\overline{\boldsymbol{I}} - \overline{\boldsymbol{R}}_{i,i-1}\cdot\widetilde{\overline{\boldsymbol{R}}}_{i,i+1})^{-1}, \tag{5.19}$$

$$\widetilde{\overline{\boldsymbol{M}}}_j = (\overline{\boldsymbol{I}} - \widetilde{\overline{\boldsymbol{R}}}_{j,j-1}\cdot\widetilde{\overline{\boldsymbol{R}}}_{j,j+1})^{-1}, \tag{5.20}$$

$$\text{for } i < j: \tag{5.21}$$

$$\widetilde{\overline{\boldsymbol{M}}}_i = (\overline{\boldsymbol{I}} - \overline{\boldsymbol{R}}_{i,i+1} \cdot \widetilde{\overline{\boldsymbol{R}}}_{i,i-1})^{-1}, \tag{5.22}$$

$$\widetilde{\overline{\boldsymbol{M}}}_j = (\overline{\boldsymbol{I}} - \widetilde{\overline{\boldsymbol{R}}}_{j,j+1} \cdot \widetilde{\overline{\boldsymbol{R}}}_{j,j-1})^{-1}, \tag{5.23}$$

$$\text{for } i = j: \tag{5.24}$$

$$\widetilde{\overline{\boldsymbol{M}}}_j = \begin{cases} (\overline{\boldsymbol{I}} - \widetilde{\overline{\boldsymbol{R}}}_{j,j-1} \cdot \widetilde{\overline{\boldsymbol{R}}}_{j,j+1})^{-1}, & \rho > \rho', \\ (\overline{\boldsymbol{I}} - \widetilde{\overline{\boldsymbol{R}}}_{j,j+1} \cdot \widetilde{\overline{\boldsymbol{R}}}_{j,j-1})^{-1}, & \rho < \rho'. \end{cases} \tag{5.25}$$

Generalized transmission matrix $\widetilde{\overline{\boldsymbol{T}}}$:

$$\widetilde{\overline{\boldsymbol{T}}}_{ji} = \overline{\boldsymbol{T}}_{i-1,i} \cdot \overline{\boldsymbol{S}}_{i-2,i-1} \cdot \cdots \cdot \overline{\boldsymbol{S}}_{j,j+1}, \qquad j < i, \tag{5.26}$$

where

$$\bar{\boldsymbol{S}}_{i,i+1} = (\bar{\boldsymbol{I}} - \overline{\boldsymbol{R}}_{i+1,i} \cdot \widetilde{\overline{\boldsymbol{R}}}_{i+1,i+2})^{-1} \cdot \overline{\boldsymbol{T}}_{i,i+1}, \tag{5.27}$$

and

$$\widetilde{\overline{\boldsymbol{T}}}_{ji} = \overline{\boldsymbol{T}}_{i+1,i} \cdot \overline{\boldsymbol{S}}_{i+2,i+1} \cdot \cdots \cdot \overline{\boldsymbol{S}}_{j,j-1}, \qquad j > i, \tag{5.28}$$

where

$$\overline{\boldsymbol{S}}_{i,i-1} = (\overline{\boldsymbol{I}} - \overline{\boldsymbol{R}}_{i-1,i} \cdot \widetilde{\overline{\boldsymbol{R}}}_{i-1,i-2})^{-1} \cdot \overline{\boldsymbol{T}}_{i,i-1}. \tag{5.29}$$

Generalized reflection matrix $\widetilde{\overline{\boldsymbol{R}}}$:

$$\widetilde{\overline{\boldsymbol{R}}}_{i,i+1} = \overline{\boldsymbol{R}}_{i,i+1} + \overline{\boldsymbol{T}}_{i+1,i} \cdot \widetilde{\overline{\boldsymbol{R}}}_{i+1,i+2} \cdot (\overline{\boldsymbol{I}} - \overline{\boldsymbol{R}}_{i,i+1} \cdot \widetilde{\overline{\boldsymbol{R}}}_{i+1,i+2})^{-1} \cdot \overline{\boldsymbol{T}}_{i,i+1}, \tag{5.30}$$

$$\widetilde{\overline{\boldsymbol{R}}}_{i,i-1} = \overline{\boldsymbol{R}}_{i,i-1} + \overline{\boldsymbol{T}}_{i-1,i} \cdot \widetilde{\overline{\boldsymbol{R}}}_{i-1,i-2} \cdot (\overline{\boldsymbol{I}} - \overline{\boldsymbol{R}}_{i-1,i} \cdot \widetilde{\overline{\boldsymbol{R}}}_{i-1,i-2})^{-1} \cdot \overline{\boldsymbol{T}}_{i,i+1}. \tag{5.31}$$

Local reflection matrix $\overline{\boldsymbol{R}}$:

$$\overline{\boldsymbol{R}}_{i+1,i} = \overline{\boldsymbol{D}}^{-1} \cdot [J_n(k_{i\rho}a) \cdot \overline{J}_n(k_{i+1\rho}a) - J_n(k_{i+1\rho}a) \cdot \overline{J}_n(k_{i\rho}a)], \tag{5.32}$$

$$\overline{\boldsymbol{R}}_{i,i+1} = \overline{\boldsymbol{D}}^{-1} \cdot [H_n^{(1)}(k_{i\rho}a) \cdot \overline{H}_n^{(1)}(k_{i+1\rho}a) - H_n^{(1)}(k_{i+1\rho}a) \cdot \overline{H}_n^{(1)}(k_{i\rho}a)]. \tag{5.33}$$

Local reflection matrix $\overline{\boldsymbol{T}}$:

$$\overline{\boldsymbol{T}}_{i+1,i} = \frac{2\omega}{\pi k_{i+1\rho} a} \cdot \overline{\boldsymbol{D}}^{-1} \cdot \begin{bmatrix} \epsilon_{i+1} & 0 \\ 0 & -\mu_{i+1} \end{bmatrix}, \tag{5.34}$$

$$\overline{\boldsymbol{T}}_{i,i+1} = \frac{2\omega}{\pi k_{i\rho} a} \cdot \overline{\boldsymbol{D}}^{-1} \cdot \begin{bmatrix} \epsilon_{i} & 0 \\ 0 & -\mu_{i} \end{bmatrix}. \tag{5.35}$$

Matrices $\overline{\boldsymbol{D}}$ and $\overline{\boldsymbol{B}}$:

$$\overline{\boldsymbol{D}} = [\overline{\boldsymbol{J}}_n(k_{i\rho}a) \cdot \overline{H}_n^{(1)}(k_{i+1\rho}a) - \overline{\boldsymbol{H}}_n^{(1)}(k_{i+1\rho}a) \cdot J_n(k_{i\rho}a)], \tag{5.36}$$

$$\overline{\boldsymbol{B}}(k_{i\rho}\rho) = \frac{1}{k_{i\rho}^2 \rho} \cdot \begin{bmatrix} i\omega\epsilon_i k_{i\rho}\rho B_n'(k_{i\rho}) & -nk_z B_n(k_{i\rho}\rho) \\ -nk_z B_n(k_{i\rho}\rho) & i\omega\mu_i k_{i\rho}\rho B_n'(k_{i\rho\rho}) \end{bmatrix}, \tag{5.37}$$

where $B_n(\bullet)$ and $B_n'(\bullet)$ represent $J_n(\bullet)$ and $J_n'(\bullet)$ or $H_n^{(1)}(\bullet)$ and $H'^{(1)}_n(\bullet)$, respectively.

For a two-layer coated PEC cylinder as shown in Fig. 5.1, the above quantities reduce to:

$\overline{\boldsymbol{D}}$ matrix:

$$\overline{\boldsymbol{D}}_{12} = \overline{\boldsymbol{J}}_n(k_{1\rho}a_2) \cdot H_n(k_{2\rho}a_2) - \overline{\boldsymbol{H}}_n^{(1)}(k_{2\rho}a_2) \cdot J_n(k_{1\rho}a_2), \tag{5.38}$$

$$\overline{\boldsymbol{D}}_{23} = \overline{\boldsymbol{J}}_n(k_{2\rho}a_3) \cdot H_n(k_{3\rho}a_3) - \overline{\boldsymbol{H}}_n^{(1)}(k_{3\rho}a_3) \cdot J_n(k_{2\rho}a_3). \tag{5.39}$$

Local and generalized reflection matrix:

$$\overline{\boldsymbol{R}}_{10} = \begin{bmatrix} -\frac{J_n(k_{1\rho}a_1)}{H_n(k_{1\rho}a_1)} & 0 \\ 0 & -\frac{J_n'(k_{1\rho}a_1)}{H_n'(k_{1\rho}a_1)} \end{bmatrix}, \tag{5.40}$$

$$\overline{\boldsymbol{R}}_{12} = \overline{\boldsymbol{D}}_{12}^{-1} \cdot \left[H_n(k_{1\rho}a_2) \cdot \overline{\boldsymbol{H}}_n^{(1)}(k_{2\rho}a_2) - H_n^{(1)}(k_{2\rho}a_2) \cdot \overline{\boldsymbol{H}}_n^{(1)}(k_{1\rho}a_2)\right], \tag{5.41}$$

$$\overline{\boldsymbol{R}}_{21} = \overline{\boldsymbol{D}}_{12}^{-1} \cdot \left[J_n(k_{1\rho}a_2) \cdot \overline{\boldsymbol{J}}_n(k_{2\rho}a_2) - J_n(k_{2\rho}a_2) \cdot \overline{\boldsymbol{J}}_n(k_{1\rho}a_2)\right], \tag{5.42}$$

$$\widetilde{\overline{\boldsymbol{R}}}_{12} = \overline{\boldsymbol{R}}_{12} + \overline{\boldsymbol{T}}_{21} \cdot \widetilde{\overline{\boldsymbol{R}}}_{23} \cdot (\overline{\boldsymbol{I}} - \overline{\boldsymbol{R}}_{21} \cdot \widetilde{\overline{\boldsymbol{R}}}_{23})^{-1} \cdot \overline{\boldsymbol{T}}_{12}, \tag{5.43}$$

$$\widetilde{\overline{\boldsymbol{R}}}_{21} = \overline{\boldsymbol{R}}_{21} + \overline{\boldsymbol{T}}_{12} \cdot \widetilde{\overline{\boldsymbol{R}}}_{10} \cdot (\overline{\boldsymbol{I}} - \overline{\boldsymbol{R}}_{12} \cdot \widetilde{\overline{\boldsymbol{R}}}_{10})^{-1} \cdot \overline{\boldsymbol{T}}_{21}, \tag{5.44}$$

$$\widetilde{\overline{\boldsymbol{R}}}_{23} = \overline{\boldsymbol{D}}_{23}^{-1} \cdot \left[H_n(k_{2\rho}a_3) \cdot \overline{\boldsymbol{H}}_n^{(1)}(k_{3\rho}a_3) - H_n^{(1)}(k_{3\rho}a_3) \cdot \overline{\boldsymbol{H}}_n^{(1)}(k_{2\rho}a_3)\right], \tag{5.45}$$

$$\overline{\boldsymbol{R}}_{23} = \overline{\boldsymbol{D}}_{23}^{-1} \cdot \left[H_n(k_{2\rho}a_3) \cdot \overline{\boldsymbol{H}}_n^{(1)}(k_{3\rho}a_3) - H_n^{(1)}(k_{3\rho}a_3) \cdot \overline{\boldsymbol{H}}_n^{(1)}(k_{2\rho}a_3)\right], \tag{5.46}$$

Local transmission matrix:

$$\overline{\boldsymbol{T}}_{12} = \frac{2\omega}{\pi k_{1\rho}^2 a_2} \cdot \overline{\boldsymbol{D}}_{12}^{-1} \cdot \begin{bmatrix} \epsilon_1 & 0 \\ 0 & -\mu_1 \end{bmatrix}, \tag{5.47}$$

$$\overline{\boldsymbol{T}}_{21} = \frac{2\omega}{\pi k_{2\rho}^2 a_3} \cdot \overline{\boldsymbol{D}}_{12}^{-1} \cdot \begin{bmatrix} \epsilon_2 & 0 \\ 0 & -\mu_2 \end{bmatrix}. \tag{5.48}$$

Define several multi-reflection matrices:

$$\widetilde{\overline{\boldsymbol{M}}}_2 = \left[\overline{\boldsymbol{I}} - \widetilde{\overline{\boldsymbol{R}}}_{21} \cdot \widetilde{\overline{\boldsymbol{R}}}_{23}\right]^{-1}, \tag{5.49}$$

$$\widetilde{\overline{\boldsymbol{M}}}_{2out} = \left[\overline{\boldsymbol{I}} - \overline{\boldsymbol{R}}_{21} \cdot \widetilde{\overline{\boldsymbol{R}}}_{23}\right]^{-1}, \tag{5.50}$$

$$\widetilde{\overline{\boldsymbol{M}}}_{2in} = \left[\overline{\boldsymbol{I}} - \overline{\boldsymbol{R}}_{23} \cdot \widetilde{\overline{\boldsymbol{R}}}_{21}\right]^{-1}, \tag{5.51}$$

$$\widetilde{\overline{\boldsymbol{M}}}_{1out} = \left[\overline{\boldsymbol{I}} - \overline{\boldsymbol{R}}_{10} \cdot \widetilde{\overline{\boldsymbol{R}}}_{12}\right]^{-1}, \tag{5.52}$$

$$\widetilde{\overline{\boldsymbol{M}}}_{1in} = \left[\overline{\boldsymbol{I}} - \overline{\boldsymbol{R}}_{12} \cdot \widetilde{\overline{\boldsymbol{R}}}_{10}\right]^{-1}. \tag{5.53}$$

5.2.2 Rearrangement of Transmission and Reflection Matrices

We normalize matrix $\overline{\boldsymbol{B}}(k_{i\rho}\rho)$ with $B_n(k_{i\rho}\rho)$ and defined the ratio as $\overline{\boldsymbol{\beta}}(k_{i\rho}\rho)$,

$$\overline{\boldsymbol{\beta}}(k_{i\rho}\rho) \equiv \frac{\overline{\boldsymbol{B}}(k_{i\rho}\rho)}{B_n(k_{i\rho}\rho)} = \frac{1}{k_{i\rho}^2\rho} \cdot \begin{bmatrix} i\omega\epsilon_i k_{i\rho}\rho \frac{B_n'(k_{i\rho}\rho)}{B_n(k_{i\rho}\rho)} & -nk_z \\ -nk_z & i\omega\mu_i k_{i\rho}\rho \frac{B_n'(k_{i\rho}\rho)}{B_n(k_{i\rho}\rho)} \end{bmatrix}. \tag{5.54}$$

Hence matrix $\overline{\boldsymbol{\beta}}(k_{i\rho}\rho)$ contains the ratio of special function and its derivative. Rearrange $\overline{\boldsymbol{D}}_{12}$ as follows,

$$\begin{aligned} \overline{\boldsymbol{D}}_{12} &= \frac{\overline{\boldsymbol{D}}_{12}}{J_n(k_{1\rho}a_2) \cdot H_n^{(1)}(k_{2\rho}a_2)} \cdot J_n(k_{1\rho}a_2) \cdot H_n^{(1)}(k_{2\rho}a_2) \\ &= \frac{\overline{\boldsymbol{J}}_n(k_{1\rho}a_2) \cdot H_n(k_{2\rho}a_2) - \overline{\boldsymbol{H}}_n^{(1)}(k_{2\rho}a_2) \cdot J_n(k_{1\rho}a_2)}{J_n(k_{1\rho}a_2) \cdot H_n^{(1)}(k_{2\rho}a_2)} \cdot J_n(k_{1\rho}a_2) \cdot H_n^{(1)}(k_{2\rho}a_2) \\ &= \left[\frac{\overline{\boldsymbol{J}}_n(k_{1\rho}a_2)}{J_n(k_{1\rho}a_2)} - \frac{\overline{\boldsymbol{H}}_n^{(1)}(k_{1\rho}a_2)}{H_n^{(1)}(k_{1\rho}a_2)}\right] \cdot J_n(k_{1\rho}a_2) \cdot H_n^{(1)}(k_{2\rho}a_2) \\ &= \overline{\boldsymbol{A}}_1 \cdot J_n(k_{1\rho}a_2) \cdot H_n^{(1)}(k_{2\rho}a_2). \end{aligned} \tag{5.55}$$

We note that matrix $\overline{\boldsymbol{A}}_1$ is in the form of $\overline{\boldsymbol{\beta}}(k_{i\rho}\rho)$, which contains the ratio of special function and its derivative. So $\overline{\boldsymbol{A}}_1$ can be evaluated recursively. Similarly,

$$\begin{aligned}\overline{\boldsymbol{D}}_{23} &= \left[\frac{\overline{\boldsymbol{J}}_n(k_{2\rho}a_3)}{J_n(k_{2\rho}a_3)} - \frac{\overline{\boldsymbol{H}}_n^{(1)}(k_{3\rho}a_3)}{H_n^{(1)}(k_{3\rho}a_3)}\right] \cdot J_n(k_{2\rho}a_3) \cdot H_n^{(1)}(k_{3\rho}a_3) \\ &= \overline{\boldsymbol{A}}_4 \cdot J_n(k_{2\rho}a_3) \cdot H_n^{(1)}(k_{3\rho}a_3). \end{aligned} \tag{5.56}$$

The other quantities such as local transmission and reflection matrices can be re-arranged similarly as follows, with matrix $\overline{\boldsymbol{A}}_2$, $\overline{\boldsymbol{A}}_3$, $\overline{\boldsymbol{A}}_4$, $\overline{\boldsymbol{A}}_5$ factored out. The matrix $\overline{\boldsymbol{A}}_2$, $\overline{\boldsymbol{A}}_3$, $\overline{\boldsymbol{A}}_4$, $\overline{\boldsymbol{A}}_5$ can be evaluated recursively. The local transmission matrix are re-arranged as

$$\overline{\boldsymbol{T}}_{12} = \frac{2\omega}{\pi k_{1\rho}^2 a_2} \cdot \overline{\boldsymbol{A}}_1^{-1} \cdot \frac{1}{J_n(k_{1\rho}a_2) \cdot H_n^{(1)}(k_{2\rho}a_2)} \begin{bmatrix} \epsilon_1 & 0 \\ 0 & -\mu_1 \end{bmatrix}, \tag{5.57}$$

$$\overline{\boldsymbol{T}}_{21} = \frac{2\omega}{\pi k_{2\rho}^2 a_3} \cdot \overline{\boldsymbol{A}}_1^{-1} \cdot \frac{1}{J_n(k_{1\rho}a_2) \cdot H_n^{(1)}(k_{2\rho}a_2)} \begin{bmatrix} \epsilon_2 & 0 \\ 0 & -\mu_2 \end{bmatrix}. \tag{5.58}$$

For $[J_n(k_{1\rho}a_2) \cdot H_n^{(1)}(k_{2\rho}a_2)]$, we can utilized recursive relation (5.6) to calculate it. The local reflection matrices are re-arranged as

$$\begin{aligned}\overline{\boldsymbol{R}}_{12} &= \overline{\boldsymbol{D}}_{12}^{-1} \cdot \left[H_n(k_{1\rho}a_2) \cdot \overline{\boldsymbol{H}}_n^{(1)}(k_{2\rho}a_2) - H_n^{(1)}(k_{2\rho}a_2) \cdot \overline{\boldsymbol{H}}_n^{(1)}(k_{1\rho}a_2)\right] \\ &= \left[\frac{\overline{\boldsymbol{J}}_n(k_{1\rho}a_2)}{J_n(k_{1\rho}a_2)} - \frac{\overline{\boldsymbol{H}}_n^{(1)}(k_{1\rho}a_2)}{H_n^{(1)}(k_{1\rho}a_2)}\right]^{-1} \frac{\left[H_n(k_{1\rho}a_2) \cdot \overline{\boldsymbol{H}}_n^{(1)}(k_{2\rho}a_2) - H_n^{(1)}(k_{2\rho}a_2) \cdot \overline{\boldsymbol{H}}_n^{(1)}(k_{1\rho}a_2)\right]}{J_n(k_{1\rho}a_2) \cdot H_n^{(1)}(k_{2\rho}a_2)} \\ &= \left[\frac{\overline{\boldsymbol{J}}_n(k_{1\rho}a_2)}{J_n(k_{1\rho}a_2)} - \frac{\overline{\boldsymbol{H}}_n^{(1)}(k_{1\rho}a_2)}{H_n^{(1)}(k_{1\rho}a_2)}\right]^{-1} \cdot \left[\frac{\overline{\boldsymbol{H}}_n^{(1)}(k_{2\rho}a_2)}{H_n^{(1)}(k_{2\rho}a_2)} - \frac{\overline{\boldsymbol{H}}_n^{(1)}(k_{1\rho}a_2)}{H_n^{(1)}(k_{1\rho}a_2)}\right] \cdot \frac{H_n^{(1)}(k_{1\rho}a_2)}{J_n(k_{1\rho}a_2)} \\ &= \overline{\boldsymbol{A}}_1^{-1} \cdot \overline{\boldsymbol{A}}_2 \cdot \frac{H_n^{(1)}(k_{1\rho}a_2)}{J_n(k_{1\rho}a_2)}, \end{aligned} \tag{5.59}$$

$$\begin{aligned}\overline{\boldsymbol{R}}_{21} &= \left[\frac{\overline{\boldsymbol{J}}_n(k_{1\rho}a_2)}{J_n(k_{1\rho}a_2)} - \frac{\overline{\boldsymbol{H}}_n^{(1)}(k_{1\rho}a_2)}{H_n^{(1)}(k_{1\rho}a_2)}\right]^{-1} \cdot \left[\frac{\overline{\boldsymbol{J}}_n(k_{2\rho}a_2)}{J_n(k_{2\rho}a_2)} - \frac{\overline{\boldsymbol{J}}_n(k_{1\rho}a_2)}{J_n(k_{1\rho}a_2)}\right] \cdot \frac{J_n(k_{2\rho}a_2)}{H_n^{(1)}(k_{2\rho}a_2)} \\ &= \overline{\boldsymbol{A}}_1^{-1} \cdot \overline{\boldsymbol{A}}_3 \cdot \frac{J_n(k_{2\rho}a_2)}{H_n^{(1)}(k_{2\rho}a_2)}, \end{aligned} \tag{5.60}$$

$$\begin{aligned}\overline{\boldsymbol{R}}_{23} &= \left[\frac{\overline{\boldsymbol{J}}_n(k_{2\rho}a_3)}{J_n(k_{2\rho}a_3)} - \frac{\overline{\boldsymbol{H}}_n^{(1)}(k_{3\rho}a_3)}{H_n^{(1)}(k_{3\rho}a_3)}\right]^{-1} \cdot \left[\frac{\overline{\boldsymbol{H}}_n^{(1)}(k_{3\rho}a_3)}{H_n^{(1)}(k_{3\rho}a_3)} - \frac{\overline{\boldsymbol{H}}_n^{(1)}(k_{2\rho}a_3)}{H_n^{(1)}(k_{2\rho}a_3)}\right] \cdot \frac{H_n^{(1)}(k_{2\rho}a_3)}{J_n(k_{2\rho}a_3)} \\ &= \overline{\boldsymbol{A}}_4^{-1} \cdot \overline{\boldsymbol{A}}_5 \cdot \frac{H_n^{(1)}(k_{2\rho}a_3)}{J_n(k_{2\rho}a_3)}. \end{aligned} \tag{5.61}$$

For the generalized reflection matrices, the re-arrangement is more complicated,

$$\begin{aligned}
\widetilde{\overline{\boldsymbol{R}}}_{21} &= \overline{\boldsymbol{A}}_1^{-1}\cdot\overline{\boldsymbol{A}}_3\cdot\frac{J_n(k_{2\rho}a_2)}{H_n^{(1)}(k_{2\rho}a_2)}+\overline{\boldsymbol{T}}_{12}\cdot\widetilde{\overline{\boldsymbol{R}}}_{10}\cdot\left(\overline{\boldsymbol{I}}-\overline{\boldsymbol{R}}_{12}\cdot\widetilde{\overline{R}}_{10}\right)^{-1}\cdot\overline{\boldsymbol{T}}_{21}\\
&= \frac{J_n(k_{2\rho}a_2)}{H_n^{(1)}(k_{2\rho}a_2)}\cdot\left[\overline{\boldsymbol{A}}_1^{-1}\cdot\overline{\boldsymbol{A}}_3+\overline{\boldsymbol{T}}_{12}\cdot\frac{H_n^{(1)}(k_{2\rho}a_2)}{J_n(k_{2\rho}a_2)}\cdot\widetilde{\overline{\boldsymbol{R}}}_{10}\left(\overline{\boldsymbol{I}}-\overline{\boldsymbol{R}}_{12}\cdot\widetilde{\overline{R}}_{10}\right)^{-1}\overline{\boldsymbol{T}}_{21}\right]\\
&= \frac{J_n(k_{2\rho}a_2)}{H_n^{(1)}(k_{2\rho}a_2)}\cdot W_{21}, \qquad (5.62)\\
\widetilde{\overline{\boldsymbol{R}}}_{12} &= \overline{\boldsymbol{A}}_1^{-1}\cdot\overline{\boldsymbol{A}}_2\cdot\frac{H_n^{(1)}(k_{2\rho}a_2)}{J_n(k_{2\rho}a_2)}+\overline{\boldsymbol{T}}_{21}\cdot\widetilde{\overline{\boldsymbol{R}}}_{23}\cdot\left(\overline{\boldsymbol{I}}-\overline{\boldsymbol{R}}_{21}\cdot\widetilde{\overline{R}}_{23}\right)^{-1}\cdot\overline{\boldsymbol{T}}_{12}\\
&= \frac{H_n^{(1)}(k_{2\rho}a_2)}{J_n(k_{2\rho}a_2)}\cdot\Big[\overline{\boldsymbol{A}}_1^{-1}\cdot\overline{\boldsymbol{A}}_2+\overline{\boldsymbol{T}}_{21}\cdot\overline{\boldsymbol{A}}_4^{-1}\cdot\overline{\boldsymbol{A}}_5\cdot\frac{J_n(k_{1\rho}a_2)}{H_n^{(1)}(k_{1\rho}a_2)}\frac{H_n^{(1)}(k_{2\rho}a_3)}{J_n(k_{2\rho}a_3)}\\
&\quad\cdot\left(\overline{\boldsymbol{I}}-\overline{\boldsymbol{R}}_{21}\cdot\widetilde{\overline{R}}_{23}\right)^{-1}\overline{\boldsymbol{T}}_{12}\Big]\\
&= \frac{H_n^{(1)}(k_{2\rho}a_2)}{J_n(k_{2\rho}a_2)}\cdot W_{12}, \qquad (5.63)
\end{aligned}$$

where

$$\begin{aligned}
\left(\overline{\boldsymbol{I}}-\overline{\boldsymbol{R}}_{12}\cdot\widetilde{\overline{R}}_{10}\right) &= \overline{\boldsymbol{I}}-\overline{\boldsymbol{A}}_1^{-1}\cdot\overline{\boldsymbol{A}}_2\cdot\frac{H_n^{(1)}(k_{1\rho}a_2)}{J_n(k_{1\rho}a_2)}\cdot\widetilde{\overline{R}}_{10}, \qquad (5.64)\\
\left(\overline{\boldsymbol{I}}-\overline{\boldsymbol{R}}_{21}\cdot\widetilde{\overline{R}}_{23}\right) &= \overline{\boldsymbol{I}}-\overline{\boldsymbol{A}}_1^{-1}\cdot\overline{\boldsymbol{A}}_3\cdot\frac{J_n(k_{2\rho}a_2)}{H_n^{(1)}(k_{2\rho}a_2)}\cdot\overline{\boldsymbol{A}}_4^{-1}\cdot\overline{\boldsymbol{A}}_5\cdot\frac{H_n^{(1)}(k_{2\rho}a_3)}{J_n(k_{2\rho}a_3)}, \qquad (5.65)
\end{aligned}$$

and the multi-reflection matrices are:

$$\begin{aligned}
\widetilde{\overline{\boldsymbol{M}}}_2 &= \left[\overline{\boldsymbol{I}}-\widetilde{\overline{\boldsymbol{R}}}_{21}\cdot\widetilde{\overline{\boldsymbol{R}}}_{23}\right]^{-1}\\
&= \left[\overline{\boldsymbol{I}}-W_{21}\cdot\frac{J_n(k_{2\rho}a_2)}{H_n^{(1)}(k_{2\rho}a_2)}\cdot\overline{\boldsymbol{A}}_4^{-1}\cdot\overline{\boldsymbol{A}}_5\cdot\frac{H_n^{(1)}(k_{2\rho}a_3)}{J_n(k_{2\rho}a_3)}\right]^{-1}, \qquad (5.66)\\
\widetilde{\overline{\boldsymbol{M}}}_{2out} &= \left[\overline{\boldsymbol{I}}-\overline{\boldsymbol{R}}_{21}\cdot\widetilde{\overline{\boldsymbol{R}}}_{23}\right]^{-1}\\
&= \left[\overline{\boldsymbol{I}}-\overline{\boldsymbol{A}}_1^{-1}\cdot\overline{\boldsymbol{A}}_3\cdot\frac{J_n(k_{2\rho}a_2)}{H_n^{(1)}(k_{2\rho}a_2)}\cdot\overline{\boldsymbol{A}}_4^{-1}\cdot\overline{\boldsymbol{A}}_5\cdot\frac{H_n^{(1)}(k_{2\rho}a_3)}{J_n(k_{2\rho}a_3)}\right]^{-1}, \qquad (5.67)\\
\widetilde{\overline{\boldsymbol{M}}}_{2in} &= \left[\overline{\boldsymbol{I}}-\overline{\boldsymbol{R}}_{23}\cdot\widetilde{\overline{\boldsymbol{R}}}_{21}\right]^{-1}\\
&= \left[\overline{\boldsymbol{I}}-\overline{\boldsymbol{A}}_4^{-1}\cdot\overline{\boldsymbol{A}}_5\cdot\frac{H_n^{(1)}(k_{2\rho}a_3)}{J_n(k_{2\rho}a_3)}\cdot W_{21}\cdot\frac{J_n(k_{2\rho}a_2)}{H_n^{(1)}(k_{2\rho}a_2)}\right]^{-1}, \qquad (5.68)\\
\widetilde{\overline{\boldsymbol{M}}}_{1out} &= \left[\overline{\boldsymbol{I}}-\overline{\boldsymbol{R}}_{10}\cdot\widetilde{\overline{\boldsymbol{R}}}_{12}\right]^{-1}\\
&= \left[\overline{\boldsymbol{I}}-\overline{\boldsymbol{R}}_{10}\cdot W_{12}\cdot\frac{H_n^{(1)}(k_{2\rho}a_3)}{J_n(k_{2\rho}a_3)}\right]^{-1}, \qquad (5.69)
\end{aligned}$$

$$\begin{aligned}\widetilde{\overline{\boldsymbol{M}}}_{1in} &= \left[\overline{\boldsymbol{I}} - \overline{\boldsymbol{R}}_{12}\cdot\widetilde{\overline{\boldsymbol{R}}}_{10}\right]^{-1} \\ &= \left[\overline{\boldsymbol{I}} - \overline{\boldsymbol{A}}_1^{-1}\cdot\overline{\boldsymbol{A}}_2\cdot\frac{H_n^{(1)}(k_{1\rho}a_2)}{J_n(k_{1\rho}a_2)}\cdot\overline{\boldsymbol{R}}_{10}\right]^{-1}. \end{aligned} \tag{5.70}$$

5.2.3 Calculation of Matrix $\overline{\boldsymbol{F}}_n$

We have completed the preliminary re-arrangement of the Green's functions so far, i.e., the reflection matrix, the transmission matrix and the multi-reflection matrix. Next, the matrix $\overline{\boldsymbol{F}}_n$ in Eq. (4.2d) will be re-arranged in this section. The new form $\overline{\boldsymbol{F}}_n$ will allow the recursive relations to be used to calculate spectral domain Green's functions or the cylindrical eigenmodes.

Case 1: $\rho = \rho' = a_2$

$$\begin{aligned}\overline{\boldsymbol{F}}_n &= H_n^{(1)}(k_{2\rho}\rho)\cdot J_n(k_{2\rho}\rho')\cdot\widetilde{\overline{\boldsymbol{M}}}_2 + J_n(k_{2\rho}\rho)\cdot J_n(k_{2\rho}\rho')\cdot\widetilde{\overline{\boldsymbol{R}}}_{23}\cdot\widetilde{\overline{\boldsymbol{M}}}_2 \\ &\quad + H_n^{(1)}(k_{2\rho}\rho)\cdot H_n^{(1)}(k_{2\rho}\rho')\cdot\widetilde{\overline{\boldsymbol{M}}}_2\cdot\widetilde{\overline{\boldsymbol{R}}}_{21} + J_n(k_{2\rho}\rho)\cdot H_n^{(1)}(k_{2\rho}\rho')\cdot\widetilde{\overline{\boldsymbol{R}}}_{23}\cdot\widetilde{\overline{\boldsymbol{M}}}_2\cdot\widetilde{\overline{\boldsymbol{R}}}_{21} \\ &= H_n^{(1)}(k_{2\rho}a_2)\cdot J_n(k_{2\rho}a_2)\cdot\widetilde{\overline{\boldsymbol{M}}}_2 + \overline{\boldsymbol{A}}_4^{-1}\cdot\overline{\boldsymbol{A}}_5\cdot\frac{J_n(k_{2\rho}a_2)}{J_n(k_{2\rho}a_3)}\cdot J_n(k_{2\rho}a_2)\cdot H_n^{(1)}(k_{2\rho}a_3)\cdot\widetilde{\overline{\boldsymbol{M}}}_2 \\ &\quad + H_n^{(1)}(k_{2\rho}a_2)\cdot J_n(k_{2\rho}a_2)\cdot\widetilde{\overline{\boldsymbol{M}}}_2\cdot W_{21} \\ &\quad + \frac{J_n(k_{2\rho}a_2)}{J_n(k_{2\rho}a_3}\cdot H_n^{(1)}(k_{2\rho}a_3)\cdot J_n(k_{2\rho}a_2)\cdot\overline{\boldsymbol{A}}_4^{-1}\cdot\overline{\boldsymbol{A}}_5\cdot\widetilde{\overline{\boldsymbol{M}}}_2\cdot W_{21} \\ &= \Big[\widetilde{\overline{\boldsymbol{M}}}_2 + \overline{\boldsymbol{A}}_4^{-1}\cdot\overline{\boldsymbol{A}}_5\cdot\frac{J_n(k_{2\rho}a_2)}{J_n(k_{2\rho}a_3)}\cdot\frac{H_n^{(1)}(k_{2\rho}a_3)}{H_n^{(1)}(k_{2\rho}a_2)}\cdot\widetilde{\overline{\boldsymbol{M}}}_2 + \widetilde{\overline{\boldsymbol{M}}}_2\cdot W_{21} \\ &\quad + \frac{J_n(k_{2\rho}a_2)}{J_n(k_{2\rho}a_3)}\cdot\frac{H_n^{(1)}(k_{2\rho}a_3)}{H_n^{(1)}(k_{2\rho}a_2)}\cdot\overline{\boldsymbol{A}}_4^{-1}\cdot\overline{\boldsymbol{A}}_5\cdot\widetilde{\overline{\boldsymbol{M}}}_2\cdot W_{21}\Big]\cdot\left[H_n^{(1)}(k_{2\rho}a_2)\cdot J_n(k_{2\rho}a_2)\right]. \end{aligned} \tag{5.71}$$

For the components in the first square bracket, $\overline{\boldsymbol{A}}_4$, $\overline{\boldsymbol{A}}_5$ can be calculated using recursive relations. $[J_n(k_{2\rho}a_2)/J_n(k_{2\rho}a_3)]$ and $[H_n^{(1)}(k_{2\rho}a_3)/H_n^{(1)}(k_{2\rho}a_2)]$ are in the form (5.4) and (5.5), respectively, and also can be evaluated recursively. For $\widetilde{\overline{\boldsymbol{M}}}_2$ and W_{21}, the recursive relations they contained are not apparent. For the convenience of our discussion, we rewrite their expression here and see how the recursive relation can be used for calculation.

For $\widetilde{\overline{\boldsymbol{M}}}_2$,

$$\widetilde{\overline{\boldsymbol{M}}}_2 = \left[\overline{\boldsymbol{I}} - W_{21}\cdot\frac{J_n(k_{2\rho}a_2)}{H_n^{(1)}(k_{2\rho}a_2)}\cdot\overline{\boldsymbol{A}}_4^{-1}\cdot\overline{\boldsymbol{A}}_5\cdot\frac{H_n^{(1)}(k_{2\rho}a_3)}{J_n(k_{2\rho}a_3)}\right]^{-1}. \tag{5.72}$$

First, we look at items other than W_{21}, i.e., $\overline{\boldsymbol{A}}_4$, $\overline{\boldsymbol{A}}_5$, $[J_n(k_{2\rho}a_2)/J_n(k_{2\rho}a_3)]$, $[H_n^{(1)}(k_{2\rho}a_3)/H_n^{(1)}(k_{2\rho}a_2)]$. They are in the form which we have discussed previously and can be evaluated recursively. Now, we examine W_{21},

$$W_{21} = \left[\overline{\boldsymbol{A}}_1^{-1}\cdot\overline{\boldsymbol{A}}_3+\overline{\boldsymbol{T}}_{12}\cdot\frac{H_n^{(1)}(k_{2\rho}a_2)}{J_n(k_{2\rho}a_2)}\cdot\widetilde{\overline{\boldsymbol{R}}}_{10}\left(\overline{\boldsymbol{I}}-\overline{\boldsymbol{R}}_{12}\cdot\widetilde{\overline{R}}_{10}\right)^{-1}\overline{\boldsymbol{T}}_{21}\right]. \quad (5.73)$$

The recursive calculation of $\overline{\boldsymbol{A}}_1$, $\overline{\boldsymbol{A}}_3$, $\overline{\boldsymbol{T}}_{12}$, $\overline{\boldsymbol{T}}_{21}$ have been discussed in previous section. Now, we need to consider quantity $[H_n^{(1)}(k_{2\rho}a_2)/J_n(k_{2\rho}a_2)]\cdot\widetilde{\overline{\boldsymbol{R}}}_{10}$ and $\left(\overline{\boldsymbol{I}}-\overline{\boldsymbol{R}}_{12}\cdot\widetilde{\overline{R}}_{10}\right)$.

$$\begin{aligned}\frac{H_n^{(1)}(k_{2\rho}a_2)}{J_n(k_{2\rho}a_2)}\cdot\widetilde{\overline{\boldsymbol{R}}}_{10} &= \frac{H_n^{(1)}(k_{2\rho}a_2)}{J_n(k_{2\rho}a_2)}\cdot\begin{bmatrix}-\frac{J_n(k_{1\rho}a_1)}{H_n(k_{1\rho}a_1)} & 0\\ 0 & -\frac{J_n'(k_{1\rho}a_1)}{H_n'(k_{1\rho}a_1)}\end{bmatrix}\\ &= \begin{bmatrix}-\frac{H_n^{(1)}(k_{2\rho}a_2)}{H_n(k_{1\rho}a_1)}\frac{J_n(k_{1\rho}a_1)}{J_n(k_{2\rho}a_2)} & 0\\ 0 & -\frac{H_n^{(1)}(k_{2\rho}a_2)}{H_n'(k_{1\rho}a_1)}\frac{J_n'(k_{1\rho}a_1)}{J_n(k_{2\rho}a_2)}\end{bmatrix}. \quad (5.74)\end{aligned}$$

We can see that the diagonal elements are in the recursive form (5.4), (5.5), (5.10) and (5.11).

$$\left(\overline{\boldsymbol{I}}-\overline{\boldsymbol{R}}_{12}\cdot\widetilde{\overline{R}}_{10}\right) = \overline{\boldsymbol{I}}-\overline{\boldsymbol{A}}_1^{-1}\cdot\overline{\boldsymbol{A}}_2\cdot\frac{H_n^{(1)}(k_{1\rho}a_2)}{J_n(k_{1\rho}a_2)}\cdot\widetilde{\overline{R}}_{10}. \quad (5.75)$$

Obviously, $[H_n^{(1)}(k_{1\rho}a_2)/J_n(k_{1\rho}a_2)]\cdot\widetilde{\overline{R}}_{10}$ takes the similar form of (5.74).

A very similar treatment can be applied to the following case 2 and case 3. The details are omitted here for brevity and only the expression of $\overline{\boldsymbol{F}}_n$ for each case is listed.

Case 2: $\rho' < a_2$, $\rho = a_2$

$$\begin{aligned}\overline{\boldsymbol{F}}_n &= H_n^{(1)}(k_{2\rho}\rho)\cdot J_n(k_{2\rho}\rho')\cdot\widetilde{\overline{\boldsymbol{M}}}_{out}+J_n(k_{2\rho}\rho)\cdot J_n(k_{1\rho}\rho')\cdot\widetilde{\overline{\boldsymbol{R}}}_{23}\cdot\widetilde{\overline{\boldsymbol{M}}}_{out}\\ &\quad +H_n^{(1)}(k_{2\rho}\rho)\cdot H_n^{(1)}(k_{1\rho}\rho')\cdot\widetilde{\overline{\boldsymbol{M}}}_{out}\cdot\overline{\boldsymbol{R}}_{10}+J_n(k_{2\rho}\rho)\cdot H_n^{(1)}(k_{1\rho}\rho')\cdot\widetilde{\overline{\boldsymbol{R}}}_{23}\cdot\widetilde{\overline{\boldsymbol{M}}}_{out}\cdot\overline{\boldsymbol{R}}_{10}\\ &= H_n^{(1)}(k_{2\rho}a_2)\cdot J_n(k_{2\rho}\rho')\cdot\widetilde{\overline{\boldsymbol{M}}}_{out}+H_n^{(1)}(k_{2\rho}a_2)\cdot H_n^{(1)}(k_{1\rho}\rho')\cdot\widetilde{\overline{\boldsymbol{M}}}_{out}\cdot\overline{\boldsymbol{R}}_{10}\\ &\quad +J_n(k_{2\rho}a_2)\cdot J_n(k_{1\rho}\rho')\cdot\frac{H_n^{(1)}(k_{2\rho}a_3)}{J_n(k_{2\rho}a_3)}\cdot\overline{\boldsymbol{A}}_4^{-1}\cdot\overline{\boldsymbol{A}}_5\cdot\widetilde{\overline{\boldsymbol{M}}}_{out}\\ &\quad +J_n(k_{2\rho}a_2)\cdot H_n^{(1)}(k_{1\rho}\rho')\cdot\frac{H_n^{(1)}(k_{2\rho}a_3)}{J_n(k_{2\rho}a_3)}\cdot\overline{\boldsymbol{A}}_4^{-1}\cdot\overline{\boldsymbol{A}}_5\cdot\widetilde{\overline{\boldsymbol{M}}}_{out}\cdot\overline{\boldsymbol{R}}_{10}\\ &= \Big[\frac{J_n(k_{2\rho}\rho')}{J_n(k_{2\rho}a_2)}\cdot\widetilde{\overline{\boldsymbol{M}}}_{out}+\frac{H_n^{(1)}(k_{1\rho}\rho')}{J_n(k_{2\rho}a_2)}\cdot\widetilde{\overline{\boldsymbol{M}}}_{out}\cdot\overline{\boldsymbol{R}}_{10}\end{aligned}$$

$$+\frac{J_n(k_{1\rho}\rho')}{J_n(k_{2\rho}a_3)}\cdot\frac{H_n^{(1)}(k_{2\rho}a_3)}{H_n^{(1)}(k_{2\rho}a_2)}\cdot\overline{\boldsymbol{A}}_4^{-1}\cdot\overline{\boldsymbol{A}}_5\cdot\widetilde{\overline{\boldsymbol{M}}}_{out}$$
$$+\frac{H_n^{(1)}(k_{1\rho}\rho')}{H_n^{(1)}(k_{2\rho}a_2)}\cdot\frac{H_n^{(1)}(k_{2\rho}a_3)}{J_n(k_{2\rho}a_3)}\cdot\overline{\boldsymbol{A}}_4^{-1}\cdot\overline{\boldsymbol{A}}_5\cdot\widetilde{\overline{\boldsymbol{M}}}_{out}\cdot\overline{\boldsymbol{R}}_{10}\Big]\cdot\Big[H_n^{(1)}(k_{2\rho}a_2)\cdot J_n(k_{2\rho}a_2)\Big], \tag{5.76}$$

where $\widetilde{\overline{\boldsymbol{M}}}_{out}=\widetilde{\overline{\boldsymbol{M}}}_{2out}\cdot\overline{\boldsymbol{T}}_{12}\cdot\widetilde{\overline{\boldsymbol{M}}}_{1out}$.

Case 3: $\rho<a_2$, $\rho'=a_2$

$$\begin{aligned}
\overline{\boldsymbol{F}}_n &= J_n(k_{1\rho}\rho)\cdot H_n^{(1)}(k_{2\rho}\rho')\cdot\widetilde{\overline{\boldsymbol{M}}}_{in}+J_n(k_{1\rho}\rho)\cdot J_n(k_{2\rho}\rho')\cdot\widetilde{\overline{\boldsymbol{M}}}_{in}\widetilde{\overline{\boldsymbol{R}}}_{23}\\
&\quad+H_n^{(1)}(k_{1\rho}\rho)\cdot H_n^{(1)}(k_{2\rho}\rho')\cdot\overline{\boldsymbol{R}}_{10}\widetilde{\overline{\boldsymbol{M}}}_{in}+H_n^{(1)}(k_{1\rho}\rho)\cdot J_n(k_{2\rho}\rho')\cdot\overline{\boldsymbol{R}}_{10}\cdot\widetilde{\overline{\boldsymbol{M}}}_{in}\cdot\widetilde{\overline{\boldsymbol{R}}}_{23}\\
&= J_n(k_{1\rho}\rho)\cdot H_n^{(1)}(k_{2\rho}a_2)\cdot\widetilde{\overline{\boldsymbol{M}}}_{in}+J_n(k_{1\rho}\rho)\cdot J_n(k_{2\rho}a_2)\cdot\frac{H_n^{(1)}(k_{2\rho}a_3)}{J_n(k_{2\rho}a_3)}\cdot\widetilde{\overline{\boldsymbol{M}}}_{in}\cdot\overline{\boldsymbol{A}}_4^{-1}\cdot\overline{\boldsymbol{A}}_5\\
&\quad+H_n^{(1)}(k_{1\rho}\rho)\cdot H_n^{(1)}(k_{2\rho}a_2)\cdot\overline{\boldsymbol{R}}_{10}\cdot\widetilde{\overline{\boldsymbol{M}}}_{in}\\
&\quad+H_n^{(1)}(k_{1\rho}\rho)\cdot J_n(k_{2\rho}a_2)\frac{H_n^{(1)}(k_{2\rho}a_3)}{J_n(k_{2\rho}a_3)}\cdot\overline{\boldsymbol{R}}_{10}\cdot\widetilde{\overline{\boldsymbol{M}}}_{in}\cdot\overline{\boldsymbol{A}}_4^{-1}\cdot\overline{\boldsymbol{A}}_5\\
&= \Big[\frac{J_n(k_{1\rho}\rho)}{J_n(k_{2\rho}a_2)}\cdot\widetilde{\overline{\boldsymbol{M}}}_{in}+\frac{J_n(k_{1\rho}\rho)}{J_n(k_{2\rho}a_3)}\cdot\frac{H_n^{(1)}(k_{2\rho}a_3)}{H_n^{(1)}(k_{2\rho}a_2)}\cdot\widetilde{\overline{\boldsymbol{M}}}_{in}\cdot\overline{\boldsymbol{A}}_4^{-1}\cdot\overline{\boldsymbol{A}}_5\\
&\quad+\frac{H_n^{(1)}(k_{1\rho}\rho)}{J_n(k_{2\rho}a_2)}\cdot\overline{\boldsymbol{R}}_{10}\cdot\widetilde{\overline{\boldsymbol{M}}}_{in}+\frac{H_n^{(1)}(k_{1\rho}\rho)}{H_n^{(1)}(k_{2\rho}a_2)}\cdot\frac{H_n^{(1)}(k_{2\rho}a_3)}{J_n(k_{2\rho}a_3)}\cdot\overline{\boldsymbol{R}}_{10}\cdot\widetilde{\overline{\boldsymbol{M}}}_{in}\cdot\overline{\boldsymbol{A}}_4^{-1}\cdot\overline{\boldsymbol{A}}_5\Big]\\
&\quad\cdot\Big[H_n^{(1)}(k_{2\rho}a_2)\cdot J_n(k_{2\rho}a_2)\Big],
\end{aligned}\tag{5.77}$$

where $\widetilde{\overline{\boldsymbol{M}}}_{in}=\widetilde{\overline{\boldsymbol{M}}}_{1in}\cdot\overline{\boldsymbol{T}}_{21}\cdot\widetilde{\overline{\boldsymbol{M}}}_{2in}$.

5.3 Reformulation of the Green's Functions: 4×4 Matrix Method

In this section, the Green's functions are derived using 4×4 matrix rather than 2×2 matrix method. In the derivation process, recursive relations are incorporated into the formulations, resulting in the Green's functions that can be evaluated recursively. The purposes of presenting the 4×4 matrix form Green's functions are to: 1) validate the reformulation of the 2×2 matrix form of Green's functions and 2) provide an alternative

way to program.

5.3.1 General Form of Tangential Fields

Consider the z components of the electromagnetic fields in layer i of a cylindrically multilayered media as shown in Fig. 3.5. E_z^i and H_z^i, which are the general solutions of Eq. (3.4), can be written in an alternative form as

$$E_z^i = A \cdot J_m(k_{i\rho}\rho) + B \cdot N_m(k_{i\rho}\rho), \tag{5.78}$$

$$H_z^i = C \cdot J_m(k_{i\rho}\rho) + D \cdot N_m(k_{i\rho}\rho), \tag{5.79}$$

where A, B, C, D are the unknown coefficients determined from the boundary conditions. From Eqs. (3.6) and (3.7), the ϕ components are

$$E_\phi^i = -\frac{nk_z}{k_{i\rho}^2\rho}E_z^i + \frac{j\omega\mu_{ri}\mu_0}{k_{i\rho}^2\rho}\frac{\partial H_z^i}{\partial\rho}, \tag{5.80}$$

$$H_\phi^i = -\frac{nk_z}{k_{i\rho}^2\rho}H_z^i - \frac{j\omega\mu_{ri}\mu_0}{k_{i\rho}^2\rho}\frac{\partial E_z^i}{\partial\rho}. \tag{5.81}$$

5.3.2 Interface Field and Transfer Matrix $\overline{\boldsymbol{T}}$

Define the tangential field at the cylindrical surface $\rho = \rho_i$ as

$$\begin{bmatrix} \boldsymbol{e}^i \\ \boldsymbol{h}^i \end{bmatrix} = \begin{bmatrix} E_z^i(\rho_i) \\ E_\phi^i(\rho_i) \\ H_z^i(\rho_i) \\ H_\phi^i(\rho_i) \end{bmatrix}. \tag{5.82}$$

From Eqs. (5.78-5.81), $[\boldsymbol{e}^i, \boldsymbol{h}^i]^T$ can be written as

$$\begin{bmatrix} \boldsymbol{e}^i \\ \boldsymbol{h}^i \end{bmatrix} = \overline{\boldsymbol{\Upsilon}}_i(k_{i\rho}\rho_i) \cdot \begin{bmatrix} A \\ B \\ C \\ D \end{bmatrix}. \tag{5.83}$$

Similarly, the tangential fields at the cylindrical surface $\rho = \rho_{i+1}$ are

$$\begin{bmatrix} \boldsymbol{e}^{i+1} \\ \boldsymbol{h}^{i+1} \end{bmatrix} = \overline{\boldsymbol{\Upsilon}}_{i+1}(k_{i\rho}\rho_{i+1}) \cdot \begin{bmatrix} A \\ B \\ C \\ D \end{bmatrix}. \tag{5.84}$$

Substitute Eq. (5.83) into Eq. (5.84), we obtain

$$\begin{bmatrix} \boldsymbol{e}^{i+1} \\ \boldsymbol{h}^{i+1} \end{bmatrix} = \overline{\boldsymbol{\Upsilon}}_{i+1}(k_{i\rho}\rho_{i+1})\overline{\boldsymbol{\Upsilon}}_{i}^{-1}(k_{i\rho}\rho_{i}) \begin{bmatrix} \boldsymbol{e}^{i} \\ \boldsymbol{h}^{i} \end{bmatrix}, \tag{5.85}$$

where

$$\begin{aligned} \overline{\boldsymbol{\Upsilon}}_{i+1}(k_{i\rho}\rho_{i+1}) &= \begin{bmatrix} \overline{\boldsymbol{\Upsilon}}_{ee} & \overline{\boldsymbol{\Upsilon}}_{eh} \\ \overline{\boldsymbol{\Upsilon}}_{he} & \overline{\boldsymbol{\Upsilon}}_{hh} \end{bmatrix}, \\ \overline{\boldsymbol{\Upsilon}}_{i}^{-1}(k_{i\rho}\rho_{i}) &= \begin{bmatrix} \overline{\boldsymbol{\Upsilon}}'_{ee} & \overline{\boldsymbol{\Upsilon}}'_{eh} \\ \overline{\boldsymbol{\Upsilon}}'_{he} & \overline{\boldsymbol{\Upsilon}}'_{hh} \end{bmatrix}, \end{aligned} \tag{5.86}$$

$$\begin{aligned} \overline{\boldsymbol{\Upsilon}}_{ee} &= \begin{bmatrix} J_n(k_{i\rho}\rho_{i+1}) & N_n(k_{i\rho}\rho_{i+1}) \\ -\frac{nk_z}{\rho_{i+1}k_{i\rho}^2}J_n(k_{i\rho}\rho_{i+1}) & -\frac{nk_z}{\rho_{i+1}k_{i\rho}^2}N_n(k_{i\rho}\rho_{i+1}) \end{bmatrix}, \\ \overline{\boldsymbol{\Upsilon}}_{eh} &= \begin{bmatrix} 0 & 0 \\ -\frac{j\omega_i\mu_i}{k_{i\rho}}J'_n(k_{i\rho}\rho_{i+1}) & -\frac{j\omega_i\mu_i}{k_{i\rho}}N'_n(k_{i\rho}\rho_{i+1}) \end{bmatrix}, \\ \overline{\boldsymbol{\Upsilon}}_{he} &= \begin{bmatrix} 0 & 0 \\ \frac{j\omega_i\epsilon_i}{k_{i\rho}}J'_n(k_{i\rho}\rho_{i+1}) & \frac{j\omega_i\epsilon_i}{k_{i\rho}}N'_n(k_{i\rho}\rho_{i+1}) \end{bmatrix}, \\ \overline{\boldsymbol{\Upsilon}}_{hh} &= \overline{\boldsymbol{\Upsilon}}_{ee}, \\ \overline{\boldsymbol{\Upsilon}}'_{ee} &= \begin{bmatrix} \frac{\pi k_{i\rho}\rho_i}{2}N'_n(k_{i\rho}\rho_i) & 0 \\ -\frac{\pi k_{i\rho}\rho_i}{2}J'_n(k_{i\rho}\rho_i) & 0 \end{bmatrix}, \\ \overline{\boldsymbol{\Upsilon}}'_{eh} &= \begin{bmatrix} -\frac{\pi nk_z\rho_i}{2j\omega\epsilon_i\rho_{i+1}}N_n(k_{i\rho}\rho_i) & -\frac{\pi k_{i\rho}^2\rho_i}{2j\omega\epsilon_i}N_n(k_{i\rho}\rho_i) \\ \frac{\pi nk_z\rho_i}{2j\omega\epsilon_i\rho_{i+1}}J_n(k_{i\rho}\rho_i) & \frac{\pi k_{i\rho}^2\rho_i}{2j\omega\epsilon_i}J_n(k_{i\rho}\rho_i) \end{bmatrix}, \\ \overline{\boldsymbol{\Upsilon}}'_{he} &= \begin{bmatrix} \frac{\pi nk_z\rho_i}{2j\omega\mu_i\rho_{i+1}}N_n(k_{i\rho}\rho_i) & \frac{\pi k_{i\rho}^2\rho_i}{2j\omega\mu_i}N_n(k_{i\rho}\rho_i) \\ -\frac{\pi nk_z\rho_i}{2j\omega\mu_i\rho_{i+1}}J_n(k_{i\rho}\rho_i) & -\frac{\pi k_{i\rho}^2\rho_i}{2j\omega\mu_i}J_n(k_{i\rho}\rho_i) \end{bmatrix}, \end{aligned}$$

$$\overline{\boldsymbol{\Upsilon}}'_{hh} = \overline{\boldsymbol{\Upsilon}}'_{ee}. \tag{5.87}$$

Defining

$$\overline{\boldsymbol{T}}(k_{i\rho}, \rho_i, \rho_{i+1}) = \overline{\boldsymbol{\Upsilon}}_{i+1}(k_{i\rho}\rho_{i+1})\overline{\boldsymbol{\Upsilon}}_i^{-1}(k_{i\rho}\rho_i), \tag{5.88}$$

from Eq. (5.85), the relation between the tangential fields on two adjacent cylindrical surface can be written as

$$\begin{bmatrix} \boldsymbol{e}^{i+1} \\ \boldsymbol{h}^{i+1} \end{bmatrix} = \overline{\boldsymbol{T}}(k_{i\rho}, \rho_i, \rho_{i+1}) \cdot \begin{bmatrix} \boldsymbol{e}^{i} \\ \boldsymbol{h}^{i} \end{bmatrix}, \tag{5.89}$$

or

$$\begin{bmatrix} \boldsymbol{e}^{i} \\ \boldsymbol{h}^{i} \end{bmatrix} = \overline{\boldsymbol{T}}^{-1}(k_{i\rho}, \rho_i, \rho_{i+1}) \cdot \begin{bmatrix} \boldsymbol{e}^{i+1} \\ \boldsymbol{h}^{i+1} \end{bmatrix}, \tag{5.90}$$

where

$$\overline{\boldsymbol{T}}(k_{i\rho}, \rho_i, \rho_{i+1}) = \begin{bmatrix} \overline{\boldsymbol{T}}_{ee} & \overline{\boldsymbol{T}}_{eh} \\ \overline{\boldsymbol{T}}_{he} & \overline{\boldsymbol{T}}_{hh} \end{bmatrix}, \tag{5.91}$$

$$\overline{\boldsymbol{T}}_{ee} = \begin{bmatrix} -\frac{\pi k_{i\rho}\rho_i}{2} R_n^{(i)} & 0 \\ \frac{\pi n k_z}{2k_{i\rho}}[\frac{\rho_i}{\rho_{i+1}} R_n^{(i)} + Q_n^{(i)}] & \frac{\pi k_{i\rho}\rho_i}{2} Q_n^{(i)} \end{bmatrix}, \tag{5.92}$$

$$\overline{\boldsymbol{T}}_{hh} = \overline{\boldsymbol{T}}_{ee}, \tag{5.93}$$

$$\overline{\boldsymbol{T}}_{eh} = \begin{bmatrix} \frac{\pi n k_z}{2j\omega\epsilon_{r_i}} P_n^{(i)} & \frac{\pi k_{i\rho}^2 \rho_i}{2j\omega\epsilon_{r_i}} P_n^{(i)} \\ -\frac{\pi\rho_i}{2j\omega\epsilon_{r_i}}[\frac{n^2 k_z^2}{k_{i\rho}^2 \rho_i \rho_{i+1}} P_n^{(i)} + k_i^2 S_n^{(i)}] & -\frac{\pi n k_z \rho_i}{2j\omega\epsilon_{r_i}\rho_{i+1}} P_n^{(i)} \end{bmatrix}, \tag{5.94}$$

$$\overline{\boldsymbol{T}}_{he} = \begin{bmatrix} -\frac{\pi n k_z}{2j\omega\mu_{r_i}} P_n^{(i)} & -\frac{\pi k_{i\rho}^2 \rho_i}{2j\omega\mu_{r_i}} P_n^{(i)} \\ \frac{\pi\rho_i}{2j\omega\mu_{r_i}}[\frac{n^2 k_z^2}{k_{i\rho}^2 \rho_i \rho_{i+1}} P_n^{(i)} + k_i^2 S_n^{(i)}] & \frac{\pi n k_z \rho_i}{2j\omega\mu_{r_i}\rho_{i+1}} P_n^{(i)} \end{bmatrix}, \tag{5.95}$$

in Eqs. (5.92-5.95),

$$P_n^{(i)} = J_n(k_{i\rho}\rho_i) \cdot N_n(k_{i\rho}\rho_{i+1}) - J_n(k_{i\rho}\rho_{i+1}) \cdot N_n(k_{i\rho}\rho_i), \tag{5.96a}$$

$$Q_n^{(i)} = J_n(k_{i\rho}\rho_i)\cdot N_n'(k_{i\rho}\rho_{i+1}) - J_n'(k_{i\rho}\rho_{i+1})\cdot N_n(k_{i\rho}\rho_i), \tag{5.96b}$$

$$R_n^{(i)} = J_n'(k_{i\rho}\rho_i)\cdot N_n(k_{i\rho}\rho_{i+1}) - J_n(k_{i\rho}\rho_{i+1})\cdot N_n'(k_{i\rho}\rho_i), \tag{5.96c}$$

$$S_n^{(i)} = J_n'(k_{i\rho}\rho_i)\cdot N_n'(k_{i\rho}\rho_{i+1}) - J_n'(k_{i\rho}\rho_{i+1})\cdot N_n'(k_{i\rho}\rho_i); \tag{5.96d}$$

and

$$\overline{\boldsymbol{T}}^{-1}(k_{i\rho},\rho_i,\rho_{i+1}) = \begin{bmatrix} \overline{\boldsymbol{T}}_{ee}' & \overline{\boldsymbol{T}}_{eh}' \\ \overline{\boldsymbol{T}}_{he}' & \overline{\boldsymbol{T}}_{hh}' \end{bmatrix}, \tag{5.97}$$

$$\overline{\boldsymbol{T}}_{ee}' = \begin{bmatrix} -\frac{\pi k_{i\rho}\rho_{i+1}}{2}W_n^{(i)} & 0 \\ \frac{\pi n k_z}{2k_{i\rho}}[\frac{\rho_{i+1}}{\rho_i}W_n^{(i)} + V_n^{(i)}] & \frac{\pi k_{i\rho}\rho_{i+1}}{2}V_n^{(i)} \end{bmatrix}, \tag{5.98}$$

$$\overline{\boldsymbol{T}}_{hh}' = \overline{\boldsymbol{T}}_{ee}', \tag{5.99}$$

$$\overline{\boldsymbol{T}}_{eh}' = \begin{bmatrix} \frac{\pi n k_z}{2j\omega\epsilon_{r_i}}U_n^{(i)} & \frac{\pi k_{i\rho}^2\rho_{i+1}}{2j\omega\epsilon_{r_i}}U_n^{(i)} \\ -\frac{\pi\rho_{i+1}}{2j\omega\epsilon_{r_i}}[\frac{n^2k_z^2}{k_{i\rho}^2\rho_i\rho_{i+1}}U_n^{(i)} + k_i^2X_n^{(i)}] & -\frac{\pi n k_z\rho_{i+1}}{2j\omega\epsilon_{r_i}\rho_i}U_n^{(i)} \end{bmatrix}, \tag{5.100}$$

$$\overline{\boldsymbol{T}}_{he}' = \begin{bmatrix} -\frac{\pi n k_z}{2j\omega\mu_{r_i}}U_n^{(i)} & -\frac{\pi k_{i\rho}^2\rho_{i+1}}{2j\omega\mu_{r_i}}U_n^{(i)} \\ \frac{\pi\rho_{i+1}}{2j\omega\mu_{r_i}}[\frac{n^2k_z^2}{k_{i\rho}^2\rho_i\rho_{i+1}}U_n^{(i)} + k_i^2X_n^{(i)}] & \frac{\pi n k_z\rho_{i+1}}{2j\omega\mu_{r_i}\rho_i}U_n^{(i)} \end{bmatrix}, \tag{5.101}$$

in Eqs. (5.98-5.101),

$$U_n^{(i)} = J_n(k_{i\rho}\rho_{i+1})\cdot N_n(k_{i\rho}\rho_i) - J_n(k_{i\rho}\rho_i)\cdot N_n(k_{i\rho}\rho_{i+1}), \tag{5.102a}$$

$$V_n^{(i)} = J_n(k_{i\rho}\rho_{i+1})\cdot N_n'(k_{i\rho}\rho_i) - J_n'(k_{i\rho}\rho_i)\cdot N_n(k_{i\rho}\rho_{i+1}), \tag{5.102b}$$

$$W_n^{(i)} = J_n'(k_{i\rho}\rho_{i+1})\cdot N_n(k_{i\rho}\rho_i) - J_n(k_{i\rho}\rho_i)\cdot N_n'(k_{i\rho}\rho_{i+1}), \tag{5.102c}$$

$$X_n^{(i)} = J_n'(k_{i\rho}\rho_{i+1})\cdot N_n'(k_{i\rho}\rho_i) - J_n'(k_{i\rho}\rho_i)\cdot N_n'(k_{i\rho}\rho_{i+1}). \tag{5.102d}$$

5.3.3 Boundary Conditions and Green's Functions

In last section, we have found the relation of the tangential fields between two adjacent cylindrical surfaces. In this section, a two-layer coated PEC cylinder as shown in Fig. 5.1

is considered for the derivation of the Green's functions. The three cylindrical interface are defined as: PEC-substrate interface (innermost cylindrical surface), substrate-superstrate interface (middle cylindrical surface) and superstrate-air interface (outermost cylindrical surface), respectively. Boundary conditions are imposed on the middle cylindrical surface and Green's functions are then obtained. The TM wave solution on the outermost cylindrical surface is

$$\begin{bmatrix} \boldsymbol{e}_{TM}^{out} \\ \boldsymbol{h}_{TM}^{out} \end{bmatrix} = \begin{bmatrix} H_n^{(1)}(k_{3\rho}a_3) \\ -\frac{nk_z}{k_{3\rho}^2 a_3} H_n^{(1)}(k_{3\rho}a_3) \\ 0 \\ \frac{j\omega\epsilon_0}{k_{3\rho}} H_n'^{(1)}(k_{3\rho}a_3) \end{bmatrix}, \tag{5.103}$$

the TE wave solution on the outermost cylindrical surface is

$$\begin{bmatrix} \boldsymbol{e}_{TE}^{out} \\ \boldsymbol{h}_{TE}^{out} \end{bmatrix} = \begin{bmatrix} 0 \\ -\frac{j\omega\mu_0}{k_{3\rho}} H_n'^{(1)}(k_{3\rho}a_3) \\ H_n^{(1)}(k_{3\rho}a_3) \\ -\frac{nk_z}{k_{3\rho}^2 a_3} H_n^{(1)}(k_{3\rho}a_3) \end{bmatrix}. \tag{5.104}$$

On the innermost cylindrical surface, since it is a PEC cylinder surface, the TM wave solution is

$$\begin{bmatrix} \boldsymbol{e}_{TM}^{in} \\ \boldsymbol{h}_{TM}^{in} \end{bmatrix} = \begin{bmatrix} 0 \\ 0 \\ 0 \\ -\frac{j\omega\epsilon_1}{\pi k_{1\rho}^2 a_1 N_n(k_{1\rho}a_1)} \end{bmatrix}. \tag{5.105}$$

The TE wave solution is

$$\begin{bmatrix} \boldsymbol{e}_{TE}^{in} \\ \boldsymbol{h}_{TE}^{in} \end{bmatrix} = \begin{bmatrix} 0 \\ 0 \\ -\frac{1}{\pi k_{1\rho} a_1 N_n'(k_{1\rho}a_1)} \\ -\frac{nk_z}{\pi k_{1\rho}^3 a_1^2 N_n'(k_{1\rho}a_1)} \end{bmatrix}. \tag{5.106}$$

The fields on the inside of the middle cylindrical surface can be related to the fields on the innermost cylindrical surface through Eq. (5.89),

$$\begin{aligned}\begin{bmatrix} \boldsymbol{e}_{TM}^{mid-} \\ \boldsymbol{h}_{TM}^{mid-} \end{bmatrix} + \begin{bmatrix} \boldsymbol{e}_{TE}^{mid-} \\ \boldsymbol{h}_{TE}^{mid-} \end{bmatrix} &= \overline{\boldsymbol{T}}(k_{1\rho}, a_1, a_2) \cdot C_{TM}^{in} \begin{bmatrix} \boldsymbol{e}_{TM}^{in} \\ \boldsymbol{h}_{TM}^{in} \end{bmatrix} \\ &\quad + \overline{\boldsymbol{T}}(k_{1\rho}, a_1, a_2) \cdot C_{TE}^{in} \begin{bmatrix} \boldsymbol{e}_{TE}^{in} \\ \boldsymbol{h}_{TE}^{in} \end{bmatrix} \\ &= C_{TM}^{in} \cdot \boldsymbol{Y}_1 + C_{TE}^{in} \cdot \boldsymbol{Y}_2, \end{aligned} \tag{5.107}$$

The fields on the outside of the middle cylindrical surface can be related to the fields on the outermost cylindrical surface through Eq. (5.90),

$$\begin{aligned}\begin{bmatrix} \boldsymbol{e}_{TM}^{mid+} \\ \boldsymbol{h}_{TM}^{mid+} \end{bmatrix} + \begin{bmatrix} \boldsymbol{e}_{TE}^{mid+} \\ \boldsymbol{h}_{TE}^{mid+} \end{bmatrix} &= \overline{\boldsymbol{T}}^{-1}(k_{2\rho}, a_2, a_3) \cdot C_{TM}^{out} \begin{bmatrix} \boldsymbol{e}_{TM}^{out} \\ \boldsymbol{h}_{TM}^{out} \end{bmatrix} \\ &\quad + \overline{\boldsymbol{T}}^{-1}(k_{2\rho}, a_2, a_3) \cdot C_{TE}^{out} \begin{bmatrix} \boldsymbol{e}_{TE}^{out} \\ \boldsymbol{h}_{TE}^{out} \end{bmatrix} \\ &= C_{TM}^{out} \cdot \boldsymbol{Y}_3 + C_{TE}^{out} \cdot \boldsymbol{Y}_4, \end{aligned} \tag{5.108}$$

where C_{TM}^{in}, C_{TE}^{in}, C_{TM}^{out} and C_{TE}^{out} are unknown coefficients, and

$$\boldsymbol{Y}_1 = \overline{\boldsymbol{T}}(k_{1\rho}, a_1, a_2) \cdot \begin{bmatrix} \boldsymbol{e}_{TM}^{in} \\ \boldsymbol{h}_{TM}^{in} \end{bmatrix}, \tag{5.109}$$

$$\boldsymbol{Y}_2 = \overline{\boldsymbol{T}}(k_{1\rho}, a_1, a_2) \cdot \begin{bmatrix} \boldsymbol{e}_{TE}^{in} \\ \boldsymbol{h}_{TE}^{in} \end{bmatrix}, \tag{5.110}$$

$$\boldsymbol{Y}_3 = \overline{\boldsymbol{T}}^{-1}(k_{2\rho}, a_2, a_3) \cdot \begin{bmatrix} \boldsymbol{e}_{TM}^{in} \\ \boldsymbol{h}_{TM}^{in} \end{bmatrix}, \tag{5.111}$$

$$\boldsymbol{Y}_4 = \overline{\boldsymbol{T}}^{-1}(k_{2\rho}, a_2, a_3) \cdot \begin{bmatrix} \boldsymbol{e}_{TE}^{in} \\ \boldsymbol{h}_{TE}^{in} \end{bmatrix}. \tag{5.112}$$

Imposing the boundary condition on the middle cylindrical surface, where there are current J_z and J_ϕ on it, we get

$$\begin{bmatrix} \boldsymbol{e}_{TM}^{mid-} \\ \boldsymbol{h}_{TM}^{mid-} \end{bmatrix} + \begin{bmatrix} \boldsymbol{e}_{TE}^{mid-} \\ \boldsymbol{h}_{TE}^{mid-} \end{bmatrix} + \begin{bmatrix} 0 \\ 0 \\ -J_\phi \\ J_z \end{bmatrix} = \begin{bmatrix} \boldsymbol{e}_{TM}^{mid+} \\ \boldsymbol{h}_{TM}^{mid+} \end{bmatrix} + \begin{bmatrix} \boldsymbol{e}_{TE}^{mid+} \\ \boldsymbol{h}_{TE}^{mid+} \end{bmatrix}. \tag{5.113}$$

Substituting Eqs. (5.107-5.112) into Eq. (5.113), we obtain

$$\begin{bmatrix} \boldsymbol{Y}_1 & \boldsymbol{Y}_2 & \boldsymbol{Y}_3 & \boldsymbol{Y}_4 \end{bmatrix} \cdot \begin{bmatrix} C_{TM}^{in} \\ C_{TE}^{in} \\ -C_{TM}^{out} \\ -C_{TE}^{out} \end{bmatrix} = \begin{bmatrix} 0 \\ 0 \\ J_\phi \\ J_z \end{bmatrix}. \tag{5.114}$$

Solving Eq. (5.114) for the unknown coefficients C_{TM}^{in}, C_{TE}^{in}, C_{TM}^{out} and C_{TE}^{out}, the fields due to current J_z and J_ϕ anywhere in the layered media can be obtained, hence the Green's functions are obtained.

5.3.4 Rearrangement of the Green's Functions

The general form of the Green's functions components can be written as

$$\begin{bmatrix} \widetilde{G}_{zz} & \widetilde{G}_{z\phi} \\ \widetilde{G}_{\phi z} & \widetilde{G}_{\phi\phi} \end{bmatrix} = \begin{bmatrix} \frac{\widetilde{E}_{zz}}{\Delta_z} & \frac{\widetilde{E}_{z\phi}}{\Delta_z} \\ \frac{\widetilde{E}_{\phi\phi}}{\Delta_\phi} & \frac{\widetilde{E}_{\phi z}}{\Delta_\phi} \end{bmatrix}, \tag{5.115}$$

The expressions of $\widetilde{E}_{zz}$, $\widetilde{E}_{z\phi}$, $\widetilde{E}_{\phi z}$, $\widetilde{E}_{\phi\phi}$, Δ_ϕ, Δ_z are list in Appendix A, and it is found that they are functions of P_n, Q_n, R_n, S_n, U_n, V_n, W_n, X_n, H_n, H_n', where

$$\begin{bmatrix} H_n \\ H_n' \end{bmatrix} = \begin{bmatrix} H_n^{(1)}(k_{3\rho}a_3) \\ H_n^{'(1)}(k_{3\rho}a_3) \end{bmatrix}, \tag{5.116}$$

$$\begin{bmatrix} U_n & P_n \\ V_n & Q_n \\ W_n & R_n \\ X_n & S_n \end{bmatrix} = \begin{bmatrix} U_n^{(2)} & P_n^{(1)} \\ V_n^{(2)} & Q_n^{(1)} \\ W_n^{(2)} & R_n^{(1)} \\ X_n^{(2)} & S_n^{(1)} \end{bmatrix}. \tag{5.117}$$

where $U_n^{(2)}$, $P_n^{(1)}$, $V_n^{(2)}$, $Q_n^{(1)}$, $W_n^{(2)}$, $R_n^{(1)}$, $X_n^{(2)}$, $S_n^{(1)}$ are defined in (5.96) and (5.102). Rearrange the Green's function $\widetilde{G}_{zz}$ as follows,

$$\begin{aligned} & \widetilde{G}_{zz}(P_n, Q_n, R_n, S_n, U_n, V_n, W_n, X_n, H_n, H_n') \\ = & \frac{E_{zz}(P_n, Q_n, R_n, S_n, U_n, V_n, W_n, X_n, H_n, H_n')}{\Delta_z(P_n, Q_n, R_n, S_n, U_n, V_n, W_n, X_n, H_n, H_n')} \\ = & \frac{E_{zz}/(P_n R_n U_n^2 H_n^2)}{\Delta_z/(P_n R_n U_n^2 H_n^2)} \\ = & \widetilde{G}_{zz}(\frac{Q_n}{P_n}, \frac{S_n}{P_n}, \frac{R_n}{P_n}, \frac{Q_n}{R_n}, \frac{S_n}{R_n}, \frac{V_n}{U_n}, \frac{W_n}{U_n}, \frac{X_n}{U_n}, \frac{H_n'}{H_n}). \end{aligned} \tag{5.118}$$

Similarly, $\widetilde{G}_{z\phi}$, $\widetilde{G}_{\phi z}$, $\widetilde{G}_{\phi\phi}$ can be re-arranged as a function of ratios (Q_n/P_n), (S_n/P_n), (R_n/P_n), (Q_n/R_n), (S_n/R_n), (V_n/U_n), (W_n/U_n), (X_n/U_n), (H_n'/H_n). These nine types of ratio can be calculated recursively using the recursive relations given in Section 5.1.

5.4 Algorithm Implemented and Numerical Results

The recursive relations developed in Section 5.1 should be implemented. Specifically, an algorithm that can accurately calculate the first three recursive relations in Section 5.1 is the most crucial, since the rest recursive relations are all based on the first three recursive relations. During the computation of recursive relations, truncation errors are involved. It is important to know how errors may propagate in the recursive process. If the error does not exceed the desired numerical accuracy for a given order, the recursive process is said to be stable. The stability is strongly depending on the direction in which the recurrence is being applied [79]. For example, the Bessel function of the second kind satisfies the forward recursive process in a manner independent of argument and order.

The same argument also applies to the first kind Hankel function. However, the forward recursive relation is not suitable for the Bessel function of the first kind since the process depends strongly on the argument, order and recursive direction. In this case, continued fraction method rather than forward recursive relation applies to the Bessel function of the first kind [79].

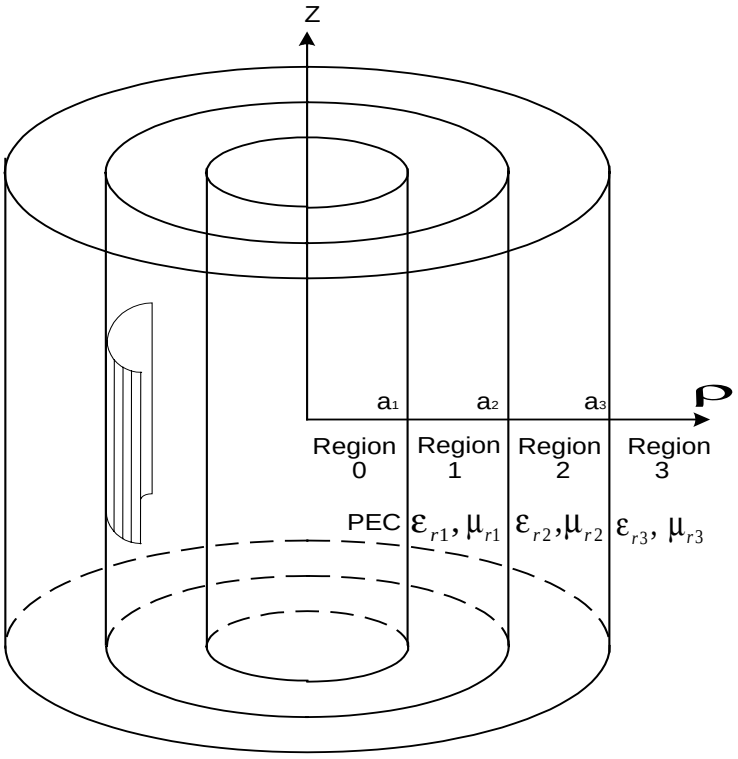

Figure 5.1: Dielectric-coated conducting cylinder with a superstrate, the shaded area denotes a conducting patch which is located at the interface of region 1 and region 2.

To verified the algorithm for recursive relation we developed, three cases are investigated for relation (5.13) using the recursive method. The results are listed in Table (5.1-5.3). The referenced results obtained by *Mathematical* 4.0 are in column $\Re[Y_m^{TM}]$ and $\Im[Y_m^{TM}]$, while the result obtained using Fortran code we have developed are in column $\Re[y_m^{TM}]$ and $\Im[y_m^{TM}]$. For the other recursive relations listed in Section 5.1, we have also found an excellent agreement between the results of our program and

Mathematical 4.0. This shows the reliability of our algorithm for the calculation of ratios using recursive relations.

Finally, cylindrical eigenmodes are computed using above recursive relations for Fig. 5.1. The results by 2×2 matrix method are compared with the results by 4×4 matrix method. They are listed in Table (5.4-5.6). In this case also, an excellent agreement can be observed.

5.5 Summary

The numerical evaluation of electrical field Green's functions is discussed in this chapter. The recursive relations and the re-arrangement of the two forms, i.e., the 2×2 and 4×4 matrix, of Green's functions are discussed. The recursive relations are important for the calculation of the Green's functions since the brutal force evaluation of cylindrical eigenmodes will definitely cause numerical overflow and underflow. After we re-arrange the spectral domain Green's functions or the cylindrical eigenmodes, the cylindrical eigenmodes are only functions of some types of ratios of special functions. These ratios of special function can be calculated recursively without numerical overflow and underflow. Numerical results in Table (5.1-5.3) show the validity of our program.

Details of re-arrangement of the Green's functions are provided. The aims are in two aspects. One is to verify the Green's functions developed in Chapter 4. As shown in Table (5.4-5.6), the spectral domain Green's functions calculated by the 2×2 and 4×4 matrix methods are in excellent agreement. This clearly shows the correctness of the multi-reflection matrix $\overline{\boldsymbol{M}}$ in Chapter 3. The other aspect is that one can select either one between these two forms of Green's functions according to one's preference. As shown in Section 5.2 and Appendix A, the expressions of the Green's functions by the 2×2 matrix method are less complicated than those by the 4×4 matrix method, but the re-arrangement of the Green's functions for the former case is more complicated

Table 5.1: Evaluation of ratio $[q(a,b)/p(a,b)]$ where $b = 0.0 + j10.0$, $a/b = 0.9$ by *Mathematical* 4.0 (in column $\Re[Y_m^{TM}]$ and $\Im[Y_m^{TM}]$) and Fortran code (in column $\Re[y_m^{TM}]$ and $\Im[y_m^{TM}]$).

Order	$\Re[Y_m^{TM}]$	$\Im[Y_m^{TM}]$	$\Re[y_m^{TM}]$	$\Im[y_m^{TM}]$
0	0.0000000	-1.262262	0.0000000	-1.262262
1	0.0000000	-1.265353	0.0000000	-1.265353
2	0.0000000	-1.274600	0.0000000	-1.274600
3	0.0000000	-1.289935	0.0000000	-1.289935
4	0.0000000	-1.311242	0.0000000	-1.311242
5	0.0000000	-1.338366	0.0000000	-1.338366
6	0.0000000	-1.371113	0.0000000	-1.371113
7	0.0000000	-1.409259	0.0000000	-1.409259
8	0.0000000	-1.452550	0.0000000	-1.452550
9	0.0000000	-1.500713	0.0000000	-1.500713
10	0.0000000	-1.553461	0.0000000	-1.553461
20	0.0000000	-2.268890	0.0000000	-2.268890
30	0.0000000	-3.165766	0.0000000	-3.165766
40	0.0000000	-4.121655	0.0000000	-4.121655
50	0.0000000	-5.097356	0.0000000	-5.097356
60	0.0000000	-6.081432	0.0000000	-6.081432
70	0.0000000	-7.070081	0.0000000	-7.070081
80	0.0000000	-8.061498	0.0000000	-8.061498
90	0.0000000	-9.054782	0.0000000	-9.054782
100	0.0000000	-10.04939	0.0000000	-10.04939
110	0.0000000	-11.04495	0.0000000	-11.04495
120	0.0000000	-12.04125	0.0000000	-12.04125
130	0.0000000	-13.03811	0.0000000	-13.03811

Table 5.2: Evaluation of ratio $[q(a,b)/p(a,b)]$ where $b = 10.0 + j10.0$, $a/b = 0.9$ by *Mathematical* 4.0 (in column $\Re[Y_m^{TM}]$ and $\Im[Y_m^{TM}]$) and Fortran code (in column $\Re[y_m^{TM}]$ and $\Im[y_m^{TM}]$).

Order	$\Re[Y_m^{TM}]$	$\Im[Y_m^{TM}]$	$\Re[y_m^{TM}]$	$\Im[y_m^{TM}]$
0	0.1921036	-0.8427190	0.1921036	-0.8427190
1	0.1941740	-0.8438992	0.1941740	-0.8438992
2	0.2003651	-0.8474354	0.2003651	-0.8474354
3	0.2106171	-0.8533145	0.2106171	-0.8533145
4	0.2248328	-0.8615147	0.2248328	-0.8615147
5	0.2428799	-0.8720055	0.2428798	-0.8720055
6	0.2645955	-0.8847476	0.2645955	-0.8847476
7	0.2897907	-0.8996932	0.2897906	-0.8996932
8	0.3182554	-0.9167865	0.3182554	-0.9167865
9	0.3497644	-0.9359634	0.3497644	-0.9359634
10	0.3840820	-0.9571529	0.3840819	-0.9571529
20	0.8315277	-1.260766	0.8315277	-1.260766
30	1.354757	-1.670491	1.354757	-1.670491
40	1.882916	-2.125725	1.882916	-2.125725
50	2.404043	-2.599897	2.404043	-2.599897
60	2.919167	-3.083022	2.919144	-3.083022
70	3.430283	-3.571098	3.430279	-3.571098
80	3.938744	-4.062186	3.938743	-4.062186
90	4.445387	-4.555269	4.445387	-4.555269
100	4.950738	-5.049743	4.950738	-5.049743
110	5.455138	-5.545225	5.455138	-5.545225
120	5.958819	-6.041461	5.958819	-6.041461
130	6.461943	-6.538278	6.461943	-6.538278

Table 5.3: Evaluation of ratio $[q(a,b)/p(a,b)]$ where $b = 10.0 + j0.0$, $a/b = 0.9$ by *Mathematical* 4.0 (in column $\Re[Y_m^{TM}]$ and $\Im[Y_m^{TM}]$) and Fortran code (in column $\Re[y_m^{TM}]$ and $\Im[y_m^{TM}]$).

Order	$\Re[Y_m^{TM}]$	$\Im[Y_m^{TM}]$	$\Re[y_m^{TM}]$	$\Im[y_m^{TM}]$
0	0.5910747	0.0000000	0.5910747	0.0000000
1	0.5951438	0.0000000	0.5951438	0.0000000
2	0.6073090	0.0000000	0.6073090	0.0000000
3	0.6274451	0.0000000	0.6274451	0.0000000
4	0.6553485	0.0000000	0.6553485	0.0000000
5	0.6907439	0.0000000	0.6907439	0.0000000
6	0.7332938	0.0000000	0.7332938	0.0000000
7	0.7826085	0.0000000	0.7826085	0.0000000
8	0.8382582	0.0000000	0.8382582	0.0000000
9	0.8997851	0.0000000	0.8997851	0.0000000
10	0.9667143	0.0000000	0.9667143	0.0000000
20	1.834651	0.0000000	1.834651	0.0000000
30	2.848544	0.0000000	2.848544	0.0000000
40	3.878381	0.0000000	3.878381	0.0000000
50	4.901334	0.0000000	4.901334	0.0000000
60	5.917484	0.0000000	5.917484	0.0000000
70	6.929230	0.0000000	6.929230	0.0000000
80	7.938038	0.0000000	7.938038	0.0000000
90	8.944890	0.0000000	8.944890	0.0000000
100	9.950374	0.0000000	9.950374	0.0000000
110	10.95486	0.0000000	10.95486	0.0000000
120	11.95861	0.0000000	11.95861	0.0000000
130	12.96178	0.0000000	12.96178	0.0000000

Table 5.4: Evaluation of Green's function components $\widetilde{G}_{zf}$ and $\widetilde{G}_{fz}$ by 4×4 and 2×2 matrix methods. The dielectric and geometry parameters in Fig. 5.1 are: $a_1 = 50$ mm, $a_2 = 53$ mm, $a_3 = 56$ mm, $\epsilon_{r1} = 2$, $\epsilon_{r2} = 5$, $\epsilon_{r3} = 1$. $\rho = \rho' = 53$ mm, $f = 7.5$ GHz.

k_z, (order = 100)	$\widetilde{G}_{zf}, \widetilde{G}_{fz}(4 \times 4$ matrix)	$\widetilde{G}_{zf}, \widetilde{G}_{fz}(2 \times 2$ matrix)
0.100619 -j5.030968E-03	-1.739939E-03 -j3.479877E-02	-1.739939E-03 -j3.479877E-02
3.87177 -j0.193588	-6.695126E-02 -j1.33903	-6.695126E-02 -j1.33903
13.0703 -j0.653513	-0.225998 -j4.52018	-0.225998 -j4.52018
27.5528 -j1.37764	-0.476294 -j9.52798	-0.476294 -j9.52798
47.0932 -j2.35466	-0.813570 -j16.2818	-0.813570 -j16.2818
71.3864 -j3.56932	-1.23172 -j24.6707	-1.23172 -j24.6707
100.053 -j5.00265	-1.72270 -j34.5535	-1.72270 -j34.5535
132.645 -j6.63227	-2.27644 -j45.7600	-2.27644 -j45.7600
168.655 -j8.43275	-2.88099 -j58.0929	-2.88099 -j58.0929
207.519 -j10.3760	-3.52280 -j71.3319	-3.52280 -j71.3319
248.631 -j12.4316	-4.18720 -j85.2383	-4.18720 -j85.2383
291.349 -j14.5674	-4.85901 -j99.5612	-4.85901 -j99.5612
335.006 -j16.7503	-5.52335 -j114.045	-5.52335 -j114.045
378.920 -j18.9460	-6.16564 -j128.438	-6.16564 -j128.438
422.405 -j21.1203	-6.77489 -j142.495	-6.77489 -j142.495
464.783 -j23.2392	-7.34492 -j156.018	-7.34492 -j156.018
505.392 -j25.2696	-7.86098 -j168.760	-7.86098 -j168.760
543.598 -j27.1799	-8.32131 -j180.560	-8.32131 -j180.560
578.804 -j28.9402	-8.72327 -j191.264	-8.72327 -j191.264
610.461 -j30.5230	-9.06617 -j200.744	-9.06617 -j200.744
638.073 -j31.9037	-9.35075 -j208.899	-9.35075 -j208.899
661.211 -j33.0606	-9.57875 -j215.648	-9.57875 -j215.648
679.513 -j33.9756	-9.75230 -j220.931	-9.75230 -j220.931

Table 5.5: Evaluation of Green's function component $\widetilde{G}_{zz}$ by 4×4 and 2×2 matrix methods. The dielectric and geometry parameters in Fig. 5.1 are: $a_1 = 50$ mm, $a_2 = 53$ mm, $a_3 = 56$ mm, $\epsilon_{r1} = 2$, $\epsilon_{r2} = 5$, $\epsilon_{r3} = 1$. $\rho = \rho' = 53$ mm, $f = 7.5$ GHz.

k_z, (order = 100)	$\widetilde{G}_{zz}(4 \times 4$ matrix)	$\widetilde{G}_{zz}(2 \times 2$ matrix)
0.100619 -j5.030968E-03	-1.879120E-07 +j15.8878	-1.879120E-07 +j15.8878
3.87177 -j0.193588	-2.782326E-04 +j15.8850	-2.782326E-04 +j15.8850
13.0703 -j0.653513	-3.170580E-03 +j15.8562	-3.170580E-03 +j15.8562
27.5528 -j1.37764	-1.408727E-02 +j15.7473	-1.408727E-02 +j15.7473
47.0932 -j2.35466	-4.113668E-02 +j15.4773	-4.113668E-02 +j15.4773
71.3864 -j3.56932	-9.444583E-02 +j14.9450	-9.444583E-02 +j14.9450
100.053 -j5.00265	-0.185267 +j14.0371	-0.185267 +j14.0371
132.645 -j6.63227	-0.324918 +j12.6384	-0.324918 +j12.6384
168.655 -j8.43275	-0.523644 +j10.6428	-0.523644 +j10.6428
207.519 -j10.3760	-0.789482 +j7.96350	-0.789482 +j7.96350
248.631 -j12.4316	-1.12726 +j4.54274	-1.12726 +j4.54274
291.349 -j14.5674	-1.53787 +j0.359695	-1.53787 +j0.359695
335.006 -j16.7503	-2.01782 -j4.56452	-2.01782 -j4.56452
378.920 -j18.9460	-2.55910 -j10.1644	-2.55910 -j10.1644
422.405 -j21.1203	-3.14997 -j16.3327	-3.14997 -j16.3327
464.783 -j23.2392	-3.77609 -j22.9266	-3.77609 -j22.9266
505.392 -j25.2696	-4.41834 -j29.7644	-4.41834 -j29.7644
543.598 -j27.1799	-5.05826 -j36.6482	-5.05826 -j36.6482
578.804 -j28.9402	-5.67642 -j43.3662	-5.67642 -j43.3662
610.461 -j30.5230	-6.25395 -j49.7040	-6.25395 -j49.7040
638.073 -j31.9037	-6.77336 -j55.4553	-6.77336 -j55.4553
661.211 -j33.0606	-7.21912 -j60.4303	-7.21912 -j60.4303
679.513 -j33.9756	-7.57813 -j64.4637	-7.57813 -j64.4637

Table 5.6: Evaluation of Green's function component $\widetilde{G}_{ff}$ by 4×4 and 2×2 matrix methods. The dielectric and geometry parameters in Fig. 5.1 are: $a_1 = 50$ mm, $a_2 = 53$ mm, $a_3 = 56$ mm, $\epsilon_{r1} = 2$, $\epsilon_{r2} = 5$, $\epsilon_{r3} = 1$. $\rho = \rho' = 53$ mm, $f = 7.5$ GHz.

k_z, (order = 100)	$\widetilde{G}_{ff}(4 \times 4$ matrix)	$\widetilde{G}_{ff}(2 \times 2$ matrix)
0.100619 -j5.030968E-03	9.276009E-08 -j636.579	9.276009E-08 -j636.579
3.87177 -j0.193588	1.373439E-04 -j636.578	1.373439E-04 -j636.578
13.0703 -j0.653513	1.565058E-03 -j636.563	1.565058E-03 -j636.563
27.5528 -j1.37764	6.953156E-03 -j636.510	6.953156E-03 -j636.510
47.0932 -j2.35466	2.029988E-02 -j636.376	2.029988E-02 -j636.376
71.3864 -j3.56932	4.658735E-02 -j636.114	4.658735E-02 -j636.114
100.053 -j5.00265	9.132232E-02 -j635.666	9.132232E-02 -j635.666
132.645 -j6.63227	0.159986 -j634.977	0.159986 -j634.977
168.655 -j8.43275	0.257438 -j633.995	0.257438 -j633.995
207.519 -j10.3760	0.387323 -j632.679	0.387323 -j632.679
248.631 -j12.4316	0.551567 -j631.003	0.551567 -j631.003
291.349 -j14.5674	0.750020 -j628.960	0.750020 -j628.960
335.006 -j16.7503	0.980296 -j626.562	0.980296 -j626.562
378.920 -j18.9460	1.24112 -j623.799	1.24112 -j623.799
422.405 -j21.1203	1.52019 -j620.814	1.52019 -j620.814
464.783 -j23.2392	1.80136 -j617.850	1.80136 -j617.850
505.392 -j25.2696	2.09641 -j614.596	2.09641 -j614.596
543.598 -j27.1799	2.38698 -j611.337	2.38698 -j611.337
578.804 -j28.9402	2.66440 -j608.174	2.66440 -j608.174
610.461 -j30.5230	2.92063 -j605.205	2.92063 -605.205
638.073 -j31.9037	3.14862 -j602.524	3.14862 -j602.524
661.211 -j33.0606	3.34240 -j600.215	3.34240 -j600.215
679.513 -j33.9756	3.49719 -j598.350	3.49719 -j598.350

than that for the latter one.

Chapter 6

Mixed Potential Green's Function for Cylindrically Layered Media

---

In Chapter 4, we have obtained the fast computational form of electric field Green's functions for the case where the source point and the field point are not located on the same cylindrical surface. How to obtain the fast computational form of Green's functions when the source point and the field point are located on the same cylindrical surface, is still a problem, since convergence problem will occur. This chapter will investigate the problem. Green's functions of another form, i.e., mixed potential Green's functions are studied instead of the electric field Green's functions for this kind of problem. A method for fast computation of mixed potential spatial domain Green's functions for cylindrically stratified media is presented. Based on the convergence behaviour of mixed potential spectral domain Green's functions, DCIM and extrapolation techniques are employed to perform the inverse Fourier transform, which is different from that of planarly stratified media. In order to evaluate the summation of cylindrical eigenmodes from negative infinity to positive infinity, the Green's functions in spectral domain are rearranged so that series acceleration technique can be well applied to speed up the

convergence of summation process. For the integral on the deformed Sommerfeld integral path with respect to k_z, DCIM is used to speed up the computation. After the quasi-static components, which correspond to the far region of the spectrum contained in the spectral domain Green's functions, are subtracted from the spectral domain Green's functions, the inverse transform of the remaining part has its simple approximated form. The mixed potential Green's functions presented here are useful for analyzing conformal patch structures mounted on cylindrically stratified media. This chapter is organized as in the following. The mixed potential Green's functions are derived in Section 6.1 from the electric field Green's functions. A fast computational procedure for the spatial domain mixed potential Green's functions is presented in Section 6.2. Some numerical examples are presented for a specific cylindrically multilayered structure in Section 6.3.

6.1 Spectral Domain Mixed Potential Green's Functions

As well known, MPIE is better than the EFIE for analyzing multilayered structures. So the mixed potential Green's functions, which are special for the MPIE, are more useful than the field Green's functions that are special for the EFIE. The mixed potential Green's functions were first developed for single-layered cylindrical structure in [87]. The extrapolation and interpolation techniques had been used in [87] to evaluate the summation of cylindrical eigenmodes. However, it only dealt with single-layered structures. For structures with more than one layer, multiple wave transmission and reflection will make it complicated to evaluate the summation of cylindrical eigenmodes. In this chpater, a more general form of the mixed potential Green's functions for multilayered cylindrical structure is developed. Several techniques including the DCIM, the large argument approximation of the zeroth-order Hankel functions and the Shanks' transform and Kummer's transform were employed to provide the so-called closed-form Green's functions.

The inverse Fourier transform of spectral domain Green's functions for cylindrically stratified media involves a summation of the cylindrical eigenmodes and an integral with respect to k_z on the complex plane. If the ρ at a field point is much larger than ρ' at a source point (the same as that in the case of [81]), the cylindrical eigenmodes form a fast convergent series. However, this is not the case when ρ and ρ' are equal to each other. In order to obtain a convergent result, the summation of a large number of cylindrical eigenmodes is needed. This is due to the slowly convergent components, i.e., the quasi-static components contained in the cylindrical eigenmodes. If the quasi-static components are not completely extracted out, then the Shanks' transform [95] is necessary for obtaining a convergent result. If the slowly convergent components in spectral domain are completely extracted out and transformed into those in spatial domain in closed form, then the summation process of the cylindrical eigenmodes will be speeded up; this is actually the application of the Kummer's transform [92] for the slowly convergent series. This scheme helps to achieve a much better convergent series of cylindrical eigenmodes, and to obtain an accurate result, especially for a small azimuthal separation. Spectral domain mixed potential Green's functions will be derived in subsection 6.1.2, followed by a step-by-step discussion of how to evaluate the spatial domain mixed potential Green's functions.

6.1.1 Spectral Domain Electric Field Green's Functions

Consider a cylindrically stratified medium as shown in Fig. 3.5, in the case of a source point in region j and a field point in region i (where the j and i in the subscript position of the formulation denote the index of the region, while j in other position in the formulation represents the complex number $j = \sqrt{-1}$), the dyadic electric field Green's functions derived in Chapter 4 are rewritten here for convenient discussion,

$\hat{z}$-oriented electrical dipole:

$$\tilde{G}^{E_n}_{zz} = -\frac{1}{8\pi\epsilon_j\omega}\cdot k^2_{j\rho} f_{11}, \tag{6.1a}$$

$$\tilde{G}^{E_n}_{\phi z} = -\frac{1}{8\pi\epsilon_j\omega k^2_{i\rho}}\cdot k^2_{j\rho}\Big(-\frac{k_z n}{\rho} f_{11} - j\omega\mu_i\frac{\partial f_{21}}{\partial\rho}\Big), \tag{6.1b}$$

$$\tilde{G}^{E_n}_{\rho z} = \frac{1}{8\pi\epsilon_j\omega k^2_{i\rho}}\cdot k^2_{j\rho}\Big(-jk_z\frac{\partial f_{11}}{\partial\rho} + \frac{n\omega\mu_i}{\rho} f_{21}\Big); \tag{6.1c}$$

$\hat{\phi}$-oriented electrical dipole:

$$\tilde{G}^{E_n}_{z\phi} = -\frac{1}{8\pi\epsilon_j\omega}\cdot\Big(j\omega\epsilon_j\frac{\partial f_{12}}{\partial\rho'} - \frac{k_z n}{\rho'} f_{11}\Big), \tag{6.2a}$$

$$\begin{aligned}\tilde{G}^{E_n}_{\phi\phi} = -\frac{1}{8\pi\epsilon_j\omega k^2_{i\rho}}\cdot\Big[&\frac{k_z n}{\rho'}\Big(\frac{k_z n}{\rho} f_{11} + j\omega\mu_i\frac{\partial f_{21}}{\partial\rho}\Big)\\ &- j\omega\epsilon_j\Big(\frac{k_z n}{\rho}\frac{\partial f_{12}}{\partial\rho'} + j\omega\mu_i\frac{\partial^2 f_{22}}{\partial\rho\partial\rho'}\Big)\Big],\end{aligned} \tag{6.2b}$$

$$\begin{aligned}\tilde{G}^{E_n}_{\rho\phi} = -\frac{1}{8\pi\epsilon_j\omega k^2_{i\rho}}\cdot\Big[&jk_z\Big(j\omega\epsilon_j\frac{\partial^2 f_{12}}{\partial\rho\partial\rho'} - \frac{k_z n}{\rho'}\frac{\partial f_{11}}{\partial\rho}\Big)\\ &- \frac{n\omega\mu_i}{\rho}\Big(j\omega\epsilon_j\frac{\partial f_{22}}{\partial\rho'} - \frac{k_z n}{\rho'} f_{21}\Big)\Big];\end{aligned} \tag{6.2c}$$

$\hat{\rho}$-oriented electrical dipole:

$$\tilde{G}^{E_n}_{z\rho} = -\frac{1}{8\pi\epsilon_j\omega}\cdot\Big(jk_z\frac{\partial f_{11}}{\partial\rho'} + \frac{n\omega\epsilon_j}{\rho'} f_{12}\Big), \tag{6.3a}$$

$$\begin{aligned}\tilde{G}^{E_n}_{\phi\rho} = -\frac{1}{8\pi\epsilon_j\omega k^2_{i\rho}}\cdot\Big[&\frac{k_z n}{\rho}\Big(jk_z\frac{\partial f_{11}}{\partial\rho'} + \frac{n\omega\epsilon_j}{\rho'} f_{12}\Big)\\ &+ j\omega\mu_i\Big(jk_z\frac{\partial^2 f_{21}}{\partial\rho\partial\rho'} + \frac{n\omega\epsilon_j}{\rho'}\frac{\partial f_{22}}{\partial\rho}\Big)\Big],\end{aligned} \tag{6.3b}$$

$$\begin{aligned}\tilde{G}^{E_n}_{\rho\rho} = \frac{1}{8\pi\epsilon_j\omega k^2_{i\rho}}\cdot\Big[&jk_z\Big(-jk_z\frac{\partial^2 f_{11}}{\partial\rho\partial\rho'} - \frac{n\omega\epsilon_j}{\rho'}\frac{\partial f_{12}}{\partial\rho}\Big)\\ &+ \frac{\omega n\mu_i}{\rho}\Big(jk_z\frac{\partial f_{21}}{\partial\rho'} + \frac{n\omega\epsilon_j}{\rho'} f_{22}\Big)\Big].\end{aligned} \tag{6.3c}$$

6.1.2 Spectral Domain Mixed Potential Green's Functions

Consider the structure as shown in Fig. 5.1. We want to construct mixed potential Green's functions for such a structure where the source and field point are located on the same cylindrical surface. First, we assume current $J_\rho = 0$. This two dimensional consideration comes from the fact that most practical circuit or antenna are conformal

to the cylindrically multilayered structure. The mixed potential Green's function will be derived from the electric field Green's functions in (6.1)-(6.3). The electric field due to the current can be expressed in a mixed potential form as

$$\boldsymbol{E} = -j\omega\boldsymbol{A} - \nabla\phi, \tag{6.4}$$

where

$$\boldsymbol{A} = \int\int_s \overline{\boldsymbol{G}}_A \cdot \boldsymbol{J}(r')ds'. \tag{6.5}$$

The electric scalar potential is related the vector potential by Lorentz gauge. To deduce the scalar potential Green's function, one must transform the divergence operator to act on the current density. A general form of ϕ is postulated as [67]

$$\phi = \int\int_s \nabla' \cdot \overline{\boldsymbol{G}}_\phi \cdot \boldsymbol{J}(r')ds'. \tag{6.6}$$

Denote $\widetilde{\overline{\boldsymbol{G}}}_E, \widetilde{\overline{\boldsymbol{G}}}_A, \widetilde{\overline{\boldsymbol{G}}}_\phi$ are the spectral domain counterpart of $\overline{\boldsymbol{G}}_E, \overline{\boldsymbol{G}}_A, \overline{\boldsymbol{G}}_\phi$, respectively,

$$\widetilde{\overline{\boldsymbol{G}}}_E = -j\omega\widetilde{\overline{\boldsymbol{G}}}_A - \nabla\nabla' \cdot (\widetilde{\overline{\boldsymbol{G}}}_\phi), \tag{6.7}$$

$$\widetilde{\overline{\boldsymbol{G}}}_E = \begin{bmatrix} \tilde{G}^{E_n}_{\rho\rho} & \tilde{G}^{E_n}_{\rho\phi} & \tilde{G}^{E_n}_{\rho z} \\ \tilde{G}^{E_n}_{\phi\rho} & \tilde{G}^{E_n}_{\phi\phi} & \tilde{G}^{E_n}_{\phi z} \\ \tilde{G}^{E_n}_{z\rho} & \tilde{G}^{E_n}_{z\phi} & \tilde{G}^{E_n}_{zz} \end{bmatrix}, \tag{6.8}$$

$$\widetilde{\overline{\boldsymbol{G}}}_A = \begin{bmatrix} \tilde{G}^{A}_{\rho\rho} & \tilde{G}^{A}_{\rho\phi} & \tilde{G}^{A}_{\rho z} \\ \tilde{G}^{A}_{\phi\rho} & \tilde{G}^{A}_{\phi\phi} & \tilde{G}^{A}_{\phi z} \\ \tilde{G}^{A}_{z\rho} & \tilde{G}^{A}_{z\phi} & \tilde{G}^{A}_{zz} \end{bmatrix}, \tag{6.9}$$

$$\widetilde{\overline{\boldsymbol{G}}}_\phi = \begin{bmatrix} \tilde{G}^{\phi}_{\rho\rho} & 0 & 0 \\ 0 & \tilde{G}^{\phi}_{\phi\phi} & 0 \\ 0 & 0 & \tilde{G}^{\phi}_{zz} \end{bmatrix}. \tag{6.10}$$

By using dyadic identities [89, 90], $\nabla\nabla' \cdot (\widetilde{\overline{\boldsymbol{G}}}_\phi)$ can be expanded as

$$\nabla\nabla' \cdot (\widetilde{\overline{\boldsymbol{G}}}_\phi) = \widehat{\boldsymbol{\rho}}[(\frac{1}{\rho'}\frac{\partial\tilde{G}^{\phi}_{\rho\rho}}{\partial\rho} + \frac{\partial^2\tilde{G}^{\phi}_{\rho\rho}}{\partial\rho\partial\rho'} - \frac{1}{\rho'}\frac{\partial\tilde{G}^{\phi}_{\phi\phi}}{\partial\rho})\widehat{\boldsymbol{\rho}}$$

$$
\begin{aligned}
&+\frac{1}{\rho'}\frac{\partial^2\widetilde{G}^{\phi}_{\phi\phi}}{\partial\rho\partial\phi'}\widehat{\boldsymbol{\phi}}+\frac{\partial^2\widetilde{G}^{\phi}_{zz}}{\partial\rho\partial z'}\widehat{\boldsymbol{z}}]\\
&+\frac{1}{\rho}\widehat{\boldsymbol{\phi}}[(\frac{1}{\rho'}\frac{\partial\widetilde{G}^{\phi}_{\rho\rho}}{\partial\phi}+\frac{\partial^2\widetilde{G}^{\phi}_{\rho\rho}}{\partial\phi\partial\rho'}-\frac{1}{\rho'}\frac{\partial\widetilde{G}^{\phi}_{\phi\phi}}{\partial\phi}\\
&-\frac{1}{\rho'}\frac{\partial\widetilde{G}^{\phi}_{\phi\phi}}{\partial\phi'})\widehat{\boldsymbol{\rho}}+(\frac{1}{\rho'}\frac{\partial^2\widetilde{G}^{\phi}_{\phi\phi}}{\partial\phi\partial\phi'}+\frac{\widetilde{G}^{\phi}_{\rho\rho}}{\rho'}+\frac{\partial\widetilde{G}^{\phi}_{\rho\rho}}{\partial\rho'}\\
&-\frac{1}{\rho'}\widetilde{G}^{\phi}_{\phi\phi})\widehat{\boldsymbol{\phi}}+\frac{\partial^2\widetilde{G}^{\phi}_{zz}}{\partial\phi\partial z'}\widehat{\boldsymbol{z}}]\\
&+\widehat{\boldsymbol{z}}[(\frac{\partial^2\widetilde{G}^{\phi}_{\rho\rho}}{\partial z\partial\rho'}+\frac{1}{\rho'}\frac{\widetilde{G}^{\phi}_{\rho\rho}}{\partial z}-\frac{1}{\rho'}\frac{\widetilde{G}^{\phi}_{\phi\phi}}{\partial z})\widehat{\boldsymbol{\rho}}\\
&+\frac{1}{\rho'}\frac{\partial^2\widetilde{G}^{\phi}_{\phi\phi}}{\partial z\partial\phi'}\widehat{\boldsymbol{\phi}}+\frac{\partial^2\widetilde{G}^{\phi}_{zz}}{\partial z\partial z'}\widehat{\boldsymbol{z}}]. \qquad (6.11)
\end{aligned}
$$

Considering (6.4), (6.8), (6.9), (6.10), (6.11), the tangential electrical field can be written as

$$
\begin{aligned}
\begin{bmatrix}\widetilde{\boldsymbol{E}}_{\phi}\\ \widetilde{\boldsymbol{E}}_{z}\end{bmatrix} &= \begin{bmatrix}\tilde{G}^{E_n}_{\phi\rho} & \tilde{G}^{E_n}_{\phi\phi} & \tilde{G}^{E_n}_{\phi z}\\ \tilde{G}^{E_n}_{z\rho} & \tilde{G}^{E_n}_{z\phi} & \tilde{G}^{E_n}_{zz}\end{bmatrix}\cdot\begin{bmatrix}J_\rho\\ J_\phi\\ J_z\end{bmatrix}\\
&= -j\omega\begin{bmatrix}\tilde{G}^{A}_{\phi\rho} & \tilde{G}^{A}_{\phi\phi} & \tilde{G}^{A}_{\phi z}\\ \tilde{G}^{A}_{z\rho} & \tilde{G}^{A}_{z\phi} & \tilde{G}^{A}_{zz}\end{bmatrix}\cdot\begin{bmatrix}J_\rho\\ J_\phi\\ J_z\end{bmatrix}-[\nabla\nabla'\cdot(\overline{\widetilde{\boldsymbol{G}}}_{\phi})]_t\cdot\begin{bmatrix}J_\rho\\ J_\phi\\ J_z\end{bmatrix}, \qquad (6.12)
\end{aligned}
$$

in which $\nabla\nabla'\cdot(\overline{\widetilde{\boldsymbol{G}}}_{\phi})_t$ is the tangential component of $\nabla\nabla'\cdot(\overline{\widetilde{\boldsymbol{G}}}_{\phi})$, that is

$$
\begin{aligned}
\nabla\nabla'\cdot(\overline{\widetilde{\boldsymbol{G}}}_{\phi})_t &= \frac{1}{\rho}\widehat{\boldsymbol{\phi}}[(\frac{1}{\rho'}\frac{\partial\widetilde{G}^{\phi}_{\rho\rho}}{\partial\phi}+\frac{\partial^2\widetilde{G}^{\phi}_{\rho\rho}}{\partial\phi\partial\rho'}-\frac{1}{\rho'}\frac{\partial\widetilde{G}^{\phi}_{\phi\phi}}{\partial\phi}\\
&-\frac{1}{\rho'}\frac{\partial\widetilde{G}^{\phi}_{\phi\phi}}{\partial\phi'})\widehat{\boldsymbol{\rho}}+(\frac{1}{\rho'}\frac{\partial^2\widetilde{G}^{\phi}_{\phi\phi}}{\partial\phi\partial\phi'}+\frac{\widetilde{G}^{\phi}_{\rho\rho}}{\rho'}+\frac{\partial\widetilde{G}^{\phi}_{\rho\rho}}{\partial\rho'}\\
&-\frac{1}{\rho'}\widetilde{G}^{\phi}_{\phi\phi})\widehat{\boldsymbol{\phi}}+\frac{\partial^2\widetilde{G}^{\phi}_{zz}}{\partial\phi\partial z'}\widehat{\boldsymbol{z}}]\\
&+\widehat{\boldsymbol{z}}[(\frac{\partial^2\widetilde{G}^{\phi}_{\rho\rho}}{\partial z\partial\rho'}+\frac{1}{\rho'}\frac{\widetilde{G}^{\phi}_{\rho\rho}}{\partial z}-\frac{1}{\rho'}\frac{\widetilde{G}^{\phi}_{\phi\phi}}{\partial z})\widehat{\boldsymbol{\rho}}\\
&+\frac{1}{\rho'}\frac{\partial^2\widetilde{G}^{\phi}_{\phi\phi}}{\partial z\partial\phi'}\widehat{\boldsymbol{\phi}}+\frac{\partial^2\widetilde{G}^{\phi}_{zz}}{\partial z\partial z'}\widehat{\boldsymbol{z}}]. \qquad (6.13)
\end{aligned}
$$

If the patch is conformal to the cylinder, it is reasonable to postulate that current component $J_\rho = 0$ (for the case of $J_\rho \neq 0$, more dyadic components will be needed

for the derivation of potential Green's functions. See Appendix B). Without loss of generality, let $\widetilde{G}^{\phi}_{\rho\rho} = 0$ and $\widetilde{G}^{\phi}_{\phi\phi} = \widetilde{G}^{\phi}_{zz} = \widetilde{G}^{\phi}$. Considering (6.13), (6.12) can be further reduced to

$$\begin{aligned}
\begin{bmatrix} \widetilde{\boldsymbol{E}}_{\phi} \\ \widetilde{\boldsymbol{E}}_{z} \end{bmatrix}_{J_\rho=0} &= \begin{bmatrix} \tilde{G}^{E_n}_{\phi\phi} & \tilde{G}^{E_n}_{\phi z} \\ \tilde{G}^{E_n}_{z\phi} & \tilde{G}^{E_n}_{zz} \end{bmatrix} \cdot \begin{bmatrix} J_\phi \\ J_z \end{bmatrix} \\
&= -j\omega \begin{bmatrix} \tilde{G}^{A}_{\phi\phi} & \tilde{G}^{A}_{\phi z} \\ \tilde{G}^{A}_{z\phi} & \tilde{G}^{A}_{zz} \end{bmatrix} \cdot \begin{bmatrix} J_\phi \\ J_z \end{bmatrix} - \nabla\nabla' \cdot (\overline{\overline{\boldsymbol{G}}}_{\phi})_t \cdot \begin{bmatrix} J_\phi \\ J_z \end{bmatrix}, \qquad (6.14)
\end{aligned}$$

where

$$\begin{aligned}
\nabla\nabla' \cdot (\overline{\overline{\boldsymbol{G}}}_{\phi})_t &= \frac{1}{\rho}\widehat{\boldsymbol{\phi}}[(\frac{1}{\rho'}\frac{\partial^2 \widetilde{G}^{\phi}}{\partial\phi\partial\phi'} - \frac{1}{\rho'}\widetilde{G}^{\phi})\widehat{\boldsymbol{\phi}} + \frac{\partial^2 \widetilde{G}^{\phi}}{\partial\phi\partial z'}\widehat{\boldsymbol{z}}] \\
&\quad + \widehat{\boldsymbol{z}}(\frac{1}{\rho'}\frac{\partial^2 \widetilde{G}^{\phi}}{\partial z\partial\phi'}\widehat{\boldsymbol{\phi}} + \frac{\partial^2 \widetilde{G}^{\phi}}{\partial z\partial z'}\widehat{\boldsymbol{z}}). \qquad (6.15)
\end{aligned}$$

By comparing it with $\widetilde{G}^{E_n}_{zz}$, $\widetilde{G}^{E_n}_{z\phi}$, $\widetilde{G}^{E_n}_{\phi z}$, $\widetilde{G}^{E_n}_{\phi\phi}$ in Eqs. (6.1)-(6.3) and from Eq. (6.14), it can be obtained that,

$$\widetilde{G}^{E_n}_{zz} = -j\omega\widetilde{G}^{A}_{zz} - k_z^2\widetilde{G}^{\phi}, \qquad (6.16a)$$

$$\widetilde{G}^{E_n}_{z\phi} = -j\omega\widetilde{G}^{A}_{z\phi} - \frac{k_z n}{\rho}\widetilde{G}^{\phi}, \qquad (6.16b)$$

$$\widetilde{G}^{E_n}_{\phi z} = -j\omega\widetilde{G}^{A}_{\phi z} - \frac{k_z n}{\rho'}\widetilde{G}^{\phi}, \qquad (6.16c)$$

$$\widetilde{G}^{E_n}_{\phi\phi} = -j\omega\widetilde{G}^{A}_{\phi\phi} - \frac{n^2-1}{\rho\rho'}\widetilde{G}^{\phi}. \qquad (6.16d)$$

Since $\widetilde{G}^{E_n}_{z\phi} = \widetilde{G}^{E_n}_{\phi z}$ when $\rho = \rho'$, let $\widetilde{G}^{A}_{z\phi} = \widetilde{G}^{A}_{\phi z} = 0$, then (6.16b) and (6.16c) can uniquely determine $\widetilde{G}^{\phi}$ as

$$\widetilde{G}^{\phi} = -\frac{1}{8\pi\epsilon_j\omega} \cdot (f_{11} + \frac{j\rho\omega\mu_i}{k_z n}\frac{\partial f_{21}}{\partial\rho}). \qquad (6.17)$$

Substituting $\widetilde{G}^{\phi}$ into (6.16a) and (B-5d) and solving for $\widetilde{G}^{A}_{zz}$ and $\widetilde{G}^{A}_{\phi\phi}$ give

$$\widetilde{G}^{A}_{zz} = -\frac{j}{8\pi\epsilon_j\omega^2} \cdot \left(k_i^2 f_{11} + \frac{j\rho\omega\mu_i k_z}{n}\frac{\partial f_{21}}{\partial\rho}\right), \qquad (6.18a)$$

$$\widetilde{G}^{A}_{\phi\phi} = -\frac{j}{8\pi\epsilon_j\omega^2 k_{i\rho}^2} \cdot \left\{k_j^2\left(\frac{n^2 f_{11}}{\rho\rho'} + \frac{j\omega\mu_i n}{\rho' k_z}\frac{\partial f_{21}}{\partial\rho}\right)\right.$$

$$-j\omega\epsilon_j\left(\frac{k_z n}{\rho}\frac{\partial f_{12}}{\partial\rho'}+j\omega\mu_i\frac{\partial^2 f_{22}}{\partial\rho\partial\rho'}\right)\Big\}$$
$$+\frac{j}{8\pi\epsilon_j\omega^2\rho\rho'}\cdot\left(f_{11}+\frac{j\rho\omega\mu_i}{k_z n}\frac{\partial f_{21}}{\partial\rho}\right). \tag{6.18b}$$

6.2 Spatial Domain Mixed Potential Green's Functions

Equations (6.17-6.18b) are the Green's functions of the MPIE in spectral domain. The source and field points are located on the same cylindrical surface, i.e., the shaded area in the Fig. 5.1. Similar to Eq. (1.4), the spatial domain mixed potential Green's functions can be obtained using the inverse Fourier transform:

$$G(\boldsymbol{r},\boldsymbol{r}')=\sum_{n=-\infty}^{\infty}\int_{-\infty}^{\infty}e^{jn(\phi-\phi')+jk_z(z-z')}\widetilde{G}(n,k_z)dk_z. \tag{6.19}$$

In equation (6.19), $\widetilde{G}(n,k_z)$ represents dyadic components in (6.17), (6.18a), and (6.18b). $k_z=\sqrt{k_i^2-k_{i\rho}^2}$, and integration over k_z is along the deformed SIP, which is shown in Fig. 4.1.

6.2.1 Property of Multi-Reflection Matrix $\overline{\boldsymbol{M}}$

The explicit expression of f_{11} is

$$\begin{aligned}f_{11}=&\Big\{\Big[H_n^{(1)}(k_{i\rho}\rho)+J_n(k_{i\rho}\rho)R_{i,i+1}(1,1)\Big]M_i(1,1)\\&+J_n(k_{i\rho}\rho)R_{i,i+1}(1,2)M_i(2,1)\Big\}\Big[J_n(k_{i\rho}\rho')\\&+H_n^{(1)}(k_{i\rho}\rho')R_{i,i-1}(1,1)\Big]+\Big\{\Big[H_n^{(1)}(k_{i\rho}\rho)\\&+J_n(k_{i\rho}\rho)R_{i,i+1}(1,1)\Big]M_i(1,2)+J_n(k_{i\rho}\rho)\\&\cdot R_{i,i+1}(1,2)M_i(2,2)\Big\}\Big[H_n^{(1)}(k_{i\rho}\rho')R_{i,i-1}(1,1)\Big],\end{aligned} \tag{6.20}$$

where $H_n^{(1)}(\bullet)$ stands for the first kind Hankel function of order n while $J_n(\bullet)$ identifies the Bessel function of order n; $R_{i,i+1}(p,q)$, $R_{i,i-1}(p,q)$, $M_i(p,q)$ with $p=1,2$ and $q=1,2$ are elements of the matrices $\widetilde{\boldsymbol{R}}_{i,i+1}$, $\widetilde{\boldsymbol{R}}_{i,i-1}$, and $\widetilde{\boldsymbol{M}}_i$, respectively [62]. It is apparent that

f_{11} contains a term $H_n^{(1)}(k_{i\rho}\rho)J_n(k_{i\rho}\rho')M_i(1,1)$. Let

$$S = \sum_{-\infty}^{\infty} H_n^{(1)}(k_{i\rho}\rho)J_n(k_{i\rho}\rho')M_i(1,1)e^{jn(\phi-\phi')}. \tag{6.21}$$

If $\rho' \gg \rho$ or $\rho' \ll \rho$, it is easy to perform the summation because the series in the right hand side of (6.21) is fast convergent. But when ρ and ρ' are in proximity, difficulty occurs. The convergence behavior of the series is very poor and a large amount of eigenmodes are needed to achieve a convergent result. The behavior of $M_i(1,1)$ can be seen from Fig. 6.1. Figure 6.1 shows that the magnitude of $[M_2(1,1) - 1.0]$ is very small

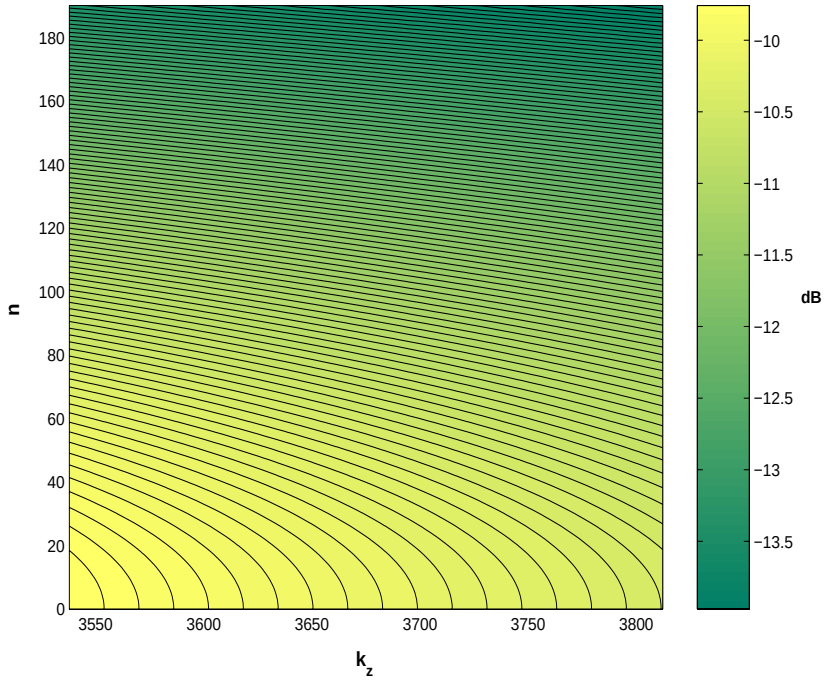

Figure 6.1: $Log_{10}[M_2(1,1) - 1.0]$ versus k_z on path Γ_3 and order of the cylindrical eigenmode n.

and $M_2(1,1)$ has the asymptotic value of 1.0 (the imaginary part of $M_2(1,1)$ is equal to zero) when k_z is sampled along path Γ_3 towards infinity and the order n approaches infinity. So $M_2(1,1)$ on path Γ_3 can be assumed to be a constant 1. This is the typical characteristic of quasi-static component contained in spectral domain Green's functions.

6.2.2 Partial Extraction of $\widehat{\phi}$-Direction Quasi-Static Components

Similar numerical investigation shows that the real parts of $M_1(1,1)$ and $M_1(2,2)$ approach 1, and the imaginary parts of $M_1(1,1)$ and $M_1(2,2)$ approach 0 when n or k_z becomes large. And both the real part and imaginary part of $M_1(1,2)$ and $M_1(2,1)$ approach 0 when n or k_z becomes large. The physical significance is that TE and TM modes are weakly coupled to each other when n or k_z becomes large. In other words, f_{11} implicitly contains a component $[H_n^{(1)}(k_{i\rho}\rho)J_n(k_{i\rho}\rho')]$.

Consider the summation of harmonics as follows:

$$S(m) = \sum_{n=-m}^{m} H_n^{(1)}(k_{i\rho}\rho)J_n(k_{i\rho}\rho')e^{jn(\phi-\phi')}. \tag{6.22}$$

The property of convergence with respect to total number of summation m is shown in Fig. 6.2 for a set of specific value. It can be seen that $S(m)$ is slowly convergent with index m. Fortunately, the following additional theorem obviates the brute force evaluation of $S(m)$:

$$H_0^{(1)}(k_{i\rho}|\boldsymbol{\rho}-\boldsymbol{\rho}'|) = \sum_{n=-\infty}^{\infty} H_n^{(1)}(k_{i\rho}\rho)J_n(k_{i\rho}\rho')e^{jn(\phi-\phi')}. \tag{6.23}$$

This fact reminds us to rearrange f_{11} as follows,

$$\begin{aligned}
f_{11} &= \Big\{ \Big[H_n^{(1)}(k_{i\rho}\rho) + J_n(k_{i\rho}\rho)R_{i,i+1}(1,1)\Big] M_i(1,1) \\
&\quad + J_n(k_{i\rho}\rho)R_{i,i+1}(1,2)M_i(2,1)\Big\} \\
&\quad \cdot \Big[J_n(k_{i\rho}\rho') + H_n^{(1)}(k_{i\rho}\rho')R_{i,i-1}(1,1)\Big] \\
&\quad + \Big\{ \Big[H_n^{(1)}(k_{i\rho}) + J_n(k_{i\rho}\rho)R_{i,i+1}(1,1)\Big] M_i(1,2) \\
&\quad + J_n(k_{i\rho}\rho)R_{i,i+1}(1,2)M_i(2,2)\Big\} \\
&\quad \cdot \Big[H_n^{(1)}(k_{i\rho}\rho')R_{i,i-1}(1,1)\Big] - H_n^{(1)}(k_{i\rho}\rho)J_n(k_{i\rho}\rho') \\
&\quad + H_n^{(1)}(k_{i\rho}\rho)J_n(k_{i\rho}\rho') \\
&= f'_{11} + H_n^{(1)}(k_{i\rho}\rho)J_n(k_{i\rho}\rho')
\end{aligned} \tag{6.24a}$$

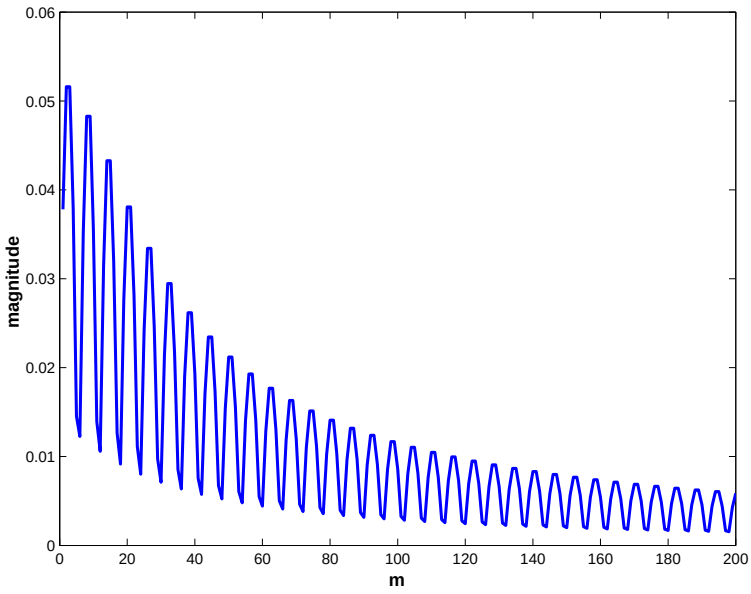

Figure 6.2: Slowly convergent behavior of summation $|S(m)|$ when $\rho = \rho' = 0.051$, $\phi - \phi' = \pi/6$, $\epsilon_{r_i} = 2.3$, $\mu_{r_i} = 1$, $f = 6.8$ GHz, $k_z = 500$ which is one sampling point located on the Sommerfeld integral path.

With the slowly convergent component extracted out, $\sum f'_{11} e^{jn(\phi-\phi')}$ converges much faster than $\sum f_{11} e^{jn(\phi-\phi')}$ when $\rho = \rho'$. The similar arrangement can be applied to f_{22}, while we keep f_{12} and f_{21} as their original forms, since they do not implicitly contain $[H_n^{(1)}(k_{i\rho}\rho) J_n(k_{i\rho}\rho')]$ as f_{11} and f_{22}. For clear understanding and completeness, the expressions of f_{12}, f_{21} and f_{22} are listed below:

$$\begin{aligned} f_{12} &= \Big\{ \Big[H_n^{(1)}(k_{i\rho}\rho) + J_n(k_{i\rho}\rho) R_{i,i+1}(1,1) \Big] M_i(1,1) \\ &\quad + J_n(k_{i\rho}\rho) R_{i,i+1}(1,2) M_i(2,1) \Big\} \\ &\quad \cdot H_n^{(1)}(k_{i\rho}\rho') R_{i,i-1}(1,2) \\ &\quad + \Big\{ \Big[H_n^{(1)}(k_{i\rho}) + J_n(k_{i\rho}\rho) R_{i,i+1}(1,1) \Big] M_i(1,2) \\ &\quad + J_n(k_{i\rho}\rho) R_{i,i+1}(1,2) M_i(2,2) \Big\} \\ &\quad \cdot \Big[J_n(k_{i\rho}\rho') + H_n^{(1)}(k_{i\rho}\rho') R_{i,i-1}(2,2) \Big] \qquad (6.24b) \\ f_{21} &= \Big\{ J_n(k_{i\rho}\rho) R_{i,i+1}(2,1) M_i(1,1) \end{aligned}$$

$$
\begin{aligned}
&+\left[H_n^{(1)}(k_{i\rho}\rho)+J_n(k_{i\rho}\rho)R_{i,i+1}(2,2)\right]M_i(2,1)\Big\}\\
&\cdot\left[J_n(k_{i\rho}\rho')+H_n^{(1)}(k_{i\rho}\rho')R_{i,i-1}(1,1)\right]\\
&+\Big\{J_n(k_{i\rho}\rho)R_{i,i+1}(2,1)M_i(1,2)\\
&+\left[H_n^{(1)}(k_{i\rho}\rho)+J_n(k_{i\rho}\rho)R_{i,i+1}(2,2)\right]M_i(2,2)\Big\}\\
&\cdot H_n^{(1)}(k_{i\rho}\rho')R_{i,i-1}(2,1) \qquad (6.24c)\\
f_{22} \;=\;& \Big\{J_n(k_{i\rho}\rho)R_{i,i+1}(2,1)M_i(1,1)\\
&+\left[H_n^{(1)}(k_{i\rho}\rho)+J_n(k_{i\rho}\rho)R_{i,i+1}(2,2)\right]M_i(2,1)\Big\}\\
&\cdot H_n^{(1)}(k_{i\rho}\rho')R_{i,i-1}(1,2)\\
&+\Big\{J_n(k_{i\rho}\rho)R_{i,i+1}(2,1)M_i(1,2)\\
&+\left[H_n^{(1)}(k_{i\rho}\rho)+J_n(k_{i\rho}\rho)R_{i,i+1}(2,2)\right]M_i(2,2)\Big\}\\
&\cdot\left[J_n(k_{i\rho}\rho')+H_n^{(1)}(k_{i\rho}\rho')R_{i,i-1}(2,2)\right]\\
&-H_n^{(1)}(k_{i\rho}\rho)J_n(k_{i\rho}\rho')+H_n^{(1)}(k_{i\rho}\rho)J_n(k_{i\rho}\rho')\\
=\;& f'_{22}+H_n^{(1)}(k_{i\rho}\rho)J_n(k_{i\rho}\rho'). \qquad (6.24d)
\end{aligned}
$$

Eqs. (6.24a-6.24d) are the formulations with the $\widehat{\phi}$-direction quasi-static components, i.e., with the term $[H_n^{(1)}(k_{i\rho}\rho)J_n(k_{i\rho}\rho')]$ in f_{11} and f_{22} extracted out. From the convergence efficiency discussion in Section 6.3, we find that the extraction of the $\widehat{\phi}$-direction quasi-static components is not complete. For some items of the vector potential Green's functions, Shanks' transform is even needed to perform the inverse Fourier transform. This shows that there are some other forms of $\widehat{\phi}$-direction quasi-static components implicitly contained in f_{11}, f_{12}, f_{21} and f_{22}. So we must consider them as a whole rather than just consider the term, $[H_n^{(1)}(k_{i\rho}\rho)J_n(k_{i\rho}\rho')]$ in f_{11} and f_{22}. The following subsection will discuss this in detail.

6.2.3 Complete Extraction of $\widehat{\phi}$-Direction Quasi-Static Components

In this subsection, a more general and hence complete extraction of the $\widehat{\phi}$-direction quasi-static components is presented. As discussed in the last subsection, if the quasi-static components, which have a closed-form summation expressions, are subtracted from the spectral domain Green's functions, the remaining part in series form will become fast convergent. Hence, (6.21) can be rewritten as

$$\begin{aligned} S &= \sum_{-\infty}^{\infty} H_n^{(1)}(k_{i\rho}\rho) J_n(k_{i\rho}\rho') M_i(1,1) e^{jn(\phi-\phi')} \\ &= \sum_{-\infty}^{\infty} H_n^{(1)}(k_{i\rho}\rho) J_n(k_{i\rho}\rho') \left[M_i(1,1) - 1 + 1\right] e^{jn(\phi-\phi')} \\ &= \sum_{-\infty}^{\infty} H_n^{(1)}(k_{i\rho}\rho) J_n(k_{i\rho}\rho') \left[M_i(1,1) - 1\right] e^{jn(\phi-\phi')} \\ &\quad + H_0^{(1)}(k_{i\rho}|\boldsymbol{\rho} - \boldsymbol{\rho}'|). \end{aligned} \tag{6.25}$$

In (6.25), the term in the summation series is actually fast decaying with its order n since the asymptotic term has been subtracted. Although only one component is considered here as an example, the same treatment can be applied to f_{11} as a whole. From the physical point of view, eigenmode f_{11} contains $[H_n^{(1)}(k_{i\rho}\rho)J_n(k_{i\rho}\rho')]$ or $[H_n^{(1)}(k_{i\rho}\rho')J_n(k_{i\rho}\rho)]$ as its "kernel" to represent the response of a point source. From this consideration, f_{11} is normalized by $[H_n^{(1)}(k_{i\rho}\rho)J_n(k_{i\rho}\rho')]$ to make a "coefficient" which is similar to $M_i(1,1)$. Thus, f_{11} can be rewritten as

$$\begin{aligned} f_{11} &= \Big\{ \Big\{ \left[H_n^{(1)}(k_{i\rho}\rho) + J_n(k_{i\rho}\rho) R_{i,i+1}(1,1)\right] M_i(1,1) \\ &\quad + J_n(k_{i\rho}\rho) R_{i,i+1}(1,2) M_i(2,1) \Big\} \left[J_n(k_{i\rho}\rho') \right. \\ &\quad \left. + H_n^{(1)}(k_{i\rho}\rho') R_{i,i-1}(1,1)\right] + \Big\{ \left[H_n^{(1)}(k_{i\rho}\rho) \right. \\ &\quad \left. + J_n(k_{i\rho}\rho) R_{i,i+1}(1,1)\right] M_i(1,2) + J_n(k_{i\rho}\rho) \\ &\quad \cdot R_{i,i+1}(1,2) M_i(2,2) \Big\} \left[H_n^{(1)}(k_{i\rho}\rho') R_{i,i-1}(1,1)\right] \Big\} \\ &\quad / \left[H_n^{(1)}(k_{i\rho}\rho) J_n(k_{i\rho}\rho')\right] \bullet \left[H_n^{(1)}(k_{i\rho}\rho) J_n(k_{i\rho}\rho')\right] \\ &= C_1 \bullet \left[H_n^{(1)}(k_{i\rho}\rho) J_n(k_{i\rho}\rho')\right]. \end{aligned} \tag{6.26}$$

The behavior of coefficient C_1 is similar to that of $M_i(1,1)$ on the path Γ_3. Because the highly complicated expression of C_1, it is not easy to find an analytical expression for the asymptotic value. However, numerical solution for the asymptotic value does exist by extrapolation. The rational function extrapolation scheme is valid here since high order value of coefficient C_1 is smooth, is slowly varying, and has an asymptotic value with respect to the order n.

The summation for the first term on the right hand side of Eqs. (6.17) and (6.18a) can be done in a similar way to that of S. Let the asymptotic value of C_1 be C_1^*. Then, we have

$$\begin{aligned}
S_1 &= \sum_{-\infty}^{\infty} f_{11} e^{jn(\phi-\phi')} \\
&= \sum_{-\infty}^{\infty} C_1 \bullet \left[H_n^{(1)}(k_{i\rho}\rho) J_n(k_{i\rho}\rho') e^{jn(\phi-\phi')} \right] \\
&= \sum_{-\infty}^{\infty} (C_1 - C_1^*) \bullet \left[H_n^{(1)}(k_{i\rho}\rho) J_n(k_{i\rho}\rho') e^{jn(\phi-\phi')} \right] \\
&\quad + \sum_{-\infty}^{\infty} C_1^* \bullet \left[H_n^{(1)}(k_{i\rho}\rho) J_n(k_{i\rho}\rho') e^{jn(\phi-\phi')} \right] \\
&= \sum_{-\infty}^{\infty} (C_1 - C_1^*) \bullet \left[H_n^{(1)}(k_{i\rho}\rho) J_n(k_{i\rho}\rho') e^{jn(\phi-\phi')} \right] \\
&\quad + C_1^* \bullet H_0^{(1)}(k_{i\rho}(|\boldsymbol{\rho} - \boldsymbol{\rho}'|)).
\end{aligned} \tag{6.27}$$

The series in the first summation in (6.27) is fast decaying. But it is different for the first term on the right hand side of (6.18b). Let

$$\begin{aligned}
S_1' &= \sum_{-\infty}^{\infty} n^2 f_{11} e^{jn(\phi-\phi')} \\
&= \sum_{-\infty}^{\infty} C_1 \bullet \left[n^2 H_n^{(1)}(k_{i\rho}\rho) J_n(k_{i\rho}\rho') e^{jn(\phi-\phi')} \right] \\
&= \sum_{-\infty}^{\infty} (C_1 - C_1^*) \bullet \left[n^2 H_n^{(1)}(k_{i\rho}\rho) J_n(k_{i\rho}\rho') e^{jn(\phi-\phi')} \right] \\
&\quad + \sum_{-\infty}^{\infty} C_1^* \bullet \left[n^2 H_n^{(1)}(k_{i\rho}\rho) J_n(k_{i\rho}\rho') e^{jn(\phi-\phi')} \right].
\end{aligned} \tag{6.28}$$

Similar to Eq. (6.27), the series in the first summation on the right hand side of Eq. (6.28) decays fast and the second summation has a closed-form (see (C-6) in Appendix).

For term f_{21} in (6.17) and (6.18a), we let

$$\begin{aligned} S_2 &= \sum_{-\infty}^{\infty} \frac{1}{k_z n} \cdot \frac{\partial f_{21}}{\partial \rho} e^{jn(\phi-\phi')} \\ &= \sum_{-\infty}^{\infty} \left\{ \frac{1}{k_z n} \cdot \frac{\partial f_{21}}{\partial \rho} \right\} / \left[H_n^{(1)}(k_{i\rho}\rho) J_n(k_{i\rho}\rho') \right] \\ &\quad \bullet \left[H_n^{(1)}(k_{i\rho}\rho) J_n(k_{i\rho}\rho') \right] e^{jn(\phi-\phi')} \\ &= \sum_{-\infty}^{\infty} C_2 \bullet \left[H_n^{(1)}(k_{i\rho}\rho) J_n(k_{i\rho}\rho') \right] e^{jn(\phi-\phi')} \\ &= \sum_{-\infty}^{\infty} (C_2 - C_2^*) \bullet \left[H_n^{(1)}(k_{i\rho}\rho) J_n(k_{i\rho}\rho') \right] e^{jn(\phi-\phi')} \\ &\quad + \sum_{-\infty}^{\infty} C_2^* \bullet \left[H_n^{(1)}(k_{i\rho}\rho) J_n(k_{i\rho}\rho') \right] e^{jn(\phi-\phi')}. \end{aligned} \tag{6.29}$$

The behavior of $C_2 k_z^2$ is similar to that of C_1 on the path Γ_3. The coefficient $C_2^* k_z^2$ has an asymptotic value which associates with the quasi-static component versus $\hat{\phi}$ coordinate. Different from coefficient C_1, the coefficient C_2 needs to be multiplied by a factor k_z^2 to give an asymptotic value with respect to k_z and n on the path Γ_3. In other words, C_2 can be assumed as a constant versus order n and decreases versus variable k_z in order of $1/k_z^2$. The second term in (6.29) has a closed-form [see (C-5) in Appendix], while the remaining part is a fast decaying series.

As for the second term in (6.18b), we let

$$\begin{aligned} S_2' &= n^2 \cdot S_2 \\ &= \sum_{-\infty}^{\infty} (C_2 - C_2^*) \bullet \left[n^2 H_n^{(1)}(k_{i\rho}\rho) J_n(k_{i\rho}\rho') \right] e^{jn(\phi-\phi')} \\ &\quad + \sum_{-\infty}^{\infty} C_2^* \bullet \left[n^2 H_n^{(1)}(k_{i\rho}\rho) J_n(k_{i\rho}\rho') \right] e^{jn(\phi-\phi')}. \end{aligned} \tag{6.30}$$

The same treatment can be applied to (6.30) as to (6.28). The series in the first summation is fast decaying and the second summation in (6.30) has a closed-form solution [see (C-6) in Appendix].

Similar to the C_2^* in (6.29), let C_3^* represent the asymptotic value which is associated with the quasi-static component versus $\hat{\phi}$ coordinate. Very similar mathematical

manipulation can be applied to the term which contains f_{12} in (6.18b).

$$\begin{aligned}
S_3 &= \sum_{-\infty}^{\infty} \frac{1}{k_z n} \cdot \frac{\partial f_{12}}{\partial \rho} e^{jn(\phi-\phi')} \\
&= \sum_{-\infty}^{\infty} \left\{ \frac{1}{k_z n} \cdot \frac{\partial f_{12}}{\partial \rho} \right\} / \left[H_n^{(1)}(k_{i\rho}\rho) J_n(k_{i\rho}\rho') \right] \\
&\quad \bullet \left[H_n^{(1)}(k_{i\rho}\rho) J_n(k_{i\rho}\rho') \right] e^{jn(\phi-\phi')} \\
&= \sum_{-\infty}^{\infty} C_3 \bullet \left[H_n^{(1)}(k_{i\rho}\rho) J_n(k_{i\rho}\rho') \right] e^{jn(\phi-\phi')} \\
&= \sum_{-\infty}^{\infty} (C_3 - C_3^*) \bullet \left[H_n^{(1)}(k_{i\rho}\rho) J_n(k_{i\rho}\rho') \right] e^{jn(\phi-\phi')} \\
&\quad + \sum_{-\infty}^{\infty} C_3^* \bullet \left[H_n^{(1)}(k_{i\rho}\rho) J_n(k_{i\rho}\rho') \right] e^{jn(\phi-\phi')}. \qquad (6.31)
\end{aligned}$$

For the second term in (6.18b) which contains f_{22}, the normalized factor should be $\partial^2[H_n^{(1)}(k_{i\rho}\rho)J_n(k_{i\rho}\rho')]/(\partial\rho\partial\rho')$ rather than $[H_n^{(1)}(k_{i\rho}\rho)J_n(k_{i\rho}\rho')]$ so that the asymptotic value associated with the quasi-static component versus $\hat{\phi}$ coordinate can be obtained. Let

$$\begin{aligned}
S_4 &= \sum_{-\infty}^{\infty} \frac{\partial^2 f_{22}}{\partial\rho\partial\rho'} e^{jn(\phi-\phi')} \\
&= \sum_{-\infty}^{\infty} \frac{\partial^2 f_{22}}{\partial\rho\partial\rho'} / \left\{ \frac{\partial^2}{\partial\rho\partial\rho'} \left[H_n^{(1)}(k_{i\rho}\rho) J_n(k_{i\rho}\rho') \right] \right\} \\
&\quad \bullet \left\{ \frac{\partial^2}{\partial\rho\partial\rho'} \left[H_n^{(1)}(k_{i\rho}\rho) J_n(k_{i\rho}\rho') \right] \right\} e^{jn(\phi-\phi')} \\
&= \sum_{-\infty}^{\infty} C_4 \bullet \left\{ \frac{\partial^2}{\partial\rho\partial\rho'} \left[H_n^{(1)}(k_{i\rho}\rho) J_n(k_{i\rho}\rho') \right] \right\} e^{jn(\phi-\phi')} \\
&= \sum_{-\infty}^{\infty} (C_4 - C_4^*) \bullet \left\{ \frac{\partial^2}{\partial\rho\partial\rho'} \left[H_n^{(1)}(k_{i\rho}\rho) J_n(k_{i\rho}\rho') \right] \right\} \cdot e^{jn(\phi-\phi')} \\
&\quad + \sum_{-\infty}^{\infty} C_4^* \bullet \left\{ \frac{\partial^2}{\partial\rho\partial\rho'} \left[H_n^{(1)}(k_{i\rho}\rho) \cdot J_n(k_{i\rho}\rho') \right] \right\} e^{jn(\phi-\phi')}, \qquad (6.32)
\end{aligned}$$

where C_4^* is also the asymptotic value associated with the quasi-static component versus $\hat{\phi}$ coordinate. The second summation in (6.32) has a closed-form [see (C-7) in Appendix] while the series in the first summation in (6.32) is fast decaying.

The spectral domain Green's function components are evaluated along the SIP for the three-layered cylindrical structure as shown in Fig. 5.1 where $a_1 = 50$ mm, $a_2 = 53$ mm,

$a_3 = 56$ mm, $\epsilon_{r1} = 2.0$, $\epsilon_{r2} = 5.0$, $\mu_{r1} = \mu_{r2} = 1$, and operating frequency $f = 7.5$ GHz. They are shown in Figs. 6.3-6.5. Summation up to 190 eigenmodes, after the quasi-static components versus $\hat{\phi}$ coordinate are completely subtracted, is found to be good enough to give a convergent result. Computational time is saved since there is no need to perform the Shank's transform when the quasi-static components are partially subtracted. It can be seen that the spectrum decays fast when k_z tends to infinity on the real axis. This is what expected. The integration over k_z is next discussed.

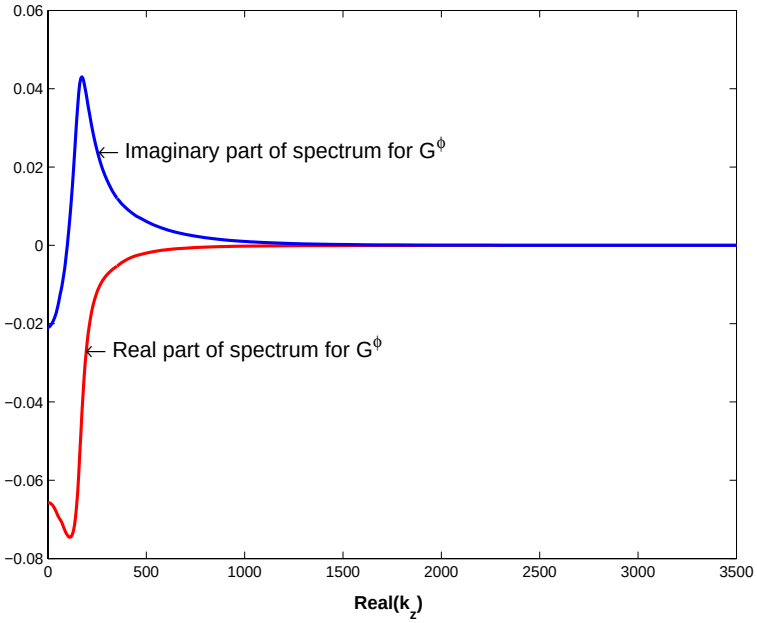

Figure 6.3: Spectral domain mixed potential Green's function $\sum \widetilde{G}^{\phi} e^{jn(\phi-\phi')}$ evaluated along the SIP where $T_1 = 0.2$, $T_2 = 10$, and $T_3 = 11$ for structures shown in Fig. 5.1 at $\phi - \phi' = 0.05$.

6.2.4 Extraction of $\hat{z}$-Direction Quasi-Static Components

At a small angle of $(\phi - \phi')$, however, the spectrum on path Γ_3 decays slowly. The integration over k_z on path Γ_3 is associated with quasi-static component versus $\hat{z}$

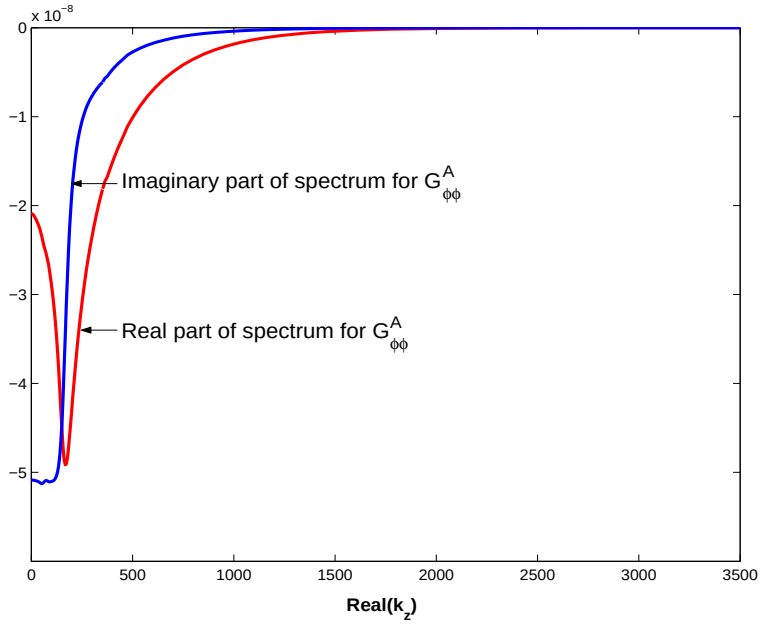

Figure 6.4: Spectral domain mixed potential Green's function $\sum \widetilde{G}^A_{\phi\phi} e^{jn(\phi-\phi')}$ evaluated along the SIP where $T_1 = 0.2$, $T_2 = 10$, and $T_3 = 11$ and for structure shown in Fig. 5.1 at $\phi - \phi' = 0.05$.

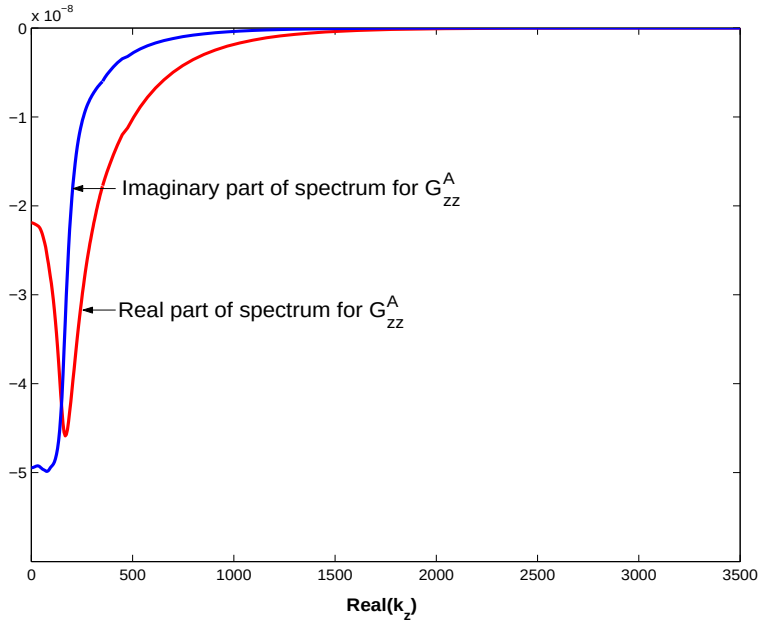

Figure 6.5: Spectral domain mixed potential Green's function $\sum \widetilde{G}^A_{zz} e^{jn(\phi-\phi')}$ evaluated along the SIP where $T_1 = 0.2$, $T_2 = 10$, and $T_3 = 11$ for structure shown in Fig. 5.1 where $\phi - \phi' = 0.05$.

coordinate and it contributes significantly to the inverse Fourier transform especially for small $(\phi - \phi')$ and $(z - z')$. This is reasonable, as the contribution of quasi-static component should be prominent for both of small $(\phi - \phi')$ and $(z - z')$. Fortunately, the contribution from integral on path Γ_3 can be well approximated through analytic formulation due to the constant behaviors of coefficients C_1, $C_2 k_z^2$, $C_3 k_z^2$, and C_4 (these four coefficients are functions of k_z and order n) on path Γ_3. In other words, the coefficients C_1^*, $C_2^* k_z^2$, $C_3^* k_z^2$, and C_4^* (associated with quasi-static component versus $\hat{\phi}$ coordinates) are constants when k_z is on path Γ_3. Denote these constant values as C_1^{**}, $C_2^{**} k_z^2$, $C_3^{**} k_z^2$, and C_4^{**}. Again, these constant values are associated with quasi-static components versus $\hat{z}$ coordinate. Considering Eq. (6.19) and Eqs. (6.27)-(6.32), we need to extract quasi-static components versus $\hat{z}$ coordinate for the following five types of integrals. Among the five, the first four types are given below:

$$
\begin{aligned}
I_0 &= \int_{-\infty}^{\infty} S_1 e^{jk_z(z-z')} dk_z \\
&= \int_{-\infty}^{\infty} \sum_{-\infty}^{\infty} (C_1 - C_1^*) \Big[H_n^{(1)}(k_{i\rho}\rho) J_n(k_{i\rho}\rho') \Big] \\
&\quad \cdot e^{jn(\phi-\phi')} e^{jk_z(z-z')} dk_z \\
&\quad + \int_{-\infty}^{\infty} (C_1^* - C_1^{**}) H_0^{(1)}(k_{i\rho}(|\boldsymbol{\rho} - \boldsymbol{\rho}'|)) e^{jk_z(z-z')} dk_z \\
&\quad + \int_{-\infty}^{\infty} C_1^{**} H_0^{(1)}(k_{i\rho}(|\boldsymbol{\rho} - \boldsymbol{\rho}'|)) e^{jk_z(z-z')} dk_z; \qquad (6.33) \\
I_1 &= \int_{-\infty}^{\infty} \frac{1}{k_{i\rho}^2} S_1 \cdot n^2 e^{jk_z(z-z')} dk_z \\
&= \int_{-\infty}^{\infty} \frac{1}{k_{i\rho}^2} \sum_{-\infty}^{\infty} (C_1 - C_1^*) \Big[n^2 H_n^{(1)}(k_{i\rho}\rho) J_n(k_{i\rho}\rho') \Big] \\
&\quad \cdot e^{jn(\phi-\phi')} e^{jk_z(z-z')} dk_z \\
&\quad + \int_{-\infty}^{\infty} \frac{1}{k_{i\rho}^2} \sum_{-\infty}^{\infty} (C_1^* - C_1^{**}) \Big[n^2 H_n^{(1)}(k_{i\rho}\rho) J_n(k_{i\rho}\rho') \Big] \\
&\quad \cdot e^{jn(\phi-\phi')} e^{jk_z(z-z')} dk_z \\
&\quad + \int_{-\infty}^{\infty} \frac{1}{k_{i\rho}^2} \sum_{-\infty}^{\infty} C_1^{**} \Big[n^2 H_n^{(1)}(k_{i\rho}\rho) J_n(k_{i\rho}\rho') \Big] \\
&\quad \cdot e^{jn(\phi-\phi')} e^{jk_z(z-z')} dk_z; \qquad (6.34) \\
I_2 &= \int_{-\infty}^{\infty} S_2 \cdot k_z^2 e^{jk_z(z-z')} dk_z
\end{aligned}
$$

$$
\begin{aligned}
&= \int_{-\infty}^{\infty} \sum_{-\infty}^{\infty} (C_2 - C_2^*) k_z^2 \left[H_n^{(1)}(k_{i\rho}\rho) J_n(k_{i\rho}\rho') \right] \\
&\cdot e^{jn(\phi-\phi')} e^{jk_z(z-z')} dk_z \\
&+ \int_{-\infty}^{\infty} \sum_{-\infty}^{\infty} (C_2^* - C_2^{**}) k_z^2 \left[H_n^{(1)}(k_{i\rho}\rho) J_n(k_{i\rho}\rho') \right] \\
&\cdot e^{jn(\phi-\phi')} e^{jk_z(z-z')} dk_z \\
&+ \int_{-\infty}^{\infty} \sum_{-\infty}^{\infty} C_2^{**} k_z^2 \left[H_n^{(1)}(k_{i\rho}\rho) J_n(k_{i\rho}\rho') \right] \\
&\cdot e^{jn(\phi-\phi')} e^{jk_z(z-z')} dk_z; \qquad (6.35)
\end{aligned}
$$

$$
\begin{aligned}
I_3 &= \int_{-\infty}^{\infty} \frac{1}{k_{i\rho}^2} S_3 \cdot n^2 k_z^2 e^{jk_z(z-z')} dk_z \\
&= \int_{-\infty}^{\infty} \frac{1}{k_{i\rho}^2} \sum_{-\infty}^{\infty} (C_3 - C_3^*) k_z^2 \left[n^2 H_n^{(1)}(k_{i\rho}\rho) J_n(k_{i\rho}\rho') \right] \\
&\cdot e^{jn(\phi-\phi')} e^{jk_z(z-z')} dk_z \\
&+ \int_{-\infty}^{\infty} \frac{1}{k_{i\rho}^2} \sum_{-\infty}^{\infty} (C_3^* - C_3^{**}) k_z^2 \left[n^2 H_n^{(1)}(k_{i\rho}\rho) J_n(k_{i\rho}\rho') \right] \\
&\cdot e^{jn(\phi-\phi')} e^{jk_z(z-z')} dk_z \\
&+ \int_{-\infty}^{\infty} \frac{1}{k_{i\rho}^2} \sum_{-\infty}^{\infty} C_3^{**} k_z^2 \left[n^2 H_n^{(1)}(k_{i\rho}\rho) J_n(k_{i\rho}\rho') \right] \\
&\cdot e^{jn(\phi-\phi')} e^{jk_z(z-z')} dk_z. \qquad (6.36)
\end{aligned}
$$

The third integral in (6.33) or (6.34) has a closed form [see (C-5) and (C-6) in Appendix] while the first and second integrals in (6.33) and (6.34) are fast decaying with k_z since $C_1 \approx C_1^* \approx C_1^{**}$ on path Γ_3. Similarly, the third integral in (6.35) or (6.36) has a closed form [see (C-8a)-(C-13) in Appendix] while the first and second integrals in (6.35) and (6.36) are fast decaying with k_z because $C_2 k_z^2 \approx C_2^* k_z^2 \approx C_2^{**} k_z^2$, $C_3 k_z^2 \approx C_3^* k_z^2 \approx C_3^{**} k_z^2$ and they are constant values on path Γ_3. Also, $\int S_2 k_z^2 dk_z$ and $\int S_3 n^2 k_z^2 dk_z$ instead of $\int S_2 dk_z$ and $\int S_3 n^2 dk_z$ are considered here. The reason is that C_2^{**} and C_3^{**} are decaying $\sim (1/k_z^2)$ on path Γ_3, so S_2 and S_3 are fast decaying with k_z. If path Γ_3 was located far away from the origin of the k_z complex plane, the contributions of $\int S_2 dk_z$ and $\int S_3 n^2 dk_z$ along path Γ_3 are negligible compared to that of $\int S_2 k_z^2 dk_z$ and $\int S_3 n^2 k_z^2 dk_z$. The fifth

type of integral is I_4,

$$\begin{aligned} I_4 &= \int_{-\infty}^{\infty} \frac{1}{k_{i\rho}^2} S_4 e^{jk_z(z-z')} dk_z \\ &= \int_{-\infty}^{\infty} \frac{1}{k_{i\rho}^2} \sum_{-\infty}^{\infty} (C_4 - C_4^*) \frac{\partial^2}{\partial\rho\partial\rho'} \left[H_n^{(1)}(k_{i\rho}\rho) J_n(k_{i\rho}\rho')\right] \\ &\quad \cdot e^{jn(\phi-\phi')} e^{jk_z(z-z')} dk_z \\ &\quad + \int_{-\infty}^{\infty} \frac{1}{k_{i\rho}^2} \sum_{-\infty}^{\infty} (C_4^* - C_4^{**}) \frac{\partial^2}{\partial\rho\partial\rho'} \left[H_n^{(1)}(k_{i\rho}\rho) J_n(k_{i\rho}\rho')\right] \\ &\quad \cdot e^{jn(\phi-\phi')} e^{jk_z(z-z')} dk_z \\ &\quad + \int_{-\infty}^{\infty} \frac{1}{k_{i\rho}^2} \sum_{-\infty}^{\infty} C_4^{**} \frac{\partial^2}{\partial\rho\partial\rho'} \left[H_n^{(1)}(k_{i\rho}\rho) J_n(k_{i\rho}\rho')\right] \\ &\quad \cdot e^{jn(\phi-\phi')} e^{jk_z(z-z')} dk_z. \end{aligned} \tag{6.37}$$

Again, the third integral in (6.37) has a closed-form [see (C-8a)-(C-13) in Appendix] while the first and second integrals in (6.37) are fast decaying with k_z since $C_4 \approx C_4^* \approx C_4^{**}$ and they can be assumed to be constant on path Γ_3.

6.3 Numerical Results and Discussion

After the quasi-static components or the slowly decaying tails have been completely subtracted from the spectral domain mixed potential Green's functions, the remaining parts of I_0, I_1, I_2, I_3, and I_4 in the last section turn out to be finite integral along paths Γ_1 and Γ_2. Therefore, the DCIM with the help of GPOF method [70] can be applied to obtain a closed-form solution of the Green's functions in spatial domain.

To validate our in-house code developed using the above mentioned procedure, a cylindrical stratified structure given in [81] is simulated, where $\rho = 70$ mm, $\rho' = 52$ mm, $\phi - \phi' = \pi/6$, $a_1 = 50$ mm, $a_2 = 51$ mm, $a_3 = 52$ mm, $\epsilon_{r1} = 2.5$, $\epsilon_{r2} = 4.0$, and $\mu_{r1} = \mu_{r2} = 1$. The component $G_{z\phi}^E$ of the spatial domain Green's function is compared with that in [81]. As shown in Fig. 6.6, they are in good agreement.

The spatial domain mixed potential Green's functions are evaluated using the

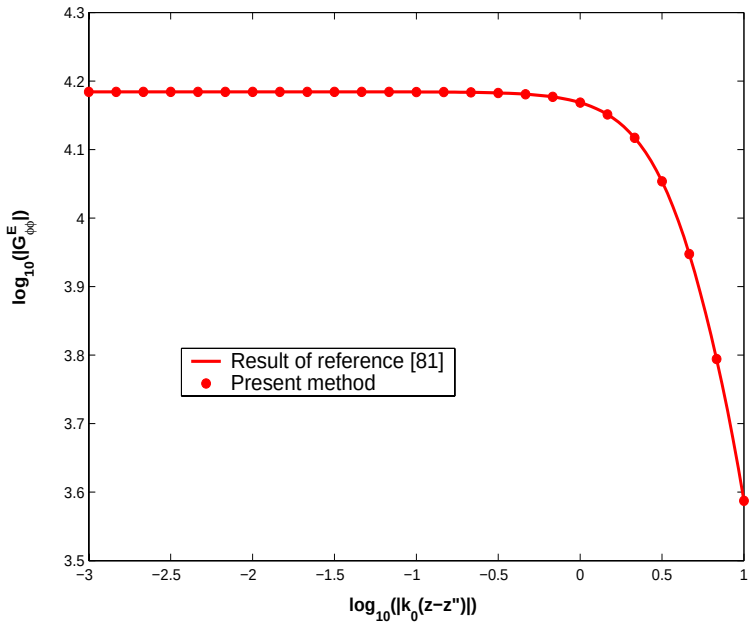

Figure 6.6: Spatial domain Green's function component $G^E_{z\phi}$.

aforementioned numerical procedure for the multilayered cylinder as shown in Fig. 5.1. The parameters of the multilayered cylinder are chosen as $a_1 = 50$ mm, $a_2 = 53$ mm, $a_3 = 56$ mm, $\epsilon_{r1} = 2.0$, $\epsilon_{r2} = 5.0$, $\mu_{r1} = \mu_{r2} = 1$. The operating frequency is $f = 7.5$ GHz. The source and field points are located both at $\rho = \rho' = 53$ mm. The results obtained by using the DCIM are compared with those obtained by using direct numerical integration and are shown in Figs. 6.7 and 6.8. Figs. 6.9-6.11 show the three Green's function's components displayed in Figs. 6.7 and 6.8, but in larger $(z - z')$. In order to see the wave phenomenon, the horizontal axial are in linear scale instead of logarithm scale. It is noted that the results obtained using the direct numerical integration are based on the accurate summation of the series. The summation of the series cannot accurately be obtained by summing up the terms of the series. This issue will be discussed later.

Figs. 6.12-6.14 show 3-D variations of the mixed potential Green's functions versus coordinates $(z - z')$ and $(\phi - \phi')$. It can be seen that when both $(z - z')$ and $(\phi - \phi')$ are small, the magnitude of the Green's functions are big. Furthermore, at the point where

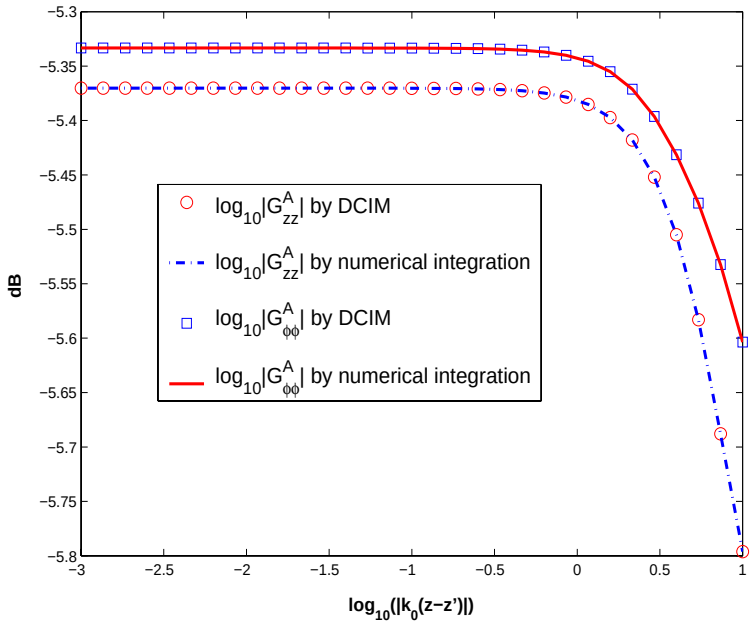

Figure 6.7: Spatial domain Green's function components $G^A_{\phi\phi}$ and G^A_{zz} at $\phi - \phi' = 0.5$.

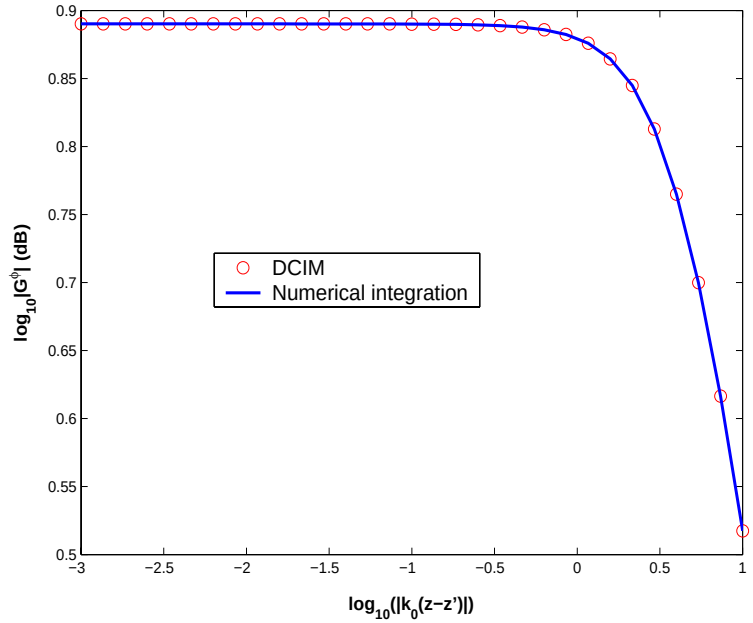

Figure 6.8: Spatial domain scalar potential Green's function G^ϕ at $\phi - \phi' = 0.5$.

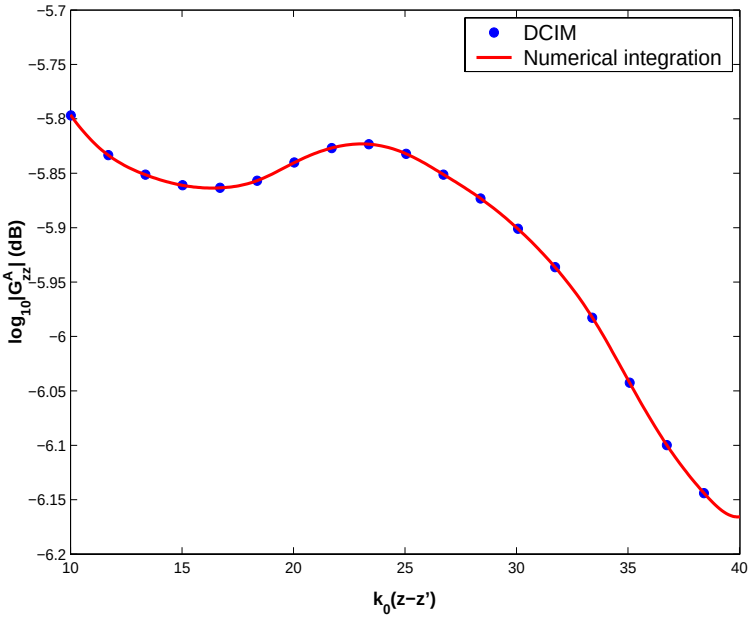

Figure 6.9: Spatial domain Green's function components G_{zz}^{A} at $\phi - \phi' = 0.5$.

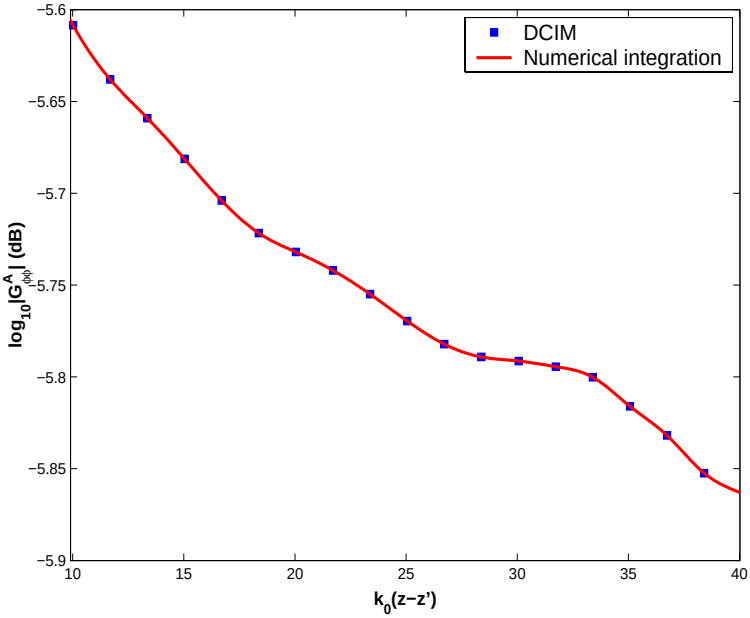

Figure 6.10: Spatial domain Green's function components $G_{\phi\phi}^{A}$ at $\phi - \phi' = 0.5$.

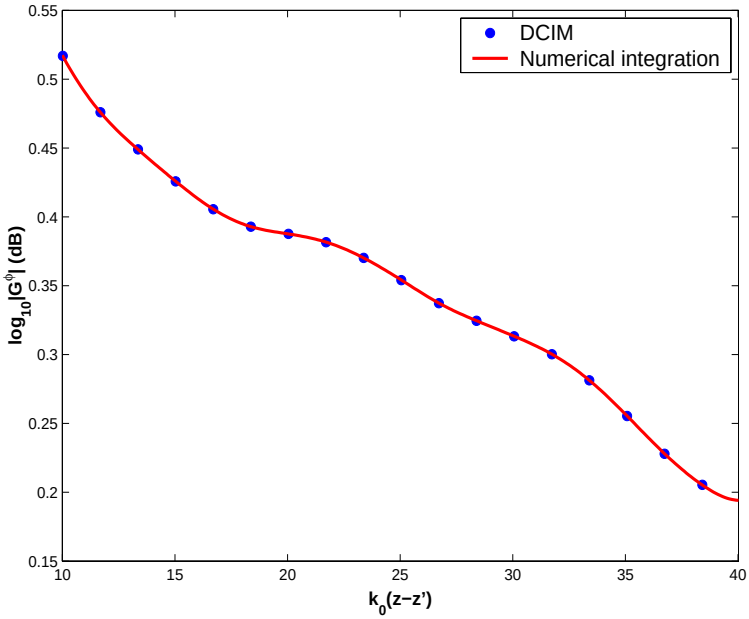

Figure 6.11: Spatial domain scalar potential Green's function G^{ϕ} at $\phi - \phi' = 0.5$.

both $(z - z') = 0$ and $(\phi - \phi') = 0$, the Green's functions are singular and cannot be numerically evaluated. This nature of the mixed potential Green's functions has clearly been described in the Figs. 6.12-6.14. The number of complex images in each segment is chosen as 7 for the paths Γ_1 and Γ_2. The sampling point numbers in each segment of the path are 50 and 200 for paths Γ_1 and Γ_2, respectively. For the deformed path parameters, $T_1 = 0.2$, $T_2 = 10.0$, and $T_3 = 12.0$. T_1 ranges from 0.1 to 0.5. It should not be too small, otherwise the spectrum will have sharp change because of the poles located on the real axis in k_z complex plane; and it cannot be too large as well since far field approximation will be inaccurate. T_2 and T_3 should be large enough to make the following condition valid:

$$
\begin{aligned}
C_1 &\approx C_1^* \approx C_1^{**}, \\
C_2 k_z^2 &\approx C_2^* k_z^2 \approx C_2^{**} k_z^2, \\
C_3 k_z^2 &\approx C_3^* k_z^2 \approx C_3^{**} k_z^2, \\
C_4 &\approx C_4^* \approx C_4^{**}.
\end{aligned}
$$

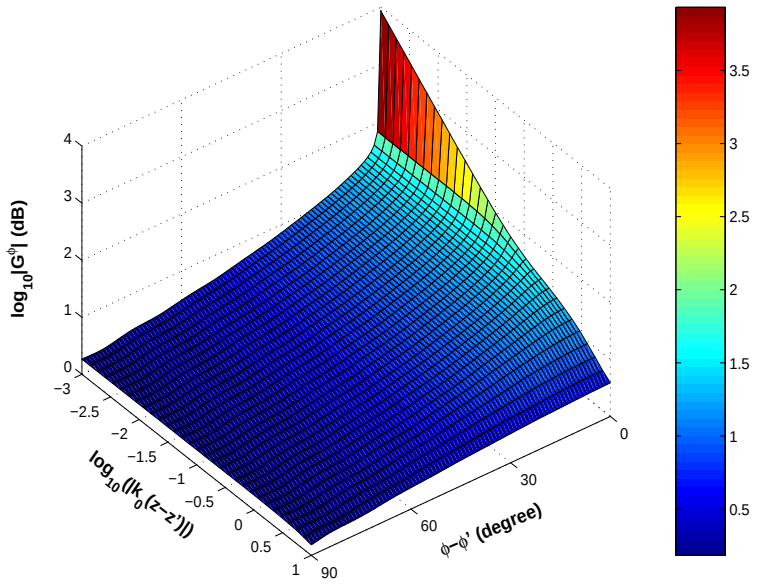

Figure 6.12: Spatial domain scalar potential Green's function G^{ϕ}.

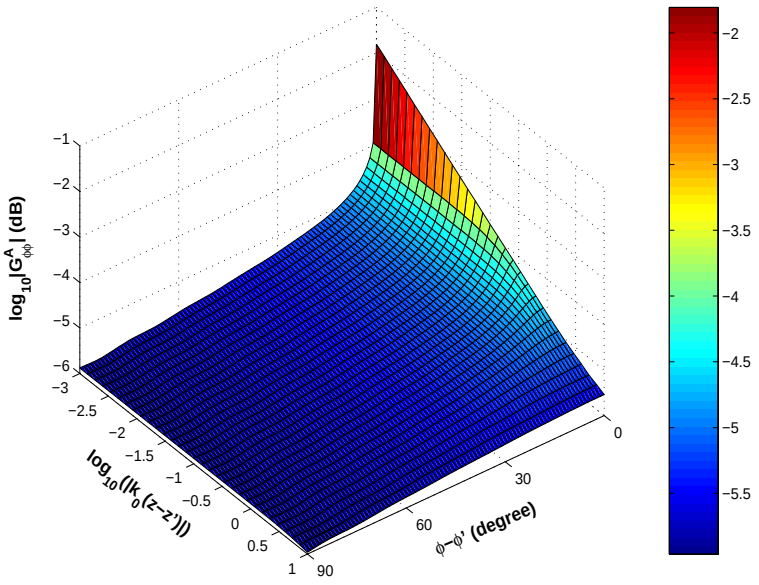

Figure 6.13: Spatial domain Green's function component $G^{A}_{\phi\phi}$.

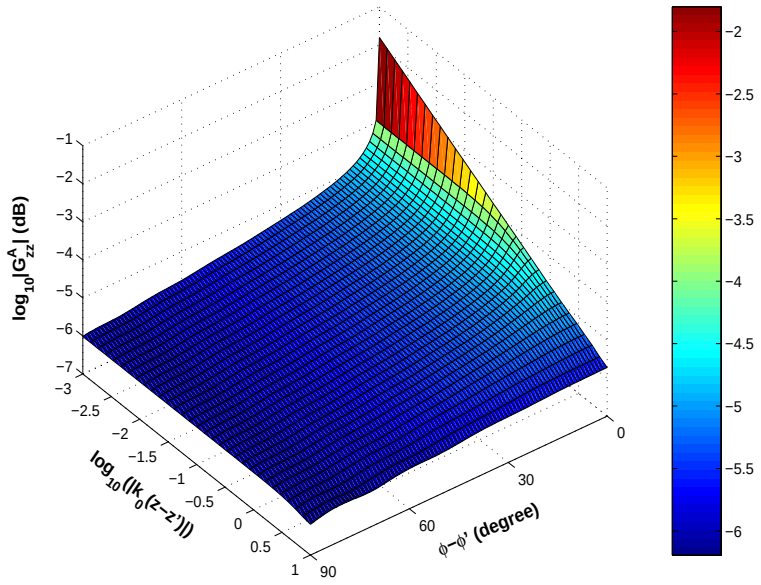

Figure 6.14: Spatial domain Green's function component G^A_{zz}.

To demonstrate the efficiency, robustness, and necessity of the new method in subsection 6.2.3 (complete extraction of the quasi-static component) compared with the old method proposed in subsection 6.2.2 (partial extraction of the quasi-static component), two cases are investigated, i.e, relatively large azimuthal separation and relatively small azimuthal separation, by calculating the relative error of the spatial domain mixed potential Green's functions G^ϕ as the function of the number of the employed terms of the series. The relative error of the G^ϕ for relatively large azimuthal separation $(\phi - \phi') = 0.5$ is shown in Fig. 6.15. It is observed from the Fig. 6.15 that the new method needs 190 terms to obtain convergent results with relative error less than 10^{-3}, while the old method needs about 200 terms. Both new and old methods can give satisfactory and convergent results. The computation time is 3.7 seconds per angle for the new method versus 3.9 seconds per angle for the previous method. However, the situation will change for the small azimuthal separation $(\phi - \phi')$. Fig. 6.16 shows the relative error of the G^ϕ for small azimuthal separation $(\phi - \phi') = 0.05$. It can be seen that only the new method can give satisfactory and convergent result when

we sum up to 190 terms. The new method still needs 190 terms to obtain convergent result with relative error less than 10^{-3}. The computation time is about 3.7 seconds per angle for the present method versus 11.1 seconds per angle for the old method, since the computation for sum up large number of terms (about 570 terms) of the series is time-consuming. Fig. 6.17 shows the relative error of the G^{ϕ} for much smaller azimuthal separation $(\phi - \phi') = 0.001$. The convergent result with relative error less than 10^{-3} can also be obtained by employing 190 terms and the computation time is about 3.7 seconds per angle for the present method, too. To obtain convergent result with relative error less than 10^{-3}, the old method needs to employ about 2000 terms and the computation time is about 38.9 seconds which is much longer than that of the new method. The Figs. 6.15-6.17 show that the convergence behaviour of the new method is much more stable and better than that of the old method, as it is independent of the angle $(\phi - \phi')$. All the computations are carried out on a Pentium-III 800 PC.

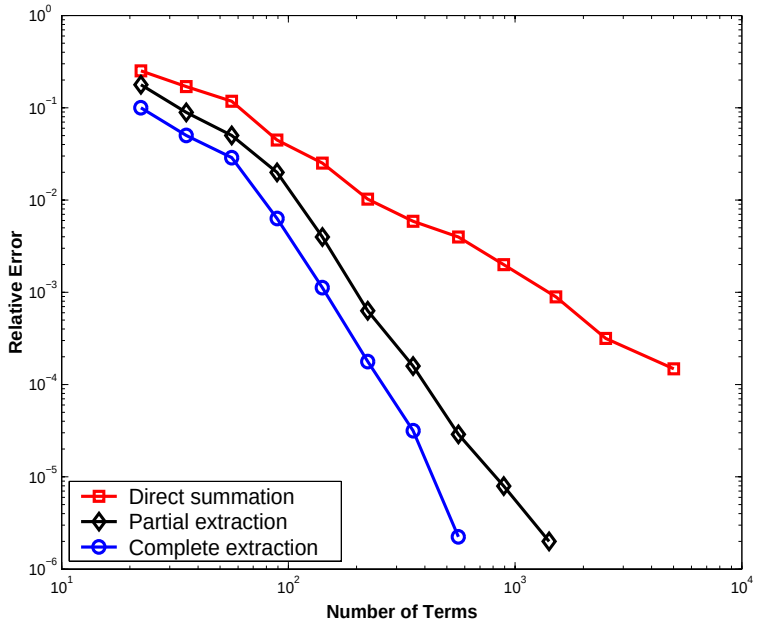

Figure 6.15: Relative error of G^{ϕ} versus number of terms for structure shown in Fig. 5.1 at $\phi - \phi' = 0.5$, $\log_{10}|k_0(z - z')| = -0.5$.

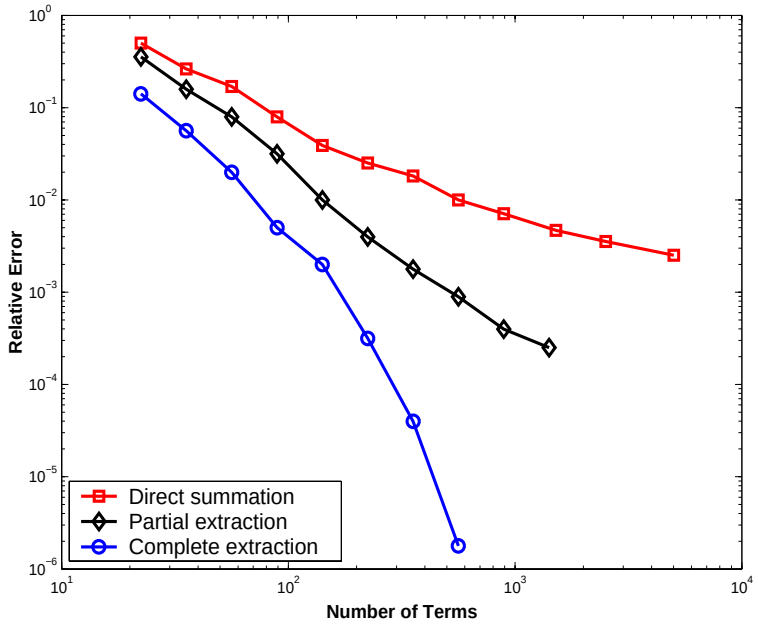

Figure 6.16: Relative error of G^{ϕ} versus number of terms for structure shown in Fig. 5.1 at $\phi - \phi' = 0.05$, $\log_{10}|k_0(z - z')| = -0.5$.

From the Fig. 6.16-6.17, it is also observed that the direct summation cannot give convergent result with relative error less than 10^{-3} even for adding about $5,000$ terms for relatively small azimuthal separation, as the convergence rate of the series is very slow. This means it is very inefficient to directly use the Eq. (6.19) to calculate the spatial domain Green's function using numerical integration. The accurate summation of the series can be obtained using the above mentioned procedure in subsection 6.2.3 and 6.2.4.

One more important observation can also be made from the Figs. 6.15-6.17 is that the accuracy of the spatial domain mixed potential Green's functions obtained using the old method cannot be easily increased by using more terms of the series. The accuracy of the spatial domain mixed potential Green's functions for small azimuthal separation directly affects the accuracy of the numerical analysis of the cylindrically stratified structure by the MPIE, especially for the structure with high dielectric properties. The reason is

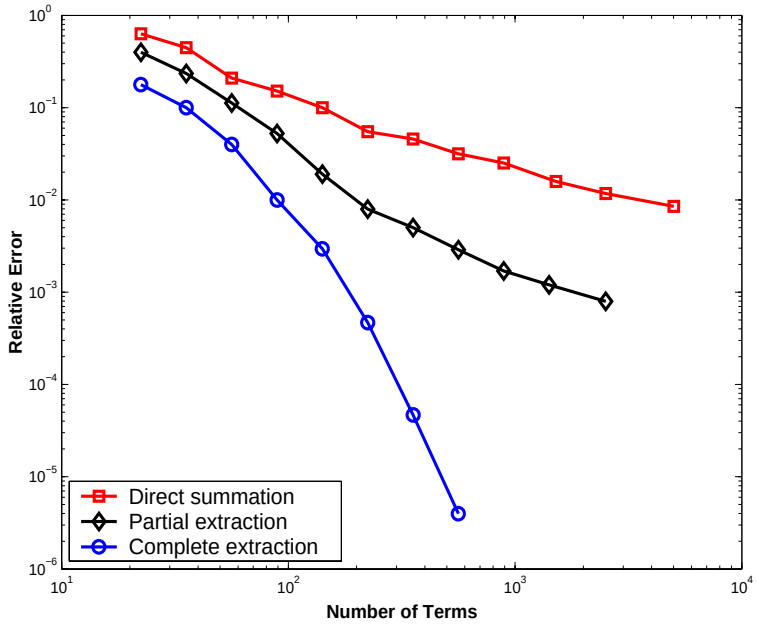

Figure 6.17: Relative error of G^{ϕ} versus number of terms for structure shown in Fig. 5.1 at $\phi - \phi' = 0.001$, $\log_{10}|k_0(z - z')| = -0.5$.

that the spatial domain mixed potential Green's functions for small azimuthal separation corresponds to the near field interaction of the MoM matrix elements resulted from the MPIE. From this point of view, the new method provides an efficient, robust, and new way to accurately calculate the mixed potential Green's functions for the MoM for solving the MPIE in spatial domain.

6.4 Summary

This chapter has presented a new method for improving the convergence behavior of the mixed potential Green's functions in spectral domain for cylindrically multilayered media. It is realized that the quasi-static components of the spectral domain Green's functions are slowly convergent but the inverse Fourier transform of the quasi-static components have a closed-form solution. After the quasi-static components are completely extracted from the vector potential and scalar potential Green's functions in spectral domain, the

remaining parts have relatively good convergence behavior which can be used to speed up the calculation of the inverse Fourier transform. This set of the mixed potential Green's functions is preferable and better than the electric field Green's functions because the mixed potential Green's functions are less singular than the electric field Green's functions in spatial domain. It is found that the electric field Green's functions in spatial domain are more difficult to evaluate when ρ and ρ' are equal to each other, as compared to the mixed potential Green's functions. This is reasonable and easily understandable, because the mixed potential Green's functions have been shown to have better convergence behaviors than the electric field Green's functions in spectral domain. Actually, as the ∇ operator is included twice in formulating the scalar potential, this operation will cause the resultant scalar potential Green's functions and vector potential Green's functions to have better convergence behaviors in spectral domain and correspondingly less singular behaviors in spatial domain.

One can easily prove that the above derived mixed potential Green's functions satisfy the Lorentz Gauge. The Coulomb Gauge can also be applied here to uniquely determine the vector potential and scalar potential. But this will cause the resultant mixed potential Green's functions to take an unnecessarily more complicated form. Also it should be noted that the mixed potential Green's functions obtained so far can be easily used to deal with a conducting patch (of a negligible thickness) mounted on cylindrical stratified structure. For a volumetric large source that occupies several layers, two considerations should be taken into account. Firstly, more dyadic components of the Green's functions should be included to account for the $\hat{\rho}$-directional current source and $\hat{\rho}$-directional field component. Secondly, an additional line integral would occur when the object occupies more than one layer. This situation is very similar to that of the planarly multilayered structure.

Chapter 7

Applications of Mixed Potential Green's Functions for Cylindrically Stratified Media

---

Applications of the mixed potential Green's functions are presented in this chapter. The resonant behaviour of a microstrip line and a rectangular patch antenna mounted on dielectric coated PEC cylinder are studied using MPIE. The effect of the superstrate on the resonance frequency is investigated. As another application, the radiation patterns of a helical antenna mounted on dielectric coated PEC cylinder is calculated by rigorously solving the MPIE for the current distribution.

7.1 Resonant Length of Microstrip Line

7.1.1 MPIE in General Form

The MPIE is solved in spatial domain with rooftop basis functions [98] for the analysis of input impedance and resonant length of microstrip line mounted on multilayered

dielectric coated PEC cylinder. Resonant length of the microstrip line as a function of permittivity of the superstrate is studied. The MPIE in component form can be written as:

$$E_z^{inc}(z,\phi) = j\omega A_z(z,\phi) + \frac{\partial}{\partial z}\Phi(z,\phi), \tag{7.1a}$$

$$E_\phi^{inc}(z,\phi) = j\omega A_\phi(z,\phi) + \frac{1}{\rho}\frac{\partial}{\partial \phi}\Phi(z,\phi), \tag{7.1b}$$

where the vector and scalar potentials are defined as

$$\boldsymbol{A}(z,\phi) = \iint_{s'} \overline{\boldsymbol{G}}_A(z,z',\phi,\phi') \cdot \boldsymbol{J}(z',\phi')ds', \tag{7.2a}$$

$$\Phi(z,\phi) = \iint_{s'} \boldsymbol{\nabla}_t' \cdot \boldsymbol{J}(z',\phi') \cdot G_\phi(z,z',\phi,\phi')ds', \tag{7.2b}$$

$$\boldsymbol{\nabla}_t' = \widehat{\boldsymbol{\phi}}\frac{1}{\rho}\frac{\partial}{\partial \phi} + \widehat{\boldsymbol{z}}\frac{\partial}{\partial z}. \tag{7.2c}$$

In (7.1a)-(7.2b), $A_z(z,\phi)$ and $A_\phi(z,\phi)$ represent the z- and ϕ-components of the vector potential $\boldsymbol{A}(z,\phi)$, respectively; while $\overline{\boldsymbol{G}}_A$ and G_ϕ denote the vector potential Green's functions and the scalar potential Green's function, respectively , which are obtained in Chapter 6. Integral equations in (7.1a) and (7.1b) are solved using the MoM with rooftop basis functions.

7.1.2 Numerical Results

The mixed potential Green's functions computed by the proposed technique are applied in the MoM to solve the problem of an axial oriented microstrip line mounted on a substrate-superstrate coated PEC cylinder as shown in Fig. 7.1, where the intermediate radius is $b = 0.5\lambda_0$, the inner radius $a = 0.9b$, the outer radius $c = 1.1b$, $\mu_{r1} = \mu_{r2} = 1.0$, $f = 6.8$ GHz, the width of the microstrip line $w = 0.005b$, the relatively permittivity of the substrate and superstrate are ϵ_{r1} and ϵ_{r2}, respectively. Before studying the aforementioned case, the input impedance of the microstrip line without the superstrate is calculated using the proposed method. The result is compared with that obtained by the commercial software *Clementine* (Fig.7.2). Fine agreement is observed. Although the

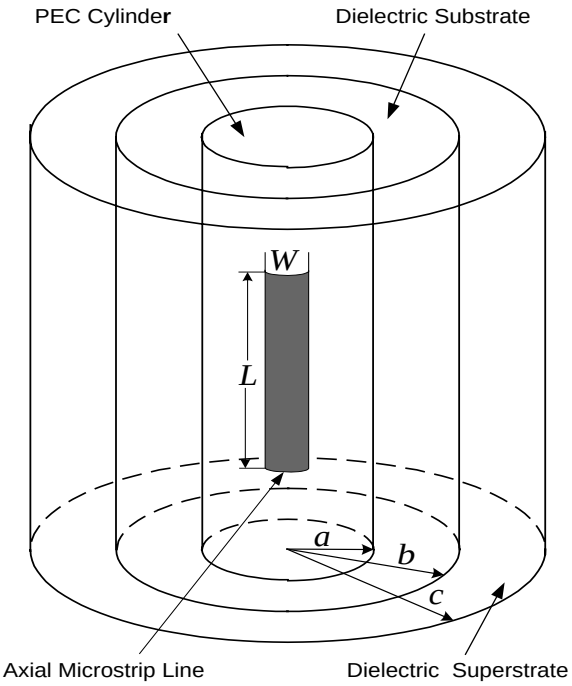

Figure 7.1: Axial oriented microstrip line. Outer radius $b = 0.5\lambda_0$, inner radius $a = 0.9b$, $w = 0.005b$, $\mu_{r1} = \mu_{r2} = 1.0$.

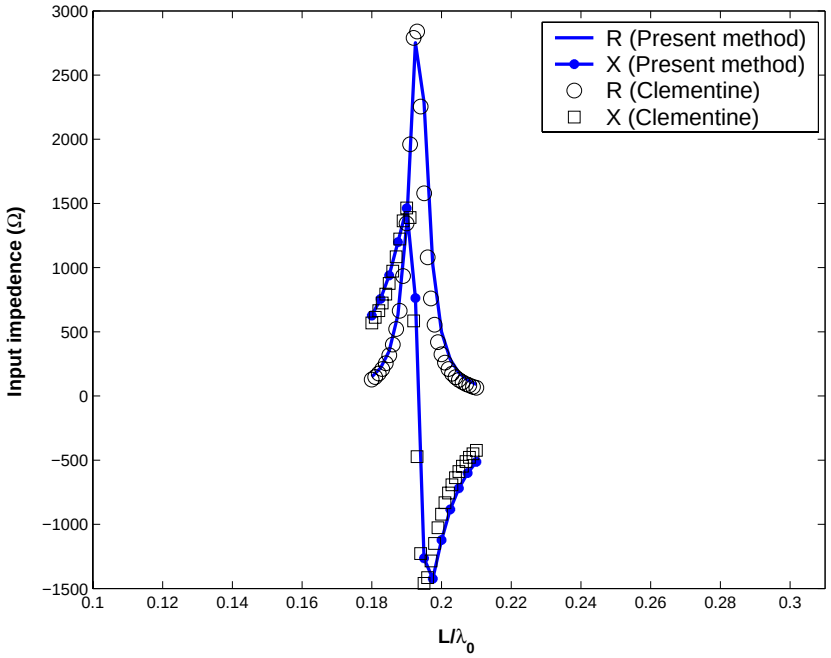

Figure 7.2: Input impedance of axial oriented microstrip line. Outer radius $b = 0.5\lambda_0$, inner radius $a = 0.9b$, $\epsilon_{r1} = 9.6$, $w = 0.005b$, $\mu_{r1} = \mu_{r2} = 1.0$, $f = 6.8$ GHz.

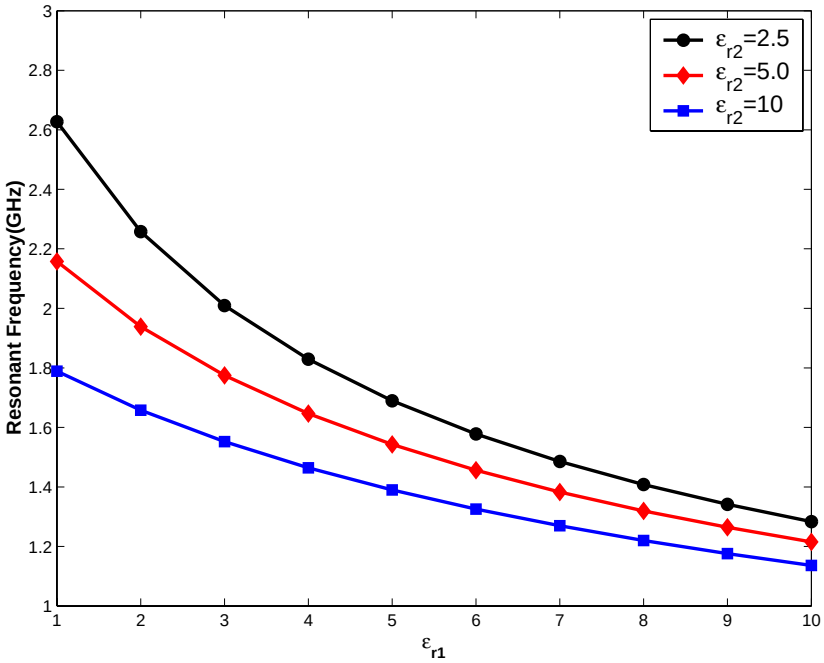

Figure 7.3: Resonant frequency versus ϵ_{r1}. Intermediate radius $b = 0.5\lambda_0$, inner radius $a = 0.9b$, outer radius $c = 1.1b$, $W = 0.005b$, $L = \lambda_0$, $\mu_{r1} = \mu_{r2} = 1.0$, $\lambda_0 = 44.12$ mm.

example is simple, the importance lies in the verification of the algorithm we developed. Then, the resonant frequency of the microstrip line with substrate and superstrate versus the permittivity of the substrate is calculated using our developed program (Fig. 7.3). From the results, we can see that for a fixed superstrate, the resonant frequency decreases smoothly when the ϵ_{r1} increases. This smooth behaviour can be utilized for numerical interpolation and extrapolation. It also can be seen that the addition of a superstrate will make the resonant frequency shift to lower end, and the increasing of the permittivity of the substrate will also make the resonant frequency lower. These are of much the similar manner to that for the planarly layered media case, where the effective permittivity will be determine by both the superstrate and substrate. The example investigated is relatively simple; however, the method presented here does provide a possible new way to study more complex problems.

7.2 Resonant Frequency of Patch Antenna

As a further application of the mixed potential Green's functions developed in the previous chapter, the resonant frequency of a rectangular microstrip patch antenna mounted in cylindrically multilayered structure is studied in this section. The most convenient way to find the resonant frequency of a patch antenna mounted on dielectric coated cylinder is cavity model method. It can only give approximate value since the fringing effect is ignored and the curvature effect of the patch is not taken into account. The most and accurate method to analyze the resonant frequency of a microstrip patch antenna is full-wave analysis, i.e., solving the integral equation using MoM. The MoM can be implemented either in spectral domain or in spatial domain. The spectral domain MoM is to formulate a characteristic equation like,

$$\overline{B}(\omega) \cdot c = 0. \tag{7.3}$$

It has a nontrivial solution for $\boldsymbol{J}(\phi', z')$ only if $\mid \overline{B}(\omega) \mid = 0$ which occurs at the resonant frequency. The resonant frequency of a structure is independent of the feed, source, etc., which is the inherent quality of a patch antenna. In this section, the MoM is implemented in spatial domain. The current distribution is first obtained under a specific excitation, i.e., a plane wave incidence. Then the resonant behaviour is obtained through the current distribution.

7.2.1 Resonant Frequency Extraction

The resonant behavior is an inherent character of the patch antenna and is independent of the feed. Similar to [99], a plane wave is assumed to be the incident field. The resonant frequency is defined as the frequency at which the imaginary part of current distribution is equal to zero. For example, a rectangular patch antenna mounted on one layered dielectric coated cylinder is studied. The configuration of the antenna is fixed and the

frequency is swept in certain range. The real and imaginary part of $\widehat{\phi}$-direction current distribution at the center of the patch antenna are plotted as a function of frequency. At the resonant frequency, the imaginary part of the current is equal to zero.

7.2.2 Numerical Results

Firstly, a rectangular patch antenna mounted on one layered dielectric coated cylinder is studied. The current distribution off the resonant frequency (3.08 GHz) are shown in Figs. (7.5-7.6), whereas the current distribution on the resonant frequency are shown in Figs. (7.7-7.8). We can see that when the patch is resonant, the imaginary part of the current distribution J_ϕ is almost zero. The current distribution at the center of the patch as a function of frequency is plotted in Fig. 7.9. From this information, we determine the resonant frequency as 3.08 GHz. Then more general case of a multilayered dielectric coated cylinder as shown in Fig. 7.4 is studied. The effect of superstrate on the resonant frequency is that the resonant frequency is shifted to the low frequency end. Fig. 7.10 shows the effect of superstrate on resonant frequency at three different configuration for ϵ_{r2}, i.e., $\epsilon_{r2} = 9$, $\epsilon_{r2} = 5$ and $\epsilon_{r2} = 1$, while $\epsilon_{r1} \in [1, 2, 3, 4.5, 5.7, 7.3, 8.5, 9.6]$.

7.3 Helical Microstrip Antenna

Analysis of a helical microstrip mounted on cylindrically stratified media has been an important subject in various antenna designs and optimizations. For example, the radiated fields of an arbitrary-shaped microstrip antenna mounted on a circular-cylindrical platform have been studied in [100], and the dispersion characteristics of the wave propagation along the helix with a conducting core and dielectric substrate have also been investigated in [101]. Most recently, a reciprocity approach for calculating the far-field radiation patterns of a center-fed helical microstrip antenna mounted on a dielectric-coated circular cylinder was reported [102]. This method is efficient if the current

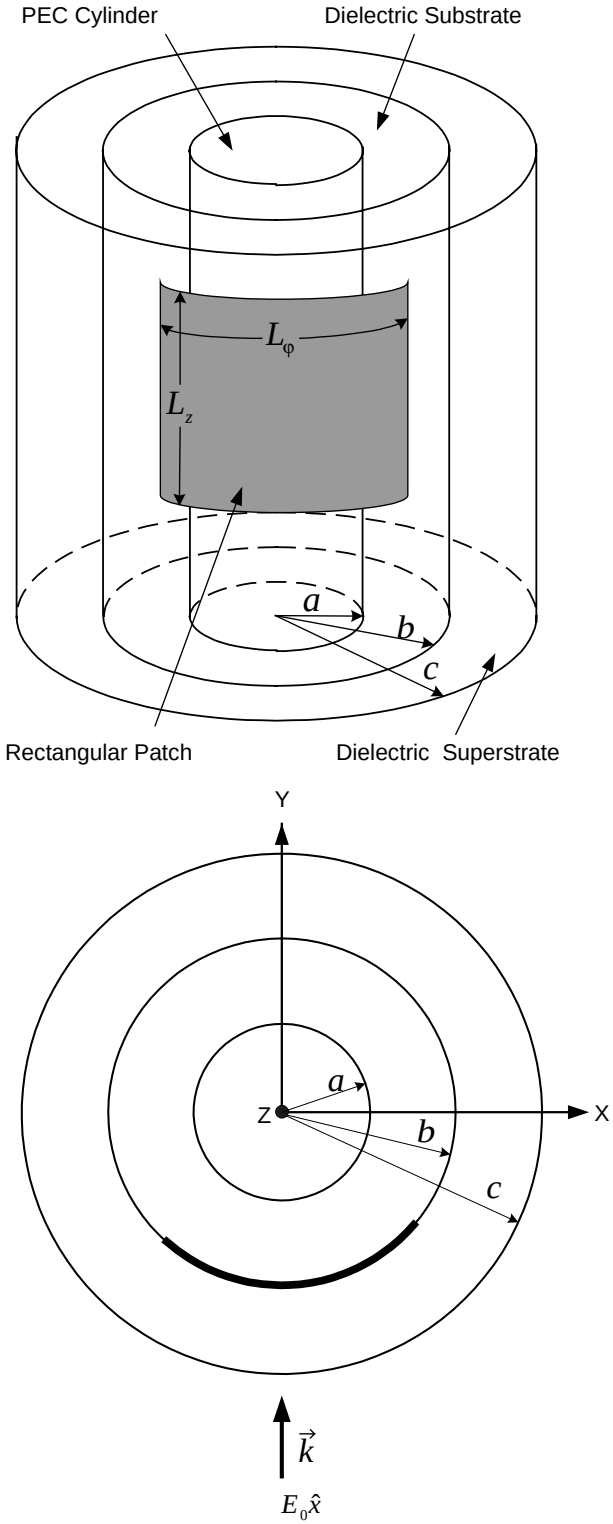

Figure 7.4: Rectangular patch antenna mounted on a substrate and superstrate coated PEC cylinder, a plane wave with $\hat{\boldsymbol{x}}$-direction polarization is the incident field.

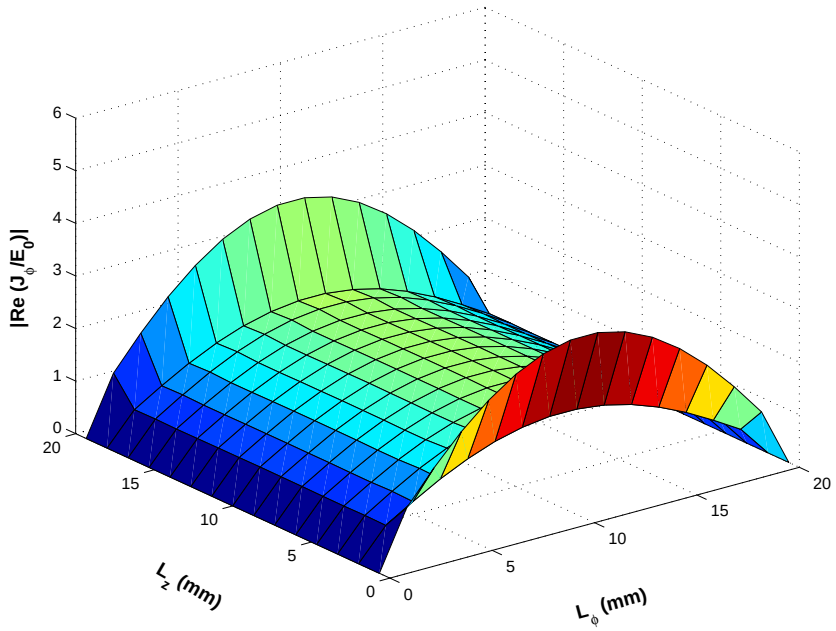

Figure 7.5: Real part of the current distribution J_ϕ, where radius $a = 19.85$ mm, $b = 22.05$ mm, $c = 24.05$ mm, $L_z = 20$ mm, $L_\phi = 20$ mm, $\epsilon_{r1} = 5.7$, $\epsilon_{r2} = 1.0$, $\mu_{r1} = \mu_{r2} = 1.0$, $f = 3.1$ GHz.

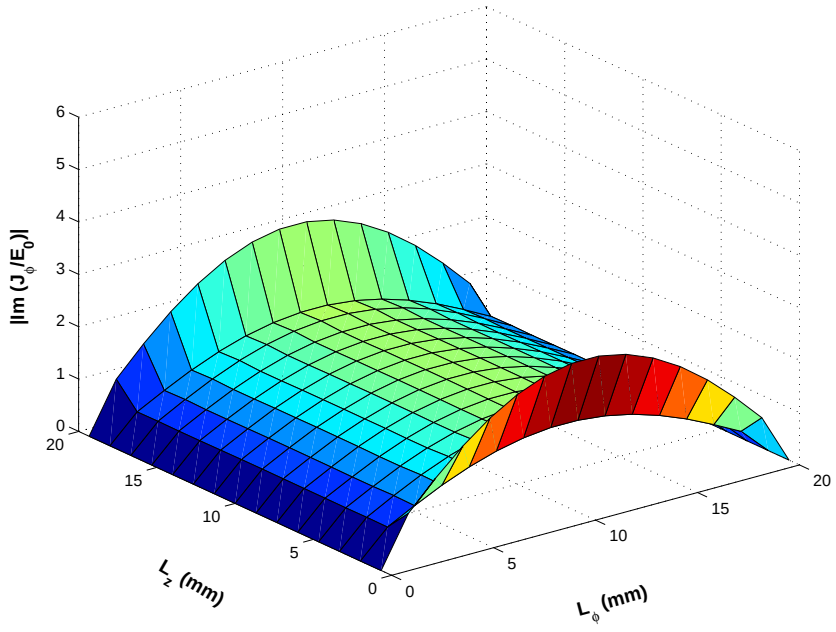

Figure 7.6: Imaginary part of the current distribution J_ϕ, where radius $a = 19.85$ mm, $b = 22.05$ mm, $c = 24.05$ mm, $L_z = 20$ mm, $L_\phi = 20$ mm, $\epsilon_{r1} = 5.7$, $\epsilon_{r2} = 1.0$, $\mu_{r1} = \mu_{r2} = 1.0$, $f = 3.1$ GHz.

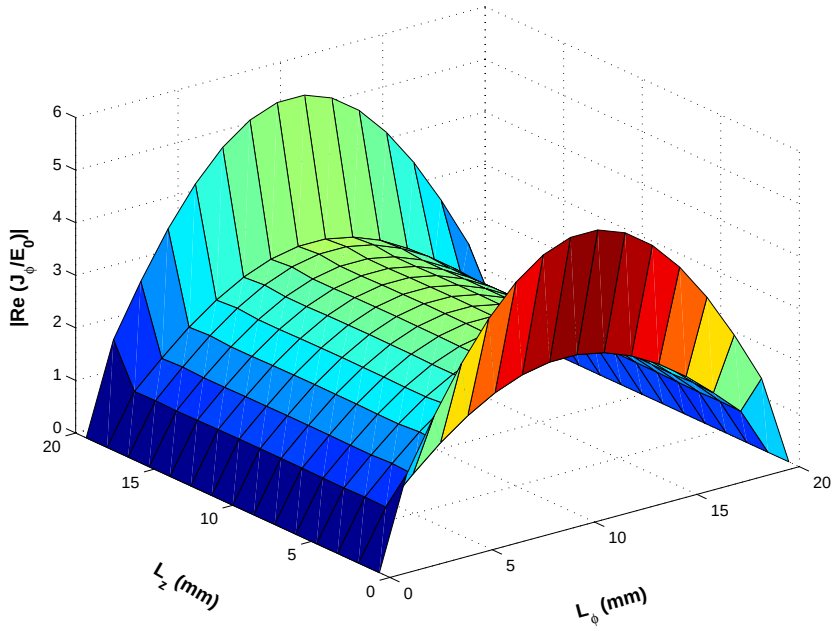

Figure 7.7: Real part of the current distribution J_ϕ, where radius $a = 19.85$ mm, $b = 22.05$ mm, $c = 24.05$ mm, $L_z = 20$ mm, $L_\phi = 20$ mm, $\epsilon_{r1} = 5.7$, $\epsilon_{r2} = 1.0$, $\mu_{r1} = \mu_{r2} = 1.0$, $f = 3.08$ GHz.

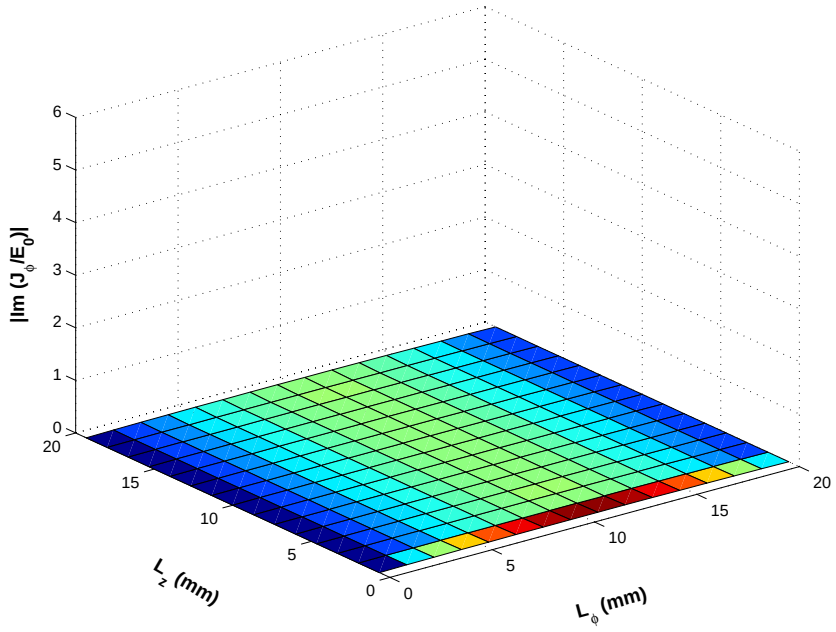

Figure 7.8: Imaginary part of the current distribution J_ϕ, where radius $a = 19.85$ mm, $b = 22.05$ mm, $c = 24.05$ mm, $L_z = 20$ mm, $L_\phi = 20$ mm, $\epsilon_{r1} = 5.7$, $\epsilon_{r2} = 1.0$, $\mu_{r1} = \mu_{r2} = 1.0$, $f = 3.08$ GHz.

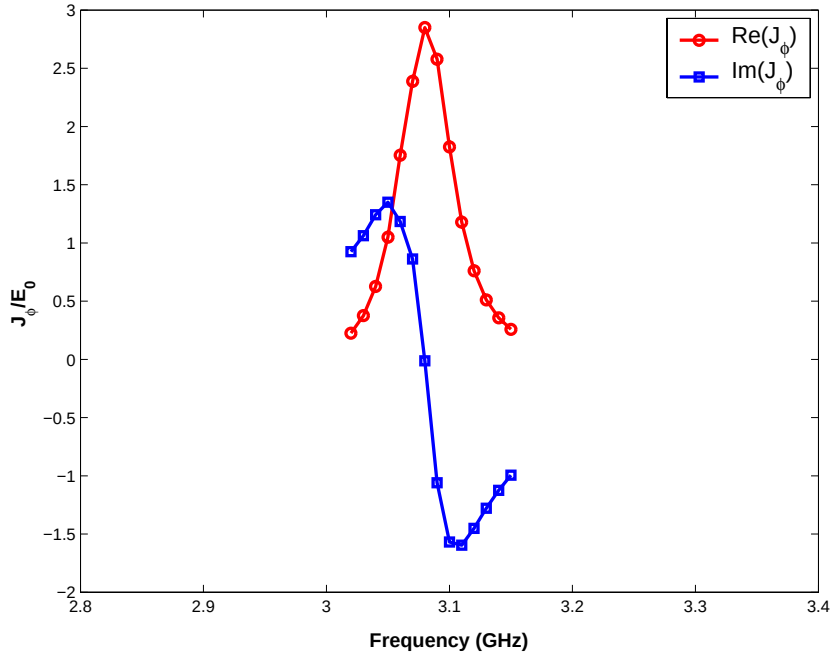

Figure 7.9: Current J_ϕ at the center of the patch, where radius $a = 19.85$ mm, $b = 22.05$ mm, $c = 24.05$ mm, $L_z = 20$ mm, $L_\phi = 20$ mm, $\epsilon_{r1} = 5.7$, $\epsilon_{r2} = 1.0$, $\mu_{r1} = \mu_{r2} = 1.0$.

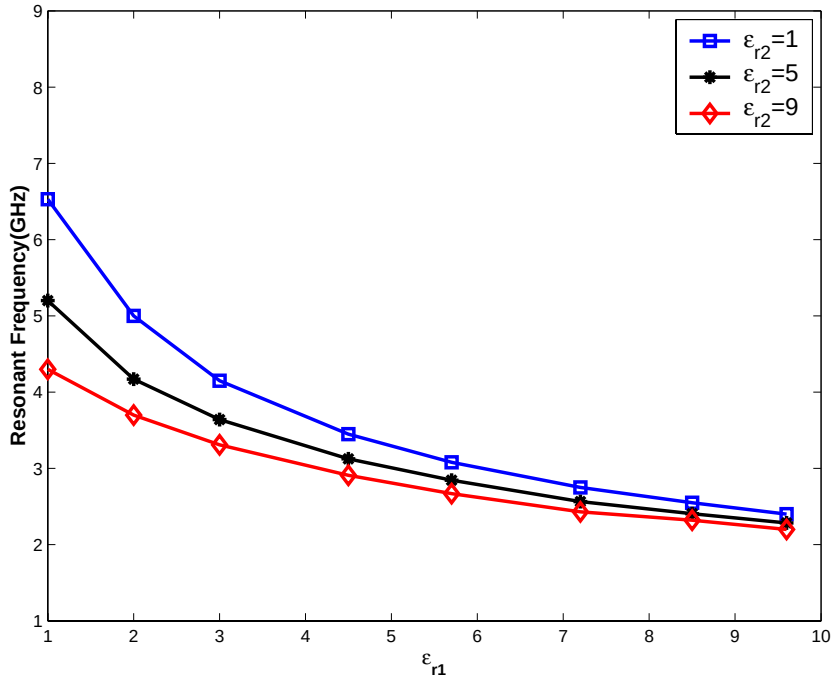

Figure 7.10: Resonant frequency versus ϵ_{r1} with a superstrate, where radius $a = 19.85$mm, $b = 22.05$mm, $c = 24.05$mm, $L_z = 20$mm, $L_\phi = 20$mm, $\mu_{r1} = \mu_{r2} = 1.0$.

distribution on the helical microstrip antenna can be easily obtained. The approximation of current distribution assumed in [102] is actually made under some conditions: a) the width of the microstrip helix, w, is small compared to a wavelength; b) the relative permittivity of the substrate is 1; and c) there is no superstrate. However, this current distribution cannot be readily obtained if the relative permittivity is no longer equal to 1 for either the superstrate or the substrate. Rigorous solution to the current distribution is thus needed. In this section, the current distribution is rigorously obtained by employing the MoM and the closed-form Green's functions obtained in previous chapter to solve the MPIE for cylindrically layered structure in spatial domain. Then the current distribution is approximated by an analytic form. Finally, the far-field Hankel transform is applied to obtain an analytical form of the radiated power due to the helical microstrip antenna.

7.3.1 Formulation of the Radiation Pattern

The geometry for the problem of interest is shown in Fig. 7.11, which is the same as that in [102] except for an additional superstrate mounted on the microstrip helix. The cylinder has an inner radius of a. The dielectric coating has a relative permittivity of ϵ_{r1} and a thickness of $h = b - a$. The superstrate has a relative permittivity of ϵ_{r2} and a thickness of $h' = c - b$. The pitch of the helix is d.

The electric field due to the current can be expressed as

$$\boldsymbol{E} = \iint_{s'} \overline{\boldsymbol{G}}(\boldsymbol{r}, \boldsymbol{r}') \cdot \boldsymbol{J}(\boldsymbol{r}') ds'. \tag{7.4}$$

The spatial domain electric field Green's function, $\overline{\boldsymbol{G}}(\boldsymbol{r}, \boldsymbol{r}')$ can be found in Chapter 4. Using the relations between cylindrical coordinates and spherical coordinates, the far field components are

$$\begin{bmatrix} E_\theta \\ E_\phi \end{bmatrix} = \iint_{s'} \begin{bmatrix} G_{\theta z} & G_{\theta\phi} \\ G_{\phi z} & G_{\phi\phi} \end{bmatrix} \cdot \begin{bmatrix} J_z \\ J_\phi \end{bmatrix} ds', \tag{7.5}$$

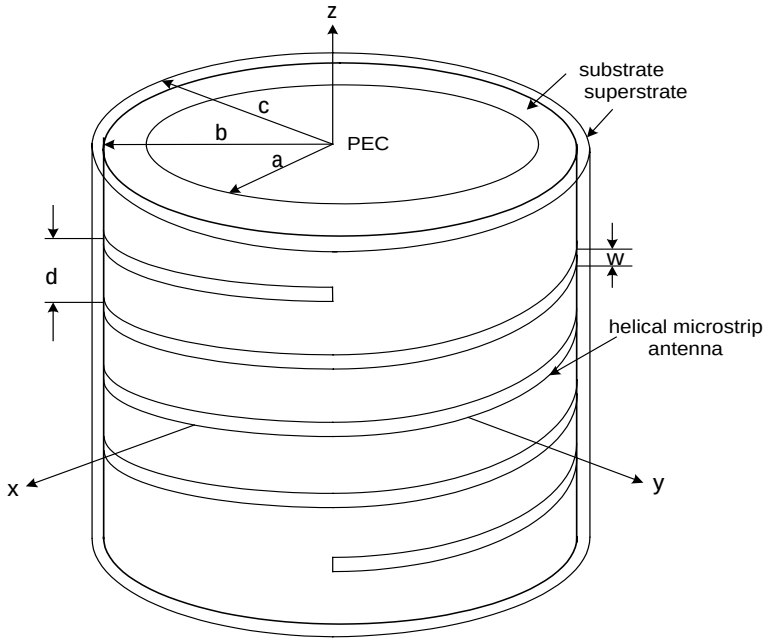

Figure 7.11: A helical microstrip antenna mounted on a dielectric-coated circular cylinder with a superstrate.

where

$$G_{\theta z} = -G_{zz}\sin\theta + G_{\rho z}\cos\theta, \tag{7.6a}$$

$$G_{\theta\phi} = -G_{z\phi}\sin\theta + G_{\rho\phi}\cos\theta. \tag{7.6b}$$

When $|\boldsymbol{r}| \to \infty$, the far field Hankel transform which relates the cylindrical wave and spherical wave is given below [103]:

$$\frac{2}{j^{n+1}}\frac{e^{ikr}}{r}G(k\cos\theta) = \int_{-\infty}^{\infty} G(k_z)H_n^{(1)}(k_\rho\rho)e^{jk_z z}dk_z, \tag{7.7}$$

where $G(\bullet)$ is the Green's function component. From above relations, the far field can be deduced as

$$\begin{aligned} E_\theta \;=\; & \sum_{n=\infty}^{\infty}(Y_{\theta z}\sin\psi + Y_{\theta\phi}\cos\psi)e^{jn\phi} \\ & \cdot \iint_{s'} \boldsymbol{J}(l')e^{-jn\phi'}e^{-jk_i\cos\theta z'}ds', \end{aligned} \tag{7.8a}$$

$$E_\phi = \sum_{n=\infty}^{\infty} (Y_{\phi z} \sin\psi + Y_{\phi\phi} \cos\psi) e^{jn\phi} \cdot \iint_{s'} \boldsymbol{J}(l') e^{-jn\phi'} e^{-jk_i \cos\theta z'} ds'. \tag{7.8b}$$

In (7.8a) and (7.8b), $\psi = \arctan[d/(2\pi b)]$ and

$$Y_{\theta z} = \frac{2(k_j^2 - k_i^2 \cos^2\theta) e^{jk_i r}}{8\pi\omega\epsilon_j j^{n+1} r \sin\theta} \frac{f_{11}(k_z, n)}{H_n^{(1)}(k_{i\rho}\rho)}\bigg|_{k_z = k_i \cos\theta}, \tag{7.9a}$$

$$Y_{\theta\phi} = \frac{2e^{jk_i r}}{8\pi\omega\epsilon_j j^{n+1} r \sin\theta H_n^{(1)}(k_{i\rho}\rho)} \left[i\omega\epsilon_j \frac{\partial f_{12}(k_z, n)}{\partial\rho'} - \frac{k_z n}{\rho'} f_{11}(k_z, n) \right]\bigg|_{k_z = k_i \cos\theta}, \tag{7.9b}$$

$$Y_{\phi z} = \frac{-2\omega\mu_i (k_j^2 - k_i^2 \cos^2\theta) e^{jk_i r}}{8\pi\omega\epsilon_j j^{n+1} r \sin\theta} \frac{f_{21}(k_z, n)}{H_n^{(1)}(k_{i\rho}\rho)}\bigg|_{k_z = k_i \cos\theta}, \tag{7.9c}$$

$$Y_{\phi\phi} = \frac{2\omega\mu_i e^{jk_i r}}{8\pi\omega\epsilon_j j^{n+1} r k_i \sin\theta H_n^{(1)}(k_{i\rho}\rho)} \left[\frac{nk_z}{\rho'} f_{21}(k_z, n) - j\omega\epsilon_j \frac{\partial f_{22}(k_z, n)}{\partial\rho'} \right]\bigg|_{k_z = k_i \cos\theta}, \tag{7.9d}$$

where $f_{11}(k_z, n)$, $f_{12}(k_z, n)$, $f_{21}(k_z, n)$, and $f_{22}(k_z, n)$ are components of Green's functions discussed in Chapter 3.

7.3.2 Current Distribution

The current distribution on the helical antenna assumed in [102] is no longer valid if the relative permittivity of the substrate or the superstrate is not equal to 1. A rigorous current distribution obtained using the MoM is necessary for the analysis of radiation pattern. On the surface of the helical antenna, the mixed potential integral equation (MPIE) in component form are found to be Eqs. (7.1a)-(7.2b).

Integral equations in (7.1a) and (7.1b) are solved using the MoM with rooftop basis functions. The unit vector along and perpendicular to the helical microstrip are $\widehat{\boldsymbol{l}}$ and $\widehat{\boldsymbol{u}}$, respectively. The currents in these two directions are assumed as $\boldsymbol{J}_u$ and $\boldsymbol{J}_l$, respectively. From our calculation, we find that $|\boldsymbol{J}_u| \ll |\boldsymbol{J}_l|$, so $\boldsymbol{J}_u$ can be neglected. Current distribution along the center line of $\widehat{\boldsymbol{l}}$ direction on a center-fed helical antenna for a

specific configuration, where $\lambda_0 = 0.04$, $a = 0.25\lambda_0$, $b = 0.3\lambda_0$, $c = 0.35\lambda_0$, $d = 0.5\lambda_0$, $L = 1.95\lambda_0$, $w = 0.005\lambda_0$, $\epsilon_{r1} = 5$, and $\epsilon_{r2} = 2$ is shown in Fig. 7.12. $\boldsymbol{J}_l$ can be fit into the form $\boldsymbol{J}_l(l') = \sin[\beta_i(\frac{L}{2} - |l'|)]\widehat{\boldsymbol{l}}$, which is similar to the assumed approximate current distribution in [102], except that β_i must be replaced by an appropriate value. This analytic form current distribution will lead to a closed-form solution for the integral in (7.8a) and (7.8b), which can be found in [102].

Numerical investigation of β_i shows that β_i is dependent on the configuration of the helical antenna system, and this includes the relative permittivity and thickness each of the substrate and superstrate, the radius of the inner cylinder, the pitch, width and length of the helical microstrip.

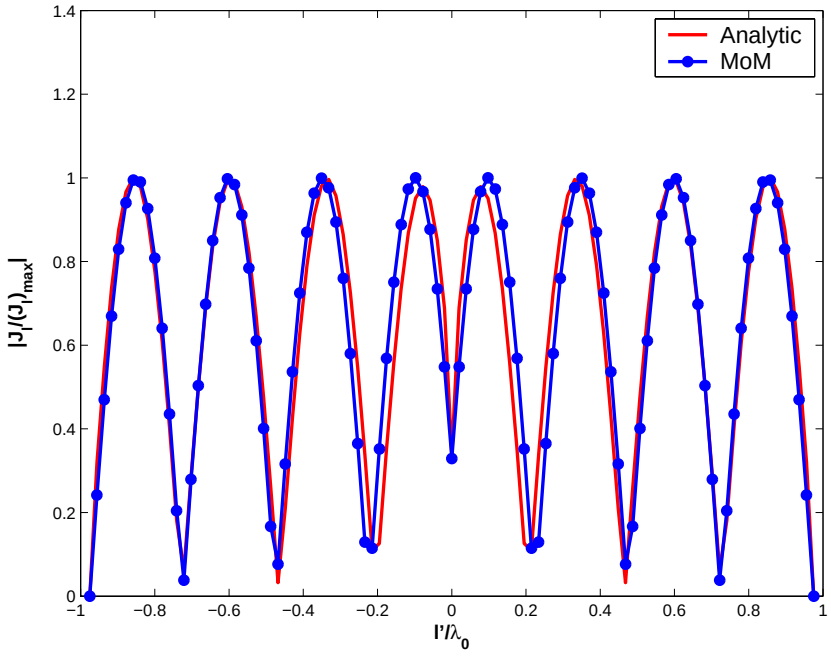

Figure 7.12: Normalized current distribution $|J_l/(J_l)_{max}|$ along the center line of $\widehat{\boldsymbol{l}}$ direction on a center-fed helical antenna. It can be approximated by an analytic form $\boldsymbol{J}_l(l') = \sin[\beta_i(\frac{L}{2} - |l'|)]\widehat{\boldsymbol{l}}$, where $\beta_i \approx (2\pi/\lambda_0)\sqrt{3.86} \approx 310.3$.

7.3.3 Numerical Results

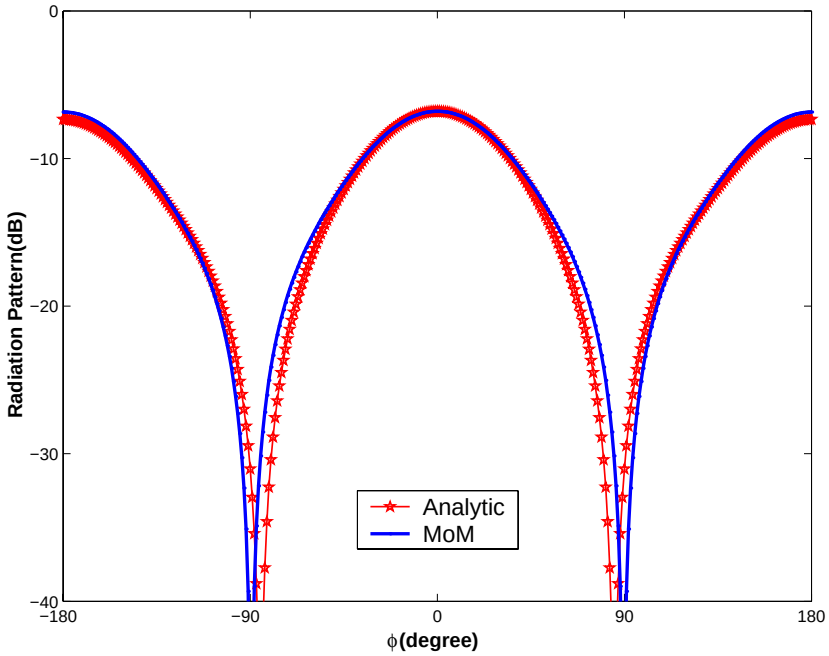

Figure 7.13: Azimuthal plane radiation pattern for one-half wavelength pitch and one-turn helical antenna. The θ-component

One case in [102] is examined using the present method as a special case of the presently more general model, where $\lambda_0 = 0.04$, $a = 0.25\lambda_0$, $b = 0.3\lambda_0$, $c = 0.35\lambda_0$, $d = 0.5\lambda_0$, $w = 0.005\lambda_0$, $\epsilon_{r1} = 1$, and $\epsilon_{r2} = 1$, the azimuthal plane bisects the helical antenna. Azimuthal plane radiation patterns of both the θ- and ϕ-components are obtained, shown in Figs. 7.13-7.14, and compared with those patterns obtained in [102]. A good agreement between the results obtained herein using the present MoM and the closed-form Green's functions approach and in [102] using the reciprocity approach provides some validation of the presently proposed method and developed code. After the method and code are further validated, more general cases are newly studied and their radiation patterns are shown in Figs. 7.15-7.17 and Figs. 7.18-7.20, where the permittivities of substrate and superstrate are set as $\epsilon_{r1} = 5$, and $\epsilon_{r2} = 2$, respectively.

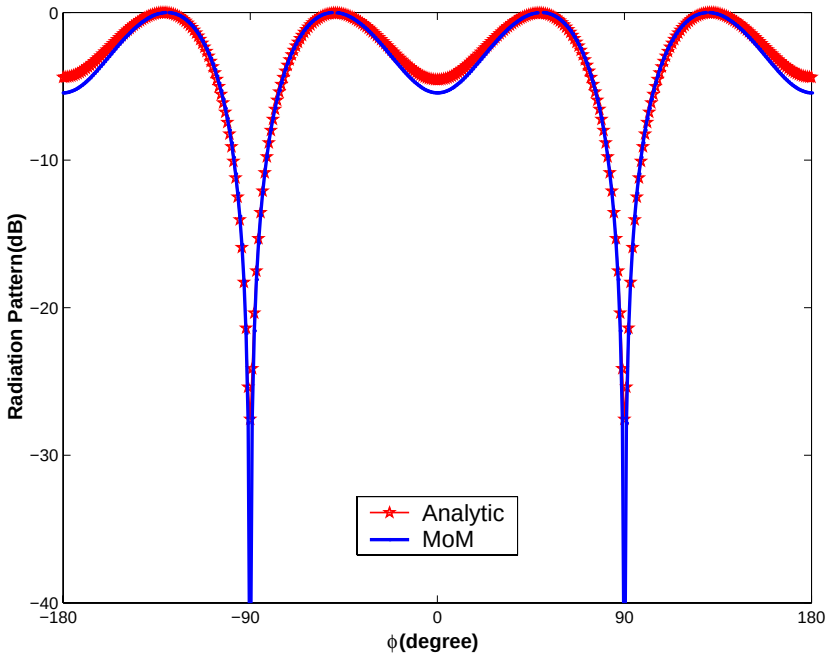

Figure 7.14: Azimuthal plane radiation pattern for one-half wavelength pitch and one-turn helical antenna. The ϕ-component.

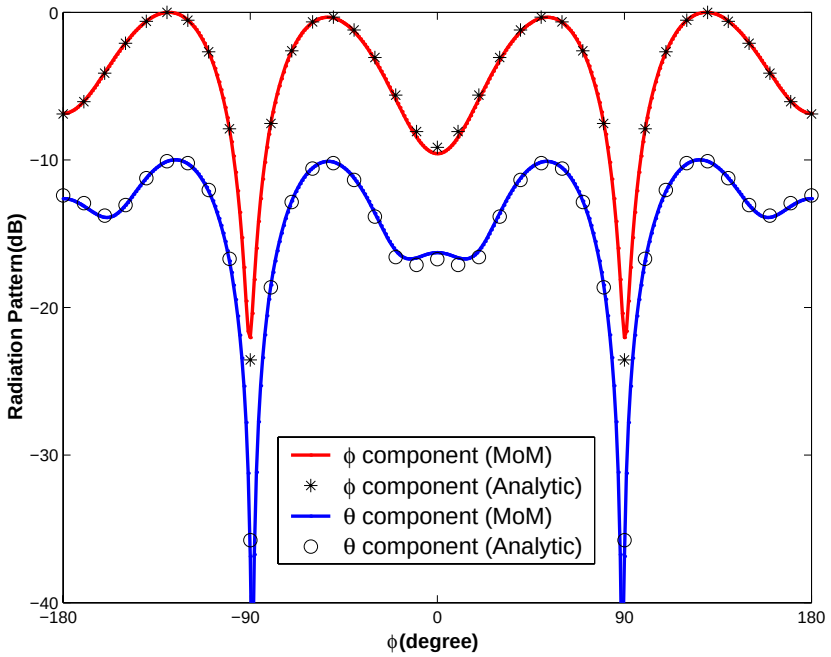

Figure 7.15: Azimuthal plane radiation patterns for one-half wavelength pitch helical antenna. One-turn helical antenna.

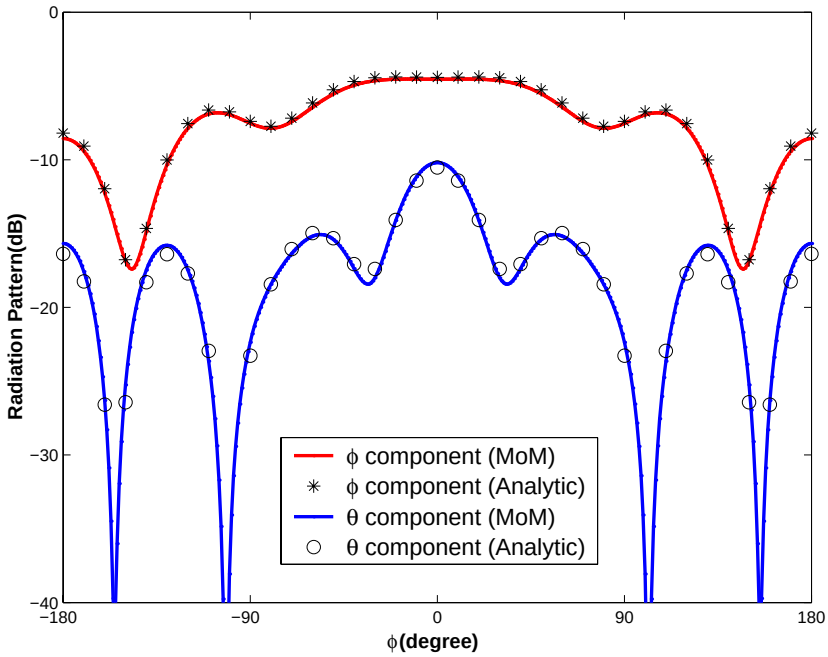

Figure 7.16: Azimuthal plane radiation patterns for one-half wavelength pitch helical antenna. Two-turn helical antenna.

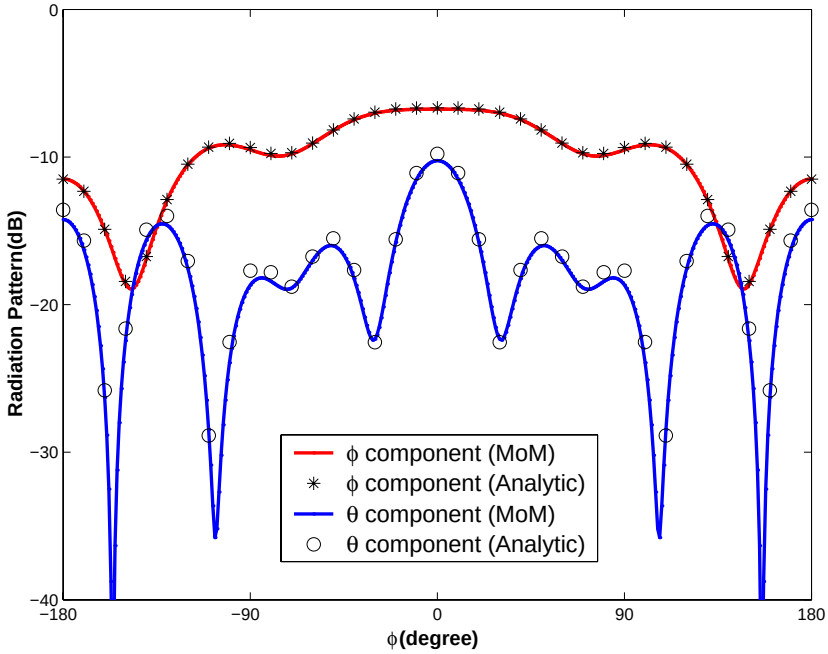

Figure 7.17: Azimuthal plane radiation patterns for one-half wavelength pitch helical antenna. Four-turn helical antenna.

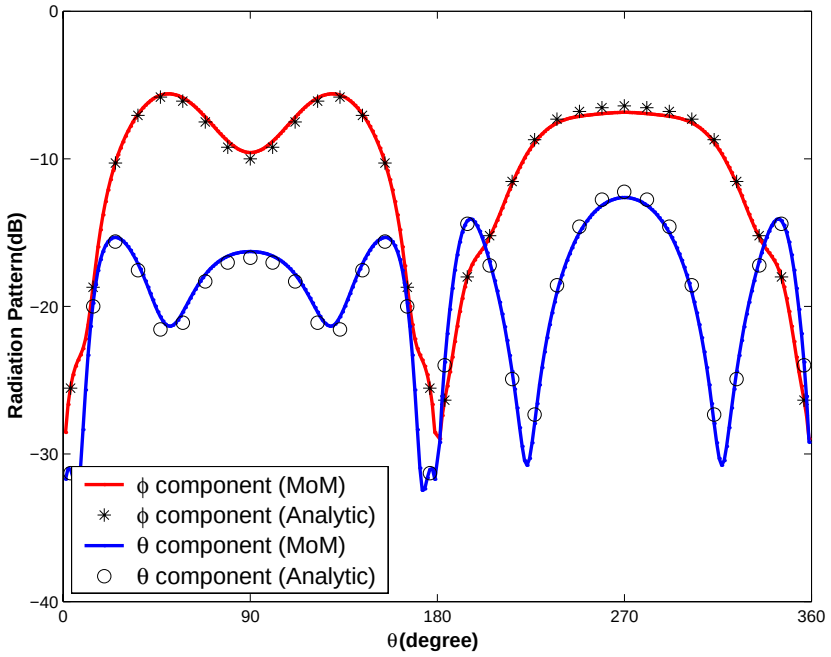

Figure 7.18: Elevation plane radiation patterns for one-half wavelength pitch helical antenna. One-turn helical antenna.

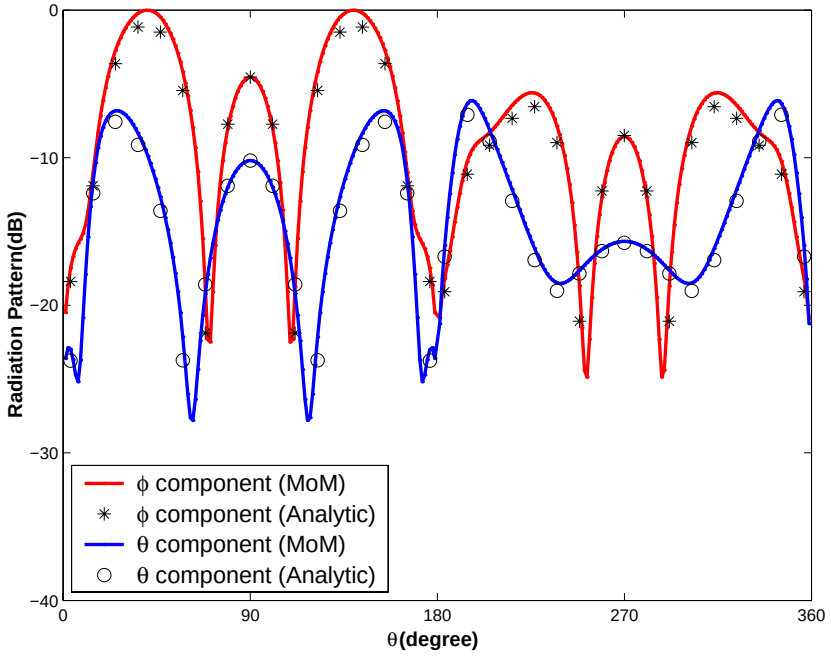

Figure 7.19: Elevation plane radiation patterns for one-half wavelength pitch helical antenna. Two-turn helical antenna.

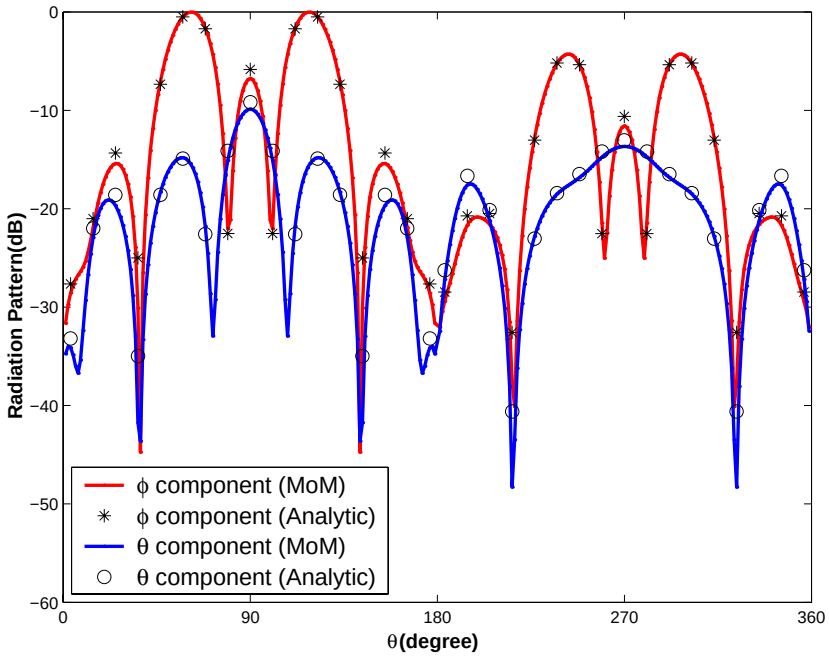

Figure 7.20: Elevation plane radiation patterns for one-half wavelength pitch helical antenna. Four-turn helical antenna.

Figs. 7.15-7.17 are the radiation patterns in azimuthal plane ($\theta = \pi/2, \phi = [0, 2\pi]$), while Figs. 7.18-7.20 are the radiation patterns in elevatio plane ($\phi = 0, \theta = [0, 2\pi]$). The radiation patterns in both planes are normalized to the maximum radiation power for each configuration, i.e., one turn, two turns and four turns, respectively. The other geometrical parameters of the helical antenna are the same as the aforementioned ones. Far-field radiation patterns are calculated by direct numerical integration. To make the obtained results more useful, the current distribution obtained by using the MoM is also approximated by the aforementioned analytic form, and then a closed-form far-field radiated power is obtained. We refer the former numeric one as "*MoM*" and the latter closed form one as "*Analytic*" through Figs. 7.15-7.17 and Figs. 7.18-7.20. It must be pointed out that the "*Analytic*" solution here is different from that in [102], and it is actually obtained based on the exact current solution obtained using the MoM rather than an assumed current distribution as used in [102]. Therefore, the present result is

more accurate, but equally fast in computation. From Figs. 7.15-7.20, we find that the radiation patterns in azimuthal plane are ϕ-symmetric in the range $[-\pi, \pi]$ referenced to $\phi = 0$ plane; while the radiation patterns in elevation plane are θ-symmetric in the range $[0, \pi]$, $[\pi, 2\pi]$ referenced to $\theta = \pi/2$ plane.

The problem we discussed is somewhat similar to the classical helical antenna, which has been studied intensively by many researchers [104], first Kraus in 1947 at Ohio State University, and then Patton, Kilgus, Wheeler, Chirex, Carver, etc. Different modes have been found as a function of the helix dimensions (diameter, spacing and pitch angle). However, the example we presented herein is basically different from the classic helical antenna. First, the classical helical antenna is not wrapped around dielectric coated PEC supports. The example we presented is a helical microstrip mounted on a dielectric coated PEC cylinder. Second, the classical helical antenna has a ground plan of (circular, square or cupped shape) at the feeding end. The example we presented has no such ground plane and is center-fed. The classical helical antenna has two main modes. In axial mode, the outgoing traveling wave is dominant and the current can be approximated as uniform traveling wave along the entire length. In normal mode, the helix is small and the current is assumed to be uniform in magnitude and in phase over the entire length of the helix. The example we presented has a typical resonant structure due to the inner PEC cylinder. The current distribution cannot take the aforementioned forms, i.e., the traveling wave and uniform wave. Due to the differences of the structures, the example we presented does not belong to the classical helical antenna. Although, from the plots in Figs. 7.15-7.20, we can observe a tendency from side radiation (the maximum lobe is in the azimuthal plane) to axial radiation (the maximum lobe is off the azimuthal plane) as the number of helix turns increases, the present example does not fall into the two typical modes, i.e., the axial mode and normal mode.

7.4 Summary

This chapter presented several applications of the mixed potential Green's functions developed in Chapter 6. The resonant behaviour of a microstrip line and a rectangular patch antenna mounted on dielectric coated PEC cylinder are studied for the resonant behaviour using MPIE. The effect of the superstrate on the resonance frequency is investigated. As another application, the radiation patterns of a helical antenna mounted on dielectric coated PEC cylinder is studied firstly using MPIE. The current distribution is obtained by rigorously solving the MPIE on the microstrip helix and far-field radiation patterns are then calculated using the electric field Green's functions developed in Chapter 4.

Chapter 8

Creeping Waves Along a Perfectly Conducting Cylinder With a Lossy Magnetic Coating

---

The effects of dielectric loss, conductor loss, surface wave mode and space wave radiation could be included, if there is any, in the spatial domain Green's functions presented Chapter 6. The surface wave mode is an important issue in designing microstrip antennas and circuits. In the previous discussion in Chapter 6, the poles corresponding to the surface wave modes are located on the certain region of the real k_z axis [83]. During the inverse Fourier transform, these poles are avoided by deforming the Sommerfeld integration path. Since the two-step DCIM is applied to the infinite integral over k_z, there is no need of the location of the poles [82]. The effect of the surface waves is implicitly contained in the spatial domain Green's functions. However, in order to explicitly investigate the surface wave propagating along the cylindrically layered media, a varied form of Green's functions, i.e, a double integral spectral representation over a continuum of azimuthal and axial wave number ν and k_z, respectively, is employed [41,43].

This formulation can be derived from the Green's functions in Chapter 6 by Watson transform [86]. Characteristic equations can be deduced from the varied form of Green's functions. In this chapter, creeping waves (one kind of surface waves) along a PEC cylinder with a lossy magnetic coating are studied.

8.1 Creeping Waves Along Cylindrically Layered Media

Consider a PEC cylinder with a coating material as shown in Fig. 8.1. The Green's functions for such structures have been studied extensively for the last several decades and the creeping waves are characterized [78,40,42,105,43,41,106]. Paknys and Wang [41]

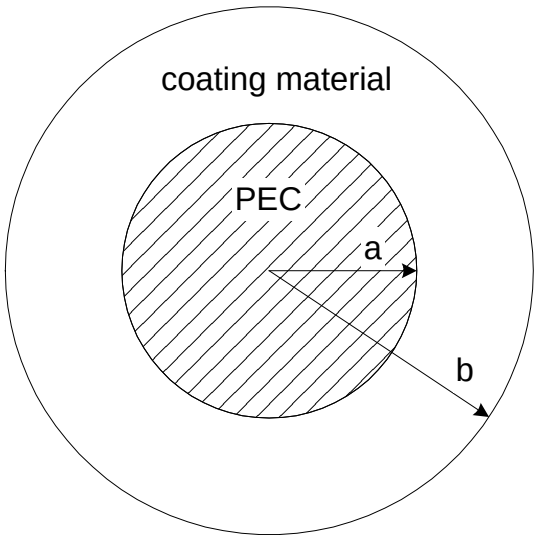

Figure 8.1: Cross section of a PEC cylinder with a coating material.

studied both transverse electric (TE) and transverse magnetic (TM) waves in the case of thick dielectric coating where $k_0 d \approx \pi$. The critical radius effect was found, where the leaky wave modes are transformed into trapped wave modes when the radius of PEC cylinder exceeds a definite critical value. A new system of poles for the Green's functions for a dielectric coated cylinder was found in [40]. These poles usually correspond

to highly attenuated creeping waves except when the coating layer is very thick. The features of creeping waves propagating in the lossy dielectric-coated cylinder were studied in [42] and critical loss effect was found, where the leaky higher-order modes switch to trapped modes when the dielectric coating losses approach definite critical values. The followed work [43] studied the dispersion behaviour of waves guided along substrate-superstrate coated cylinder, emphasizing various effects of superstrate. Most recently, some researchers studied electromagnetic scattering by a PEC cylinder coated with a thin lossy magnetic layer [105].

In this chapter, we will study the same structure with a coating material as in [105], but focus our attention on the behavior of creeping waves guided along the lossy magnetic-coated cylinder. The material is assumed to be dispersive or frequency-dependent in property. The complex propagation constants which correspond to the poles on the complex plane are obtained by solving the dispersion equation. The random search is used to obtain the coarse values of the poles for the case of $d = 0$, which are the initial values for further iterations in the secant method for the refined and accurate values for the cases of increased coating thickness. The hypothetical dielectric permittivity and magnetic permeability can be considered as a representative of a class of widely available microwave materials [105]. In this sense, the analysis conducted herein is generalized and very useful.

8.2 Theory and Formulation

In order to find poles of the Green's function components for a dielectric coated cylinder, we must solve the transcendental characteristic equation, which can be written as follows [41]:

$$F(\nu) = H_{\nu}^{'(1)}(k_0 b) + jCH_{\nu}^{(1)}(k_0 b) = 0, \tag{8.1}$$

where the coefficient C is defined as follows:

for transverse electric (TE) polarization,

$$C_\nu^h = j\frac{k_1\epsilon_0}{k_0\epsilon_1}\frac{H_\nu^{'(1)}(k_1b)H_\nu^{'(2)}(k_1a)-H_\nu^{'(1)}(k_1a)H_\nu^{'(2)}(k_1b)}{H_\nu^{(1)}(k_1b)H_\nu^{'(2)}(k_1a)-H_\nu^{'(1)}(k_1a)H_\nu^{(2)}(k_1b)}; \tag{8.2a}$$

and for transverse magnetic (TM) polarization,

$$C_\nu^s = j\frac{k_1\mu_0}{k_0\mu_1}\frac{H_\nu^{'(1)}(k_1b)H_\nu^{(2)}(k_1a)-H_\nu^{(1)}(k_1a)H_\nu^{'(2)}(k_1b)}{H_\nu^{(1)}(k_1b)H_\nu^{(2)}(k_1a)-H_\nu^{(1)}(k_1a)H_\nu^{(2)}(k_1b)}; \tag{8.2b}$$

in which $H_\nu^{(1,2)}(\bullet)$ denotes the first or second kind of Hankel function, whereas $H_\nu^{'(1,2)}(\bullet)$ stands for its derivative with respect to the argument; k, ϵ and μ with subscript 0 or 1 refer to wave number, permittivity, permeability in free space or dielectric medium, respectively; a identifies the radius of PEC cylinder while b represents the outer radius of the dielectric-coated cylinder, and d denotes the thickness of the dielectric coating, i.e., $d = b - a$.

The solution of (8.1) is used to define the azimuthal surface waves with modal complex propagation constants $\nu_p = \nu_p' + j\nu_p''$. Usually, the azimuthal waves can be classified as leaky waves, creeping waves or trapped waves depending on whether $\nu_p' < k_0b$, $\nu_p' \approx k_0b$, or $\nu_p' > k_0b$, respectively. This classification is made, based on the phase matching condition for the tangential field on the outer boundary at $r = b$ [41].

In order to solve Eq. (8.1), we must correctly evaluate the Hankel function $H_\nu^{(1,2)}(z)$ of complex order and argument. The proper computation seems easy but is actually not, because whether exact or asymptotic representations must be implemented for different cases in which the order and argument may be nearly equal or far apart (Appendix D). The Olver asymptotic expansions are tested and then implemented [92]. This form of expansion is preferable to Debye approximation and Watson approximation, because the Olver asymptotic expansions are uniformly valid, regardless of whether the argument and order are very close or far apart. The leading term for Olver asymptotic expansions is given by [41].

The roots of Eq. (8.1) are found using random search combined with the secant method. The root points for $d = 0$ lie on the Stokes' line of $H_\nu^{(1)}(k_0 b)$ and $H_\nu^{'(1)}(k_0 b)$, and we can find these roots using random search. Since the root loci for increased d will emanate from the points located on the Stokes' line [106], we can find this root loci using the secant method by setting the root value for $d = 0$ as an initial guess for iteration.

8.3 Numerical Results

To verify the program codes and to show how the magnetic losses affect the previous results, it is worth reproducing independently the results in [42] and [106]. Numerical results for the first three creeping modes are shown in Figs. 8.2-8.4, respectively, but for different outer radii of the cylinder, i.e., $k_0 b = 10$, 20 and 40. The coating thickness starts from $d = 0$ (which actually corresponds to a PEC cylinder) to $d = 0.5\lambda$. Figs. 8.5-8.8 are the results for the case of dielectric lossy coating [42].

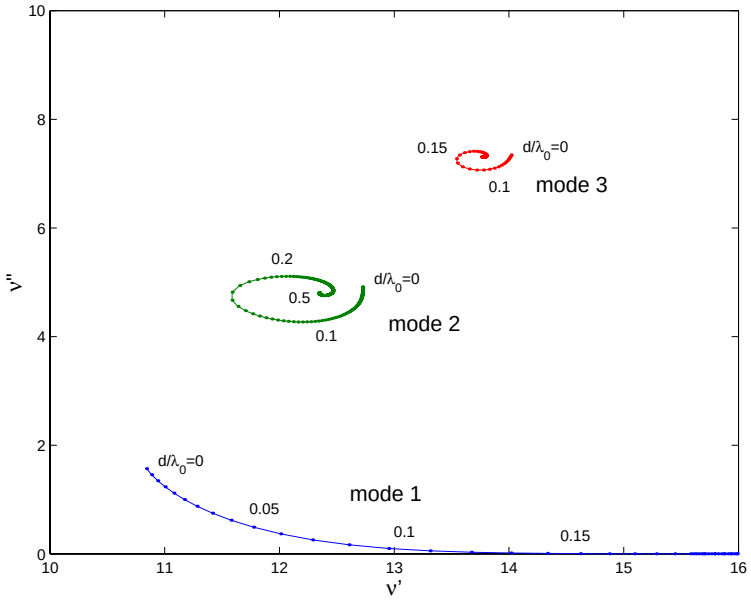

Figure 8.2: Propagation constants of the first three creeping wave modes in the case of lossless coating: $\epsilon_r = 4$, $\mu_r = 1$, and $k_0 b = 10$.

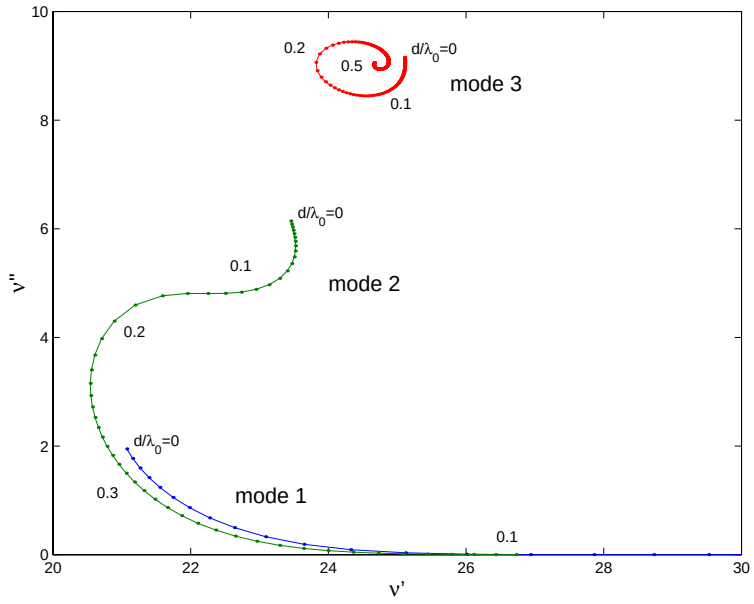

Figure 8.3: Propagation constants of the first three creeping wave modes in the case of lossless coating: $\epsilon_r = 4$, $\mu_r = 1$, and $k_0 b = 20$.

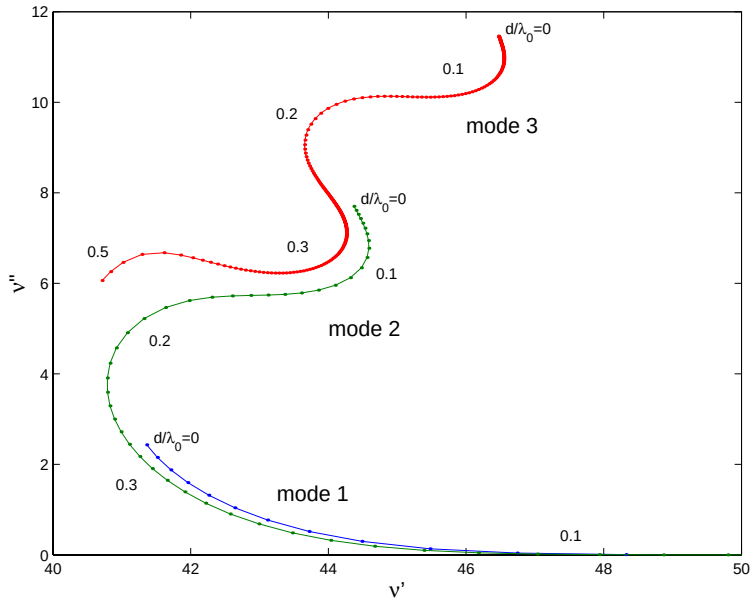

Figure 8.4: Propagation constants of the first three creeping wave modes for in case of lossless coating: $\epsilon_r = 4$, $\mu_r = 1$, and $k_0 b = 40$.

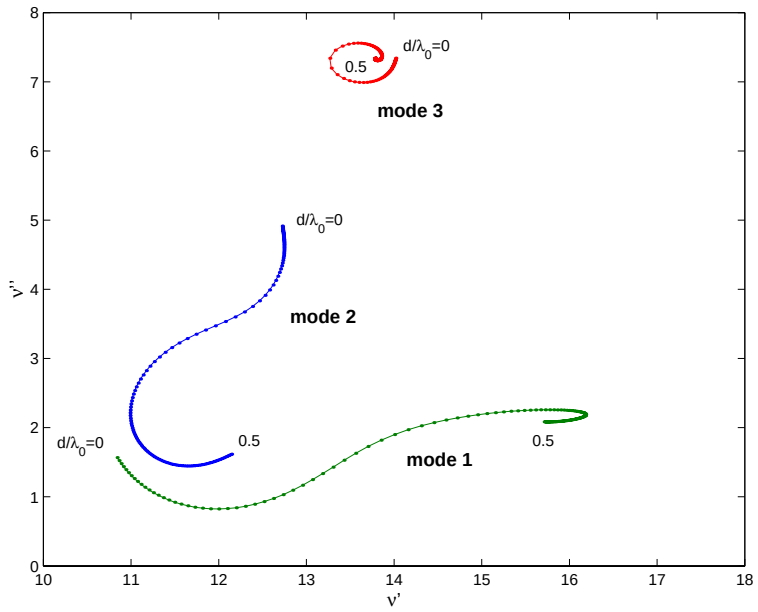

Figure 8.5: Propagation constants of the first three creeping wave modes in the case of dielectric lossy coating: $\epsilon_r = 4 + i$, $\mu_r = 1$, and $k_0 b = 10$.

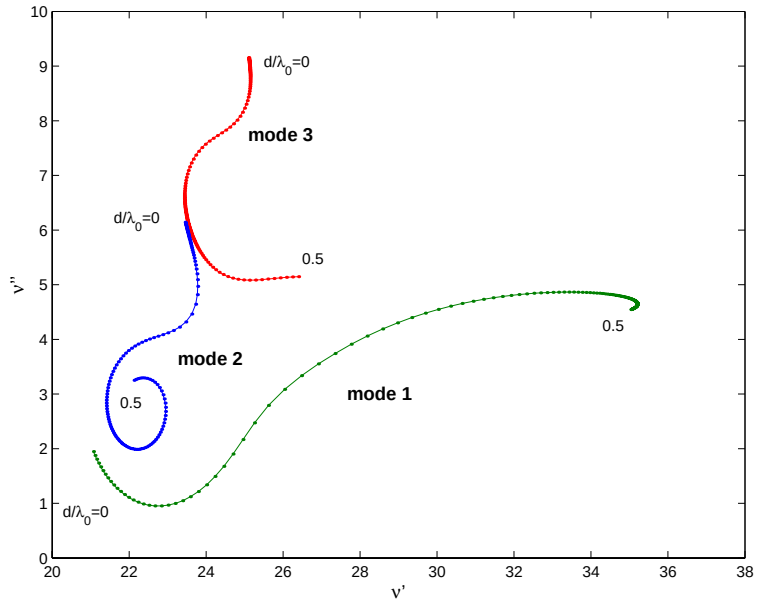

Figure 8.6: Propagation constants of the first three creeping wave modes in the case of dielectric lossy coating: $\epsilon_r = 4 + i$, $\mu_r = 1$, and $k_0 b = 20$.

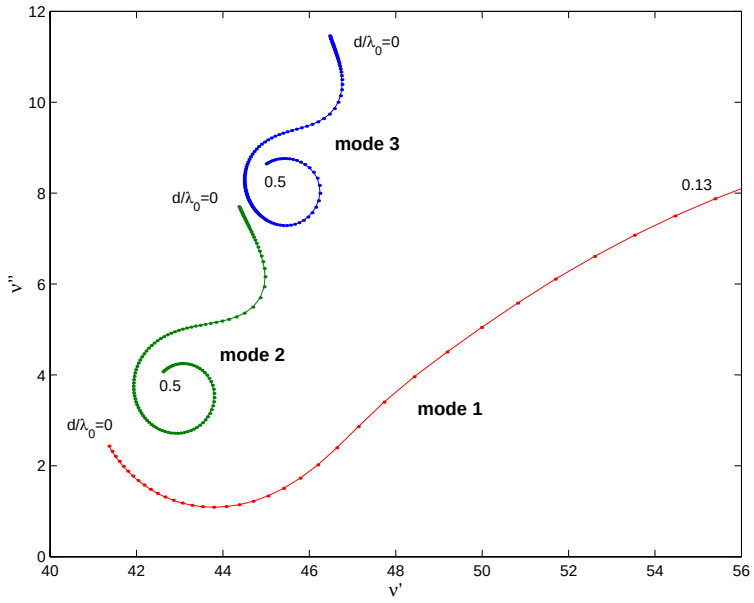

Figure 8.7: Propagation constants of the first three creeping wave modes for in case of dielectric lossy coating: $\epsilon_r = 4 + i$, $\mu_r = 1$, and $k_0 b = 40$.

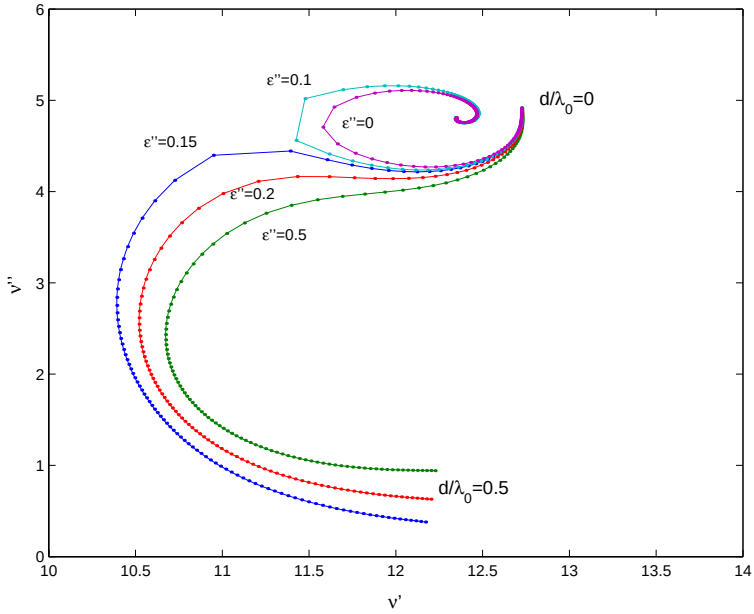

Figure 8.8: Critical dielectric losses effect for the second mode: $\epsilon' = 4$, $\mu_r = 1$, and $k_0 b = 40$.

The first three modes shown in Figs. 8.9-8.11 are for the case where a magnetic loss is included for the coating material, i.e., $\mu_r = 1 + 0.25j$; and the first three modes shown in Figs. 8.12-8.14 are for the case where both magnetic loss and dieletric loss are included for the coating material, i.e., $\mu_r = 1 + 0.25j$ and $\epsilon_r = 4 + 1j$. Several effects can be seen from Figs. 8.9-8.18 and summarized subsequently.

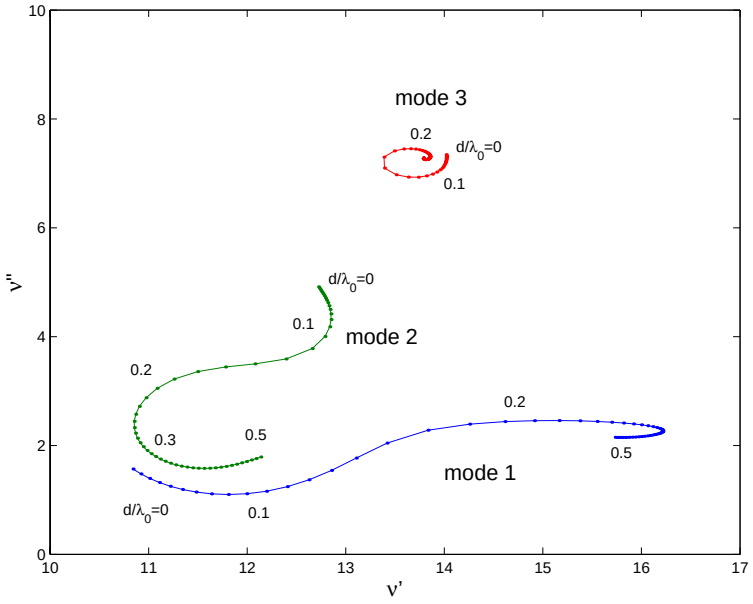

Figure 8.9: Propagation constants of the first three creeping wave modes in the case of magnetic lossy coating: $\epsilon_r = 4$, $\mu_r = 1 + 0.25j$, and $k_0 b = 10$.

From Figs. 8.9-8.11, an inverse critical radius effect similar to that in [42] is also observed. This means that when the other parameters are maintained, the radius of the cylinder plays an important role in determining which modes will appear in the structure. For a cylinder of radius larger than the critical radius, the trapped mode transforms to leaky mode due to the magnetic loss of a large radius cylinder. For example, for the large-radius cylinder $k_0 b = 40$, the higher-order modes, i.e., leaky modes with high attenuation, are present; for $k_0 b = 20$, some of the higher-order modes (mode 2 and mode 3) exist in the form of trapped modes; and for $k_0 b = 10$ the higher-order mode (i.e., mode 2)

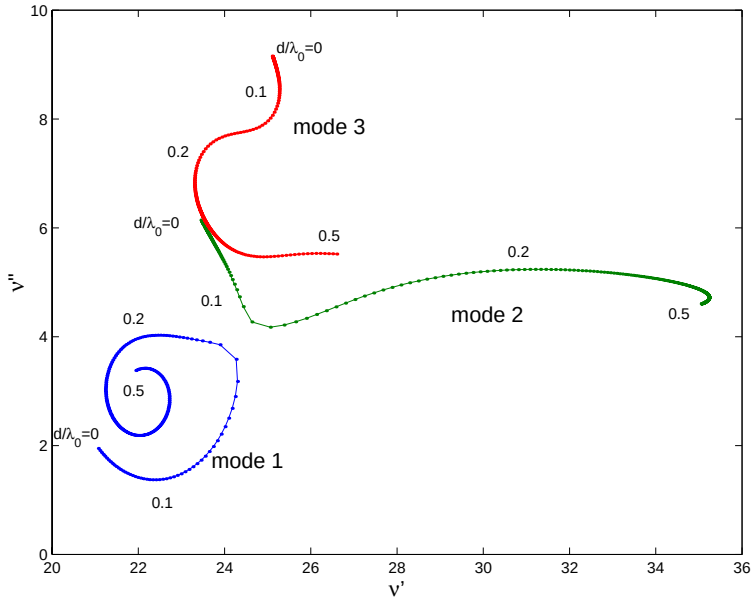

Figure 8.10: Propagation constants of the first three creeping wave modes in the case of magnetic lossy coating: $\epsilon_r = 4$, $\mu_r = 1 + 0.25j$, and $k_0 b = 20$.

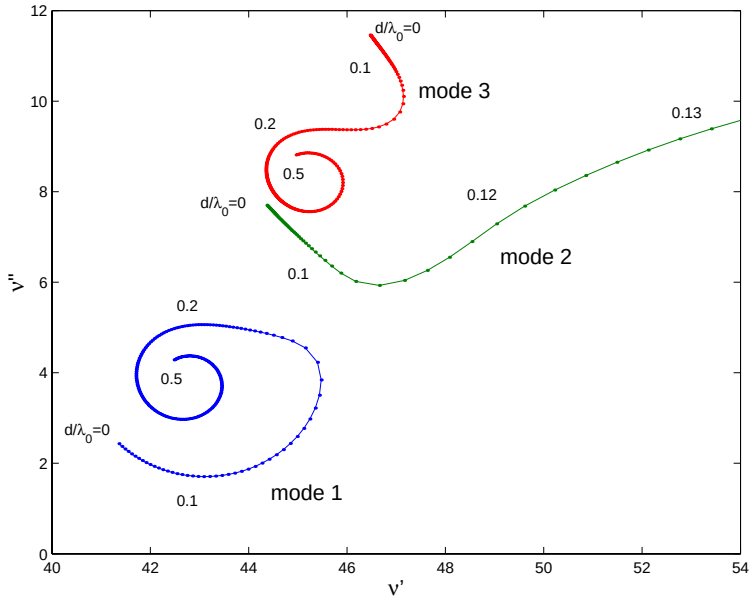

Figure 8.11: Propagation constants of the first three creeping wave modes in the case of magnetic lossy coating: $\epsilon_r = 4$, $\mu_r = 1 + 0.25j$, and $k_0 b = 40$.

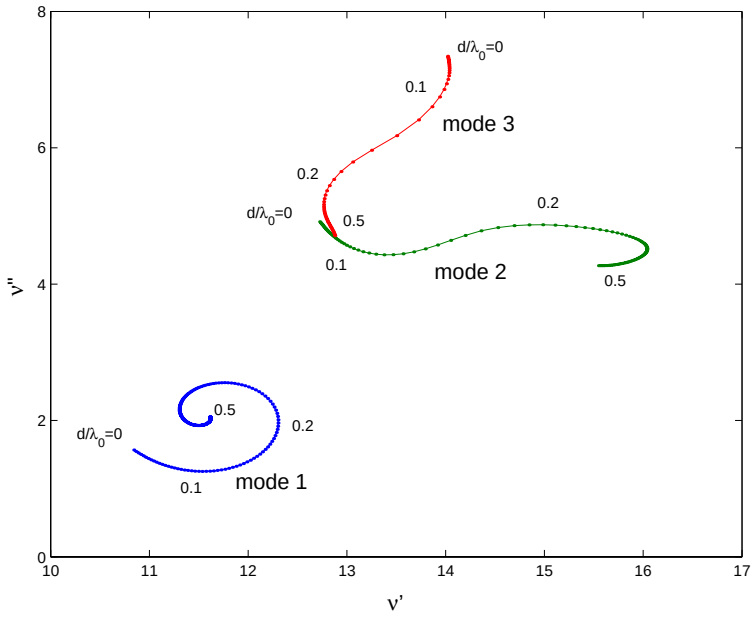

Figure 8.12: Propagation constants of the first three creeping wave modes in the case of dielectric and magnetic lossy coating: $\epsilon_r = 4 + 1.0j$, $\mu_r = 1 + 0.25j$, and $k_0 b = 10$.

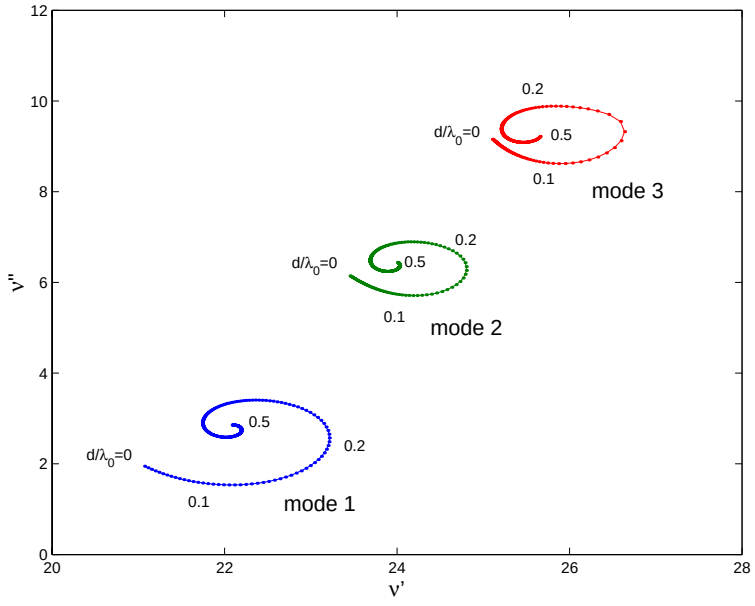

Figure 8.13: Propagation constants of the first three creeping wave modes in the case of dielectric and magnetic lossy coating: $\epsilon_r = 4 + 1.0j$, $\mu_r = 1 + 0.25j$, and $k_0 b = 20$.

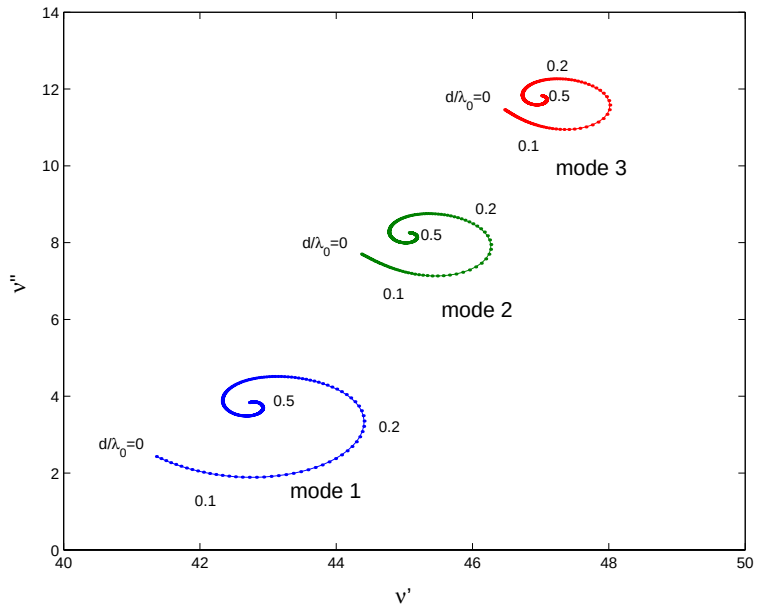

Figure 8.14: Propagation constants of the first three creeping wave modes in the case of dielectric and magnetic lossy coating: $\epsilon_r = 4 + 1j$, $\mu_r = 1 + 0.25j$, and $k_0 b = 40$.

apparently demonstrates the characteristics of trapped modes.

Also, the inverse critical radius effect can be significantly enhanced when both electric and magnetic losses are included. Figs. 8.12-8.14 depict the results for $\mu_r = 1 + 0.25j$ and $\epsilon_r = 4 + 1j$. Comparing these in Figs. 8.12-8.14 with those in Figs. 8.9-8.11 and Figs. 8.2-8.4, we can see that with imaginary part included into both μ_r and ϵ_r, the inverse critical radius effect becomes more apparent and stronger. The trapped modes only exist in the case of a small cylinder (e.g., $k_0 b = 10$), while all of them are highly attenuated for relatively large cylinder.

In addition, the magnetic loss effect is observed. To show this effect, the second mode for $k_0 b = 10$ is shown in Figs. 8.15-8.16, but for various μ'' values. With μ'' increased from 0 to 0.1, the leaky mode transforms to trapped mode, where the critical value for the turning is around $\mu'' = 0.04$. The same effects for the other leaky modes are observed for different radii of coated cylinder. The argument of the impedance function C_ν^h shown in Fig. 11 also depicts this transition where inductive impedance occurs. It is noted that

the critical loss effect here is similar to that found by [42], where the leaky modes will transform to trapped modes when increasing the dielectric loss from zero to a certain critical value.

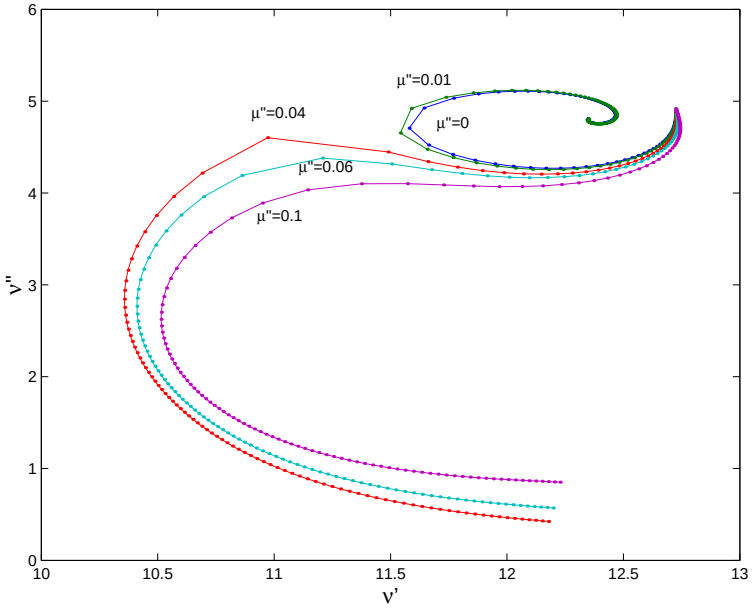

Figure 8.15: Critical magnetic loss effect for the second mode, $\epsilon_r = 4$, $\mu_r' = 1$, and $k_0 b = 10$.

When the cylindrical radius is increased, however, the magnetic loss effect that we observed previously can be entirely opposite. For instance, the second mode (trapped mode) will transform to leaky modes when we increase the magnetic loss from zero to a certain critical value (as shown in Figs. 8.17-8.18) for $k_0 b = 20$. This transition point is also be depicted in Fig. 8.18.

8.4 Summary

Creeping waves guided along a perfectly conducting cylinder with a lossy magnetic coating are studied and characterized in this chapter. The complex propagation constants

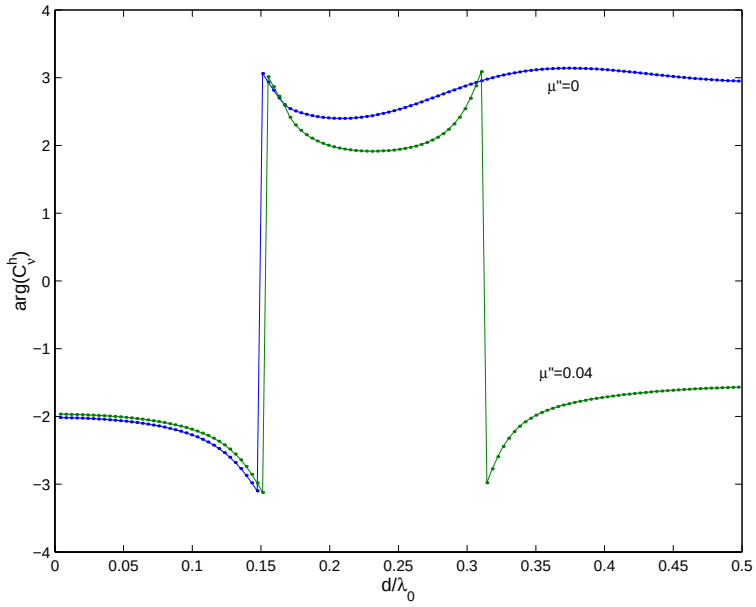

Figure 8.16: Argument of the impedance function for the second mode, $\epsilon_r = 4$, $\mu_r' = 1$, and $k_0 b = 10$.

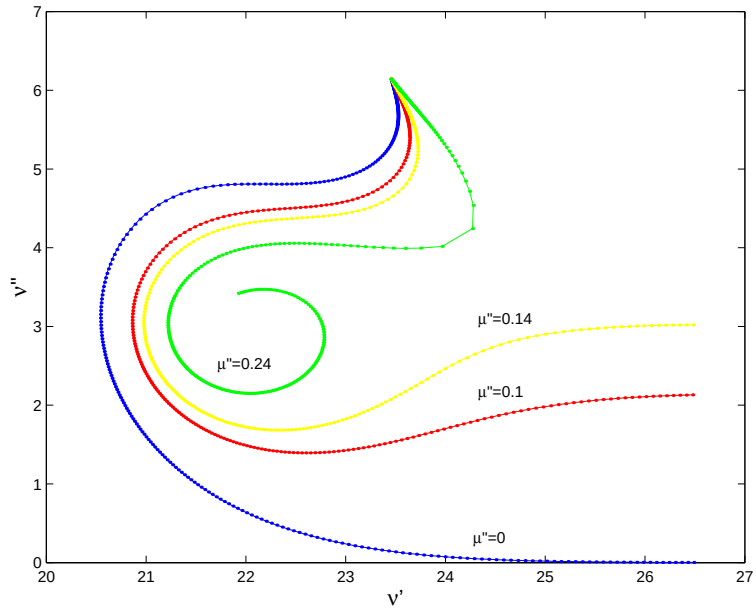

Figure 8.17: Critical magnetic loss effect for the second mode, $\epsilon_r = 4$, $\mu_r' = 1$, and $k_0 b = 20$.

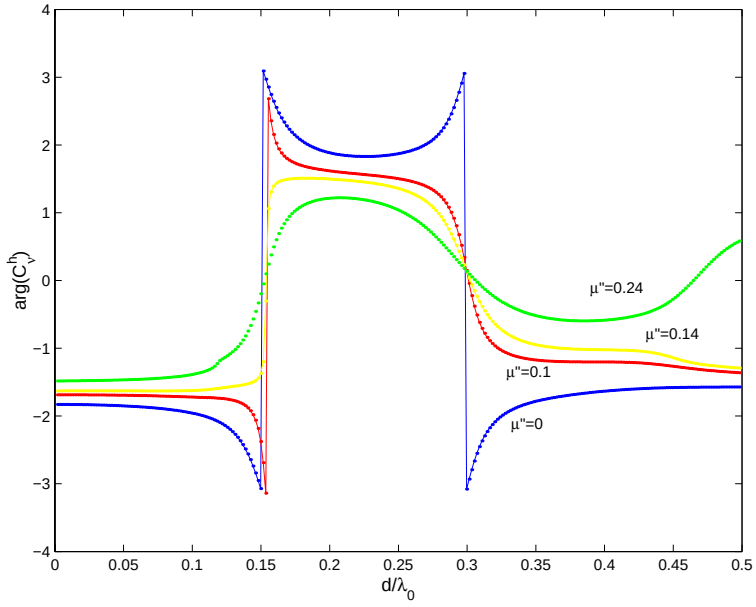

Figure 8.18: Argument of the impedance function for the second mode, $\epsilon_r = 4$, $\mu_r' = 1$, and $k_0 b = 20$.

are obtained by solving the dispersion equation. The first three modes are calculated in the case of different coating thicknesses ranging form 0 to $d/\lambda_0 = 0.5$. Highly attenuated leaky wave modes are observed from both the lower- and higher-order modes due to the included magnetic loss. A similar inverse critical radius effect to that in [42] is noted and two different kinds of critical magnetic loss effects are observed for all the three modes at different radii of the coated cylinder. The present analysis provides an greater insight into the physical features and charateristics of the guided creeping waves.

Chapter 9

Conclusions and Suggestions for Future Work

9.1 Conclusions

This thesis presents spatial domain Green's functions (electric field Green's functions for EFIE and mixed potential Green's funcitons for MPIE) in fast computational forms and the applications of MPIE for cylindrically stratified media. A number of methods were employed to achieve the goals.

9.1.1 On the Work

Firstly, electric field Green's functions for cylindrically stratified media were studied. After the spectral domain Green's functions were obtained, closed-form or fast computational form electric field Green's functions in the spatial domain were given through the inverse Fourier transform. This was for the case where the source point and the field point were not on the same cylindrical surface.

Secondly, mixed potential Green's functions were given both in the spectral domain

and spatial domain. This was for the case where the source point and the field point were on the same cylindrical surface. The inverse Fourier transform of the spectral domain Green's functions was much more difficult if the the source point and the field point were on the same cylindrical surface, since the convergence property of the series of the cylindrical eigenmodes broke down. Several techniques, such as series acceleration technique and DCIM were used to obtain the spatial domain Green's functions.

Finally, as examples of the applications of mixed potential Green's functions, a rectangular patch antenna and a helical microstrip antenna were studied. Current distributions were obtained rigorously by solving the MPIE in spatial domain. Resonant frequency for the rectangular patch antenna and far field radiation patterns for the helical microstrip antenna were calculated from the current distributions. The creeping wave propagating along the multilayered cylinder was studied in final part of this thesis. FORTRAN, MATHEMATICA, MATALAB and other math tools were utilized to carry out the numerical computations and investigations.

9.1.2 On the Methods

The electromagnetic waves are normally coupled TE and TM waves while propagating through cylindrically multilayered media, which causes difficulties in expressing the fields in terms of solutions of transmission line model. Two methods, i.e., 2×2 and 4×4 matrix methods, were employed to derive the spectral domain Green's functions. Both methods are based on the solution of vector wave equations, hence they are essentially equivalent. The 2×2 matrix method gives a compact form of Green's functions, while the 4×4 matrix method gives relatively tedious expressions. However, from the discussion in Chapter 5, the reformulation of the Green's functions in 2×2 matrix form is rather complicated than that of the Green's functions in 4×4 matrix form. From this point of view, the Green's functions in 4×4 matrix form is more suitable for the inverse Fourier transform,

since large order cylindrical eigenmodes are easier to calculated. Although the DCIM is employed to perform the inverse Fourier transform, it is not straightforward as that in the planarly multilayered media case. Series acceleration technique should be used to sum the cylindrical eigenmodes firstly. After that, two-step DCIM could be employed to evaluate the Sommerfeld integration.

The purpose of obtaining the fast computational form of mixed potential Green's functions is to construct MPIE for the cylindrically conformal structures. Analysis and design of conformal structures, such as conformal microstrip antennas and arrays, play an important role in many practical applications. Multilayered cylindrical structures are good physical models for rigorously numerical modeling of such structures using the MoM. The MoM procedure can be applied either in the spatial domain or in the spectral domain. In contrast with spectral domain MoM, the spatial domain MoM, which is specifically MPIE here, can be considered to be a more general and promising way for solving large and complex problem, as it can be easily applied to objects of arbitrary shape and particularly when the Fourier transform cannot be directly applied to formulate and simplify the Green's functions of the problem. The spatial domain MoM has also more potential to enhance its capability to solve real and large problem by combining it with fast algorithms.

9.1.3 On the Results

In this thesis, spectral domain electric field Green's functions were derived systematically. Several misleading contents in the literature [62] are identified and the correct expressions were given. The correctness was proved by comparing the numerical results between two forms of Green's functions. Spatial domain Green's functions both in electric form and mixed potential form are then obtained in fast computational form. Numerical results show that the two-step DCIM technique can be applied to the inverse Fourier transform

of the spectral domain Green's functions for the cylindrically layered media as that for the planarly layered media, as long as the convergence problem of the cylindrical eigenmodes is solved. The spatial domain mixed potential Green's functions are finally utilized to analyze a rectangular microstrip patch antenna for the resonant behaviour. Numerical results show that the addition of a superstrate will shift the resonant frequency to the lower end. A helical microstrip antenna is also analyzed using the MPIE. Rigorous current distributions are obtained and far field radiation patterns are calculated from these current distributions. Numerical results show that the far field radiation patterns are significantly affected by geometry configuration of the helical antenna.

9.2 Suggestions for Future Work

The work reported in this thesis was done during my PhD study period. The mixed potential Green's functions both in the spectral domain and spatial domain for cylindrically stratified media were successfully derived. Correspondingly, the MPIE for cylindrically conformal structures was also successfully developed. Based on the knowledge acquired, the work can be further extended to large body size problem [107]. One of the difficulties in doing this may be the accurate evaluation of the Green's functions in the far field region, since the surface wave will be dominant in the far field. More delicate methods rather than the two-step DCIM for the treatment of the poles which corresponds to the surface wave are needed. The MPIE presented in this thesis can also be extended to the PEC 3-D object (the PEC patch studied in Chpater 6 is a 2-D object in the cylindrical coordinate) problem where the object penetrates one layer [108], as long as the complete components of the mixed potential Green's functions are available or can be obtained.

Appendix A

Expressions of Green's Functions

The explicit expressions of $\widetilde{E}_{zz}$, $\widetilde{E}_{z\phi}$, $\widetilde{E}_{\phi z}$, $\widetilde{E}_{\phi\phi}$, Δ_z, Δ_ϕ are

$$
\begin{aligned}
\widetilde{E}_{zz} \;=\; & -jn^2 H_n^2 k_1^2 k_z^2 k_{1\rho}^3 k_{2\rho}^8 P_n U_n^2 S_n \epsilon_2 \mu_2 \rho_2^2 \\
& +2jn^2 H_n^2 k_1^2 k_z^2 k_{1\rho}^3 k_{2\rho}^6 k_{3\rho}^2 P_n U_n^2 S_n \epsilon_2 \mu_2 \rho_2^2 \\
& -jn^2 H_n^2 k_1^2 k_z^2 k_{1\rho}^3 k_{2\rho}^4 k_{3\rho}^4 P_n U_n^2 S_n \epsilon_2 \mu_2 \rho_2^2 \\
& +jn^2 \omega^2 H_n^2 k_z^2 k_{1\rho}^4 k_{2\rho}^7 P_n U_n V_n R_n \epsilon_1 \epsilon_2 \mu_2^2 \rho_2^2 \\
& -2jn^2 \omega^2 H_n^2 k_z^2 k_{1\rho}^4 k_{2\rho}^5 k_{3\rho}^2 P_n U_n V_n R_n \epsilon_1 \epsilon_2 \mu_2^2 \rho_2^2 \\
& +jn^2 \omega^2 H_n^2 k_z^2 k_{1\rho}^4 k_{2\rho}^3 k_{3\rho}^4 P_n U_n V_n R_n \epsilon_1 \epsilon_2 \mu_2^2 \rho_2^2 \\
& -j\omega^2 H_n^2 k_2^2 k_{1\rho}^4 k_{2\rho}^5 k_{3\rho}^4 P_n R_n W_n X_n \epsilon_1 \epsilon_2 \mu_2^2 \rho_2^2 \rho_3^2 \\
& +j\omega^2 H_n^2 k_1^2 k_{1\rho}^3 k_{2\rho}^6 k_{3\rho}^4 P_n W_n^2 S_n \epsilon_2^2 \mu_2^2 \rho_2^2 \rho_3^2 \\
& +j\omega^2 H_n H_n^{'} k_2^2 k_{1\rho}^4 k_{2\rho}^6 k_{3\rho}^3 P_n U_n R_n X_n \epsilon_1 \epsilon_3 \mu_2^2 \rho_2^2 \rho_3^2 \\
& -j\omega^2 H_n H_n^{'} k_1^2 k_{1\rho}^3 k_{2\rho}^7 k_{3\rho}^3 P_n U_n W_n S_n \epsilon_2 \epsilon_3 \mu_2^2 \rho_2^2 \rho_3^2 \\
& -j\omega^2 H_n H_n^{'} k_1^2 k_{1\rho}^3 k_{2\rho}^7 k_{3\rho}^3 P_n U_n W_n S_n \epsilon_2^2 \mu_2 \mu_3 \rho_2^2 \rho_3^2 \\
& +j\omega^2 H_n^{'2} k_1^2 k_{1\rho}^3 k_{2\rho}^8 k_{3\rho}^2 P_n U_n^2 S_n \epsilon_2 \epsilon_3 \mu_2 \mu_3 \rho_2^2 \rho_3^2 \\
& +j\omega^4 H_n H_n^{'} k_{1\rho}^4 k_{2\rho}^6 k_{3\rho}^3 P_n V_n R_n W_n \epsilon_1 \epsilon_2^2 \mu_2^2 \mu_3 \rho_2^2 \rho_3^2 \\
& -j\omega^4 H_n^{'2} k_{1\rho}^4 k_{2\rho}^7 k_{3\rho}^2 P_n U_n V_n R_n \epsilon_1 \epsilon_2 \epsilon_3 \mu_2^2 \mu_3 \rho_2^2 \rho_3^2, \qquad \text{(A-1)}
\end{aligned}
$$

$$
\begin{aligned}
\widetilde{E}_{z\phi} &= -jn^3H_n^2k_1^2k_z^3k_{1\rho}^3k_{2\rho}^6P_nU_n^2S_n\epsilon_2\mu_2\rho_2 \\
&\quad +2jn^3H_n^2k_1^2k_z^3k_{1\rho}^3k_{2\rho}^4k_{3\rho}^2P_nU_n^2S_n\epsilon_2\mu_2\rho_2 \\
&\quad -jn^3H_n^2k_1^2k_z^3k_{1\rho}^3k_{2\rho}^2k_{3\rho}^4P_nU_n^2S_n\epsilon_2\mu_2\rho_2 \\
&\quad +jn^3\omega^2H_n^2k_z^3k_{1\rho}^2k_{2\rho}^7P_nU_nV_nR_n\epsilon_1\epsilon_2\mu_2^2\rho_2 \\
&\quad -2jn^3\omega^2H_n^2k_z^3k_{1\rho}^2k_{2\rho}^5k_{3\rho}^2P_nU_nV_nR_n\epsilon_1\epsilon_2\mu_2^2\rho_2 \\
&\quad +jn^3\omega^2H_n^2k_z^3k_{1\rho}^2k_{2\rho}^3k_{3\rho}^4P_nU_nV_nR_n\epsilon_1\epsilon_2\mu_2^2\rho_2 \\
&\quad +jnH_n^2k_1^2k_2^2k_zk_{1\rho}^3k_{2\rho}^6k_{3\rho}^2P_nU_nS_nX_n\epsilon_2\mu_2\rho_2^2\rho_3 \\
&\quad -jnH_n^2k_1^2k_2^2k_zk_{1\rho}^3k_{2\rho}^4k_{3\rho}^4P_nU_nS_nX_n\epsilon_2\mu_2\rho_2^2\rho_3 \\
&\quad -jn\omega^2H_n^2k_1^2k_zk_{1\rho}^3k_{2\rho}^6k_{3\rho}^2P_nV_nW_nS_n\epsilon_2^2\mu_2^2\rho_2^2\rho_3 \\
&\quad +jn\omega^2H_n^2k_1^2k_zk_{1\rho}^3k_{2\rho}^4k_{3\rho}^4P_nV_nW_nS_n\epsilon_2^2\mu_2^2\rho_2^2\rho_3 \\
&\quad -jn\omega^2H_n^2k_2^2k_zk_{1\rho}^2k_{2\rho}^5k_{3\rho}^4P_nR_nW_nX_n\epsilon_1\epsilon_2\mu_2^2\rho_2\rho_3^2 \\
&\quad +jn\omega^2H_n^2k_1^2k_zk_{1\rho}^3k_{2\rho}^4k_{3\rho}^4P_nW_n^2S_n\epsilon_2^2\mu_2^2\rho_2\rho_3^2 \\
&\quad +jn\omega^2H_nH_n^{'}k_2^2k_zk_{1\rho}^2k_{2\rho}^6k_{3\rho}^3P_nU_nR_nX_n\epsilon_1\epsilon_3\mu_2^2\rho_2\rho_3^2 \\
&\quad -jn\omega^2H_nH_n^{'}k_1^2k_zk_{1\rho}^3k_{2\rho}^5k_{3\rho}^3P_nU_nW_nS_n\epsilon_2\epsilon_3\mu_2^2\rho_2\rho_3^2 \\
&\quad -jn\omega^2H_nH_n^{'}k_1^2k_zk_{1\rho}^3k_{2\rho}^5k_{3\rho}^3P_nU_nW_nS_n\epsilon_2^2\mu_2\mu_3\rho_2\rho_3^2 \\
&\quad +jn\omega^2H_n^{'2}k_1^2k_zk_{1\rho}^3k_{2\rho}^6k_{3\rho}^2P_nU_n^2S_n\epsilon_2\epsilon_3\mu_2\mu_3\rho_2\rho_3^2 \\
&\quad +jn\omega^4H_nH_n^{'}k_zk_{1\rho}^2k_{2\rho}^6k_{3\rho}^3P_nV_nR_nW_n\epsilon_1\epsilon_2^2\mu_2^2\mu_3\rho_2\rho_3^2 \\
&\quad -jn\omega^4H_n^{'2}k_zk_{1\rho}^2k_{2\rho}^7k_{3\rho}^2P_nU_nV_nR_n\epsilon_1\epsilon_2\epsilon_3\mu_2^2\mu_3\rho_2\rho_3^2, \qquad \text{(A-2)} \\
\Delta_z &= n^4\omega H_n^2k_z^4k_{1\rho}^4k_{2\rho}^4P_nU_n^2R_n\epsilon_1\epsilon_2\mu_2 \\
&\quad -2n^4\omega H_n^2k_z^4k_{1\rho}^2k_{2\rho}^6P_nU_n^2R_n\epsilon_1\epsilon_2\mu_2 \\
&\quad +n^4\omega H_n^2k_z^4k_{2\rho}^8P_nU_n^2R_n\epsilon_1\epsilon_2\mu_2 \\
&\quad -2n^4\omega H_n^2k_z^4k_{1\rho}^4k_{2\rho}^2k_{3\rho}^2P_nU_n^2R_n\epsilon_1\epsilon_2\mu_2 \\
&\quad +4n^4\omega H_n^2k_z^4k_{1\rho}^2k_{2\rho}^4k_{3\rho}^2P_nU_n^2R_n\epsilon_1\epsilon_2\mu_2 \\
&\quad -2n^4\omega H_n^2k_z^4k_{2\rho}^6k_{3\rho}^2P_nU_n^2R_n\epsilon_1\epsilon_2\mu_2
\end{aligned}
$$

$$+n^4\omega H_n^2 k_z^4 k_{1\rho}^4 k_{3\rho}^4 P_n U_n^2 R_n \epsilon_1 \epsilon_2 \mu_2$$

$$-2n^4\omega H_n^2 k_z^4 k_{1\rho}^2 k_{2\rho}^2 k_{3\rho}^4 P_n U_n^2 R_n \epsilon_1 \epsilon_2 \mu_2$$

$$+n^4\omega H_n^2 k_z^4 k_{2\rho}^4 k_{3\rho}^4 P_n U_n^2 R_n \epsilon_1 \epsilon_2 \mu_2$$

$$-n^2\omega H_n^2 k_1^2 k_z^2 k_{1\rho}^2 k_{2\rho}^8 U_n^2 Q_n S_n \epsilon_1 \epsilon_2 \mu_2 \rho_2^2$$

$$+2n^2\omega H_n^2 k_1^2 k_z^2 k_{1\rho}^2 k_{2\rho}^6 k_{3\rho}^2 U_n^2 Q_n S_n \epsilon_1 \epsilon_2 \mu_2 \rho_2^2$$

$$-n^2\omega H_n^2 k_1^2 k_z^2 k_{1\rho}^2 k_{2\rho}^4 k_{3\rho}^4 U_n^2 Q_n S_n \epsilon_1 \epsilon_2 \mu_2 \rho_2^2$$

$$+n^2\omega H_n^2 k_1^2 k_z^2 k_{1\rho}^3 k_{2\rho}^7 P_n U_n V_n S_n \epsilon_2^2 \mu_2 \rho_2^2$$

$$-2n^2\omega H_n^2 k_1^2 k_z^2 k_{1\rho}^3 k_{2\rho}^5 k_{3\rho}^2 P_n U_n V_n S_n \epsilon_2^2 \mu_2 \rho_2^2$$

$$+n^2\omega H_n^2 k_1^2 k_z^2 k_{1\rho}^3 k_{2\rho}^3 k_{3\rho}^4 P_n U_n V_n S_n \epsilon_2^2 \mu_2 \rho_2^2$$

$$+n^2\omega^3 H_n^2 k_z^2 k_{1\rho}^3 k_{2\rho}^7 U_n Q_n V_n R_n \epsilon_1^2 \epsilon_2 \mu_2^2 \rho_2^2$$

$$-2n^2\omega^3 H_n^2 k_z^2 k_{1\rho}^3 k_{2\rho}^5 k_{3\rho}^2 U_n Q_n V_n R_n \epsilon_1^2 \epsilon_2 \mu_2^2 \rho_2^2$$

$$+n^2\omega^3 H_n^2 k_z^2 k_{1\rho}^3 k_{2\rho}^3 k_{3\rho}^4 U_n Q_n V_n R_n \epsilon_1^2 \epsilon_2 \mu_2^2 \rho_2^2$$

$$-n^2\omega^3 H_n^2 k_z^2 k_{1\rho}^4 k_{2\rho}^6 P_n V_n^2 R_n \epsilon_1 \epsilon_2^2 \mu_2^2 \rho_2^2$$

$$+2n^2\omega^3 H_n^2 k_z^2 k_{1\rho}^4 k_{2\rho}^4 k_{3\rho}^2 P_n V_n^2 R_n \epsilon_1 \epsilon_2^2 \mu_2^2 \rho_2^2$$

$$-n^2\omega^3 H_n^2 k_z^2 k_{1\rho}^4 k_{2\rho}^2 k_{3\rho}^4 P_n V_n^2 R_n \epsilon_1 \epsilon_2^2 \mu_2^2 \rho_2^2$$

$$-2n^2\omega H_n^2 k_2^2 k_z^2 k_{1\rho}^4 k_{2\rho}^4 k_{3\rho}^2 P_n U_n R_n X_n \epsilon_1 \epsilon_2 \mu_2 \rho_2 \rho_3$$

$$+2n^2\omega H_n^2 k_2^2 k_z^2 k_{1\rho}^2 k_{2\rho}^6 k_{3\rho}^2 P_n U_n R_n X_n \epsilon_1 \epsilon_2 \mu_2 \rho_2 \rho_3$$

$$+2n^2\omega H_n^2 k_2^2 k_z^2 k_{1\rho}^4 k_{2\rho}^2 k_{3\rho}^4 P_n U_n R_n X_n \epsilon_1 \epsilon_2 \mu_2 \rho_2 \rho_3$$

$$-2n^2\omega H_n^2 k_2^2 k_z^2 k_{1\rho}^2 k_{2\rho}^4 k_{3\rho}^4 P_n U_n R_n X_n \epsilon_1 \epsilon_2 \mu_2 \rho_2 \rho_3$$

$$+2n^2\omega^3 H_n^2 k_z^2 k_{1\rho}^4 k_{2\rho}^4 k_{3\rho}^2 P_n V_n R_n W_n \epsilon_1 \epsilon_2^2 \mu_2^2 \rho_2 \rho_3$$

$$-2n^2\omega^3 H_n^2 k_z^2 k_{1\rho}^2 k_{2\rho}^6 k_{3\rho}^2 P_n V_n R_n W_n \epsilon_1 \epsilon_2^2 \mu_2^2 \rho_2 \rho_3$$

$$-2n^2\omega^3 H_n^2 k_z^2 k_{1\rho}^4 k_{2\rho}^2 k_{3\rho}^4 P_n V_n R_n W_n \epsilon_1 \epsilon_2^2 \mu_2^2 \rho_2 \rho_3$$

$$+2n^2\omega^3 H_n^2 k_z^2 k_{1\rho}^2 k_{2\rho}^4 k_{3\rho}^4 P_n V_n R_n W_n \epsilon_1 \epsilon_2^2 \mu_2^2 \rho_2 \rho_3$$

$$-n^2\omega^3 H_n^2 k_z^2 k_{1\rho}^4 k_{2\rho}^2 k_{3\rho}^4 P_n R_n W_n^2 \epsilon_1 \epsilon_2^2 \mu_2^2 \rho_3^2$$

$$+2n^2\omega^3 H_n^2 k_z^2 k_{1\rho}^2 k_{2\rho}^4 k_{3\rho}^4 P_n R_n W_n^2 \epsilon_1 \epsilon_2^2 \mu_2^2 \rho_3^2$$

$$-n^2\omega^3 H_n^2 k_z^2 k_{2\rho}^6 k_{3\rho}^4 P_n R_n W_n^2 \epsilon_1 \epsilon_2^2 \mu_2^2 \rho_3^2$$

$$+n^2\omega^3 H_n H_n^{'} k_z^2 k_{1\rho}^4 k_{2\rho}^3 k_{3\rho}^3 P_n U_n R_n W_n \epsilon_1 \epsilon_2 \epsilon_3 \mu_2^2 \rho_3^2$$

$$-2n^2\omega^3 H_n H_n^{'} k_z^2 k_{1\rho}^2 k_{2\rho}^5 k_{3\rho}^3 P_n U_n R_n W_n \epsilon_1 \epsilon_2 \epsilon_3 \mu_2^2 \rho_3^2$$

$$+n^2\omega^3 H_n H_n^{'} k_z^2 k_{2\rho}^7 k_{3\rho}^3 P_n U_n R_n W_n \epsilon_1 \epsilon_2 \epsilon_3 \mu_2^2 \rho_3^2$$

$$+n^2\omega^3 H_n H_n^{'} k_z^2 k_{1\rho}^4 k_{2\rho}^3 k_{3\rho}^3 P_n U_n R_n W_n \epsilon_1 \epsilon_2^2 \mu_2 \mu_3 \rho_3^2$$

$$-2n^2\omega^3 H_n H_n^{'} k_z^2 k_{1\rho}^2 k_{2\rho}^5 k_{3\rho}^3 P_n U_n R_n W_n \epsilon_1 \epsilon_2^2 \mu_2 \mu_3 \rho_3^2$$

$$+n^2\omega^3 H_n H_n^{'} k_z^2 k_{2\rho}^7 k_{3\rho}^3 P_n U_n R_n W_n \epsilon_1 \epsilon_2^2 \mu_2 \mu_3 \rho_3^2$$

$$-n^2\omega^3 H_n^{'2} k_z^2 k_{1\rho}^4 k_{2\rho}^4 k_{3\rho}^2 P_n U_n^2 R_n \epsilon_1 \epsilon_2 \epsilon_3 \mu_2 \mu_3 \rho_3^2$$

$$+2n^2\omega^3 H_n^{'2} k_z^2 k_{1\rho}^2 k_{2\rho}^6 k_{3\rho}^2 P_n U_n^2 R_n \epsilon_1 \epsilon_2 \epsilon_3 \mu_2 \mu_3 \rho_3^2$$

$$-n^2\omega^3 H_n^{'2} k_z^2 k_{2\rho}^8 k_{3\rho}^2 P_n U_n^2 R_n \epsilon_1 \epsilon_2 \epsilon_3 \mu_2 \mu_3 \rho_3^2$$

$$+\omega H_n^2 k_2^4 k_{1\rho}^4 k_{2\rho}^4 k_{3\rho}^4 P_n R_n {X_n}^2 \epsilon_1 \epsilon_2 \mu_2 \rho_2^2 \rho_3^2$$

$$-\omega H_n^2 k_1^2 k_2^2 k_{1\rho}^3 k_{2\rho}^5 k_{3\rho}^4 P_n W_n S_n X_n \epsilon_2^2 \mu_2 \rho_2^2 \rho_3^2$$

$$-\omega^3 H_n^2 k_2^2 k_{1\rho}^3 k_{2\rho}^5 k_{3\rho}^4 Q_n R_n W_n X_n \epsilon_1^2 \epsilon_2 \mu_2^2 \rho_2^2 \rho_3^2$$

$$+\omega^3 H_n^2 k_1^2 k_{1\rho}^2 k_{2\rho}^6 k_{3\rho}^4 Q_n W_n^2 S_n \epsilon_1 \epsilon_2^2 \mu_2^2 \rho_2^2 \rho_3^2$$

$$+\omega^3 H_n H_n^{'} k_2^2 k_{1\rho}^3 k_{2\rho}^6 k_{3\rho}^3 U_n Q_n R_n X_n \epsilon_1^2 \epsilon_3 \mu_2^2 \rho_2^2 \rho_3^2$$

$$-\omega^3 H_n H_n^{'} k_1^2 k_{1\rho}^2 k_{2\rho}^7 k_{3\rho}^3 U_n Q_n W_n S_n \epsilon_1 \epsilon_2 \epsilon_3 \mu_2^2 \rho_2^2 \rho_3^2$$

$$-\omega^3 H_n H_n^{'} k_2^2 k_{1\rho}^4 k_{2\rho}^5 k_{3\rho}^3 P_n V_n R_n X_n \epsilon_1 \epsilon_2 \epsilon_3 \mu_2^2 \rho_2^2 \rho_3^2$$

$$+\omega^3 H_n H_n^{'} k_1^2 k_{1\rho}^3 k_{2\rho}^6 k_{3\rho}^3 P_n V_n W_n S_n \epsilon_2^2 \epsilon_3 \mu_2^2 \rho_2^2 \rho_3^2$$

$$+\omega H_n H_n^{'} k_1^2 k_2^2 k_{1\rho}^3 k_{2\rho}^6 k_{3\rho}^3 P_n U_n S_n X_n \epsilon_2^2 \mu_3 \rho_2^2 \rho_3^2$$

$$-\omega^3 H_n H_n^{'} k_1^2 k_{1\rho}^2 k_{2\rho}^7 k_{3\rho}^3 U_n Q_n W_n S_n \epsilon_1 \epsilon_2^2 \mu_2 \mu_3 \rho_2^2 \rho_3^2$$

$$-\omega^3 H_n H_n^{'} k_2^2 k_{1\rho}^4 k_{2\rho}^5 k_{3\rho}^3 P_n V_n R_n X_n \epsilon_1 \epsilon_2^2 \mu_2 \mu_3 \rho_2^2 \rho_3^2$$

$$+\omega^3 H_n^{'2} k_1^2 k_{1\rho}^2 k_{2\rho}^8 k_{3\rho}^2 U_n^2 Q_n S_n \epsilon_1 \epsilon_2 \epsilon_3 \mu_2 \mu_3 \rho_2^2 \rho_3^2$$

$$-\omega^3 H_n^{'2} k_1^2 k_{1\rho}^3 k_{2\rho}^7 k_{3\rho}^2 P_n U_n V_n S_n \epsilon_2^2 \epsilon_3 \mu_2 \mu_3 \rho_2^2 \rho_3^2$$

$$
\begin{aligned}
&+\omega^5 H_n H_n^{'} k_{1\rho}^3 k_{2\rho}^6 k_{3\rho}^3 Q_n V_n R_n W_n \epsilon_1^2 \epsilon_2^2 \mu_2^2 \mu_3 \rho_2^2 \rho_3^2 \\
&-\omega^5 H_n^{'2} k_{1\rho}^3 k_{2\rho}^7 k_{3\rho}^2 U_n Q_n V_n R_n \epsilon_1^2 \epsilon_2 \epsilon_3 \mu_2^2 \mu_3 \rho_2^2 \rho_3^2 \\
&+\omega^5 H_n^{'2} k_{1\rho}^4 k_{2\rho}^6 k_{3\rho}^2 P_n V_n^2 R_n \epsilon_1 \epsilon_2^2 \epsilon_3 \mu_2^2 \mu_3 \rho_2^2 \rho_3^2, \qquad \text{(A-3)} \\
\widetilde{E}_{\phi\phi} \;=\; &-jn^4 H_n^2 k_1^2 k_z^4 k_{1\rho}^3 k_{2\rho}^4 P_n U_n^2 S_n \epsilon_2 \mu_2 \\
&+2jn^4 H_n^2 k_1^2 k_z^4 k_{1\rho}^3 k_{2\rho}^2 k_{3\rho}^2 P_n U_n^2 S_n \epsilon_2 \mu_2 \\
&-jn^4 H_n^2 k_1^2 k_z^4 k_{1\rho}^3 k_{3\rho}^4 P_n U_n^2 S_n \epsilon_2 \mu_2 \\
&+jn^4 \omega^2 H_n^2 k_z^4 k_{2\rho}^7 P_n U_n V_n R_n \epsilon_1 \epsilon_2 \mu_2^2 \\
&-2jn^4 \omega^2 H_n^2 k_z^4 k_{2\rho}^5 k_{3\rho}^2 P_n U_n V_n R_n \epsilon_1 \epsilon_2 \mu_2^2 \\
&+jn^4 \omega^2 H_n^2 k_z^4 k_{2\rho}^3 k_{3\rho}^4 P_n U_n V_n R_n \epsilon_1 \epsilon_2 \mu_2^2 \\
&-jn^2 \omega^2 H_n^2 k_1^2 k_z^2 k_{1\rho}^2 k_{2\rho}^7 U_n Q_n V_n S_n \epsilon_1 \epsilon_2 \mu_2^2 \rho_2^2 \\
&+2jn^2 \omega^2 H_n^2 k_1^2 k_z^2 k_{1\rho}^2 k_{2\rho}^5 k_{3\rho}^2 U_n Q_n V_n S_n \epsilon_1 \epsilon_2 \mu_2^2 \rho_2^2 \\
&-jn^2 \omega^2 H_n^2 k_1^2 k_z^2 k_{1\rho}^2 k_{2\rho}^3 k_{3\rho}^4 U_n Q_n V_n S_n \epsilon_1 \epsilon_2 \mu_2^2 \rho_2^2 \\
&+jn^2 \omega^2 H_n^2 k_1^2 k_z^2 k_{1\rho}^3 k_{2\rho}^6 P_n V_n^2 S_n \epsilon_2^2 \mu_2^2 \rho_2^2 \\
&-2jn^2 \omega^2 H_n^2 k_1^2 k_z^2 k_{1\rho}^3 k_{2\rho}^4 k_{3\rho}^2 P_n V_n^2 S_n \epsilon_2^2 \mu_2^2 \rho_2^2 \\
&+jn^2 \omega^2 H_n^2 k_1^2 k_z^2 k_{1\rho}^3 k_{2\rho}^2 k_{3\rho}^4 P_n V_n^2 S_n \epsilon_2^2 \mu_2^2 \rho_2^2 \\
&+2jn^2 H_n^2 k_1^2 k_2^2 k_z^2 k_{1\rho}^3 k_{2\rho}^4 k_{3\rho}^2 P_n U_n S_n X_n \epsilon_2 \mu_2 \rho_2 \rho_3 \\
&-2jn^2 H_n^2 k_1^2 k_2^2 k_z^2 k_{1\rho}^3 k_{2\rho}^2 k_{3\rho}^4 P_n U_n S_n X_n \epsilon_2 \mu_2 \rho_2 \rho_3 \\
&-2jn^2 \omega^2 H_n^2 k_1^2 k_z^2 k_{1\rho}^3 k_{2\rho}^4 k_{3\rho}^2 P_n V_n W_n S_n \epsilon_2^2 \mu_2^2 \rho_2 \rho_3 \\
&+2jn^2 \omega^2 H_n^2 k_1^2 k_z^2 k_{1\rho}^3 k_{2\rho}^2 k_{3\rho}^4 P_n V_n W_n S_n \epsilon_2^2 \mu_2^2 \rho_2 \rho_3 \\
&-jn^2 \omega^2 H_n^2 k_2^2 k_z^2 k_{2\rho}^5 k_{3\rho}^4 P_n R_n W_n X_n \epsilon_1 \epsilon_2 \mu_2^2 \rho_3^2 \\
&+jn^2 \omega^2 H_n^2 k_1^2 k_z^2 k_{1\rho}^3 k_{2\rho}^2 k_{3\rho}^4 P_n W_n^2 S_n \epsilon_2^2 \mu_2^2 \rho_3^2 \\
&+jn^2 \omega^2 H_n H_n^{'} k_2^2 k_z^2 k_{2\rho}^6 k_{3\rho}^3 P_n U_n R_n X_n \epsilon_1 \epsilon_3 \mu_2^2 \rho_3^2 \\
&-jn^2 \omega^2 H_n H_n^{'} k_1^2 k_z^2 k_{1\rho}^3 k_{2\rho}^3 k_{3\rho}^3 P_n U_n W_n S_n \epsilon_2 \epsilon_3 \mu_2^2 \rho_3^2 \\
&-jn^2 \omega^2 H_n H_n^{'} k_1^2 k_z^2 k_{1\rho}^3 k_{2\rho}^3 k_{3\rho}^3 P_n U_n W_n S_n \epsilon_2^2 \mu_2 \mu_3 \rho_3^2
\end{aligned}
$$

$$
\begin{aligned}
&+jn^2\omega^2 H_n^{'2}k_1^2k_z^2k_{1\rho}^3k_{2\rho}^4k_{3\rho}^2P_nU_n^2S_n\epsilon_2\epsilon_3\mu_2\mu_3\rho_3^2\\
&+jn^2\omega^4 H_nH_n^{'}k_z^2k_{2\rho}^6k_{3\rho}^3P_nV_nR_nW_n\epsilon_1\epsilon_2^2\mu_2^2\mu_3\rho_3^2\\
&-jn^2\omega^4 H_n^{'2}k_z^2k_{2\rho}^7k_{3\rho}^2P_nU_nV_nR_n\epsilon_1\epsilon_2\epsilon_3\mu_2^2\mu_3\rho_3^2\\
&-jH_n^2k_1^2k_2^4k_{1\rho}^3k_{2\rho}^4k_{3\rho}^4P_nS_n{X_n}^2\epsilon_2\mu_2\rho_2^2\rho_3^2\\
&+j\omega^2 H_n^2k_1^2k_2^2k_{1\rho}^2k_{2\rho}^5k_{3\rho}^4Q_nW_nS_nX_n\epsilon_1\epsilon_2\mu_2^2\rho_2^2\rho_3^2\\
&-j\omega^2 H_nH_n^{'}k_1^2k_2^2k_{1\rho}^2k_{2\rho}^6k_{3\rho}^3U_nQ_nS_nX_n\epsilon_1\epsilon_3\mu_2^2\rho_2^2\rho_3^2\\
&+j\omega^2 H_nH_n^{'}k_1^2k_2^2k_{1\rho}^3k_{2\rho}^5k_{3\rho}^3P_nV_nS_nX_n\epsilon_2\epsilon_3\mu_2^2\rho_2^2\rho_3^2\\
&+j\omega^2 H_nH_n^{'}k_1^2k_2^2k_{1\rho}^3k_{2\rho}^5k_{3\rho}^3P_nV_nS_nX_n\epsilon_2^2\mu_2\mu_3\rho_2^2\rho_3^2\\
&-j\omega^4 H_nH_n^{'}k_1^2k_{1\rho}^2k_{2\rho}^6k_{3\rho}^3Q_nV_nW_nS_n\epsilon_1\epsilon_2^2\mu_2^2\mu_3\rho_2^2\rho_3^2\\
&+j\omega^4 H_n^{'2}k_1^2k_{1\rho}^2k_{2\rho}^7k_{3\rho}^2U_nQ_nV_nS_n\epsilon_1\epsilon_2\epsilon_3\mu_2^2\mu_3\rho_2^2\rho_3^2\\
&-j\omega^4 H_n^{'2}k_1^2k_{1\rho}^3k_{2\rho}^6k_{3\rho}^2P_nV_n^2S_n\epsilon_2^2\epsilon_3\mu_2^2\mu_3\rho_2^2\rho_3^2, \qquad \text{(A-4)}\\
\widetilde{E}_{\phi z} \quad = \quad & jn^3H_n^2k_1^2k_z^3k_{1\rho}^3k_{2\rho}^6P_nU_n^2S_n\epsilon_2\mu_2\rho_2\\
&-2jn^3H_n^2k_1^2k_z^3k_{1\rho}^3k_{2\rho}^4k_{3\rho}^2P_nU_n^2S_n\epsilon_2\mu_2\rho_2\\
&+jn^3H_n^2k_1^2k_z^3k_{1\rho}^3k_{2\rho}^2k_{3\rho}^4P_nU_n^2S_n\epsilon_2\mu_2\rho_2\\
&-jn^3\omega^2H_n^2k_z^3k_{1\rho}^2k_{2\rho}^7P_nU_nV_nR_n\epsilon_1\epsilon_2\mu_2^2\rho_2\\
&+2jn^3\omega^2H_n^2k_z^3k_{1\rho}^2k_{2\rho}^5k_{3\rho}^2P_nU_nV_nR_n\epsilon_1\epsilon_2\mu_2^2\rho_2\\
&-jn^3\omega^2H_n^2k_z^3k_{1\rho}^2k_{2\rho}^3k_{3\rho}^4P_nU_nV_nR_n\epsilon_1\epsilon_2\mu_2^2\rho_2\\
&-jnH_n^2k_1^2k_2^2k_zk_{1\rho}^3k_{2\rho}^6k_{3\rho}^2P_nU_nS_nX_n\epsilon_2\mu_2\rho_2^2\rho_3\\
&+jnH_n^2k_1^2k_2^2k_zk_{1\rho}^3k_{2\rho}^4k_{3\rho}^4P_nU_nS_nX_n\epsilon_2\mu_2\rho_2^2\rho_3\\
&+jn\omega^2H_n^2k_1^2k_zk_{1\rho}^3k_{2\rho}^6k_{3\rho}^2P_nV_nW_nS_n\epsilon_2^2\mu_2^2\rho_2^2\rho_3\\
&-jn\omega^2H_n^2k_1^2k_zk_{1\rho}^3k_{2\rho}^4k_{3\rho}^4P_nV_nW_nS_n\epsilon_2^2\mu_2^2\rho_2^2\rho_3\\
&+jn\omega^2H_n^2k_2^2k_zk_{1\rho}^2k_{2\rho}^5k_{3\rho}^4P_nR_nW_nX_n\epsilon_1\epsilon_2\mu_2^2\rho_2\rho_3^2\\
&-jn\omega^2H_n^2k_1^2k_zk_{1\rho}^3k_{2\rho}^4k_{3\rho}^4P_nW_n^2S_n\epsilon_2^2\mu_2^2\rho_2\rho_3^2\\
&-jn\omega^2H_nH_n^{'}k_2^2k_zk_{1\rho}^2k_{2\rho}^6k_{3\rho}^3P_nU_nR_nX_n\epsilon_1\epsilon_3\mu_2^2\rho_2\rho_3^2
\end{aligned}
$$

$$
\begin{aligned}
&+jn\omega^2 H_n H_n^{'} k_1^2 k_z k_{1\rho}^3 k_{2\rho}^5 k_{3\rho}^3 P_n U_n W_n S_n \epsilon_2 \epsilon_3 \mu_2^2 \rho_2 \rho_3^2 \\
&+jn\omega^2 H_n H_n^{'} k_1^2 k_z k_{1\rho}^3 k_{2\rho}^5 k_{3\rho}^3 P_n U_n W_n S_n \epsilon_2^2 \mu_2 \mu_3 \rho_2 \rho_3^2 \\
&-jn\omega^2 H_n^{'2} k_1^2 k_z k_{1\rho}^3 k_{2\rho}^6 k_{3\rho}^2 P_n U_n^2 S_n \epsilon_2 \epsilon_3 \mu_2 \mu_3 \rho_2 \rho_3^2 \\
&-jn\omega^4 H_n H_n^{'} k_z k_{1\rho}^2 k_{2\rho}^6 k_{3\rho}^3 P_n V_n R_n W_n \epsilon_1 \epsilon_2^2 \mu_2^2 \mu_3 \rho_2 \rho_3^2 \\
&+jn\omega^4 H_n^{'2} k_z k_{1\rho}^2 k_{2\rho}^7 k_{3\rho}^2 P_n U_n V_n R_n \epsilon_1 \epsilon_2 \epsilon_3 \mu_2^2 \mu_3 \rho_2 \rho_3^2, \qquad \text{(A-5)}
\end{aligned}
$$

$$
\begin{aligned}
\Delta_\phi \;=\;& n^4 \omega H_n^2 k_z^4 k_{1\rho}^4 k_{2\rho}^4 P_n U_n^2 R_n \epsilon_1 \epsilon_2 \mu_2 \\
&-2n^4 \omega H_n^2 k_z^4 k_{1\rho}^2 k_{2\rho}^6 P_n U_n^2 R_n \epsilon_1 \epsilon_2 \mu_2 \\
&+n^4 \omega H_n^2 k_z^4 k_{2\rho}^8 P_n U_n^2 R_n \epsilon_1 \epsilon_2 \mu_2 \\
&-2n^4 \omega H_n^2 k_z^4 k_{1\rho}^4 k_{2\rho}^2 k_{3\rho}^2 P_n U_n^2 R_n \epsilon_1 \epsilon_2 \mu_2 \\
&+4n^4 \omega H_n^2 k_z^4 k_{1\rho}^2 k_{2\rho}^4 k_{3\rho}^2 P_n U_n^2 R_n \epsilon_1 \epsilon_2 \mu_2 \\
&-2n^4 \omega H_n^2 k_z^4 k_{2\rho}^6 k_{3\rho}^2 P_n U_n^2 R_n \epsilon_1 \epsilon_2 \mu_2 \\
&+n^4 \omega H_n^2 k_z^4 k_{1\rho}^4 k_{3\rho}^4 P_n U_n^2 R_n \epsilon_1 \epsilon_2 \mu_2 \\
&-2n^4 \omega H_n^2 k_z^4 k_{1\rho}^2 k_{2\rho}^2 k_{3\rho}^4 P_n U_n^2 R_n \epsilon_1 \epsilon_2 \mu_2 \\
&+n^4 \omega H_n^2 k_z^4 k_{2\rho}^4 k_{3\rho}^4 P_n U_n^2 R_n \epsilon_1 \epsilon_2 \mu_2 \\
&-n^2 \omega H_n^2 k_1^2 k_z^2 k_{1\rho}^2 k_{2\rho}^8 U_n^2 Q_n S_n \epsilon_1 \epsilon_2 \mu_2 \rho_2^2 \\
&+2n^2 \omega H_n^2 k_1^2 k_z^2 k_{1\rho}^2 k_{2\rho}^6 k_{3\rho}^2 U_n^2 Q_n S_n \epsilon_1 \epsilon_2 \mu_2 \rho_2^2 \\
&-n^2 \omega H_n^2 k_1^2 k_z^2 k_{1\rho}^2 k_{2\rho}^4 k_{3\rho}^4 U_n^2 Q_n S_n \epsilon_1 \epsilon_2 \mu_2 \rho_2^2 \\
&+n^2 \omega H_n^2 k_1^2 k_z^2 k_{1\rho}^3 k_{2\rho}^7 P_n U_n V_n S_n \epsilon_2^2 \mu_2 \rho_2^2 \\
&-2n^2 \omega H_n^2 k_1^2 k_z^2 k_{1\rho}^3 k_{2\rho}^5 k_{3\rho}^2 P_n U_n V_n S_n \epsilon_2^2 \mu_2 \rho_2^2 \\
&+n^2 \omega H_n^2 k_1^2 k_z^2 k_{1\rho}^3 k_{2\rho}^3 k_{3\rho}^4 P_n U_n V_n S_n \epsilon_2^2 \mu_2 \rho_2^2 \\
&+n^2 \omega^3 H_n^2 k_z^2 k_{1\rho}^3 k_{2\rho}^7 U_n Q_n V_n R_n \epsilon_1^2 \epsilon_2 \mu_2^2 \rho_2^2 \\
&-2n^2 \omega^3 H_n^2 k_z^2 k_{1\rho}^3 k_{2\rho}^5 k_{3\rho}^2 U_n Q_n V_n R_n \epsilon_1^2 \epsilon_2 \mu_2^2 \rho_2^2 \\
&+n^2 \omega^3 H_n^2 k_z^2 k_{1\rho}^3 k_{2\rho}^3 k_{3\rho}^4 U_n Q_n V_n R_n \epsilon_1^2 \epsilon_2 \mu_2^2 \rho_2^2 \\
&-n^2 \omega^3 H_n^2 k_z^2 k_{1\rho}^4 k_{2\rho}^6 P_n V_n^2 R_n \epsilon_1 \epsilon_2^2 \mu_2^2 \rho_2^2
\end{aligned}
$$

$$+2n^2\omega^3 H_n^2 k_z^2 k_{1\rho}^4 k_{2\rho}^4 k_{3\rho}^2 P_n V_n^2 R_n \epsilon_1 \epsilon_2^2 \mu_2^2 \rho_2^2$$

$$-n^2\omega^3 H_n^2 k_z^2 k_{1\rho}^4 k_{2\rho}^2 k_{3\rho}^4 P_n V_n^2 R_n \epsilon_1 \epsilon_2^2 \mu_2^2 \rho_2^2$$

$$-2n^2\omega H_n^2 k_2^2 k_z^2 k_{1\rho}^4 k_{2\rho}^4 k_{3\rho}^2 P_n U_n R_n X_n \epsilon_1 \epsilon_2 \mu_2 \rho_2 \rho_3$$

$$+2n^2\omega H_n^2 k_2^2 k_z^2 k_{1\rho}^2 k_{2\rho}^6 k_{3\rho}^2 P_n U_n R_n X_n \epsilon_1 \epsilon_2 \mu_2 \rho_2 \rho_3$$

$$+2n^2\omega H_n^2 k_2^2 k_z^2 k_{1\rho}^4 k_{2\rho}^2 k_{3\rho}^4 P_n U_n R_n X_n \epsilon_1 \epsilon_2 \mu_2 \rho_2 \rho_3$$

$$-2n^2\omega H_n^2 k_2^2 k_z^2 k_{1\rho}^2 k_{2\rho}^4 k_{3\rho}^4 P_n U_n R_n X_n \epsilon_1 \epsilon_2 \mu_2 \rho_2 \rho_3$$

$$+2n^2\omega^3 H_n^2 k_z^2 k_{1\rho}^4 k_{2\rho}^4 k_{3\rho}^2 P_n V_n R_n W_n \epsilon_1 \epsilon_2^2 \mu_2^2 \rho_2 \rho_3$$

$$-2n^2\omega^3 H_n^2 k_z^2 k_{1\rho}^2 k_{2\rho}^6 k_{3\rho}^2 P_n V_n R_n W_n \epsilon_1 \epsilon_2^2 \mu_2^2 \rho_2 \rho_3$$

$$-2n^2\omega^3 H_n^2 k_z^2 k_{1\rho}^4 k_{2\rho}^2 k_{3\rho}^4 P_n V_n R_n W_n \epsilon_1 \epsilon_2^2 \mu_2^2 \rho_2 \rho_3$$

$$+2n^2\omega^3 H_n^2 k_z^2 k_{1\rho}^2 k_{2\rho}^4 k_{3\rho}^4 P_n V_n R_n W_n \epsilon_1 \epsilon_2^2 \mu_2^2 \rho_2 \rho_3$$

$$-n^2\omega^3 H_n^2 k_z^2 k_{1\rho}^4 k_{2\rho}^2 k_{3\rho}^4 P_n R_n W_n^2 \epsilon_1 \epsilon_2^2 \mu_2^2 \rho_3^2$$

$$+2n^2\omega^3 H_n^2 k_z^2 k_{1\rho}^2 k_{2\rho}^4 k_{3\rho}^4 P_n R_n W_n^2 \epsilon_1 \epsilon_2^2 \mu_2^2 \rho_3^2$$

$$-n^2\omega^3 H_n^2 k_z^2 k_{2\rho}^6 k_{3\rho}^4 P_n R_n W_n^2 \epsilon_1 \epsilon_2^2 \mu_2^2 \rho_3^2$$

$$+n^2\omega^3 H_n H_n^{'} k_z^2 k_{1\rho}^4 k_{2\rho}^3 k_{3\rho}^3 P_n U_n R_n W_n \epsilon_1 \epsilon_2 \epsilon_3 \mu_2^2 \rho_3^2$$

$$-2n^2\omega^3 H_n H_n^{'} k_z^2 k_{1\rho}^2 k_{2\rho}^5 k_{3\rho}^3 P_n U_n R_n W_n \epsilon_1 \epsilon_2 \epsilon_3 \mu_2^2 \rho_3^2$$

$$+n^2\omega^3 H_n H_n^{'} k_z^2 k_{2\rho}^7 k_{3\rho}^3 P_n U_n R_n W_n \epsilon_1 \epsilon_2 \epsilon_3 \mu_2^2 \rho_3^2$$

$$+n^2\omega^3 H_n H_n^{'} k_z^2 k_{1\rho}^4 k_{2\rho}^3 k_{3\rho}^3 P_n U_n R_n W_n \epsilon_1 \epsilon_2^2 \mu_2 \mu_3 \rho_3^2$$

$$-2n^2\omega^3 H_n H_n^{'} k_z^2 k_{1\rho}^2 k_{2\rho}^5 k_{3\rho}^3 P_n U_n R_n W_n \epsilon_1 \epsilon_2^2 \mu_2 \mu_3 \rho_3^2$$

$$+n^2\omega^3 H_n H_n^{'} k_z^2 k_{2\rho}^7 k_{3\rho}^3 P_n U_n R_n W_n \epsilon_1 \epsilon_2^2 \mu_2 \mu_3 \rho_3^2$$

$$-n^2\omega^3 H_n^{'2} k_z^2 k_{1\rho}^4 k_{2\rho}^4 k_{3\rho}^2 P_n U_n^2 R_n \epsilon_1 \epsilon_2 \epsilon_3 \mu_2 \mu_3 \rho_3^2$$

$$+2n^2\omega^3 H_n^{'2} k_z^2 k_{1\rho}^2 k_{2\rho}^6 k_{3\rho}^2 P_n U_n^2 R_n \epsilon_1 \epsilon_2 \epsilon_3 \mu_2 \mu_3 \rho_3^2$$

$$-n^2\omega^3 H_n^{'2} k_z^2 k_{2\rho}^8 k_{3\rho}^2 P_n U_n^2 R_n \epsilon_1 \epsilon_2 \epsilon_3 \mu_2 \mu_3 \rho_3^2$$

$$+\omega H_n^2 k_2^4 k_{1\rho}^4 k_{2\rho}^4 k_{3\rho}^4 P_n R_n {X_n}^2 \epsilon_1 \epsilon_2 \mu_2 \rho_2^2 \rho_3^2$$

$$-\omega H_n^2 k_1^2 k_2^2 k_{1\rho}^3 k_{2\rho}^5 k_{3\rho}^4 P_n W_n S_n X_n \epsilon_2^2 \mu_2 \rho_2^2 \rho_3^2$$

$$
\begin{aligned}
&-\omega^3 H_n^2 k_2^2 k_{1\rho}^3 k_{2\rho}^5 k_{3\rho}^4 Q_n R_n W_n X_n \epsilon_1^2 \epsilon_2 \mu_2^2 \rho_2^2 \rho_3^2 \\
&+\omega^3 H_n^2 k_1^2 k_{1\rho}^2 k_{2\rho}^6 k_{3\rho}^4 Q_n W_n^2 S_n \epsilon_1 \epsilon_2^2 \mu_2^2 \rho_2^2 \rho_3^2 \\
&+\omega^3 H_n H_n^{'} k_2^2 k_{1\rho}^3 k_{2\rho}^6 k_{3\rho}^3 U_n Q_n R_n X_n \epsilon_1^2 \epsilon_3 \mu_2^2 \rho_2^2 \rho_3^2 \\
&-\omega^3 H_n H_n^{'} k_1^2 k_{1\rho}^2 k_{2\rho}^7 k_{3\rho}^3 U_n Q_n W_n S_n \epsilon_1 \epsilon_2 \epsilon_3 \mu_2^2 \rho_2^2 \rho_3^2 \\
&-\omega^3 H_n H_n^{'} k_2^2 k_{1\rho}^4 k_{2\rho}^5 k_{3\rho}^3 P_n V_n R_n X_n \epsilon_1 \epsilon_2 \epsilon_3 \mu_2^2 \rho_2^2 \rho_3^2 \\
&+\omega^3 H_n H_n^{'} k_1^2 k_{1\rho}^3 k_{2\rho}^6 k_{3\rho}^3 P_n V_n W_n S_n \epsilon_2^2 \epsilon_3 \mu_2^2 \rho_2^2 \rho_3^2 \\
&+\omega H_n H_n^{'} k_1^2 k_2^2 k_{1\rho}^3 k_{2\rho}^6 k_{3\rho}^3 P_n U_n S_n X_n \epsilon_2^2 \mu_3 \rho_2^2 \rho_3^2 \\
&-\omega^3 H_n H_n^{'} k_1^2 k_{1\rho}^2 k_{2\rho}^7 k_{3\rho}^3 U_n Q_n W_n S_n \epsilon_1 \epsilon_2^2 \mu_2 \mu_3 \rho_2^2 \rho_3^2 \\
&-\omega^3 H_n H_n^{'} k_2^2 k_{1\rho}^4 k_{2\rho}^5 k_{3\rho}^3 P_n V_n R_n X_n \epsilon_1 \epsilon_2^2 \mu_2 \mu_3 \rho_2^2 \rho_3^2 \\
&+\omega^3 H_n^{'2} k_1^2 k_{1\rho}^2 k_{2\rho}^8 k_{3\rho}^2 U_n^2 Q_n S_n \epsilon_1 \epsilon_2 \epsilon_3 \mu_2 \mu_3 \rho_2^2 \rho_3^2 \\
&-\omega^3 H_n^{'2} k_1^2 k_{1\rho}^3 k_{2\rho}^7 k_{3\rho}^2 P_n U_n V_n S_n \epsilon_2^2 \epsilon_3 \mu_2 \mu_3 \rho_2^2 \rho_3^2 \\
&+\omega^5 H_n H_n^{'} k_{1\rho}^3 k_{2\rho}^6 k_{3\rho}^3 Q_n V_n R_n W_n \epsilon_1^2 \epsilon_2^2 \mu_2^2 \mu_3 \rho_2^2 \rho_3^2 \\
&-\omega^5 H_n^{'2} k_{1\rho}^3 k_{2\rho}^7 k_{3\rho}^2 U_n Q_n V_n R_n \epsilon_1^2 \epsilon_2 \epsilon_3 \mu_2^2 \mu_3 \rho_2^2 \rho_3^2 \\
&+\omega^5 H_n^{'2} k_{1\rho}^4 k_{2\rho}^6 k_{3\rho}^2 P_n V_n^2 R_n \epsilon_1 \epsilon_2^2 \epsilon_3 \mu_2^2 \mu_3 \rho_2^2 \rho_3^2 . \qquad \text{(A-6)}
\end{aligned}
$$

Appendix B

Mixed Potential Green's Functions for Radial Directed Dipole Source

---

Tangential electrical field can be written as

$$\begin{aligned}
\begin{bmatrix} \widetilde{\boldsymbol{E}}_\phi \\ \widetilde{\boldsymbol{E}}_z \end{bmatrix} &= \begin{bmatrix} \tilde{G}^{E_n}_{\phi\rho} & \tilde{G}^{E_n}_{\phi\phi} & \tilde{G}^{E_n}_{\phi z} \\ \tilde{G}^{E_n}_{z\rho} & \tilde{G}^{E_n}_{z\phi} & \tilde{G}^{E_n}_{zz} \end{bmatrix} \cdot \begin{bmatrix} J_\rho \\ J_\phi \\ J_z \end{bmatrix} \\
&= -j\omega \begin{bmatrix} \tilde{G}^{A}_{\phi\rho} & \tilde{G}^{A}_{\phi\phi} & \tilde{G}^{A}_{\phi z} \\ \tilde{G}^{A}_{z\rho} & \tilde{G}^{A}_{z\phi} & \tilde{G}^{A}_{zz} \end{bmatrix} \cdot \begin{bmatrix} J_\rho \\ J_\phi \\ J_z \end{bmatrix} - [\nabla\nabla' \cdot (\widetilde{\overline{\boldsymbol{G}}}_\phi)]_t \cdot \begin{bmatrix} J_\rho \\ J_\phi \\ J_z \end{bmatrix}, \quad \text{(B-1)}
\end{aligned}$$

in which $\nabla\nabla' \cdot (\widetilde{\overline{\boldsymbol{G}}}_\phi)_t$ is the tangential component of $\nabla\nabla' \cdot (\widetilde{\overline{\boldsymbol{G}}}_\phi)$, that is

$$\begin{aligned}
\nabla\nabla' \cdot (\widetilde{\overline{\boldsymbol{G}}}_\phi)_t &= \frac{1}{\rho}\widehat{\boldsymbol{\phi}}[(\frac{1}{\rho'}\frac{\partial \widetilde{G}^{\phi}_{\rho\rho}}{\partial\phi} + \frac{\partial^2 \widetilde{G}^{\phi}_{\rho\rho}}{\partial\phi\partial\rho'} - \frac{1}{\rho'}\frac{\partial \widetilde{G}^{\phi}_{\phi\phi}}{\partial\phi} \\
&\quad -\frac{1}{\rho'}\frac{\partial \widetilde{G}^{\phi}_{\phi\phi}}{\partial\phi'})\widehat{\boldsymbol{\rho}} + (\frac{1}{\rho'}\frac{\partial^2 \widetilde{G}^{\phi}_{\phi\phi}}{\partial\phi\partial\phi'} + \frac{\widetilde{G}^{\phi}_{\rho\rho}}{\rho'} + \frac{\partial \widetilde{G}^{\phi}_{\rho\rho}}{\partial\rho'} \\
&\quad -\frac{1}{\rho'}\widetilde{G}^{\phi}_{\phi\phi})\widehat{\boldsymbol{\phi}} + \frac{\partial^2 \widetilde{G}^{\phi}_{zz}}{\partial\phi\partial z'}\widehat{\boldsymbol{z}}]
\end{aligned}$$

$$+\widehat{\boldsymbol{z}}[(\frac{\partial^2\widetilde{G}^{\phi}_{\rho\rho}}{\partial z\partial\rho'}+\frac{1}{\rho'}\frac{\widetilde{G}^{\phi}_{\rho\rho}}{\partial z}-\frac{1}{\rho'}\frac{\widetilde{G}^{\phi}_{\phi\phi}}{\partial z})\widehat{\boldsymbol{\rho}}$$
$$+\frac{1}{\rho'}\frac{\partial^2\widetilde{G}^{\phi}_{\phi\phi}}{\partial z\partial\phi'}\widehat{\boldsymbol{\phi}}+\frac{\partial^2\widetilde{G}^{\phi}_{zz}}{\partial z\partial z'}\widehat{\boldsymbol{z}}]. \tag{B-2}$$

Without loss of generality, let $\widetilde{G}^{\phi}_{\rho\rho}=0$ and $\widetilde{G}^{\phi}_{\phi\phi}=\widetilde{G}^{\phi}_{zz}=\widetilde{G}^{\phi}$. Considering (B-2), (B-1) can be further reduced to

$$\begin{aligned}\begin{bmatrix}\widetilde{\boldsymbol{E}}_{\phi}\\ \widetilde{\boldsymbol{E}}_{z}\end{bmatrix} &= \begin{bmatrix}\tilde{G}^{E_n}_{\phi\rho} & \tilde{G}^{E_n}_{\phi\phi} & \tilde{G}^{E_n}_{\phi z}\\ \tilde{G}^{E_n}_{z\rho} & \tilde{G}^{E_n}_{z\phi} & \tilde{G}^{E_n}_{zz}\end{bmatrix}\cdot\begin{bmatrix}J_\rho\\ J_\phi\\ J_z\end{bmatrix}\\ &= -j\omega\begin{bmatrix}\tilde{G}^{A}_{\phi\rho} & \tilde{G}^{A}_{\phi\phi} & \tilde{G}^{A}_{\phi z}\\ \tilde{G}^{A}_{z\rho} & \tilde{G}^{A}_{z\phi} & \tilde{G}^{A}_{zz}\end{bmatrix}\cdot\begin{bmatrix}J_\rho\\ J_\phi\\ J_z\end{bmatrix}-\nabla\nabla'\cdot(\overline{\widetilde{\boldsymbol{G}}}_{\phi})_t\cdot\begin{bmatrix}J_\rho\\ J_\phi\\ J_z\end{bmatrix},\end{aligned} \tag{B-3}$$

where

$$\begin{aligned}\nabla\nabla'\cdot(\overline{\widetilde{\boldsymbol{G}}}_{\phi})_t &= \frac{1}{\rho}\widehat{\boldsymbol{\phi}}[(\frac{1}{\rho'}\frac{\partial^2\widetilde{G}^{\phi}}{\partial\phi\partial\phi'}-\frac{1}{\rho'}\widetilde{G}^{\phi})\widehat{\boldsymbol{\phi}}+\frac{\partial^2\widetilde{G}^{\phi}}{\partial\phi\partial z'}\widehat{\boldsymbol{z}}]\\ &\quad+\widehat{\boldsymbol{z}}(-\frac{1}{\rho'}\frac{\partial\widetilde{G}^{\phi}}{\partial z}\widehat{\boldsymbol{\rho}}+\frac{1}{\rho'}\frac{\partial^2\widetilde{G}^{\phi}}{\partial z\partial\phi'}\widehat{\boldsymbol{\phi}}+\frac{\partial^2\widetilde{G}^{\phi}}{\partial z\partial z'}\widehat{\boldsymbol{z}}).\end{aligned} \tag{B-4}$$

By comparing it with $\widetilde{G}^{E_n}_{\phi\rho}$, $\widetilde{G}^{E_n}_{z\rho}$, $\widetilde{G}^{E_n}_{zz}$, $\widetilde{G}^{E_n}_{z\phi}$, $\widetilde{G}^{E_n}_{\phi z}$ and $\widetilde{G}^{E_n}_{\phi\phi}$ in Eqs. (6.1)-(6.3) and from Eq. (B-3), it can be obtained that,

$$\widetilde{G}^{E_n}_{\phi\rho} = -j\omega\widetilde{G}^{A}_{\phi\rho} \tag{B-5a}$$
$$\widetilde{G}^{E_n}_{z\rho} = -j\omega\widetilde{G}^{A}_{z\rho}+\frac{ik_z}{\rho'}\widetilde{G}^{\phi} \tag{B-5b}$$
$$\widetilde{G}^{E_n}_{zz} = -j\omega\widetilde{G}^{A}_{zz}-k_z^2\widetilde{G}^{\phi}, \tag{B-5c}$$
$$\widetilde{G}^{E_n}_{z\phi} = -j\omega\widetilde{G}^{A}_{z\phi}-\frac{k_z n}{\rho'}\widetilde{G}^{\phi}, \tag{B-5d}$$
$$\widetilde{G}^{E_n}_{\phi z} = -j\omega\widetilde{G}^{A}_{\phi z}-\frac{k_z n}{\rho}\widetilde{G}^{\phi}, \tag{B-5e}$$
$$\widetilde{G}^{E_n}_{\phi\phi} = -j\omega\widetilde{G}^{A}_{\phi\phi}-\frac{n^2-1}{\rho\rho'}\widetilde{G}^{\phi}. \tag{B-5f}$$

From Eq. (B-5a), $\widetilde{G}^{A}_{\phi\rho}$ can be determined. Without loss of generality, let $\widetilde{G}^{A}_{z\rho}=0$, solving Eq. (B-5b) for $\widetilde{G}^{\phi}$, and substitute $\widetilde{G}^{\phi}$ in to Eqs. (B-5c)-(B-5f) for other components of potential Green's functions.

Appendix C

Some Intermediates

C.1 Sommerfeld Identity

The Sommerfeld identity is given by

$$\frac{e^{jk_0 r}}{r} = j\int_0^\infty dk_\rho \frac{k_\rho}{k_z} J_0(k_\rho \rho) e^{jk_z|z|}. \tag{C-1}$$

By using $J_0(k_\rho\rho) = \frac{1}{2}[H_0^{(1)}(k_\rho\rho) + H_0^{(2)}(k_\rho\rho)]$ and $H_0^{(1)}(e^{j\pi}x) = -H_0^{(2)}(x)$, a variation of the above identity can be derived as

$$\frac{e^{jk_0 r}}{r} = \frac{j}{2}\int_{-\infty}^\infty dk_\rho \frac{k_\rho}{k_z} H_0^{(1)}(k_\rho \rho) e^{jk_z|z|}. \tag{C-2}$$

Another useful identity is

$$\frac{e^{jk_0 r}}{r} = \frac{j}{2}\int_{-\infty}^\infty dk_z e^{jk_z z} H_0^{(1)}(k_\rho \rho). \tag{C-3}$$

C.2 Some Intermediates

The addition theorem are given below:

$$\frac{e^{jk|\boldsymbol{r}-\boldsymbol{r}'|}}{|\boldsymbol{r}-\boldsymbol{r}'|} = \sum_{n=-\infty}^{\infty} \frac{je^{jn(\phi-\phi')}}{2}\int_{-\infty}^\infty e^{jk_z(z-z')} \cdot J_n(k_\rho\rho_<) H_n^{(1)}(k_\rho\rho_>) dk_z, \tag{C-4}$$

$$H_0^{(1)}(k_{i\rho}|\boldsymbol{\rho}-\boldsymbol{\rho}'|) = \sum_{n=-\infty}^{\infty} H_n^{(1)}(k_{i\rho}\rho)J_n(k_{i\rho}\rho')e^{jn(\phi-\phi')}, \tag{C-5}$$

where

$$\begin{aligned} |\boldsymbol{r}-\boldsymbol{r}'| &= \sqrt{(z-z')^2+\rho^2+\rho'^2-2\rho\rho'\cos(\phi-\phi')}, \\ |\boldsymbol{\rho}-\boldsymbol{\rho}'| &= \sqrt{\rho^2+\rho'^2-2\rho\rho'\cos(\phi-\phi')}. \end{aligned}$$

It can be derived from (C-5) that

$$\begin{aligned} \frac{\partial^2}{\partial\phi\partial\phi'}H_0^{(1)}(k_{i\rho}|\boldsymbol{\rho}-\boldsymbol{\rho}'|) = \\ &- \frac{1}{|\boldsymbol{\rho}-\boldsymbol{\rho}'|}k_{i\rho}\rho\rho'\cos(\phi-\phi')H_0^{'(1)}(k_{i\rho}|\boldsymbol{\rho}-\boldsymbol{\rho}'|) \\ &+ \frac{1}{|\boldsymbol{\rho}-\boldsymbol{\rho}'|^{\frac{3}{2}}}k_{i\rho}\rho^2\rho'^2\sin(\phi-\phi')H_0^{'(1)}(k_{i\rho}|\boldsymbol{\rho}-\boldsymbol{\rho}'|) \\ &- \frac{1}{|\boldsymbol{\rho}-\boldsymbol{\rho}'|^2}k_{i\rho}\rho^2\rho'^2\sin^2(\phi-\phi')H_0^{''(1)}(k_{i\rho}|\boldsymbol{\rho}-\boldsymbol{\rho}'|), \end{aligned} \tag{C-6}$$

$$\begin{aligned} \frac{\partial^2}{\partial\rho\partial\rho'}H_0^{(1)}(k_{i\rho}|\boldsymbol{\rho}-\boldsymbol{\rho}'|) = \\ &- \frac{1}{4|\boldsymbol{\rho}-\boldsymbol{\rho}'|^{\frac{3}{2}}}k_{i\rho}[2\rho'-2\rho\cos(\phi-\phi')] \\ &\cdot [2\rho-2\rho'\cos(\phi-\phi')]H_0^{'(1)}(k_{i\rho}|\boldsymbol{\rho}-\boldsymbol{\rho}'|) \\ &+ \frac{1}{4|\boldsymbol{\rho}-\boldsymbol{\rho}'|^2}k_{i\rho}^2[2\rho'-2\rho\cos(\phi-\phi')] \\ &\cdot [2\rho-2\rho'\cos(\phi-\phi')]H_0^{''(1)}(k_{i\rho}|\boldsymbol{\rho}-\boldsymbol{\rho}'|) \\ &- \frac{1}{|\boldsymbol{\rho}-\boldsymbol{\rho}'|}k_{i\rho}\cos(\phi-\phi')H_0^{'(1)}(k_{i\rho}|\boldsymbol{\rho}-\boldsymbol{\rho}'|), \end{aligned} \tag{C-7}$$

where $H_0^{\prime(1)}$ and $H_0^{\prime\prime(1)}$ in (C-6) and (C-7) denote the first order derivative and second order derivative of the zeroth order Hankel function of the first kind, respectively. In order to get the closed-form solution to the following two infinite integrals:

$$\frac{1}{k_{i\rho}^2}\int \frac{\partial^2}{\partial\phi\partial\phi'}H_0^{(1)}(k_{i\rho}|\boldsymbol{\rho}-\boldsymbol{\rho}'|)e^{jk_z(z-z')}dk_z, \tag{C-8a}$$

$$\frac{1}{k_{i\rho}^2}\int \frac{\partial^2}{\partial\rho\partial\rho'}H_0^{(1)}(k_{i\rho}|\boldsymbol{\rho}-\boldsymbol{\rho}'|)e^{jk_z(z-z')}dk_z, \tag{C-8b}$$

we define the following two integrals W_1 and W_2:

$$W_1 = \int_{-\infty}^{\infty}\frac{1}{k_{i\rho}}H_0^{'(1)}(k_{i\rho}|\boldsymbol{\rho}-\boldsymbol{\rho}'|)e^{jk_z(z-z')}dk_z, \tag{C-9a}$$

$$W_2 = \int_{-\infty}^{\infty} H_0^{''(1)}(k_{i\rho}|\boldsymbol{\rho}-\boldsymbol{\rho}'|)e^{jk_z(z-z')}dk_z. \tag{C-9b}$$

By taking integration by part, the closed form solutions to W_1 and W_2 can be found as

$$W_{1c} = \left(\frac{1}{|\boldsymbol{\rho}-\boldsymbol{\rho}'|}\right)\frac{e^{jk_s|\boldsymbol{r}-\boldsymbol{r}'|}}{k_s}, \tag{C-10a}$$

$$W_{2c} = -\left(\frac{2}{|\boldsymbol{\rho}-\boldsymbol{\rho}'|^2}\right)\frac{e^{jk_s|\boldsymbol{r}-\boldsymbol{r}'|}}{k_s} - \left(\frac{2}{j}\right)\frac{e^{jk_s|\boldsymbol{r}-\boldsymbol{r}'|}}{|\boldsymbol{r}-\boldsymbol{r}'|}. \tag{C-10b}$$

Let C be a constant, then we have

$$\begin{aligned}
P_1 &= \int_{-\infty}^{\infty} C\cdot H_0^{(1)}(k_{i\rho}(|\boldsymbol{\rho}-\boldsymbol{\rho}'|))e^{jk_z(z-z')}dk_z \\
&= \frac{2C}{j}\frac{e^{jk|\boldsymbol{r}-\boldsymbol{r}'|}}{|\boldsymbol{r}-\boldsymbol{r}'|},
\end{aligned} \tag{C-11}$$

$$\begin{aligned}
P_2 =& \int_{-\infty}^{\infty}\frac{1}{k_{i\rho}^2}\sum_{-\infty}^{\infty} C[n^2H_n^{(1)}(k_{i\rho}\rho)J_n(k_{i\rho}\rho')] \\
&\cdot e^{jn(\phi-\phi')}e^{jk_z(z-z')}dk_z \\
=& \int_{-\infty}^{\infty}\frac{1}{k_{i\rho}^2}\frac{\partial^2}{\partial\phi\partial\phi'}\Big\{\sum_{-\infty}^{\infty} C\left[H_n^{(1)}(k_{i\rho}\rho)J_n(k_{i\rho}\rho')\right] \\
&\cdot e^{jn(\phi-\phi')}\Big\}e^{jk_z(z-z')}dk_z \\
=& \int_{-\infty}^{\infty}\frac{1}{k_{i\rho}^2}\frac{\partial^2}{\partial\phi\partial\phi'}\left[CH_0^{(1)}(k_{i\rho}|\boldsymbol{\rho}-\boldsymbol{\rho}'|)\right]e^{jk_z(z-z')}dk_z \\
=& \int_{-\infty}^{\infty}\frac{C}{k_{i\rho}^2}\Big\{\frac{-1}{|\boldsymbol{\rho}-\boldsymbol{\rho}'|}k_{i\rho}\rho\rho'\cos(\phi-\phi')H_0^{\prime(1)}(k_{i\rho}|\boldsymbol{\rho}-\boldsymbol{\rho}'|) \\
&+\frac{1}{|\boldsymbol{\rho}-\boldsymbol{\rho}'|^{\frac{3}{2}}}k_{i\rho}\rho^2\rho'^2\sin^2(\phi-\phi')H_0^{\prime(1)}(k_{i\rho}|\boldsymbol{\rho}-\boldsymbol{\rho}'|) \\
&-\frac{1}{|\boldsymbol{\rho}-\boldsymbol{\rho}'|^2}k_{i\rho}^2\rho^2\rho'^2\sin^2(\phi-\phi')H_0^{\prime\prime(1)}(k_{i\rho}|\boldsymbol{\rho}-\boldsymbol{\rho}'|)\Big\} \\
&\cdot e^{jk_z(z-z')}dk_z \\
=& C\Big\{-\frac{1}{|\boldsymbol{\rho}-\boldsymbol{\rho}'|}\rho\rho'\cos(\phi-\phi')W_{1c} \\
&+\frac{1}{|\boldsymbol{\rho}-\boldsymbol{\rho}'|^{\frac{3}{2}}}\rho^2\rho'^2\sin^2(\phi-\phi')W_{1c} \\
&-\frac{1}{|\boldsymbol{\rho}-\boldsymbol{\rho}'|^2}\rho^2\rho'^2\sin^2(\phi-\phi')W_{2c}\Big\},
\end{aligned} \tag{C-12}$$

$$\begin{aligned}
P_3 =& \int_{-\infty}^{\infty}\frac{1}{k_{i\rho}^2}\frac{\partial^2}{\partial\rho\partial\rho'}\Big\{\sum_{-\infty}^{\infty} C\cdot[H_n^{(1)}(k_{i\rho}\rho)J_n(k_{i\rho}\rho')] \\
&\cdot e^{jn(\phi-\phi')}\Big\}e^{jk_z(z-z')}dk_z
\end{aligned}$$

$$
\begin{aligned}
&= \int_{-\infty}^{\infty} \frac{1}{k_{i\rho}^2} \frac{\partial^2}{\partial\rho\partial\rho'} \left[C H_0^{(1)}(k_{i\rho}|\boldsymbol{\rho}-\boldsymbol{\rho}'|) \right] e^{jk_z(z-z')} dk_z \\
&= \int_{-\infty}^{\infty} \frac{C}{k_{i\rho}^2} \Big\{ -\frac{1}{|\boldsymbol{\rho}-\boldsymbol{\rho}'|^{\frac{3}{2}}} k_{i\rho} \left[\rho' - \rho\cos(\phi-\phi')\right] \\
&\quad \cdot \left[\rho - \rho'\cos(\phi-\phi')\right] H_0^{'(1)}(k_{i\rho}|\boldsymbol{\rho}-\boldsymbol{\rho}'|) \\
&\quad + \frac{1}{|\boldsymbol{\rho}-\boldsymbol{\rho}'|^2} k_{i\rho}^2 [\rho' - \rho\cos(\phi-\phi')] \\
&\quad \cdot \left[\rho - \rho'\cos(\phi-\phi')\right] H_0^{''(1)}(k_{i\rho}|\boldsymbol{\rho}-\boldsymbol{\rho}'|) \\
&\quad - \frac{1}{|\boldsymbol{\rho}-\boldsymbol{\rho}'|} k_{i\rho}\cos(\phi-\phi') H_0^{'(1)}(k_{i\rho}|\boldsymbol{\rho}-\boldsymbol{\rho}'|) \Big\} \\
&\quad \cdot e^{jk_z(z-z')} dk_z \\
&= C \Big\{ -\frac{1}{|\boldsymbol{\rho}-\boldsymbol{\rho}'|^{\frac{3}{2}}} \left[\rho' - \rho\cos(\phi-\phi')\right] \\
&\quad \cdot [\rho - \rho'\cos(\phi-\phi')] W_{1c} + \frac{1}{|\boldsymbol{\rho}-\boldsymbol{\rho}'|^2} \\
&\quad \cdot \left[\rho' - \rho\cos(\phi-\phi')\right] \left[\rho - \rho'\cos(\phi-\phi')\right] W_{2c} \\
&\quad - \frac{1}{|\boldsymbol{\rho}-\boldsymbol{\rho}'|} \cos(\phi-\phi') W_{1c} \Big\}. \qquad \text{(C-13)}
\end{aligned}
$$

The closed-form solutions to integrals P_1, P_2, P_3 are used in Section II for obtaining the closed form inverse Fourier transformation for quasi-static components.

Appendix D

Approximations of Special Functions

D.1 Large Argument Behaviour

The scalar wave equation in cylindrical coordinate has four types of special functions as its solution, they are Bessel function $J_n(k_\rho\rho)$, Neumann function $N_n(k_\rho\rho)$, Hankel function of the first kind $H_n^{(1)}(k_\rho\rho)$ and Hankel function of the second kind $H_n^{(2)}(k_\rho\rho)$. These special functions behave differently when the argument $k_\rho\rho \to \infty$. When $k_\rho\rho \to \infty$,

$$J_n(k_\rho\rho) \sim \sqrt{\frac{2}{\pi k_\rho\rho}}\cos(k_\rho\rho - \frac{n\pi}{2} - \frac{\pi}{2}) \tag{D-1}$$

$$N_n(k_\rho\rho) \sim \sqrt{\frac{2}{\pi k_\rho\rho}}\sin(k_\rho\rho - \frac{n\pi}{2} - \frac{\pi}{2}) \tag{D-2}$$

$$J_n(k_\rho\rho) \sim \sqrt{\frac{2}{\pi k_\rho\rho}}e^{i(k_\rho\rho - \frac{n\pi}{2} - \frac{\pi}{2})} \tag{D-3}$$

$$J_n(k_\rho\rho) \sim \sqrt{\frac{2}{\pi k_\rho\rho}}e^{-i(k_\rho\rho - \frac{n\pi}{2} - \frac{\pi}{2})} \tag{D-4}$$

D.2 Uniform Expansion

$$
\begin{aligned}
J_\nu(z) &\sim \left(\frac{4\xi}{1-C^2}\right)^{\frac{1}{4}} \cdot \left[\frac{A_i(\nu^{2/3}\xi)}{\nu^{1/3}}\right], \\
Y_\nu(z) &\sim -\left(\frac{4\xi}{1-C^2}\right)^{\frac{1}{4}} \cdot \left[\frac{B_i(\nu^{2/3}\xi)}{\nu^{1/3}}\right], \\
J'_\nu(z) &\sim -\frac{2}{C}\left(\frac{1-C^2}{4\xi}\right)^{\frac{1}{4}} \cdot \left[\frac{A'_i(\nu^{2/3}\xi)}{\nu^{2/3}}\right], \\
Y'_\nu(z) &\sim \frac{2}{C}\left(\frac{1-C^2}{4\xi}\right)^{\frac{1}{4}} \cdot \left[\frac{B'_i(\nu^{2/3}\xi)}{\nu^{2/3}}\right], \\
H^{(1)}_\nu(z) &\sim 2e^{-j\pi/3}\left(\frac{4\xi}{1-C^2}\right)^{\frac{1}{4}} \cdot \left[\frac{A_i(e^{j2\pi/3}\nu^{2/3}\xi)}{\nu^{1/3}}\right], \\
H^{'(1)}_\nu(z) &= 4e^{j4\pi/3}C\left(\frac{1-C^2}{4\xi}\right)^{\frac{1}{4}} \cdot \left[\frac{A'_i(e^{j2\pi/3}\nu^{2/3}\xi)}{\nu^{2/3}}\right],
\end{aligned}
\tag{D-5}
$$

where A_i and B_i are Airy functions; A'_i and B'_i are derivatives of Airy functions A_i and B_i, respectively.

D.3 Debye Approximation

Debye expansion of first and second kind Bessel function:

for $|\nu| > |z|$, $\alpha = \text{ArcCosh}(\nu/z)$

$$
\begin{aligned}
J_\nu(z) &\sim \frac{e^{\nu(\tanh\alpha-\alpha)}}{\sqrt{2\pi\nu\tanh\alpha}}, \\
Y_\nu(z) &\sim -\frac{e^{\nu(\alpha-\tanh\alpha)}}{\sqrt{\frac{1}{2}\pi\nu\tanh\alpha}}, \\
J'_\nu(z) &\sim \sqrt{\frac{\sinh 2\alpha}{4\pi\nu}}e^{\nu(\tanh\alpha-\alpha)}, \\
Y'_\nu(z) &\sim \sqrt{\frac{\sinh 2\alpha}{\pi\nu}}e^{\nu(\alpha-\tanh\alpha)}.
\end{aligned}
\tag{D-6}
$$

for $|\nu| < |z|$, $\beta = \text{ArcCosh}(\nu/z)$

$$
J_\nu(z) \sim \sqrt{\frac{2}{\pi\nu\tan\beta}}\cos\left[\nu(\tan\beta-\beta)-\frac{\pi}{4}\right],
$$

$$
\begin{aligned}
J'_\nu(z) &\sim -\sqrt{\frac{\sin 2\beta}{\pi\nu}}\sin\left[\nu(\tan\beta-\beta)-\frac{\pi}{4}\right],\\
Y_\nu(z) &\sim \sqrt{\frac{2}{\pi\nu\tan\beta}}\sin\left[\nu(\tan\beta-\beta)-\frac{\pi}{4}\right],\\
Y'_\nu(z) &\sim -\sqrt{\frac{\sin 2\beta}{\pi\nu}}\cos\left[\nu(\tan\beta-\beta)-\frac{\pi}{4}\right]. \qquad \text{(D-7)}
\end{aligned}
$$

Debye expansion of first and second kind Hankel function and logarithmic derivatives:

for $|\nu-z|\geq|\nu|^{1/3}$,

$$
\begin{aligned}
H_\nu^{(1,2)}(z) &\sim \sqrt{\frac{2}{\pi\nu\tan\gamma}}e^{\pm j\pi/4}e^{\pm j\nu(\tan\gamma-\gamma)}\cdot\left[1\mp j\frac{3t+5t^2}{24\nu}+O(\nu^{-2})\right],\\
&\quad \cos\gamma=\nu/z, \qquad t=\cot\gamma,\\
&\quad 0<\Re\gamma<\pi, \qquad |\nu|<|z| \qquad \text{(D-8)}\\
H_\nu^{(1,2)}(z) &\sim \mp j\frac{e^{\nu(\alpha-\tanh\alpha)}}{\frac{1}{2}\pi\nu\tanh\alpha}\cdot\left[1+j\frac{5t^3-3t}{24\nu}+O(\nu^{-2})\right],\\
&\quad \cosh\alpha=\nu/z, \qquad t=\coth\alpha,\\
&\quad \Re\gamma>0, \qquad |\nu|>|z| \qquad \text{(D-9)}\\
H_\nu^{(1,2)}(z) &\sim \frac{e^{\pm\nu(\alpha-\tanh\alpha)}}{\frac{1}{2}\pi\nu\tanh\alpha}e^{j5\pi/4\pm j\pi/4}\cdot\left[1\pm j\frac{5t^3-3t}{24\nu}+O(\nu^{-2})\right],\\
&\quad \cosh\alpha=\nu/z, \qquad t=\coth\alpha,\\
&\quad \Re\gamma>0, \qquad |\nu|>|z|, \qquad \arg(\nu/z)\sim 0, \qquad \text{(D-10)}
\end{aligned}
$$

$$
\begin{aligned}
\frac{H_\nu^{'(1,2)}(z)}{H_\nu^{(1,2)}(z)} &\sim \pm j\sin\gamma-\frac{1}{2z\sin^2\gamma}+\frac{1}{z}\frac{12\sin^2\gamma-15}{\mp j24\sin^5\gamma+2\sin^4\gamma-5\sin^2\gamma}+O(\nu^{-3})\\
&\quad \cos\gamma=\nu/z, \qquad t=\cot\gamma,\\
&\quad 0<\Re\gamma<\pi, \qquad |\nu|<|z| \qquad \text{(D-11)}\\
\frac{H_\nu^{'(1,2)}(z)}{H_\nu^{(1,2)}(z)} &\sim -\sinh\alpha+\frac{1}{2z\sinh^2\alpha}+\frac{1}{z}\frac{12\sinh^2\gamma+15}{j24\sinh^5\alpha+2\sinh^4\alpha+5\sinh^2\alpha}+O(\nu^{-3})\\
&\quad \cosh\alpha=\nu/z, \qquad t=\coth\alpha,\\
&\quad \Re\gamma>0, \qquad |\nu|>|z| \qquad \text{(D-12)}\\
\frac{H_\nu^{'(1,2)}(z)}{H_\nu^{(1,2)}(z)} &\sim \mp\sinh\alpha+\frac{1}{2z\sinh^2\alpha}+\frac{1}{z}\frac{12\sinh^2\gamma+15}{\pm j24\sinh^5\alpha+2\sinh^4\alpha+5\sinh^2\alpha}+O(\nu^{-3})\\
&\quad \cosh\alpha=\nu/z, \qquad t=\coth\alpha,\\
&\quad \Re\gamma>0, \qquad |\nu|>|z|, \qquad \arg(\nu/z)\sim 0, \qquad \text{(D-13)}
\end{aligned}
$$

for $|\nu - z| < |\nu|^{1/3}$,

$$\begin{aligned} \frac{H_\nu^{'(1,2)}(z)}{H_\nu^{(1,2)}(z)} &\sim -\frac{1}{m}\frac{w_{1,2}'(t)}{w_{1,2}(t)}, \\ & m = (z/2)^{1/3}, \qquad t = (\nu - z)/m, \\ & w_{1,2}(t) = \sqrt{\pi}\,[B_i(t) \pm jA_i(t)]\,. \end{aligned} \tag{D-14}$$

Bibliography

[1] J. Q. Howell, "Microstrip antennas", *IEEE AP-S Int.Symp.Digest*, pp. 177–180, 1972.

[2] R. E. Munson, "Conformal microstrip antennas and microstrip phased arrays", *IEEE Trans.Antennas Propagat.*, vol. 22, pp. 74–78, 1974.

[3] K. R. Carver and J. W. Mink, "Microstrip antenna technology", *IEEE Trans. Antennas Propagat.*, vol. 29, pp. 2–24, 1981.

[4] J. R. James and P. S. Hall, *Handbook of Microstrip Antennas*, Peter Peregrinus, London, UK, 1989.

[5] D. M. Pozar and D. H. Schaubert, *The Analysis and Design of Microstrip Antennas and Arrays*, IEEE Press, New York, 1996.

[6] D. M. Pozar, "Microstrip antennas", *Proc. IEEE*, vol. 80, pp. 79–91, 1992.

[7] G. Ramesh, B. Prakash, B. Inder, and I. Apisak, *Microstrip Antenna Design Handbook*, Artech House, Boston, 2000.

[8] A. Derneryd, "Linearly polarized microstrip antennas", *IEEE Trans.Antennas Propagat.*, vol. 24, pp. 846–851, 1976.

[9] A. Derneryd, "A theoretical investigation of the rectangular microstrip antenna element", *IEEE Trans.Antennas Propagat.*, vol. 26, pp. 532–535, 1978.

[10] A. K. Bhattacharyya, L. Shafai, and R. Garg, "Micostrip antenna-a generalised transmission line", *Progress in Electromagnetics Research*, vol. 4, pp. 45–84, 1991.

[11] A. K. Bhattacharyya and R. Garg, "Generalized transmission line model for microstrip patches", *IEE Proc.Pt.H*, vol. 132, pp. 93–98, 1985.

[12] A. K. Bhattacharyya and R. Garg, "Analysis of annular sector and circular sector microsrtip patch antennas", *Electromagnetics*, vol. 6, no. 3, pp. 229–242, 1986.

[13] A. K. Bhattacharyya and R. Garg, "A microstrip array of concentric annular rings", *IEEE Trans.Antennas Propagat.*, vol. 33, pp. 655–659, 1985.

[14] Y. T. Lo, D. Soloman, and W. F. Richards, "Theory and experiment on microstrip antennas", *IEEE Trans.Antennas Propagat.*, vol. 27, pp. 137–145, 1979.

[15] K. F. Lee, K. M. Luk, and J. S. Dahele, "Characteristics of the equilateral triangular patch antenna", *IEEE Trans. Antennas Propagat.*, vol. 36, pp. 1510–1818, 1988.

[16] J. S. Dahele and K. F. Lee, "Effect of substrate thickness on the performance of a circular-disk microstrip antenna", *IEEE Trans.Antennas Propagat.*, vol. 31, pp. 358–360, 1983.

[17] J. W. Mink, "Circular ring microstrip antenna element", *IEEE AP-S Int.Symp.Digest*, pp. 605–608, 1980.

[18] V. Palanisamy and R. Garg, "Analysis of arbitrary shaped microstrip patch antennas using segmentation technnique and cavity model", *IEEE Trans.Antennas Propagat.*, vol. 34, pp. 1208–1213, 1986.

[19] A. Taflove, *Computational Electrodynamics: The Finite Difference Time Domain Method*, Artech House, Norwood, MA, 1995.

[20] J. M. Jin, *The finite element method in electromagnetics*, New York : Wiley, 1993.

[21] D. M. Pozar, "Radiation and scattering from a microstrip patch on a uniaxial subatrate", *IEEE Trans.Antennas Propagat.*, vol. 35, pp. 613–621, 1987.

[22] M. D. Deshpande and M. C. Bailey, "Input impedence of microstrip antennas", *IEEE Trans.Antennas Propagat.*, vol. 30, pp. 645–650, 1982.

[23] J. R. Mosig and F. E. Gardiol, "Analytic and numerical techniques in the green's function treatment of microstrip antennas and scatters", *IEE Proc.*, vol. 130. Pt.H, pp. 175–182, 1983.

[24] J. R. Mosig and F. E. Gardiol, "General integration equation formilation for microstrip antennas and scatters", *IEE Proc.*, vol. 132. Pt.H, pp. 424–432, 1985.

[25] J. R. Mosig, "Arbitrarily shaped microstrip structures and their analysis with a mixed potential integral equation", *IEEE Trans.Microwave Theory Tech.*, vol. 36, pp. 314–323, 1988.

[26] D. G. Fang, J. J. Yang, and G. Y. Delisle, "Discrete image theory for horizontal electric dipole in a multilayer medium", *Proc. Inst. Elect. Eng. H*, vol. 135, pp. 297–303, Oct. 1988.

[27] Y. L. Chow, J. J. Yang, D. G. Fang, and G. E. Howard, "A closed-form spatial Green's function for the thick microstrip substrate", *IEEE Trans. Microwave Theory Tech.*, vol. 39, pp. 558–592, Mar. 1991.

[28] M. Kahrizi, T. K. Sarkar, and Z. A. Maricevic, "Analysis of a wide radiating slot in the ground plane of a microstrip line", *IEEE Trans. Microwave Theory Tech.*, vol. 41, pp. 29–37, 1993.

[29] C. Chen and N. G. Alexopoulos, "Modeling microstrip line fed slot antennas with arbitrary shape", *Electromagnetics*, vol. 15, pp. 567–586, 1995.

[30] R. C. Hall and J. R. Mosig, "The analysis of arbitrarily shaped aperture-couple patch antennas via a mixed-potential integral equation", *IEEE Trans.Antennas Propagat.*, vol. 44, pp. 608–614, 1996.

[31] L. Barlatey, J. R. Mosig, and T. Sphicopoulos, "Analysis of stacked microstrip patches with a mixed potential integral equation", *IEEE Trans.Antennas Propagat.*, vol. 38, pp. 608–615, 1990.

[32] G. A. E. Vandenbosch and A. R. Van de Capelle, "Mixed-potential integral expression formulation of electric field in a sttatified dielectric medium appication to the case of a prob current source", *IEEE Trans.Antennas Propagat.*, vol. 40, pp. 806–817, 1992.

[33] K. A. Michalski and J. R. Mosig, "Discret complex image mixed-potential integral equation analysis of microstrip patch antennas with vertical probe feeds", *Electromagnetics*, vol. 15, pp. 377–392, 1995.

[34] K. M. Luk and K. F. Lee, "Characterristics of the cylindrical-circular patch antenna", *IEEE Trans. Antennas Propagat.*, vol. 38, no. 7, pp. 1119–1123, Jul. 1990.

[35] T. M. Habashy, S. M. Ali, and J. A. Kong, "Input impedance and radiation pattern of cylindrical-rectangular and wraparound microstrip antennas", *IEEE Trans. Antennas Propagat.*, vol. 38, pp. 722–732, May. 1990.

[36] F. C. Silva, S. B. A. Fonseca, A. J. M. Soares, and A. J. Giarola, "Analysis of microstrip antennas on circular-cylindrical substrates with a dielectric overlay", *IEEE Trans. Antennas Propagat.*, vol. 39, no. 9, pp. 1398–1404, 1991.

[37] K. L. Wong, Y. T. Cheng, and J. S. Row, "Resonance in a superstrate-loaded cylindrical-rectangular microstrip structure", *IEEE Trans. Microwave Theory Tech.*, vol. 41, no. 5, pp. 814–819, May 1993.

[38] R. F. Harrington, *Field Computation by Moment Methods*, Macmillan, NY, 1968.

[39] K. L. Wong, *Design of Nonplanar Microstrip Antennas and Transmission Lines*, New York: Wiley, 1999.

[40] N. C. Abertsen, "Creeping wave modes for a dielectric coated cylinder", *IEEE Trans. Antennas Propagat.*, vol. 37, no. 12, pp. 1642–1644, 1989.

[41] R. Paknys and N. Wang, "Creeping wave propagation constants and model impedence for a dielectric coated cylinder", *IEEE Trans. Antennas Propagat.*, vol. 34, no. 6, pp. 674–680, 1986.

[42] A. P. Krasnojen, "Features of creeping waves propagation on the dielectric-coated circular cylinder", *IEE Proc. Microw. Antennas Propag.*, vol. 145, no. 2, pp. 179–183, 1998.

[43] K. Naishadham and L. B. Felsen, "Dispersion of waves guided along a cylindrical substrate-superstrate layered medium", *IEEE Trans. Antennas Propagat.*, vol. 41, no. 3, pp. 304–313, 1993.

[44] S. H. Talisa, "Application of davidenko's method to the solution of dispersion relation in lossy waveguiding systems", *IEEE Trans. Microwave Theory Tech.*, vol. 33, pp. 967–971, 1985.

[45] C. M. Krowne, "Cylindrical-rectangular microstrip antenna", *IEEE Trans. Antennas Propagat.*, vol. 31, pp. 194–199, Jan.1983.

[46] K. M. Luk, K. F. Lee, and J. S. Dahele, "Analysis of the cylindrical-rectangular patch antenna", *IEEE Trans. Antennas Propagat.*, vol. 37, no. 2, pp. 143–147, 1989.

[47] J. Helszajn and D. S. James, "Planar triangular resonator with magnetic wall", *IEEE Trans. Microwave Theory Tech.*, vol. 26, pp. 95–100, 1978.

[48] K. L. Wong and S. C. Pan, "Resonance in a cylindrical-triangular microstrip structure", *IEEE Trans. Microwave Theory Tech.*, vol. 45, pp. 1270–1272, 1997.

[49] S. B. A Fonseca and A. J. Giarola, "Analysis of microstrip wraparound antannas using dyadic Green's functions", *IEEE Trans. Antennas Propagat.*, vol. 31, pp. 248–253, Mar.1983.

[50] N. Herscovici, Z. Sipus, and P. S. Kildal, "The cylindrical omnidirectional patch antenna", *IEEE Trans. Antennas Propagat.*, vol. 49, no. 12, pp. 1746–1753, Dec.1995.

[51] N. G. Alexopoulos and A. Nakatani, "Cylindrical substarte microstrip line charaterization", *IEEE Trans. Microwave Theory Tech.*, vol. 35, pp. 843–849, 1987.

[52] L. R. Zeng and Y. Wang, "Accurate solutions of elliptical and cylindrical striplines and microstrip lines", *IEEE Trans. Microwave Theory Tech.*, vol. 34, pp. 259–264, 1986.

[53] H. M. Chen and K. L. Wong, "Characterizations of coupled cylindrical microstriplines mounted inside a ground cylinder", *Micorwave Opt. Tech. Lett.*, vol. 10, pp. 330–333, 1995.

[54] H. M. Chen and K. L. Wong, "Characterizations of cylindrical microstrip gap discontinuities", *Micorwave Opt. Tech. Lett.*, vol. 9, pp. 260–263, 1995.

[55] J. H. Lu and K. L. Wong, "Analysis of slot-couple double-side cylindrical microstrip lines", *IEEE Trans. Microwave Theory Tech.*, vol. 44, pp. 1167–1170, 1996.

[56] H. C. Su and K. L. Wong, "Dispersion characteristic of cylindrical coplannar waveguide", *IEEE Trans. Microwave Theory Tech.*, vol. 44, pp. 2120–2122, 1996.

[57] J. Ashkenazy, S. Shtrikman, and D. Treves, "Electric surface current model for the analysis of microstrip antennas on cylindrical body", *IEEE Trans. Antennas Propagat.*, vol. 33, no. 3, pp. 295–300, 1985.

[58] J. Ashkenazy, S. Shtrikman, and D. Treves, "Conformal microstrip arrays on cylinders", *IEE Proc.*, vol. 135. Pt.H, pp. 132–134, 1988.

[59] J. R. Wait, *Electromagnetic Waves in Stratified Media*, Pergamon, Elmsford, NY, 1970.

[60] L. B. Felson and N. Marcuvitz, *Radiation and Scattering of Waves*, Prentice-Hall, Englewood Cliff, NJ, 1973.

[61] A. Dreher, "A new approach to dyadic Green's functions in spectral domain", *IEEE Trans. Antennas Propagat.*, vol. 43, pp. 1297–1302, Nov.1995.

[62] W. C. Chew, *Waves and Fields in Inhomogeneous Media*, Vannostrand, New York, 1990.

[63] C. T. Tai, *Dyadic Green's Fuunctions in electromagnetic Theory*, 2nd ed. Piscataway, NI: IEEE Press, 1994.

[64] L. W. Li, P. S. Kooi, M. S. Leong, and T. S. Yeo, "On the eigenfunction expansion of the dyadic Green's function in planarly stratified media", *J. Electromag. Waves Applic.*, vol. 8, no. 6, pp. 663–678, June 1994.

[65] K. A. Michalski and D. Zheng, "Electromagnetic scattering and radiation by surface of arbitrary shape in layered media- Part I: Theory", *IEEE Trans. Antennas Propagat.*, vol. 38, pp. 335–344, Mar. 1990.

[66] S. M. Rao, D. R. Wilton, and A. W. Glission, "Electromagnetic scattering by surfaces of arbitrary shape", *IEEE Trans. Antennas Propagat.*, vol. 30, pp. 409–418, May. 1982.

[67] J. Chen, A. A. Kishk, and A. W. Glisson, "Application of a new MPIE formulation to the analysis of a dielecric resonator embedded in a multilayered medium couple to a microstrip circuit", *IEEE Trans. Microwave Theory Tech.*, vol. 49, no. 2, pp. 263–279, 2001.

[68] A. Sommerfeld, *Partial Differential Equations in Physics*, New York: Academic, 1967.

[69] A. J. Mackay and A. McCowan, "An improved pencil-of-function method for extracting poles of an Em system from its transient response", *IEEE Trans. Antennas Propagat.*, vol. 35, pp. 435–441, 1987.

[70] Y. Hua and T. K. Sarkar, "Generalized pencil-of-function method for extracting poles of an EM system from its transient response", *IEEE Trans.Antennas Propagat.*, vol. 37, pp. 229–234, Feb. 1989.

[71] J. J. Yang, Y. L. Chow, G. E. Howard, and D. G. Fang, "Complex images of an electric dipole in homogeneous and layered dielectrics between two grounded planes", *IEEE Trans. Microwave Theory Tech.*, vol. 40, pp. 595–600, Mar. 1992.

[72] R. A. Kipp and C. H. Chan, "Complex image method for sources in bounded regions of multilayer structures", *IEEE Trans. Microwave Theory Tech.*, vol. 42, pp. 860–865, May 1994.

[73] G. Dural and M. I. Aksun, "Closed-form Green's functions for general sources and stratified media", *IEEE Trans.Microwave Theory Tech.*, vol. 43, pp. 1545–1552, July. 1995.

[74] F. J. Demuynck, Guy A. E. Vandenbosch, and Antoine R. Van de Capelle, "The expansion wave concept-Part I: efficient calculation of spatial green's functions in a stratified dielectric medium", *IEEE Trans. Antennas Propagat.*, vol. 46, no. 3, pp. 397–406, Mar. 1998.

[75] F. Ling and J. M. Jin, "Discrete complex image method for Green's functions of general multilayer media", *IEEE Microwave Guided Wave Lett.*, vol. 10, pp. 400–402, Oct. 2000.

[76] J. R. Wait, *Electromagnetic Propagation from Cylindrical Structures*, New York: Pergamon, 1959.

[77] L. W. Pearson, "On the spectral expansion of the electric and magnetic dyadic Green's functions in cylindrical harmonics", *Radio Sci*, vol. 18, pp. 166–174, 1983.

[78] L. W. Li, M. S. Leong, T. S. Yeo, and P. S. Kooi, "Electromagnetic dyadic Green's functions in spectral domain for multilayered cylinders", *Journal of Electromagnetic Waves and Applications*, vol. 14, pp. 961–986, Jul. 2000.

[79] A. Nakatani, *Modeling microstrip and antennas on cylindrical substrate*, Ph.D. dissertation, Dept. Elec. Eng., University of California at Los Angeles, 1988.

[80] M. Thiel and A. Dreher, "Dyadic green's function of multilayer cylindrical closed and sector structures for waveguide, microstrip-antenna and network analysis", *IEEE Trans. Microwave Theory Tech.*, vol. 50, pp. 2576–2579, Nov. 2002.

[81] C. Tokgöz and G. Dural, "Closed-form Green's functions for cylindrically stratified media", *IEEE Trans.Microwave Theory Tech.*, vol. 48, pp. 40–49, Jan. 2000.

[82] M. I. Aksun, "A robust approch for the derivation of closed-form spatial Green's functions", *IEEE Trans.Microwave Theory Tech.*, vol. 44, pp. 651–658, May. 1996.

[83] W. C. Chew, "The singularities of a fourier-type integral in a multicylindrical layer problem", *IEEE Trans. Antennas Propagat.*, vol. 31, no. 4, pp. 653–655, July. 1983.

[84] V. B. Ertürk and R. G. Rojas, "Efficient computation of surface fields excited on a dielectric-coated circular cylinder", *IEEE Trans. Antennas Propagat.*, vol. 48, no. 10, pp. 1507–1516, 2000.

[85] V. B. Ertürk and R. G. Rojas, "Paraxial space-domain formulation for surface fields on a large dielectric-coated circular cylinder", *IEEE Trans. Antennas Propagat.*, vol. 50, no. 11, pp. 1577–1587, 2002.

[86] A. Ishimaru, *Electromagnetics Wave Propagation, Radiation, and Scattering*, New Jersey: Prentice-Hall, 1991.

[87] R. C. Hall, C. H. Thng, and D. C. Chang, "Mixed potential Green's functions for cylindrical microstrip structures", *IEEE Antennas Propagat. Soc. Int. Symp.*, vol. 4, pp. 1776–1779, 1995.

[88] J. A. Kong, *Electromagnetics Wave Theory*, John Wiley & Sons, Inc., 1990.

[89] C. T. Tai, *Generalized Vector and Dyadic Analysis*, New York, IEEE Press, 1997.

[90] J.Van Bladel, *Electromagnetic Fields*, Bristol,PA: Hemisphere, 1985.

[91] L. W. Pearson, "A construction of the fields radiated by z-directed point sources of current in the presence of a cylindrically layered obstacle", *Radio Sci*, vol. 21, no. 4, pp. 559–569, 1986.

[92] M. Abramowitz and I. Stegun, *Handbook of Mathematical Functions*, New York: Dover, 1965.

[93] R. Lampe, P. Klock, and P. Mayes, "Integral transforms useful for the accelerated summation of peridic, free-space green's functions", *IEEE Trans. Microwave Theory Tech.*, vol. 33, pp. 734–736, Aug. 1985.

[94] S. Singh, W. F. Richards, J. R. Zinecker, and D. R. Wilton, "Accelerating the convergence of series representing the free space periodic green's fucntion", *IEEE Trans. Antennas Propagat.*, vol. 38, pp. 1958–1962, Dec. 1990.

[95] D. Shanks, "Non-linear transformations of divergent and slowly convergent sequences", *Journal of Mathematical Physics*, vol. 34, pp. 1–42, 1955.

[96] P. Wynn, "On a device for computing the $e_m(s_n)$ transformation", *Mathematical Tables and Other Aids for Computation*, vol. 10, pp. 91–96, 1956.

[97] M. I. Aksun and R. Mittra, "Derivation of closed-form spatial Green's functions for a general microstrip geometry", *IEEE Trans.Microwave Theory Tech.*, vol. 40, pp. 2055–2062, Nov. 1992.

[98] A. W. Glission and D. R. Wilton, "Simple and efficient numerical methods for problems of electromagnetic radiation and scattering from surface", *IEEE Trans. Antennas Propagat.*, vol. 28, pp. 593–603, 1980.

[99] M. C. Bailey and M. D. Deshpande, "Integral equation formulation of microstrip antennas", *IEEE Trans. Antennas Propagat.*, vol. 30, no. 4, pp. 651–656, 1982.

[100] R. J. Allard, D. H. Werner, and J. S. Zmysl, "A domain decomposition/ reciprocity technique for the analysis of arbitrarily-shaped microstrip antennas with dielectric substrates and superstrates mounted on circularly-cylindrical platforms", *Proc.16th Ann. Rev. Progress Appl. Comput. Electromagn.*, pp. 173–180, Mar. 2000.

[101] A. F. Peterson, B. S. Greene, and R. Mittra, "Propagation and radiation characteristics of the taped helix with a conducting core and dielectric substrate", *IEEE Trans. Antennas Propagat.*, vol. 38, pp. 578–583, Apr. 1990.

[102] R. A. Martin and D. H. Werner, "A reciprocity approach for calculating the far-field radiation patterns of a center-fed helical microstrip antenna mounted on a dielectric-coated circular cylinder", *IEEE Trans. Antennas Propagat.*, vol. 49, no. 12, pp. 1754–1762, Dec. 2001.

[103] S. Lu and P. G. Xu, *Analytic Methods in Electromagnetic Fields* (in Chinese), Wuhan : Wuhan University, 1992.

[104] J. D. Kraus and R. J. Marhefka, *Antennas for All Applications*, Mc Graw Hill, Third Edition, 2002.

[105] H. C. Strifors and G. C. Gaunaurd, "Scattering of electromagnetic waves by a perfectly conducting cylinder with a thin lossy magnetic coating", *IEEE Trans. Antennas Propagat.*, vol. 48, no. 10, pp. 1528–1532, Oct. 2000.

[106] R. Paknys, "Evaluation of Hankel function with complex argument and complex order", *IEEE Trans. Antennas Propagat.*, vol. 40, no. 5, pp. 569–578, May. 1992.

[107] F. Ling, C. F. Wang, and J. M. Jin, "An efficient algorithm for analyzing large-scale microstrip structures using adaptive integral method combined with discrete complex-image method", *IEEE Trans. Microwave Theory Tech.*, vol. 48, pp. 832–839, May. 2000.

[108] K. A. Michalski and D. Zheng, "Electromagnetic scattering and radiation by surface of arbitrary shape in layered media- Part II: Implementation and results for contiguous half-sapces", *IEEE Trans. Antennas Propagat.*, vol. 38, pp. 345–352, Mar. 1990.